

CONF-8510166--

DE86 010354

PROCEEDINGS OF THE
FIRST INTERNATIONAL INFORMATION MEETING
ON THE TMI-2 ACCIDENT

Convened by

U. S. Department of Energy--Headquarters
October 21, 1985
Germantown, MD 20874

Compiled By

Sidney Langer
Idaho National Engineering Laboratory
EG&G Idaho, Inc.

and

Willis R. Young
U. S. Department of Energy
Idaho Operations Office

MASTER

DISTRIBUTION OF THIS DOCUMENT IS UNLIMITED

ENB

ACKNOWLEDGMENT

The Editors would like to thank all of the contributors for their cooperation in promptly supplying the manuscripts that permitted the publication of this document within about six months of the actual conference. We also appreciate the invaluable assistance of Mss. Judy Gordon and Sandy Lord in rapidly completing the technical editing and preparing the manuscript for printing.

Technical review of all the papers was carried out by Dr. R. R. Hobbins in addition to the undersigned, and we wish to acknowledge his valuable comments. It is our hope that this document will contribute to the increasing knowledge of the behavior of nuclear power plants under severe accident conditions.

Sidney Langer
Willis R. Young

CONTENTS

ACKNOWLEDGMENT	11
ACRONYMS	v
INTRODUCTION AND ACCIDENT EVALUATION PROGRAM	1
Introduction	
G. Donald McPherson, DOE-HQ	3
TMI-2 Programs Overview	
H. M. Burton, INEL	5
Core Condition and Accident Scenario	
J. M. Broughton, INEL	7
TMI-2 Accident Evaluation Program Overview	
E. L. Tolman, INEL	19
TMI-2 Accident Evaluation Program Sample Acquisition and Examination Plan	
R. K. McCardell et al., INEL	27
PLANT INSTRUMENT BEHAVIOR	43
In-Core Instrument Survivability	
R. D. Meininger, INEL	45
TMI-2 Pressurizer-Level Response	
J. L. Anderson, INEL	47
TMI SPND Interpretation	
D. J. N. Taylor, INEL	65
CORE DEBRIS BED AND FISSION-PRODUCT BEHAVIOR	75
TMI-2 Core Debris Analysis	
B. A. Cook and E. R. Carlson, INEL	77
Fission-Product Transport at Three Mile Island	
D. E. Owen, Nuclear Engineering Consultant	
T. E. Cox, Bechtel National, Inc.	
J. M. Broughton, INEL	97
Fission-Product and Core Material Behavior	
S. Langer, M. L. Russell, D. W. Akers, INEL	123
CORE AND POTENTIAL STRUCTURAL DAMAGE	141
Core Relocation Phenomenology	
R. E. Henry et al., Fauske & Associates	143

Debris Thermal Interaction with Lower Plenum Structures A. W. Cronenberg, Engineering Science and Analysis S. R. Behling, W. F. Domenico, J. M. Broughton, INEL	177
Chemical Interactions Between Core and Structural Materials E. R. Carlson and B. A. Cook, INEL	191
SUMMARY	207
Future Meetings and Information Transfer S. Langer, INEL	209

ACRONYMS

ANL	Argonne National Laboratory (West and East)
B&W	Babcock & Wilcox Company
DOE	U. S. Department of Energy
EPRI	Electric Power Research Institute
GEND	The TMI Research Group composed of GPU Nuclear, EPRI, NRC, and Doe
GPU Nuclear	General Public Utilities Nuclear Corporation
HEDL	Hanford Engineering Development Laboratory
INEL	Idaho National Engineering Laboratory
KFK	Kernforschungszentrum, Karlsruhe (Federal Republic of Germany)
NRC	U. S. Nuclear Regulatory Commission
ORNL	Oak Ridge National Laboratory
TMI	Three Mile Island

AEP	Accident Evaluation Program
ANS	American Nuclear Society
ECCS	Emergency Core Cooling System
EPICOR-II	Liners for prefilter demineralizer resins (organic and zeolite)
ESF	Engineered Safety Feature
HPI	High Pressure Injection
HPIS	High Pressure Injection System
ICS	Integrated Control System
IDCOR	Industry Degraded Core Research Program
IWTS	Industrial Waste Treatment System
LOFT	Loss-of-Fluid-Test Facility
LWR	Light Water Reactor

MOV	Motor-Operated Valve
MUP	Makeup/Purification System
NNI	Nonnuclear Instrumentation
PBF	Power Burst Facility
PORV	Pilot-Operated Relief Valve
PWR	Pressurized Water Reactor
R&D	Research and Development
RB	Reactor Basement
RCBHT	Reactor Coolant Bleed Holdup Tank
RCBT	Reactor Coolant Bleed Tank
RCDT	Reactor Coolant Drain Tank
RCP	Reactor Coolant Pump
RCS	Reactor Coolant System
RELAP5	Reactor Excursion and Leak Analysis Program
RQSA	Rig of Safety Assessment (a Japanese Test Facility)
RPV	Reactor Pressure Vessel
RTD	Resistance Thermal Detector
SA&E	Sample Acquisition and Examination Plan
SCD	Severe Core Damage
SCDAP	Severe Core Damage Analysis Program
SDS	Submerged Demineralizer System
SEM	Scanning Electron Microscope
SFD	Severe Fuel Damage
SPND	Self-Powered Neutron Detector
SRM	Source Range Monitor
TMI-2	TMI Nuclear Power Station Unit 2
TRU	Transuranic

INTRODUCTION AND ACCIDENT EVALUATION PROGRAM

INTRODUCTION

G. Donald McPherson, Manager
TMI-2 Accident Evaluation Program
U.S. Department of Energy--Headquarters
Germantown, MD 20874

DOE is working in cooperation with GPU Nuclear, owner of the TMI-2 nuclear power plant, to remove, transport, and dispose of the damaged core from TMI-2. In 1984, when it became apparent that the core had been damaged much worse than originally thought, DOE, in collaboration with GPU Nuclear, EPRI, and NRC undertook an extensive program of examination and analysis, with the following objectives:

- Determine the core damage progression
- Determine the plant-wide fission-product behavior (source term), concentrating on release from the fuel and transport and retention in the primary cooling system
- Enhance the understanding of controlling processes and phenomena and identify those that are not currently included in codes or are modeled improperly
- Provide a Standard Problem for the TMI-2 accident, against which the severe accident analysis codes can be evaluated.

Progress toward meeting those objectives was reported during the one-day First International Information Meeting on the TMI-2 Accident and is recorded in detail in these Proceedings. The reader will discover the vast amount of information that has been uncovered and developed during the early stages of this program; a great deal is now understood about the accident. Furthermore, it now appears that the consequences to the reactor are fairly typical of severe accidents; therefore, it is even more important to today's current severe accident and source-term issues that the above objectives are met.

After the Information Meeting, held on October 21, 1985, we received many commendations for the organization of material and the content and quality of presentations. We sincerely hope that the reader will be equally impressed with the quality of the papers contained in these Proceedings.

TMI-2 PROGRAMS OVERVIEW

Harold M. Purton
Idaho National Engineering Laboratory
EG&G Idaho, Inc.
P.O. Box 1625, Idaho Falls, ID 83415

In 1980, GPU Nuclear, EPRI, NRC, and DOE (collectively known as GEND) established the TMI-2 Technical Information and Examination Program under a cooperative agreement. EG&G Idaho, Inc., is managing the DOE portions of this program. The DOE TMI-2 programs have two key objectives. The first is supporting recovery of the TMI-2 reactor--this paper focuses on that objective. The second is obtaining a complete understanding of the TMI-2 accident. Other papers in these Proceedings of the First International Information Meeting on the TMI-2 Accident focus on that objective.

DOE support of the recovery effort is being achieved through four specific programs. The Waste Disposition Program is providing unique support through disposition of accident-generated wastes that cannot be accommodated by commercial disposal. The Reactor Disassembly Program is developing equipment and techniques for disassembling the severely damaged TMI-2 reactor that also have generic applications for future, potentially difficult disassembly tasks. The Fuel Shipping and Storage Program is fulfilling requirements of a DOE/GPU Nuclear contract, whereby DOE will take possession of the TMI-2 core for R&D. That program also is contributing significantly to R&D efforts by handling, transporting, storing, and dispositioning severely damaged nuclear fuel. The Data Acquisition Program is providing unique applications of technology in a particularly difficult environment to acquire data to support both the recovery effort and evaluation of the accident.

The Waste Disposition Program is providing a TMI-specific solution for industry-wide application of managing nuclear wastes. There were six categories of accident-generated wastes from TMI-2: gases, EPICOR-II prefilters, high-activity zeolites, MUP resins, abnormal wastes, and core debris. The gases were dispositioned via radioactive decay and controlled releases to the environment. Those releases resulted in insignificant exposure to the public. EPICOR-II prefilters were used in processing water in the TMI-2 Auxiliary and Fuel Handling Buildings after the accident. They contained mixed ion-exchange resins and zeolites in steel liners and were loaded up to 1000 Ci/m³. Except for four prefilters retained at INEL for research, the EPICOR-II prefilters were disposed of in high-integrity containers at the commercial disposal site in the State of Washington. High-activity zeolites in stainless steel containers, loaded up to 350,000 Ci/m³, resulted from processing water in the Reactor Building and RCS. MUP demineralizer resins were damaged by loading with postaccident fission products, principally iodine. After the iodine decayed, the remaining significant radionuclides, principally cesium, were eluted in order to handle the damaged resins with existing systems. Abnormal waste is the generic term applied to all high specific-activity wastes, particularly those with levels of TRU contaminant that preclude disposal at commercial sites. The only solution for removing abnormal

waste from the TMI-2 site is to provide interim storage at a DOE site--INEL--while the capability for long-term storage in a Federal repository is being developed. Finally, the TMI-2 core debris has significant research value; examination of many samples is a prerequisite to understanding the accident. To enable efficient examination of the core debris, the entire core will be stored at INEL until examination is complete and a Federal repository is developed.

The Reactor Disassembly Program already has achieved several major milestones: removal of the head in July 1984, removal of the plenum in May 1985, and initiation of defueling in October 1985. Future milestones include initiating core transport and bulk defueling in early 1986, completing reactor vessel defueling in early 1987, and completing core transport in early 1988. These milestones will constitute major DOE program activities and, upon completion, will demonstrate that recovery of a severely damaged reactor can occur safely, with only slight extensions of existing technology.

Recovery of TMI-2 is providing valuable information to the nuclear industry for future decontamination/decommissioning and fuel transportation activities. It also is providing essential information to the Accident Evaluation Program, as described in the papers in these Proceedings of the First International Information Meeting on the TMI-2 Accident.

CORE CONDITION AND ACCIDENT SCENARIO

James M. Broughton
Idaho National Engineering Laboratory
EG&G Idaho, Inc.
P.O. Box 1625, Idaho Falls, ID 83415

INTRODUCTION

The TMI-2 accident has had a profound impact on the nuclear industry, in spite of the fact that adverse public health effects were insignificant. Understanding the progression of this severe core damage accident and its relationship to the very small releases of radioactivity to the environment can have significant impact on the nuclear power industry. The TMI-2 accident is the only source of full-scale, severe-accident data for addressing the outstanding technical issues. An overview of the current understanding of the accident is presented in this paper. The damage state of the reactor, an accident scenario, temperature estimates in both the core debris and structural material in the upper plenum, and an accounting of fission-product inventory in the plant are presented.

An understanding of the accident is being sought by a combination of methods, including:

- Interpretation of the response of online instruments during the accident
- Visual and ultrasonic examination of the reactor vessel interior
- Physical and chemical examination of materials removed from the reactor vessel
- Examination of materials transported to RCS and containment system components
- Calculations of accident damage and fission-product behavior by severe-accident analysis codes
- First-principles engineering calculations of specific phenomena.

DAMAGE STATE WITHIN THE REACTOR VESSEL

The currently known damage state of the reactor core and the reactor vessel internal structures, as determined by various examinations and measurements, is shown in Figure 1. A void now exists in the upper region of the original core, encompassing approximately one-third of the total core volume and extending to the outermost, partially damaged fuel assemblies. A debris bed about 1 m deep lies at the bottom of the core cavity. Efforts to probe down through the debris indicate that a layer of hard, impenetrable material exists underneath the debris bed at about the mid-core elevation. Video scans of the lower regions of the reactor vessel

indicate that 10 to 20% of the core material now rests on the reactor vessel lower head, about 2 m below the bottom of the original core. A photograph of the debris in the lower plenum is shown in Figure 2. Gamma measurements¹ through an instrument tube suggest that the material at the very bottom of the lower plenum may be non-fuel material (perhaps silver from melted control rods and steel from melted structural components). The particle size and texture of the material in the lower plenum varies, ranging from uniform pea-like gravel a few millimeters in diameter to larger pieces of lava-like material at least 20 cm dia. The extent of damage to the lower core-support assembly is not known, since the video scans were unable to view the central regions of the lower plenum. The peripheral regions of both the lower core-support structures and the reactor head do not appear to be damaged.

Particles retrieved from the core debris bed have been examined^{2,3} to determine the physical, chemical, and radioisotopic characteristics of the debris. Particles greater than 1 mm dominate the size distribution in the debris, and there is a trend toward smaller particles lower in the bed. A significant depletion (up to 50%) of the zirconium content has occurred and less than 10% of the silver from the control rods is accounted for in the debris bed. Ceramographic examination showed extensive oxidation of fuel and cladding, molten oxygen-saturated alpha-phase zircaloy ($T > 2250$ K), molten UO_2 - ZrO_2 ceramic ($T > 2800$ K), molten UO_2 ($T > 3100$ K), and relatively unaffected fuel ($T < 1900$ K). An average temperature of 2200 K has been roughly estimated for a debris-bed sample weighing about 1 kg. Additional and larger samples of the debris bed will be taken, permitting the determination of more accurate bulk characteristics of the debris bed. The samples taken from various places in the debris bed are quite heterogeneous on a microscale (from particle to particle and even within individual particles), but are fairly uniform from sample to sample in terms of fuel structure, elemental composition, and uranium enrichment.

The damage to the underside of the core upper-grid structure exhibited strong local variations, as shown in Figure 3. Areas of foamed stainless steel components, caused by rapid oxidation near the melting point of steel (1720 K), were adjacent to intact stainless steel components and also melted stainless steel exhibiting no evidence of foaming. These observations suggest local variations in the composition of the gas exiting the core during the high-temperature phase of the accident. Some gas streams were strongly oxidizing, others were largely absent of steam (probably containing mostly hydrogen), and some were much hotter than others. Such evidence of inhomogeneity in composition and temperature of the gaseous effluent from the core suggests that there were damaged regions in the core that blocked gas flow and diverted it into channels (perhaps circuitous) through the core with different degrees of oxygen uptake from steam by zircaloy.

A significant axial temperature gradient existed in the upper plenum⁴ during the high-temperature phase of the accident, according to analyses of microstructure and microhardness of two control rod drive leadscrews removed from the reactor. Maximum temperatures of 1255 K near the bottom of the plenum assembly and 700 K near the top were estimated, based

on analysis of the steel samples from a leadscrew in a central position. Analysis of a sample from a leadscrew near the periphery showed a maximum temperature of 1033 K near the bottom of the upper plenum. Fission-product and aerosol deposition can be expected on steel surfaces at temperatures in the range 700 to 1255 K. The plenum surfaces had been submerged in reactor coolant for about 4 y before the leadscrews were removed for examination. As a result, only insoluble fission-product deposition remains on the leadscrew surfaces.

FISSION-PRODUCT DISTRIBUTION

Only about 1% of the noble gases and $3 \times 10^{-5}\%$ of the iodine escaped to the environment during the accident. To date, measurements of fission products have been made in the core debris, reactor coolant, Reactor and Auxiliary Building sumps and tanks, and on surfaces in the reactor vessel, RCS, and Reactor and Auxiliary Buildings. The estimated radioisotope accounting based on these measurements is summarized in Table 1 (Reference 5). The fission products are primarily in the core debris or in sumps and tanks in the Reactor and Auxiliary Buildings. About 10% of iodine and cesium was found in the reactor coolant immediately following the accident. No more than 1% of any other fission product was measured in the coolant. The retention of fission products on surfaces, including the upper plenum, is generally less than 1% of the core inventory.

About 20% of the iodine and cesium remain in the core debris, and about 40% is in the sumps and tanks of the Reactor and Auxiliary Buildings. About 4% of the core inventory of tellurium was found in sumps and tanks. At this time, data on tellurium in the debris bed are too few to estimate retention in core debris; although, tellurium⁶ has been found on leadscrew surfaces in amounts corresponding to about 2% of its core inventory, based on extrapolating results from the two leadscrews examined to the entire upper plenum surface area. This is the largest measured deposition in the RCS for any of the fission products.⁷ The remaining depositions are less than 1% of core inventory. It is of interest to fission-product chemistry to note that cesium was found primarily to be bound to an oxide layer on the leadscrew surfaces. Silver was found to be deposited on the leadscrews in amounts corresponding to about 1% of its inventory in Ag-In-Cd control rods, if extrapolated to the entire upper plenum surface area. Most of the fission-product deposition was found near the top of the plenum assembly where the temperature was lower during the accident. The debris retained approximately 94% of its strontium and practically all of its cerium. One percent of the core inventory of strontium has been found in the reactor coolant water and about 2% in sumps and tanks. Approximately 53% of the antimony and 61% of the ruthenium inventories were retained in the core debris, and less than 1% of the core inventory of these materials has been found elsewhere. There is evidence⁸ that molten stainless steel tends to concentrate available ruthenium into a separate metal phase. Measurements have not been performed yet on the fission-product content of the core below the debris bed nor in the material located in the lower plenum.

ACCIDENT SCENARIO

The accident scenario developed here for the the initial 4 h of the accident is based on:

- The known end-state conditions of the core and reactor vessel
- Data from plant instrumentation recorded during the accident
- The results from best-estimate analyses of the accident employing the SCDAP code⁹
- Damage mechanisms deduced from severe fuel damage experiments.¹⁰

The important features of the accident scenario are discussed here to identify the primary mechanisms controlling core-damage progression and the primary questions remaining to be resolved.

Core uncover started between 100 and 120 min after turbine trip, which is considered the beginning of the accident. This is substantiated by the measurement of superheated steam detected in the hot legs at 113 min. Best-estimate predictions indicate that core temperatures were high enough to balloon and rupture the fuel rod cladding at about 140 min, releasing the noble gases and other more volatile fission products such as iodine and cesium into the gap between the fuel pellets and the cladding. Fission products were detected in the containment at about 143 min. These predictions also indicate that cladding temperatures rapidly increased at about 150 min, due to cladding oxidation, and quickly exceeded the cladding melting temperature. The molten zircaloy dissolved some fuel; the liquefied fuel flowed down and solidified in lower, cooler regions of the core. The lowest level where the molten material flowed to was probably coincident with the coolant liquid level, which is estimated to have been into the lower one-third of the core.

By 174 min (just prior to the primary pump transient, as discussed later), core temperatures had probably reached fuel melting in the central, highest-temperature regions of the core; and between one-quarter and one-half of the core probably attained cladding melting temperatures with subsequent fuel dissolution and relocation. During the time period between 150 and 174 min, a relatively solid region of core materials composed of previously molten and intact fuel rods formed, as illustrated in Figure 3a. The top of the core probably consisted of highly oxidized and embrittled fuel rod remnants. High-temperature molten material had not yet penetrated below about 0.75 m above the bottom of the core, otherwise the SPNDs at Level 1 and about half of those at Level 2 (0.25 and 0.75 m above the core bottom, respectively) would have indicated anomalous behavior upon contact with the hot material as determined by later tests.¹¹

The primary system pump transient at 174 min injected some coolant into the core. However, the extent of core cooling is not known because of the unknown flow blockage resulting from the relocated material in the lower regions of the core. Thermal and mechanical shock resulting from the injected coolant would result in fragmentation of the embrittled fuel rod remnants in the upper regions of the core. These fuel rod fragments could have collapsed onto the solidified surface of previously molten material, forming the debris bed shown in Figure 3b. Thermal calculations indicate that the zone of the relocated core materials continued to heat up even

after injection of coolant into the core.¹² These calculations are consistent with recent analysis of the in-core thermocouple alarms. The peripheral thermocouples responded to coolant injection into the core by coming back from a high-temperature alarm state. The central thermocouples remained in their high-temperature alarm state even after the core was flooded with coolant, indicating a non-coolable geometry in the central part of the core before the pump transient.

Most, if not all, of the molten core materials found in the lower plenum probably relocated at approximately 227 min in a molten form. This relocation was indicated by anomalous output from the Levels 1 and 2 SPNDs and by a very rapid increase in the primary system pressure of approximately 2 MPa. The increased system pressure apparently was caused by the generation of substantial quantities of steam as the hot core material flowed into water in the lower plenum. The steam and water probably fragmented the molten material as it relocated into the lower plenum. This fragmentation may have resulted in formation of a coolable configuration in the lower plenum. The progression of core-configuration change was essentially halted at this time by the presence of water in the lower plenum and the continued injection of water into the RCS by the HPIS. The postulated end-state and configuration of the reactor core and its support structures is illustrated in Figure 3c.

INSIGHTS FROM TMI-2

Our current understanding of the TMI-2 accident has provided significant insights into severe accident phenomenology:

- The TMI-2 damage state is basically consistent with the calculations of core-damage progression (such as fuel liquefaction, relocation and solidification, and fragmentation of embrittled rods) by detailed severe core damage codes such as SCDAP.
- Results of laboratory severe fuel damage experiments can be used to describe the principal severe core damage phenomena.
- The accident demonstrates that damage to the upper plenum and reactor vessel itself can be minimal in spite of very severe core damage. This implies that hot gas flow and heat transfer from the core to the upper plenum can be quite limited due to core flow blockage.
- Large, but very localized, variations in damage to the core upper-grid structure suggest core damage and the coolant conditions within the core were highly nonuniform during the period when high-temperature gas flowed to the upper plenum.
- Little irreversible fission-product deposition in the upper plenum (generally <1% of core inventory) occurred, which is consistent with recent in-pile test results in PBF at the INEL. At the temperature range experienced by the upper plenum during the accident, deposition that was later removed by reactor coolant could have been quite large.

- The TMI-2 damage state and postulated accident scenario suggest that the initial melt relocation within the core by localized candling of liquefied core materials can form a non-coolable geometry, ending with remelt and relocation to the lower plenum. If water is present in the lower plenum, core-melt progression can be terminated with a coolable geometry in the lower plenum.
- The present estimated releases of noble gases, iodine, and cesium from the core are consistent with our current understanding. The strong retention of strontium and cerium in the core debris is not unexpected, based on NUREG-0772 release rates, nor is the significant release of antimony. The significant depletion of ruthenium measured in the core debris is unexpected, based on its NUREG-0772 release rate.
- Current evidence suggests that much of the silver inventory in control rods has disappeared from the upper core debris and may have relocated into the lower plenum.

REFERENCES

1. General Public Utilities, Nuclear Division, Unpublished Data, June 1985.
2. D. W. Akers et al., TMI-2 Core Debris Grab Samples--Examination and Analysis, EGG-TMI-6853, July 1985.
3. B. A. Cook and E. R. Carlson, "TMI-2 Core Debris Analysis", Proceedings of the First International Information Meeting on the TMI-2 Accident, Germantown, MD, October 21, 1985.
4. K. Vinjamuri et al., Preliminary Report: Examination of H8 and B8 Leadscrews from Three Mile Island Unit 2 (TMI-2), EGG-TMI-6685, April 1985.
5. D. E. Owen, T. E. Cox, J. M. Broughton, "Fission Product Transport at Three Mile Island", Proceedings of the First International Information Meeting on the TMI-2 Accident, Germantown, MD, October 21, 1985. (In Press).
6. K. Vinjamuri et al., Tellurium Chemistry, Tellurium Release and Deposition During the TMI-2 Accident, EGG-TMI-6894, August 1985.
7. R. Davis et al., Radionuclide Mass Balances for the TMI-2 Accident: Data Through 1979 and Preliminary Assessments of Uncertainties, GEND-INF-047, November 1984.
8. G. W. Parker et al., "Source Term Evaluation from Recent Core-Melt Experiments", International Symposium on Source Term Evaluations for Accident Conditions, Columbus, Ohio, October 28 to November 1, 1985, IAEA-SM-281 (1986).

9. C. Allison et al., SCDAP/MOD1 Analysis of the Progression of Core Damage During the TMI-2 Accident, SE-CMD-84, 009, EG&G Idaho, Inc.
10. R. K. McCardell et al., Severe Fuel Damage Test 1-1--Quick Look Report, 1983.
11. D. J. N. Taylor, "TMI SPND Interpretation", Proceedings of the First International Information Meeting on the TMI-2 Accident, Germantown, MD, October 21, 1985.
12. A. W. Cronenberg et al., "Debris Thermal Interaction with Lower Plenum Structures", Proceedings of the First International Information Meeting on the TMI-2 Accident, Germantown, MD, October 21, 1985.

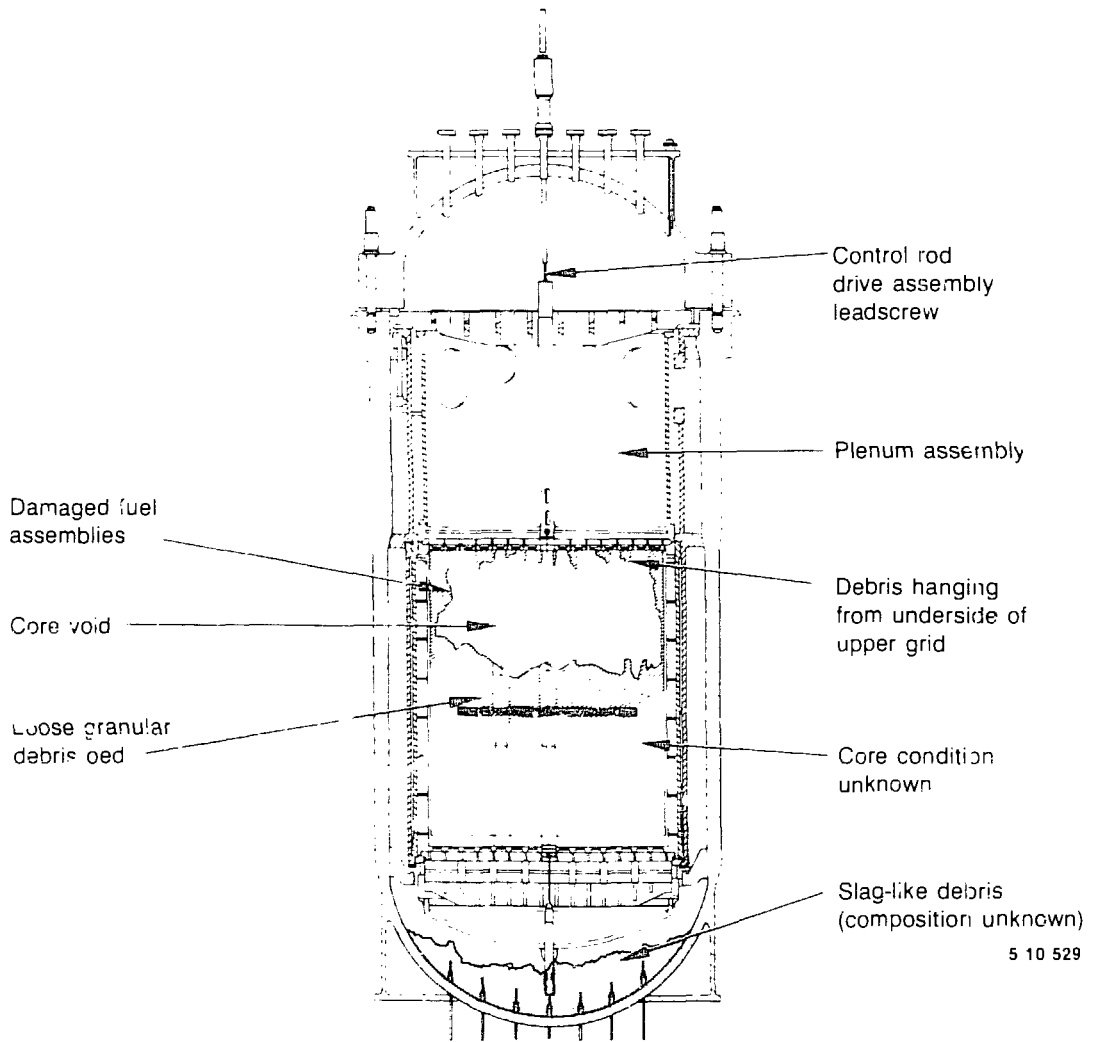


Figure 1. Known core and reactor vessel conditions.

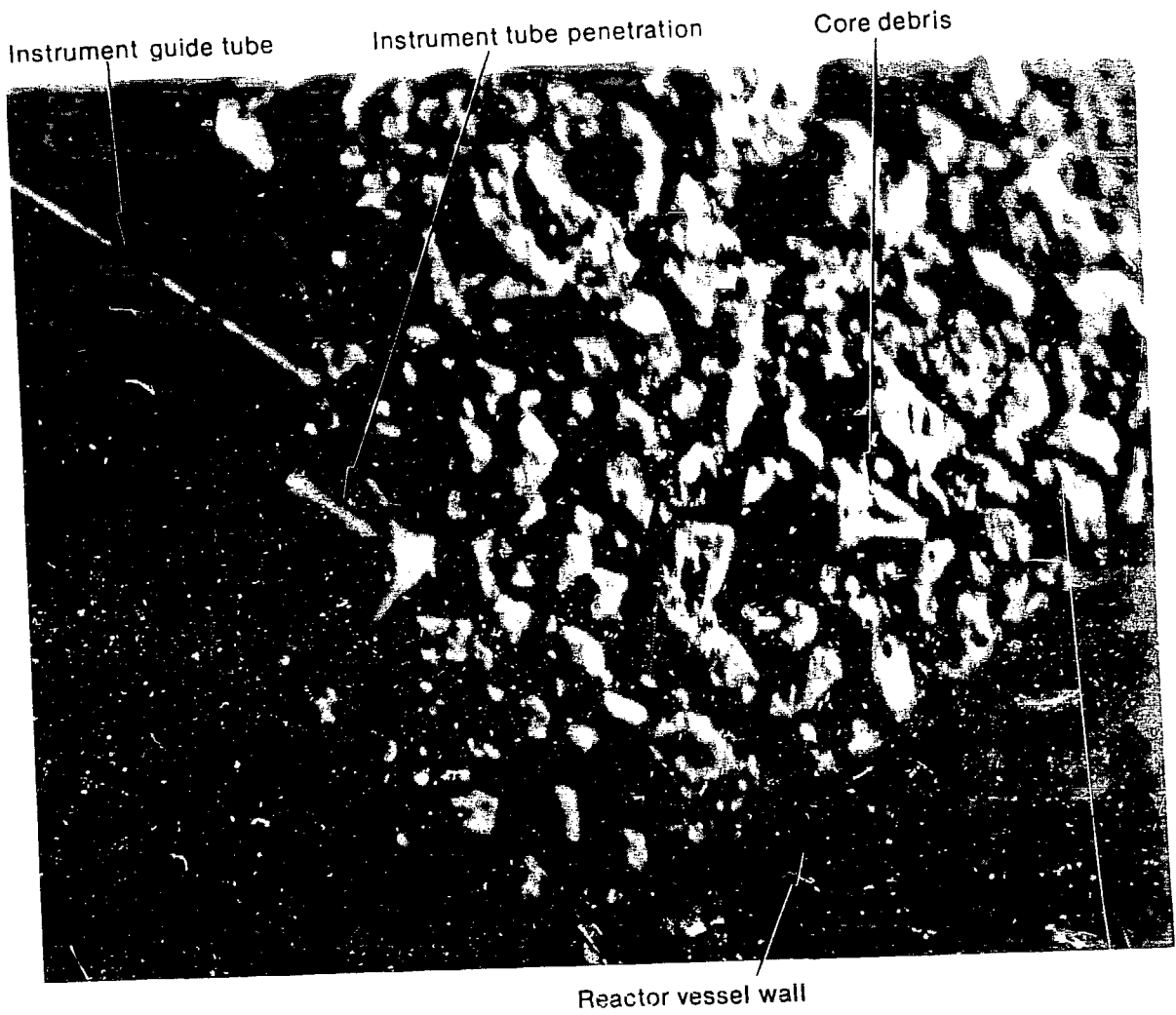
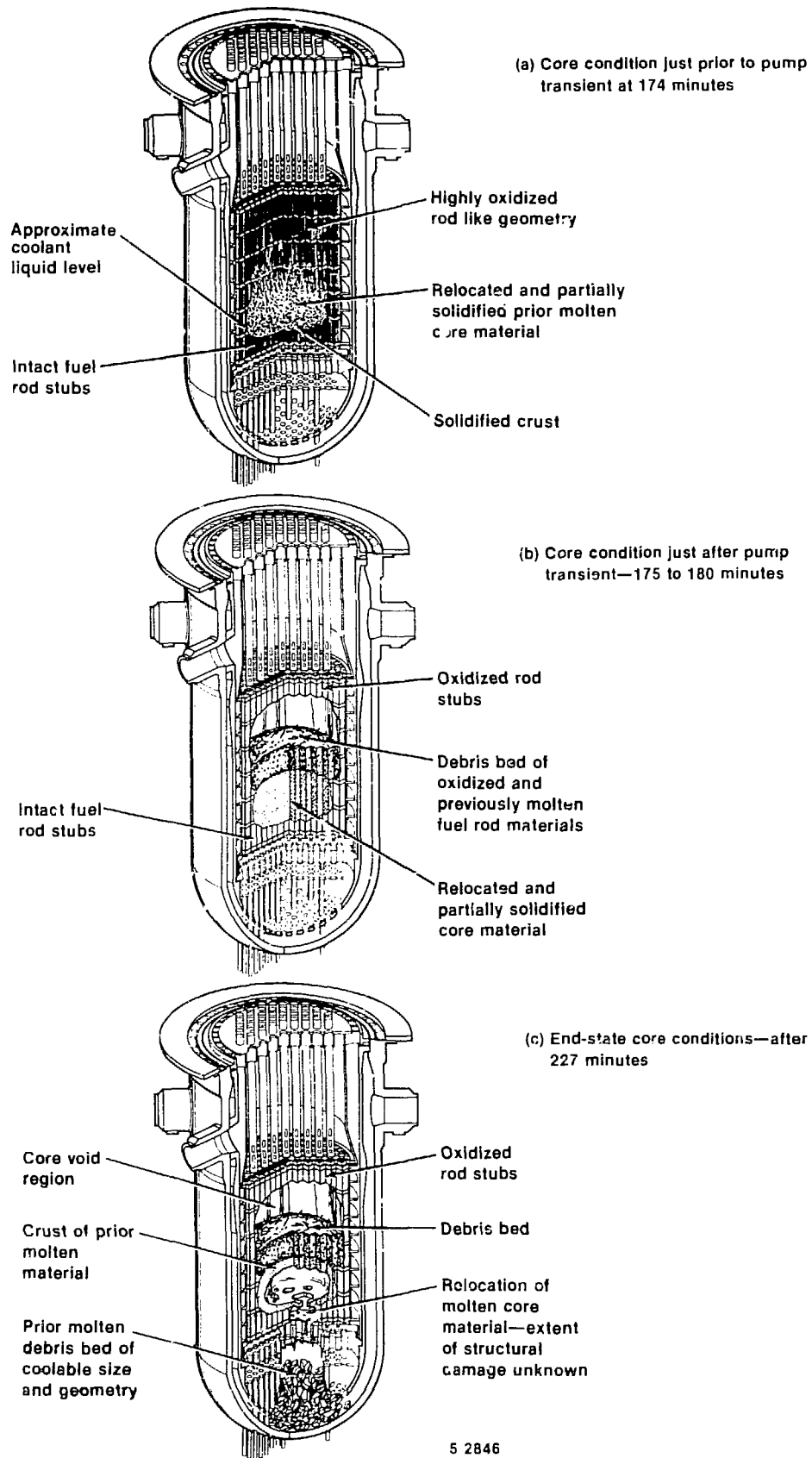


Figure 2. Lower plenum debris (from video data).



5 2846

Figure 3. Hypothesized stages of the TMI-2 accident progression.

TMI-2 ACCIDENT EVALUATION PROGRAM OVERVIEW

E. L. (Bert) Tolman
Idaho National Engineering Laboratory
EG&G Idaho, Inc.
P.O. Box 1625, Idaho Falls, ID 83415

The DOE-supported TMI-2 recovery program consists of two major efforts:

- o Provide support in defueling the TMI-2 reactor vessel and final disposition of the core material
- o Perform accident evaluation work to complete our understanding of the accident progression.

An overview of the defueling support work is discussed in another paper in these Proceedings of The First International Information Meeting on the TMI-2 Accident. This paper presents an overview of the work necessary to complete our understanding of the TMI-2 accident, and utilize this understanding to address technical issues related to severe accidents

Our current understanding of the TMI-2 core damage progression is discussed in Reference 2. An increased understanding of the core-damage progression prior to the pump transient is emerging based on the observed end-state core conditions, supporting engineering analysis to interpret the TMI data, and independent severe accident research work. However, the core degradation after the pump transient is not understood satisfactorily, particularly the evidence that indicates: (a) formation of large non-coolable regions of molten core materials, (b) failure mechanisms of the core-support structures, and (c) interaction of the molten fuel with the coolant in the reactor vessel and with the vessel itself. It is hoped that the TMI Accident Evaluation Program will complete our understanding of these aspects of the TMI-2 accident. Specific program objectives include:

- o Establishing an understanding of the coupled reactor system thermal hydraulics that controlled the core-damage progression and fission-product release and transport during the accident
- o Developing a TMI Standard Problem for assessing the TMI data and evaluating the capabilities of the severe accident computer models
- o Relating the major TMI research findings to other severe accident research for addressing unresolved severe accident technical issues.

A discussion of the work necessary to achieve each of these objectives is presented below, followed by a brief description of the program structure and a tentative schedule for completing the work.

TMI-2 ACCIDENT EVALUATION PROGRAM OVERVIEW

E. L. (Bert) Tolman
Idaho National Engineering Laboratory
EG&G Idaho, Inc.
P.O. Box 1625, Idaho Falls, ID 83415

The DOE-supported TMI-2 recovery program consists of two major efforts:

- Provide support in defueling the TMI-2 reactor vessel and final disposition of the core material
- Perform accident evaluation work to complete our understanding of the accident progression.

An overview of the defueling support work is discussed in another paper in these Proceedings of The First International Information Meeting on the TMI-2 Accident. This paper presents an overview of the work necessary to complete our understanding of the TMI-2 accident, and utilize this understanding to address technical issues related to severe accidents.

Our current understanding of the TMI-2 core damage progression is discussed in Reference 2. An increased understanding of the core-damage progression prior to the pump transient is emerging based on the observed end-state core conditions, supporting engineering analysis to interpret the TMI data, and independent severe accident research work. However, the core degradation after the pump transient is not understood satisfactorily, particularly the evidence that indicates: (a) formation of large non-coolable regions of molten core materials, (b) failure mechanisms of the core-support structures, and (c) interaction of the molten fuel with the coolant in the reactor vessel and with the vessel itself. It is hoped that the TMI Accident Evaluation Program will complete our understanding of these aspects of the TMI-2 accident. Specific program objectives include:

- Establishing an understanding of the coupled reactor system thermal hydraulics that controlled the core-damage progression and fission-product release and transport during the accident
- Developing a TMI Standard Problem for assessing the TMI data and evaluating the capabilities of the severe accident computer models
- Relating the major TMI research findings to other severe accident research for addressing unresolved severe accident technical issues.

A discussion of the work necessary to achieve each of these objectives is presented below, followed by a brief description of the program structure and a tentative schedule for completing the work.

Currently, it is anticipated that the TMI Standard Problem will be conducted in two phases. The first phase will be limited to the accident progression out to 174 min (initiation of the pump transient). The data necessary to understand this phase of the of the accident is, for the most part, available. The second phase will include the accident progression after 174 min and will emphasize core-failure mechanisms, fuel-coolant and fuel-vessel interactions, final core coolability, and fission-product behavior during the latter stages of the accident. The second phase of the Standard Problem must wait for results from sample acquisition, video data from the lower core and plenum regions, and the examination results of the lower core and plenum samples.

WORK NECESSARY TO RELATE TMI FINDINGS TO UNRESOLVED TECHNICAL ISSUES

The TMI-2 accident is unique in three important aspects:

- o The accident occurred in a large reactor system
- o The prototypicality of the reactor system thermal-hydraulic conditions that resulted in severe damage to the core
- o In general, core damage is much more extensive than predicted from most previous analyses.

Because of the extensive damage to the reactor core and the large-scale prototypicality of TMI, the accident provides the only current possibility to obtain data to confirm our understanding of:

- o In-reactor core-damage progression, including reactor vessel challenge from molten core materials
- o The mechanisms controlling in-reactor fission-product behavior
- o The in-reactor coupling between reactor system thermal hydraulics and core degradation.

Important technical questions that can be assessed from the TMI data were identified in a two-step process. The first step was to identify all technical questions requiring additional research to resolve. These issues were compiled from the major source term reviews recently completed (References 7-10) and recommendations from the industry-sponsored IDCOR program (Reference 11). The second step was to evaluate each issue against our current understanding of the TMI-2 accident progression to evaluate if (a) data could be obtained from the accident to directly impact our understanding of the issue, and (b) the data would also provide additional information to increase our understanding of the accident progression. If TMI data could be obtained to meet these two objectives, the issue was categorized as high priority. This process was carried out by EG&G Idaho researchers based on NRC research information and independently by industry researchers based on the results of the IDCOR program (Reference 12.). From these two efforts, those technical issues summarized in Appendix A were identified for which TMI data will have a high impact in resolving.

The TMI research findings will not only increase our understanding of important technical questions regarding core degradation and fission-product behavior, but will also allow assessment of scaling questions associated with reactor system size and the typicality of boundary conditions utilized for the small scale, separate effects experiments.

PROGRAM ORGANIZATION AND TENTATIVE SCHEDULE

The structure of the TMI Accident Evaluation Program is shown in Figure 1 and consists of four major elements: (a) Examination Requirements and System Evaluation, (b) Sample Acquisition and Examination, (c) Analytical Support, and (d) Information and Industry Coordination.

The Examination Requirements and System Evaluation program element will define the overall program requirements, the Standard Problem requirements, and conduct engineering analysis to improve our understanding of the core-degradation processes, particularly those mechanisms that would result in relocation of the molten core into the lower plenum regions. Analytical work is currently being conducted by both government and industry researchers and will provide the bases for specifying sample acquisition requirements and interpreting the end-state core conditions. In addition, a TMI Accident Evaluation Program Document is being drafted to summarize our current understanding of the accident progression and the data and analysis requirements necessary to complete our understanding of the accident. Near-term milestones (to be completed in FY-86) for this program element include (a) final documentation of the TMI Accident Evaluation Program Document, (b) definition of the TMI Standard Problem (174 min), and (c) documentation of initial analysis results to study the core-melt progression and reactor-system response during the latter stages of the accident.

The Sample Acquisition and Examination program element will obtain and analyze the necessary physical samples from the reactor system to complete our understanding of the end-state core condition. Near-term milestones include (a) complete the TMI Sample Acquisition and Examination Plan, (b) complete the core sample acquisition tasks, and (c) prepare the core samples for hot cell examination and complete the examination results from the lower plenum debris samples recently received.

The Analytical Support program element will catalog and qualify the TMI data for use in the TMI Standard Problem and/or in model development and assessment. Near-term milestones include (a) complete the data base configuration, and (b) qualify the reactimeter data (power range detector data), and the in-core instrumentation data.

The Information and Industry Coordination program element will coordinate input from various organizations to the TMI Accident Evaluation Program Plan and disseminate results from the analytical studies and examination work. Near-term milestones include (a) initial coordination for the TMI Standard Problem work, (b) distribution of major findings related to the core removal and sample acquisition activities, (c) complete digitization, (d) qualify data, (e) prepare inputs for personal computers, (f) archive original data, and (g) select and add to the NRC file.

A tentative schedule for completing the TMI evaluation work is shown in Figure 2. The Sample Acquisition and Examination Tasks control the program schedule since these tasks are dependent on the defueling schedule, which estimates core removal will be completed by mid-FY-87. Sample acquisition of the core-former walls, core-support structures, and vessel head may be examined after core removal when funds are available. Although the sample examination activities will not be completed before mid-FY-88, preliminary findings showing the damage extent to the lower core and plenum regions will be available in mid-FY-86. The reactor system data consolidation and qualification will be completed by the end of FY-87. Final integration of the sample examination results and the supporting engineering analysis work to identify a consistent accident scenario will be completed by FY-88. Extensive engineering analysis work will be required during FY-86 to evaluate the initial core-defueling data as it becomes available and to guide the sample acquisition and examination work. Final application of the TMI findings to severe accident issues will be completed in FY-89. As noted earlier, the Standard Problem will be conducted in two phases. The first phase, out to the pump transient at 174 min, will be defined during FY-86. The second phase, which will extend the analysis to core failure, melt progression into the lower plenum regions and final core coolability, will be defined by mid-FY-88.

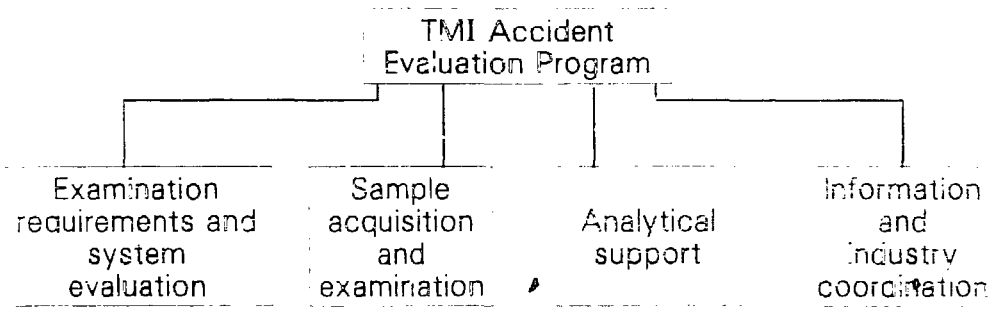
CONCLUSIONS

The TMI-2 accident resulted in extensive core damage and fuel relocation. The large scale uniqueness of TMI offers the opportunity to confirm our understanding of both the integral reactor system response during a severe accident, and to increase our understanding of the mechanisms controlling core degradation and fission-product behavior. The work outlined in this paper will complete our understanding of the end-state core damage extent and provide the necessary resources for interpreting the TMI data and establishing a consistent understanding of the core-damage progression and resulting fission-product behavior. Completing our understanding of the TMI accident will provide the necessary information to evaluate the implications of the accident against our current perspective of reactor safety, particularly the ability of reactor systems to withstand severe core damage.

REFERENCES

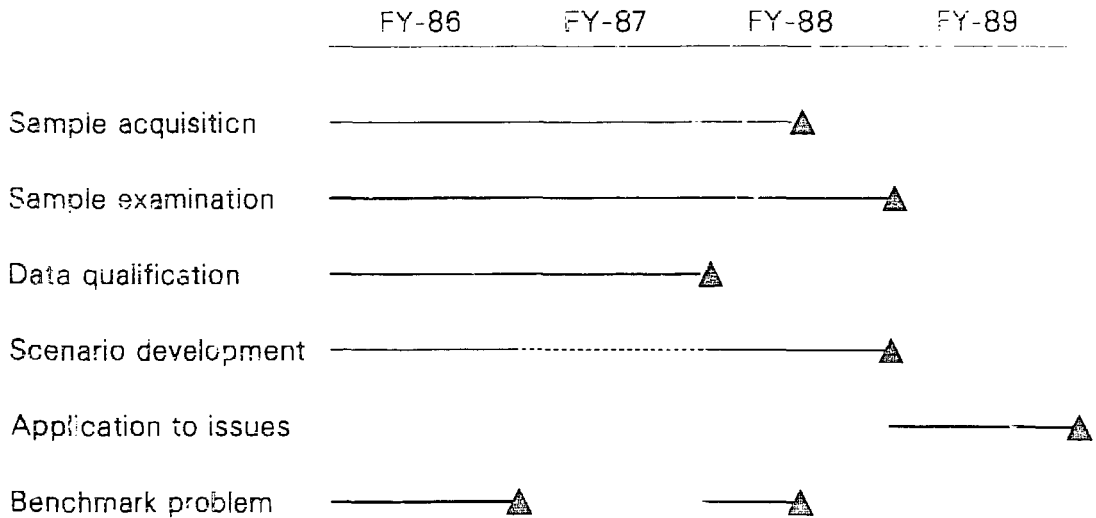
1. H. Burton, "TMI-2 Programs Overview", Proceedings of the First International Information Meeting on the TMI-2 Accident, Germantown, MD, October 21, 1985.
2. J. Broughton, "Core Condition and Accident Scenario", Proceedings of the First International Information Meeting on the TMI-2 Accident, Germantown, MD, October 21, 1985.
3. R. McCardell et al., "TMI-2 Sample Acquisition and Examination Plan", Proceedings of the First International Information Meeting on the TMI-2 Accident, Germantown, MD, October 21, 1985.

4. R. Henry et al., "Core Relocation Phenomenology", Proceedings of the First International Information Meeting on the TMI-2 Accident, Germantown, MD, October 21, 1985.
5. A. Cronenberg et al., "Debris Thermal Interaction With Lower Plenum Structures", Proceedings of the First International Information Meeting on the TMI-2 Accident, Germantown, MD, October 21, 1985.
6. B. Cook, "Chemical Interaction Between Core and Structural Materials", Proceedings of the First International Information Meeting on TMI-2 Accident, Germantown, MD, October 21, 1985.
7. Report of the Special Committee on Source Terms, American Nuclear Society, September 1984.
8. Radionuclide Release from Severe Accident at Nuclear Power Plants, American Physical Society, February 1985.
9. Assessment of Radionuclide Source Term Research, DOE/ID-10126, March 1985.
10. Reassessment of the Technical Bases for Estimating Source Terms, NUREG-0956, June 1985.
11. A. Buhl et al., "IDCOR--The Severe Accident Issues, Individual Plan Examinations, and Source Term Reductions", Paper presented at the Atomic Industrial Forum Conference on New Directives in Licensing, Dallas, Texas, May 1985.
12. M. Fontana et al., Needs for Results of TMI Data Acquisition and Analysis Program, ENERGEX Associates, Inc., Report prepared for EG&G, Idaho Inc., June 1985.



P230 ST-0158-01

Figure 1. TMI Accident Evaluation Program Structure.



P230 ST-0158-02

Figure 2. Tentative TMI Accident Evaluation Program Schedule.

APPENDIX A

SEVERE ACCIDENT TECHNICAL ISSUES TO BE ADDRESSED VIA THE TMI ACCIDENT EVALUATION PROGRAM

Reactor System Thermal Hydraulics

1. Reactor system natural convection
2. Coupling between core degradation, reactor vessel thermal hydraulics, and fission-product behavior
3. Confirmatory data for integrated reactor systems computer codes.

Core-Damage Progression and RPV Failure

1. Damage progression in core
2. Core slump and collapse
3. Reactor vessel failure modes
4. Release of control rod materials
5. Hydrogen generation after core disruption
6. Core-concrete interaction
7. Aerosol-generation mechanisms
8. Containment failure by in-vessel steam explosions
9. Confirmatory data for integrated reactor systems computer codes.

Fission-Product Release and Transport

1. Release of low volatility fission products during fuel degradation
2. Chemical reactions affecting fission-product transport
3. Tellurium behavior
4. Fission-product and aerosol deposition in the reactor cooling system
5. Deposition model for fission products in containment
6. In-containment volatilization of iodine
7. Revaporization of fission products in the upper plenum
8. Confirmatory data for integrated reactor systems computer codes.

TMI-2 ACCIDENT EVALUATION PROGRAM SAMPLE ACQUISITION AND EXAMINATION PLAN

Richard K. McCardell, Malcolm L. Russell, Michael D. Peters
Idaho National Engineering Laboratory
EG&G Idaho, Inc.
P.O. Box 1625, Idaho Falls, ID 83415

INTRODUCTION

The purpose of the Sample Acquisition and Examination (SA&E) Plan of the TMI-2 Accident Evaluation Program is to develop and implement a test and inspection plan that completes the characterization of the (a) TMI-2 equipment that may have been damaged during the accident, and (b) TMI-2 core fission-product inventory. The characterization program includes both sample acquisition/examination and in situ measurements. Fission-product characterization involves locating fission products, as well as determining their chemical form and material association.

The SA&E Plan is responsible for collecting samples from the TMI-2 plant, examining those samples (to provide data specified by the Examination Requirements and Systems Evaluation element), interpreting and reporting examination results, and coordinating examination activities at other laboratories. The SA&E Plan also provides engineering support for obtaining and transporting samples.

BACKGROUND AND HISTORY

The SA&E Plan has been in existence since the TMI-2 accident, evolving from the requirements set forth in the document entitled, TMI-2 Accident Evaluation Program.¹ The program description provides the guidelines for characterizing the postaccident core condition and fission-product inventory. Examination requirements documents written previously include the GEND Planning Report² and the TMI-2 Core Examination Plan.³ The current program description is an extension of the preceding examination requirements documents with appropriate additions and changes to account for our enhanced understanding of the TMI-2 accident and the resultant refinements in sample and examination requirements.

The already-completed portion of the SA&E Plan includes in situ measurements and sample acquisition/examinations involving private organizations and state and federal agencies. It has provided post-accident core and fission-product end-state data indicating the following:

- o Large regions of the core exceeded the melting temperature of the fuel rod cladding (~2200 K). Significant fuel liquefaction by molten zircaloy and some fuel melting occurred with temperatures up to at least 3100 K.
- o Core materials relocated into the lower plenum region of the reactor vessel from the core, leaving a void in the upper core region equivalent to approximately 26% of the original core volume. Between 10 and 20 metric tons of core and structural

materials now reside in the space between the lower head of the reactor vessel and the elliptical flow distributor.

- Fission-product retention in the core materials is significant. The retention of fission products outside the core was primarily in RCS water, water in the basement of the Reactor Building, and in basement sediment.

Significant consequences resulted from these findings. They are:

- Increased technical interest in the TMI-2 accident, because it represents a full-scale SCD event and provides evidence of a large inconsistency in the understanding of offsite radiation release from the SCD event
- Reconsideration of plans and equipment for defueling the TMI-2 reactor
- Expansion of the TMI-2 accident examination plan to determine:
 - Consequences of high temperature interactions between core materials and reactor vessel lower plenum structural and pressure boundary components
 - Release from the fuel of the lower volatility fission products.

ASSUMPTIONS

Development of the SA&E Plan included consideration of the following assumptions:

- The total budget allowance, including prior years, is \$20.6M from DOE and \$600K from, and administered by, NRC.
- Sample retrieval and in situ measurements will be accomplished in conjunction with the TMI-2 recovery program of GPU Nuclear and with support from the TMI-2 Reactor Evaluation Program of DOE in developing special defueling tools and collecting defueling-related samples and in situ measurements.
- Prioritization of the Sample Acquisition and Examination tasks is summarized in Table 1. This prioritization is based on technical needs identified and discussed in Reference 1 and shown in Table 2.

These assumptions, along with the enhanced understanding we have of the TMI-2 accident, were considered in developing the examination plan described in the following section.

EXAMINATION PLAN

The technical background and purpose, previous accomplishments, sample examination plans, product lists and schedules, and resource allocation are

described in the SA&E Plan. The plan is divided into three categories as follows:

- Reactor vessel, which includes the reactor vessel, its internal structures, and the core
- RCS fission-product inventory, which includes the core materials and fission products now residing in the ex-vessel portion of the RCS, including the core flood tanks.
- Ex-RCS fission-product inventory, which includes the core materials and fission products now residing in areas, buildings, and equipment external to the RCS.

Table 3 is a summary of the in situ measurements and sample acquisitions and examinations that will satisfy the technical information needs identified Reference 1 and listed in Table 2. Table 3 includes prior-year sample acquisitions and examinations and in situ measurements for completeness. The Sample Acquisition and Examination Plan includes:

- Acquisition of all samples, distinct components, and in situ measurements listed in the Future Additional Samples column under Quantity.
- Sample examination and in situ measurement analysis of only those items listed in the Proposed Future Exams column. Only the high priority tasks can be accomplished within the allocated resources. Selection was made using the examination priority list shown in Table 1.

The proposed acquisition and examination plan for the core bore will provide as much flexibility as possible, since the core bores will be taken from the unexplored region below the core cavity. The purpose of this plan is to obtain as many core bore samples as possible, using the recommended locations and priorities shown on Figure 1. Each bore location will yield two or three samples (segments); one from the core region, and one or two from the region beneath the core, depending on whether or not the lower flow distributor is encountered. The 12 bore locations shown on Figure 1 will provide for radial and azimuthal variations in core damage; characterize the differences between control and burnable poison rod assemblies; and infer location, composition, and tensile properties of the core materials. This information will be derived from bore cutting tool data (cutting speed, tool location, cutter material, etc.) obtained during boring operations. Because of funding constraints, the examination plan includes only the segments (three from the core region, five from the region beneath the core) from the three (K9, F10, and N5) high priority locations shown on Figure 1. Medium priority or contingency location segments will be examined if the higher priority location segments cannot be acquired. Examination of these eight core bore samples will yield information on the quantity and physical and chemical state of the fused core materials located beneath the loose debris and in the lower plenum.

These examinations will also provide data on fission-product concentration and chemical form. However, with only three core locations being examined, only the axial and radial variation in these parameters will be determined. Measurement of azimuthal variation would require that more samples be examined.

Four fuel rod segments, two each from a part-length peripheral control rod assembly and a part-length peripheral burnable poison rod assembly will be examined. One fuel rod segment will be obtained from a location near a control rod position and another one from a location not near a control rod position. The control rod remnant also will be obtained. Examination of these three (two fuel rods, one control rod) rod segments will help determine the effect of control rod materials on the damage to adjacent fuel rods. The examination of two fuel rods and one burnable poison rod remnant will be structured in a similar manner. Fuel rod segments from a burnable poison rod and a control rod assembly in the lower core region will be obtained and examined also, if possible.

The large-debris sample from the debris bed below the upper cavity will help reduce the uncertainty in the retained fission products (especially tellurium) that was measured from the 11 grab samples already examined. Analysis of this large sample will also help determine the homogeneity of the upper debris bed and, therefore, the applicability of the data from the 11 small samples to the entire debris bed.

Eleven other small-debris samples have been obtained from the lower vessel debris bed. Examination of these samples will indicate the fission-product retention in a mixture of materials that probably contains more structural material than the upper core debris bed. A large sample of this lower vessel debris will also be obtained and examined to determine homogeneity. A large sample of loose debris will be obtained from the lower core-support-structure region also, if possible. The debris examination programs are intended to yield data on the prior peak temperature, materials interactions, and material composition and tensile properties.

In order to determine fission-product-chemical form and fission product and aerosol interaction with structural materials, samples will be obtained from both the RCS and the Ex-RCS fission-product transport pathways. Of high priority in the Ex-RCS are the sediment samples and concrete samples from the basement walls and floor of the Reactor Building. Samples of high priority in the RCS are adherent surface deposits on the B-loop RTD thermowell, the handhole cover liner on the A-loop steam generator, the manway cover backing plate on the B-loop steam generator, and the manway cover backing plate on the pressurizer. Sediment will be obtained for examination from the lower head of the steam generator, the top of the steam generator tube sheet, and the bottom of the pressurizer.

The SA&E Plan provides for the following:

- o Acquisition of the samples listed in Table 3 in the "Future Additional Samples" column. For FY-1986, this includes:

- As many core bores as possible from up to 12 locations during the 30 days scheduled for core boring, six approximately 6-in.-long fuel rod segments, control rod and burnable poison rod spiders, fuel assembly upper end fittings, fuel assembly upper sections, additional core material samples from the loose debris at the floor of the core cavity and the lower head region
- RCS adherent surface deposit samples from a RTD thermowell, a handhole cover liner from the steam generator, and manway cover backing plates from the pressurizer and steam generator
- RCS loose debris samples from the top of the steam generator tube sheets, the steam generator lower plenum, and the pressurizer lower head; and approximately 17 sediment samples from the reactor building basement floor.

Acquisition of the remaining samples is planned for FY-1987 and beyond.

- ① Examination of the samples listed in the "Proposed Future Exams" column of Table 3. For FY-1986, this includes:

- Initiating the examination of six core bore segments, four fuel rod segments, one control rod segment, one burnable poison rod segment
- Examining nine particles of the reactor vessel lower head debris
- Examining two "large" samples of core cavity floor loose debris
- Examining the B-loop hot leg RTD thermowell
- Examining approximately 12 Reactor Building basement sediment samples.

Initial examination of the remaining "Proposed" samples is planned for FY-1987 and FY-1988.

- ① The TMI-2 AEP will evaluate the availability of and pursue other resources to examine all the samples listed in the "Future Additional Samples" column of Table 3. Potential resources include the NRC, OECD/CSNI,^a and domestic fuel suppliers.

a. Organization for Economic Cooperation and Development, Committee on the Safety of Nuclear Installations.

SUMMARY

The TMI-2 Sample Acquisition and Examination Plan presents a challenging, high-technology program that addresses the severe core damage accident issues set forth in Reference 1. The issues addressed include reactor system thermal hydraulics, core damage and damage progression, reactor vessel failure, and fission-product release from the fuel and transport and retention within the RCS. The planned examinations include the following:

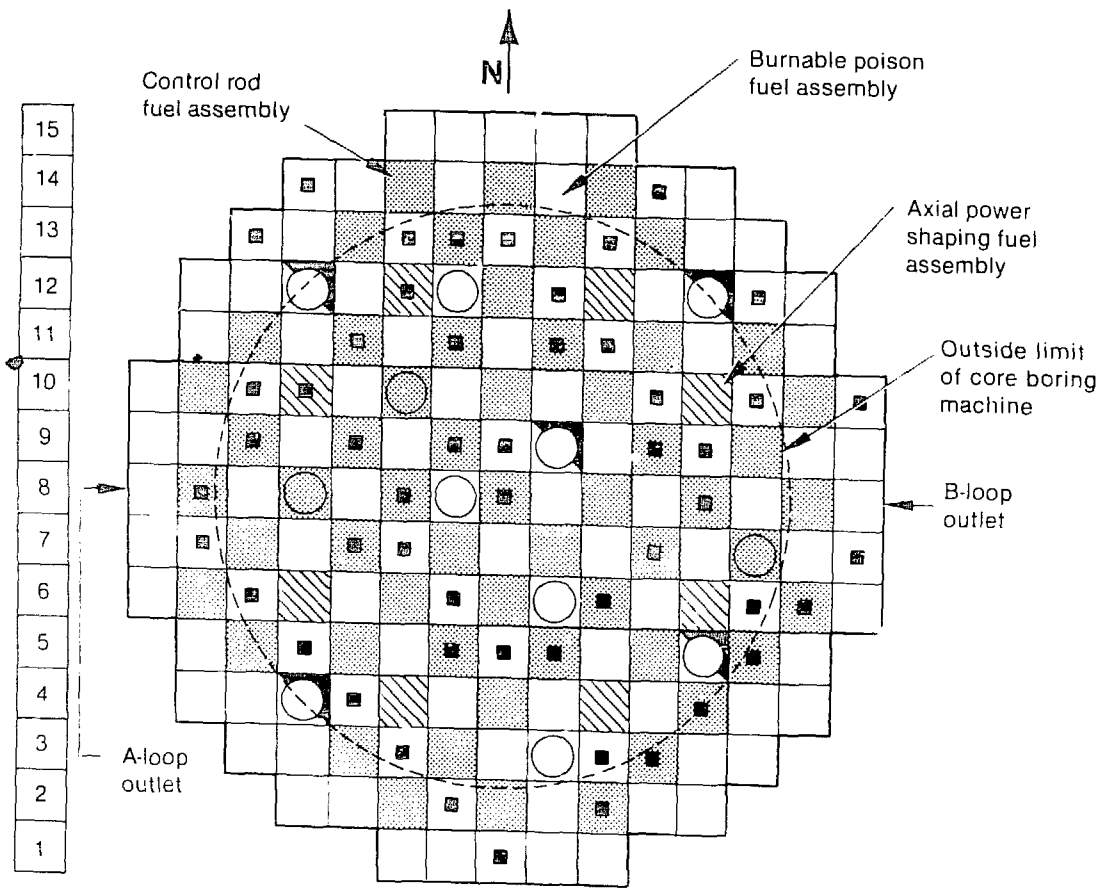
- o Physical samples from the upper plenum, RCS piping, and vessel internals to determine temperature distribution
- o Core debris grab samples from the core and lower plenum regions to characterize materials interactions and fission-product behavior
- o Fuel rod segments from the upper and lower portion of intact peripheral assemblies to provide estimates of temperature, fission-product retention, and the effects of control and poison rod materials on core damage
- o Core stratification samples for spatial determination of core damage, material interactions, and relocation of previously molten materials
- o Lower core support, core instrument support, and vessel lower head area structural component samples to help determine the extent of damage to core boundary material and reactor vessel walls
- o Ex-vessel and balance-of-plant samples to provide data on fission products, such as chemical form, material associations, and the extent of release from the reactor vessel and transport to the TMI-2 plant.

In addition, the Sample Acquisition and Examination Plan is designed to be:




- o Flexible to accommodate new findings, information, and knowledge that may become available from either this examination plan, the GPU Nuclear defueling program, or any SCD research program
- o Updated annually during the evolution of the TMI-2 Accident Evaluation Program
- o Conducted in accordance with DOE contractor business practices for effective accomplishment of government-funded projects.

REFERENCES

1. TMI-2 Accident Evaluation Program, EGG Draft Report, distributed September 24, 1985, under transmittal letter No. JMB-39-85.
2. GEND Planning Report, GEND-001, June 1980.
3. TMI-2 Core Examination Plan, Johan O. Carlson (ed.), EGG-TMI-6169, Rev. 1, July 1984.



A B C D E F G H K L M N O P R

-  Positions where Inspection holes line up
-  Recommended Core Bore Locations
-  Core Instrument String Locations

High Priority

K9
F10
N5

Medium Priority

K6
N12
D12
G8
D8

Contingency

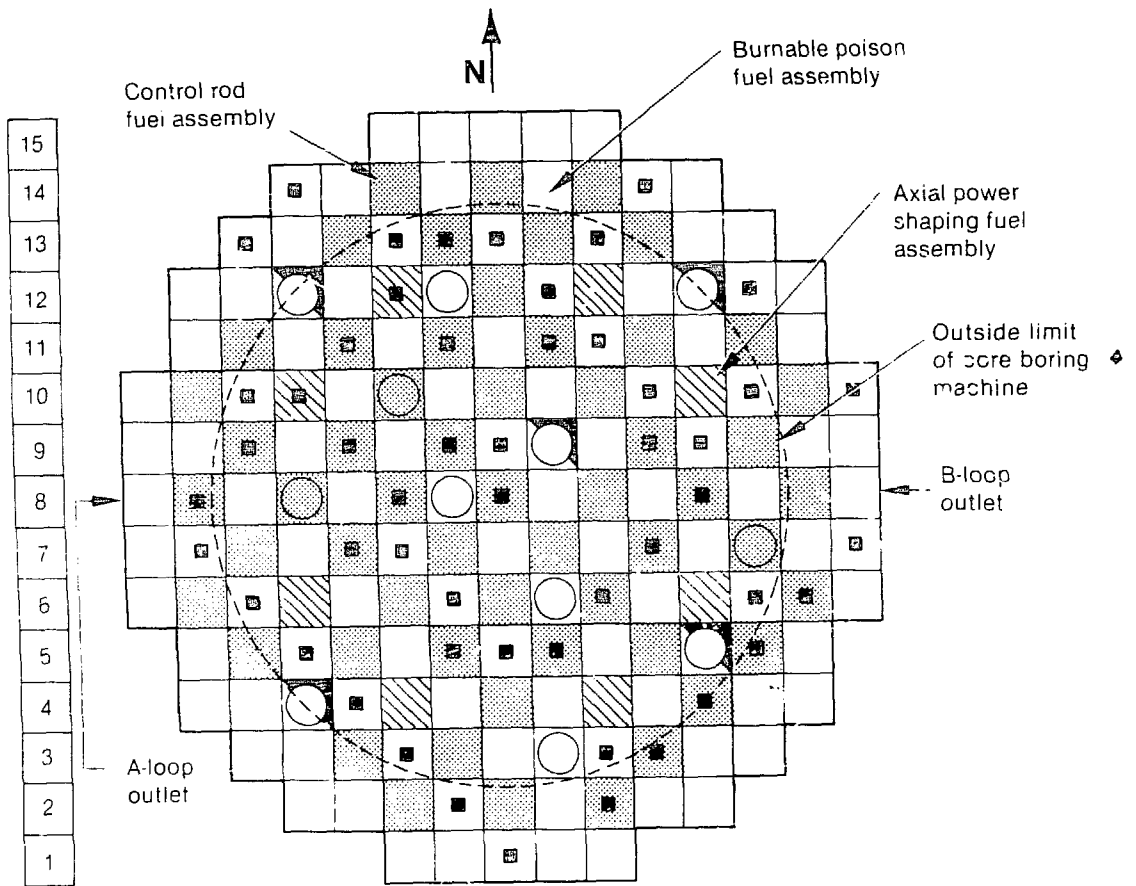
D4
G12
K3
D7

6 3067

Figure 1. Core bore locations.

REFERENCES

1. TMI-2 Accident Evaluation Program, EGG Draft Report, distributed September 24, 1985, under transmittal letter Nr. JMB-39-85.
2. GEND Planning Report, GEND-001, June 1980.
3. TMI-2 Core Examination Plan, Johan O. Carlson (ed.), EGG-TMI-6169, Rev. 1, July 1984.



A B C D E F G H K L M N O P R



Positions where Inspection holes line up



Recommended Core Bore Locations



Core Instrument String Locations

High Priority

K9
F10
N5

Medium Priority

K6
N12
D12
G8
D8

Contingency

D4
G12
K3
D7

6 3067

Figure 1. Core bore locations.

TABLE 1. SUMMARY OF PRIORITIZED SAMPLE ACQUISITION AND/OR ACQUISITION TASKS

1. Video inspection of core--core bores and defueling operation.
 2. Acoustic topography of core cavity after removal of loose debris and fuel rod segments.
 3. Acquisition of core bores.
 4. Documentation of core defueling operations.
 5. Core bore samples.
 6. Large-volume samples of debris from the core and the lower plenum.
 7. Partial-length fuel assemblies from control rod, poison rod, and non-control material locations.
 8. Sludge samples from the Reactor Building basement .
 9. Concrete samples from the walls of the Reactor Building basement.
 10. Primary cooling system surface and sediment samples from A and B loop steam generators, pressurizer, hot leg RTD thermowells, and manway and handhole covers from the steam generator.
 11. Samples of the interaction zone between the core materials and lower core-support assembly.
 12. Samples of the interaction zone between the instrument-guide-tube structures and core material.
 13. Samples of the interaction zone between the reactor vessel lower head surface and the lower core debris materials.
 14. Samples of the interaction zone between the core former wall and core.
 15. Fission-product retention surfaces in upper plenum.
 16. Upper plenum leadscrews.
 17. Upper end boxes, control rod spiders, and spring from top of core.
 18. Fuel rod segments from debris bed.
-

TABLE 2. PRIORITIZATION OF TMI-2 PHYSICAL SAMPLES

Information Needs	Physical Sample	Applicability To		
		Technical Issue	Accident Scenario	Weighted Priority
1. Gross structure of core and RPV internals	a. Video inspection	High	High	High
	b. Acoustic topography	High	High	High
	c. Acquisition of core bores	High	High	High
	d. Core disassembly documentation	High	High	High
2. Core damage progression peak temperature, material physical, and chemical interactions, extent of material oxidation, effect of Ag-In-Cd and B ₄ C/Al ₂ O ₃ on core damage, physical and chemical characteristics of core materials	a. Core bores	High	High	High
	b. Distinct fuel assemblies	High	High	High
	c. Large-volume core debris	High	High	High
	d. Core former wall	Low	Low	Low
	e. Core support assembly	Medium	Medium	Medium
	f. Instrument structures	Medium	Medium	Medium
	g. PRV lower head	Medium	Medium	Medium
	h. Fuel assembly upper-grid and end boxes	Low	Low	Low
	i. Fuel rod segments from upper core	Low	Low	Low
3. Retention of fission products in the fuel, chemical form, physical and/or chemical association with core and structural materials, fission-product distribution throughout RCS and auxiliary piping	a. Core bores	High	High	High
	b. Distinct fuel assemblies	High	High	High
	c. Large-volume debris	High	High	High
	d. Upper plenum surfaces	Low	Medium	Medium-Low
	e. RCS surfaces	Medium	Medium	Medium
	f. RB Basement sludge	Low	High	Medium
	g. Basement concrete wall core bores	Low	High	Medium
	h. Auxiliary piping and components outside RB basement	Low	Low	Low

TABLE 3. TMI-2 ACCIDENT EVALUATION IN-SITU MEASUREMENTS AND SAMPLE ACQUISITIONS AND EXAMINATIONS

Measurement/Examination Activity	Quantity			Priority ^e	Examine ^a	Justification/Information
	Completed Exams	Future Additional Samples	Proposed future Exams			
A. Reactor vessel visual examination						Explain accident scenario and support sample selection.
1. Closed circuit television surveys	3 areas ^d	NA	1 area	1	RIP/ALP	Determine lower core-support structure ablation and approximate location and volume of internal cavities.
2. Periscope survey	0	NA	1 area	4	RIP	Improved images of loose debris in core cavity region.
3. Sonar topography survey	1 area	NA	1 area	4	RIP/AEP	Core cavity dimensions after loose debris and distinct core component removal.
B. Core bore samples of fused/joined core material						Determine condition and quantity of fused/joined core material under loose debris and between core and reactor vessel head. Determine retained fission-product concentration and chemical form.
1. Under loose debris	0	up to 12	3	1, 5, 9	ALP-INEL	
2. Subcore	0	up to 18	5	2, 5, 9	NRC-ANL ^c	
C. Core distinct components						
1. Upper core region						
a. 6-in. fuel rod segments from core cavity periphery	0	6	0	20	-- ^b	Determine condition of unrecalibrated fuel rods in upper core region. In situ separation of segments. Reduce uncertainty in retained fission-product inventory (especially tellurium) from previous grab sample examination.
b. Small grab samples from upper core debris	11	4	0	--		Study interactions between fuel rods and control or burnable poison material and variations in fuel rod damage around the core periphery. Segment separation from fuel assembly remnant will be performed in INEL hot cell.
c. Large grab samples from upper core debris	0	2	1	3		
d. Fuel assembly upper section:						
(1) Fuel rod segments from core cavity periphery fuel assembly remnants	0	25	4	8	AEP-INEL ^b	
(2) Guide tube/burnable poison rod (BPR) segments	0	5	1	8	AEP-INEL ^b	

TABLE 3. (continued)

Measurement/Examination Activity	Quantity			Priority ^e	Examiner ^a	Justification/Information
	Completed Exams	Future Additional Samples	Proposed Future Exams			
(3) Guide tube/control rod segments	0	5	1	8	ALP-INEL ^b	
(4) Instr. tube/Instr. string segments	0	3	0	19	--b	
(5) Instrument tube segments	0	3	0	19	--b	
(6) Spacer grids	0	9	0	19	--b	
(7) Upper end boxes	0	16	0	19	--b	
(8) Hold-down springs	0	14	0	19	--b	
e. Burnable poison rod spiders	0	6	0	19	--b	
f. Control rod spiders	0	7	0	19	--b	
g. Axial power shaping rod (APSR) spider surface deposit	0	1	0	19	--b	
2. Lower core region						Additional data needed to complete selection.
a. Fuel rod segments	0	TBD	4	TBD	ALP-INEL	
b. Guide tube/BPR segments	0	TBD	1	TBD	ALP-INEL	
c. Guide tube/control rod segments	0	TBD	1	TBD	ALP-INEL	
d. Instr. tube/Instr. string segments	0	TBD	0	19	--b	May provide information on thermocouple junction relocation.
e. Instrument tube segments	0	TBD	0	19	--b	
f. Spacer grids	0	TBD	0	19	--b	
g. Lower end boxes	0	TBD	0	19	--b	
D. Lower Vessel Debris						
1. Core material samples from lower head region						
a. Small	0	10	10	7	RLP-INEL NRC-ANLE	
b. Large		1	1	7	REP-INEL NRC-ANLE	From two azimuthal locations via downcomer access.
2. Reactor vessel lower region gamma scans through instrument strings	0	--	--	--	--b	Ion-chamber survey of any of 35 unsurveyed core instrument string calibration tubes. Data may be convertible to location of fuel and nonfuel materials.
3. Samples of loose debris in lower core-support structure region	0	1	1	6	ALP-INEL	Character of loose debris in lower core support structure region.

TABLE 3. (continued)

Measurement/Examination Activity	Quantity			Priority ^e	Examiner ^a	Justification/Information
	Completed Exams	Future Additional Samples	Proposed Future Exams			
E. Reactor vessel internals examinations						
1. Control rod lead screws	2	7	0	18	--b	Fission-product transport path, temperature gradient, and reactor vessel natural recirculation routes.
2. Core former wall samples	0	TBD	4	16	AEP-PL	Data for Isotherm maps and materials interactions at core periphery.
3. Lead screw support tube lower section	1	0	0	Low	AEP-BCL	Characterization of surface deposits in reactor vessel dome region.
4. Lower core-support structure plate samples	0	TBD	6	13	AEP-PL	Data for Isotherm maps and materials interactions along core material relocation path. Fission-product inventory and materials interactions.
5. Reactor vessel lower head samples	0	TBD	2	15	AEP-PL	Data for Isotherm maps and materials interactions.
6. Lower plenum horizontal surface deposits	0	TBD	0	17	--b	Fission-product inventory data.
7. Lower plenum instrument structures	0	TBD	6	14	AEP-PL	Materials interactions.
F. Reactor coolant system (RCS) characterization						
1. RCS Gamma Scans						Capability to convert data to radionuclide and uranium abundance & location uncertain.
a. A loop steam generator (external)	7	N/A	0	Low	GPUN/AEP	
b. Pressurizer (external)	6	N/A	0	Low	GPUN/AEP	
c. Core Flood Tank B	9	N/A	0	Low	GPUN/AEP	
d. Steam generator inside	0	N/A	TBD	Low	GPUN/AEP	
e. Pressurizer inside	0	N/A	TBD	Low	GPUN/AEP	
f. Pressurizer surge line	0	N/A	TBD	Low	GPUN/AEP	
g. Decay heat removal line	0	N/A	TBD	Low	GPUN/AEP	
h. Pump volutes	0	N/A	TBD	Low	GPUN/AEP	
i. Hot legs	0	N/A	TBD	Low	GPUN/AEP	
2. RCS adherent surface deposits						Adherent fission-product deposits.
a. A loop RTD thermowell	1	0	0	12		
b. B loop RTD thermowell	3	1	1	12	AEP-PL	
c. A loop steam generator handhole cover liner	0	1	1	12	AEP-PL	

TABLE 3. (continued)

Measurement/Examination Activity	Quantity			Priority ^e	Examiner ^a	Justification/Information
	Completed Exams	Future Additional Samples	Proposed Future Exams			
d. B loop steam generator manway cover backing plate	0	1	1	12	AFP-PL	
e. Pressurizer manway cover backing plate	0	1	1	12	AFP-PL	
3. RCS sediment						
a. Steam generator tube sheet top loose debris	0	2	2	12	AEP-PL	Character of sediment in both steam generator upper heads. GPU Nuclear project. Character of sediment in both steam generator lower heads. Character of sediment in pressurizer lower head.
b. Steam generator lower head loose debris	0	2	2	12	AEP-PL	
c. Pressurizer sediment	0	1	1	12	AEP-PL	
G. Ex-reactor-coolant-system characterization						
1. Reactor Building						
a. Liquid						Basement liquid has been drained and decontaminated.
(1) Basement-305 ft el.	110 mL	0	0	Low	AEP-INEL	
(2) Basement-325 ft el.	120 mL	0	0	Low	AEP-INEL	
(3) Bottom open stairwell	45 mL	0	0	Low	AEP-INEL/ HEDL	
(4) Basement sump pit	200 mL	0	0	Low	AEP-INEL/ HEDL	
(5) Reactor coolant drain tank (RCDT)	120 mL	0	0	Low	AEP-INEL/ HEDL	
b. Sediment						Sediment includes Susquehanna River silt as well as core fission products and materials.
(1) Basement-305 ft el.	108 g	0	0	10	AEP-INEL	
(2) Basement-325 ft el.	25 g	0	0	10	AEP-INEL	
(3) Bottom open stairwell	1 g	0	0	10	AEP-INEL/ HEDL	
(4) Basement sump pit	72 g	0	0	10	AEP-INEL/ HEDL	
(5) Reactor coolant drain tank	0.5 mg	0	0	10	AEP-INEL/ HEDL	
(6) Basement floor (282 ft el.) (a) RCDT discharge area	0	3	3	10	AEP-PL	
(b) Leakage cooler room, RCDT room, inside D-ring, outside D-ring areas	0	10	10	10	AEP-PL	

TABLE 3. (continued)

Measurement/Examination Activity	Quantity			Priority ^e	Examiner ^a	Justification/Information
	Completed Exams	Future Additional Samples	Proposed future Exams			
(c) Core instrument cable chase	0	2	2	10	AEP-PL	
c. Concrete bores						
(1) Floors: 347 ft el.	8	0	0	Low	GPUN/AEP	GPUN proposal, bore depth not specified, after floor dewatering and desludging.
305 ft el.	6	0	0	11	GPUN/AEP	
282 ft el.	0	10	13	11	AEP-PL	
(2) D-ring walls: 347 ft el.	1	0	0	Low	GPUN/AEP	GPUN proposal, bore depth not specified.
305 ft el.	2	0	0	11	GPUN/AEP	
flooded region	3	8	3	11	AEP-PL	
(3) 3000 psi (shield) wall (flooded region)	3	8	3	11	AEP-PL	GPUN proposal, bore depth not specified.
(4) Block (elevator/stairwell) walls (flooded region)	3	8	3	11	AEP-PL	GPUN proposal, bore depth not specified.
d. Adherent surface deposits						
(1) Air cooler panels	5	0	0	Low	AEP-INEL	Acquisition and examination plan under consideration.
(2) Basement outer wall steel liner	0	TBD	TBD	Low	AEP-PL	
2. Auxiliary and Fuel Handling Buildings						
a. Liquid						
(1) Reactor coolant bleed Tank A	125 mL	0	0	Low	AEP-INEL	All equipment in the Auxiliary and Fuel Handling Buildings has been fully or partially decontaminated by flushing, filter removal, water treatment, and resin removal or treatment.
(2) Reactor coolant bleed Tank B	150 mL	0	0	Low	AEP-INEL	
(3) Reactor coolant bleed Tank C	150 mL	0	0	Low	AEP-INEL	
(4) Makeup and purification demineralizer B	40 mL	0	0	Low	AEP-ORNL	
b. Sediment						
(1) Reactor coolant bleed Tank A	60 g	0	0	Low	AEP-INEL/ HE DL	
(2) Makeup and purification demineralizer A (resin)	10 g	0	0	Low	AEP-ORNL	
(3) Makeup and purification demineralizer B (resin)	40 mL	0	0	Low	AEP-ORNL	
c. Filter housing contents (filter paper, liquid, and collected solids)						

TABLE 3. (continued)

Measurement/Examination Activity	Quantity			Priority ^e	Examiner ^a	Justification/Information
	Completed Exams	Future Additional Samples	Proposed Future Exams			
(1) Makeup and purification system						
(a) Demineralizer prefilters	both	0	0	Low	AEP-INEL/ LANL, NRC- ANL	
(b) Demineralizer after filters	both	0	0	Low	AEP-INEL/ LANL, NRC- ANL	
(2) RC pump seal water injection system filters	both	0	0	Low	AEP-INEL/ LANL, NRC- ANL	

a. Examination responsibility is shown with the funding organization (AEP, REP, NRC, and/or GPUN) shown first (xxx/xxx indicates joint funding and/or performance responsibility), and the sample examination location shown second. Names of funding organizations are abbreviated as follows: Accident Evaluation Program, AEP; Reactor Evaluation Program, REP; Nuclear Regulatory Commission, NRC; GPU Nuclear, GPUN. Names of examination locations are abbreviated as follows: Idaho National Engineering Laboratory, INEL; Argonne National Laboratory-East, ANLE; Battelle Columbus Laboratories, BCL; Hanford Engineering Development Laboratory, HEDL; Oak Ridge National Laboratory, ORNL; Los Alamos National Laboratory, LANL. PL indicates an outside private laboratory is expected to perform the examination.

b. Possible examination by foreign laboratory, including funding.

c. Possible examination of two core bores and lower plenum debris by ANL using NRC funding.

d. Completed reactor vessel CCTV surveys include the following areas: all sides of the upper core region cavity, core cavity region loose debris after dislodging core components from plenum assembly, plenum assembly, and accessible areas of the downcomer and reactor vessel lower head periphery regions.

e. Priority values 1 through 20 are listed in table 1.

TABLE 1. TMI-2 FISSION PRODUCT PARTITIONING

Plant Location	Estimated Percentage of Inventory at Time of Accident							
	Cs	I	Xe	Kr	Sr	Sb	Ru	Ce
Fuel and core debris within the vessel	27	33	13 ^a	13 ^a	115	41	61	~100
Vessel internals and primary system piping	~1	<1	nm	nm	<1	<1	<<1	<<1
Primary system coolant	~10	~8	<1	nm	~1	nm	<<1	nm
Reactor and Auxiliary Building sumps and tanks	~45	~41	nm	nm	~2	nm	<1	nm
Reactor and Auxiliary Building surfaces	<1	<1	nm	nm	<<1	nm	nm	nm
Reactor Building atmosphere	<<1	<<1	nm	54	<<1	nm	nm	nm
Environment	nd	<<1	1	~1	nd	nd	nd	nd
Total accounted for (%)	83	92	68 ^b	68	118	41	61	100

nm = not measured.

nd = not detected above background.

a. Calculation only; assumes the apparently intact fuel rods contain their initial inventory.

b. Assumes Xe retained in Reactor Building atmosphere to the same extent as Kr, but had decayed at time of measurement.

PLANT INSTRUMENT BEHAVIOR

TMI-2 PRESSURIZER-LEVEL RESPONSE

J. L. Anderson
Idaho National Engineering Laboratory
EG&G, Idaho Inc.
P.O. Box 1625, Idaho Falls, ID 83415

ABSTRACT

Results of a study to evaluate and understand the pressurizer-level response to the reactor system thermal-hydraulic conditions during the first 1000 min of the TMI-2 accident are presented in this paper. An evaluation of the measurement system with regards to postulated problems determined that these problems were insufficient to discount the observed pressurizer-level response. It has been determined that the observed level changes can be explained in terms of response to the thermal-hydraulic conditions in the reactor coolant system. A comparison of the TMI-2 pressurizer-level response and the level response observed during integral system experiments is made. In those experiments where a TMI accident scenario was simulated, the pressurizer level responded in a manner very similar to the measured TMI response.

INTRODUCTION

During normal plant operation, the function of the pressurizer is to control the system pressure. This is accomplished by using pressurizer heaters to increase the fluid temperature in the saturated pressurizer, thus increasing system pressure; and by using the spray line to inject cold liquid into the pressurizer, thus reducing temperature and pressure. The pressurizer is also equipped with a PORV to quickly relieve pressure under conditions such as a feedwater pump trip. This is the valve that stuck open and resulted in the severity of the TMI-2 accident. The level in the pressurizer is normally used as an indication of total system mass inventory, and is controlled through the use of the letdown and makeup systems. Level in the pressurizer is normally maintained between 508 and 660 cm (200 and 260 in.) The level just prior to the feedwater pump trip was 569 cm (224 in.).

Since the March 28, 1979, accident at the TMI-2 nuclear plant, there has been considerable controversy²⁻⁴ as to the reliability of the pressurizer-level measurements during the accident, and as to the reasons for the response of the pressurizer level if the level indications were correct. This paper is a summary of a study that has been performed by the TMI-2 Accident Evaluation Program of EG&G, Idaho Inc., in an attempt to clarify pressurizer response to the thermal-hydraulic conditions in the RCS during the first 1000 min of the accident. The detailed analysis and results of the study are provided in Reference 1. The approach taken in the study consisted of:

- A description of the pressurizer-level-measurement system and evaluation of the various reasons that have been set forth for disbelieving the measurements

- o An analysis of the pressurizer-level response to the thermal-hydraulic conditions in the primary and secondary systems, assuming that the trends of the level measurements were correct
- o Supporting data from integral systems experiments were evaluated and compared to the measured TMI-2 pressurizer-level response
- o The results from thermal-hydraulic code calculations that have been performed in support of accident evaluation were evaluated with respect to the predicted pressurizer-level response.

At this time, the RELAP5 analysis is not complete and will not be presented in this paper.

There are two reasons for studying the pressurizer-level measurements during the first day of the accident. First, understanding the mechanism causing changes in the pressurizer level can provide valuable insight into the conditions existing in the RCS during major events, such as core uncover and heatup. Unfortunately, there were insufficient measurements recorded during the accident to determine the RCS conditions directly; therefore, information inferred from the pressurizer-level response is extremely useful. Second, prediction of the correct pressurizer level by the thermal-hydraulic codes (such as RELAP5) is critical to the calculation of the overall system response leading up to core uncover. Prediction of the correct level is necessary for the calculation of the correct mass flow rate out the open PORV. In addition, the impact of the pressurizer-level response (remaining near full or draining) is especially significant during the time period when initial core uncover and core damage occurred. RELAP5 calculations indicate that if the pressurizer had drained, as some investigators have speculated, then the additional liquid in the core would have delayed core uncover and heatup by as much as 1 h. For these reasons, the study was undertaken to determine if the measured liquid level could be used for analysis of the accident. The remainder of this paper will summarize the results from the study.

In this paper, the measurement system will be described and evaluated. The pressurizer-level response to several of the major events will then be presented and discussed. Results from one of the integral system experiments (the Semiscale TMI simulations) will be presented and compared to the TMI-2 pressurizer-level response. Finally, conclusions reached from the study will be presented.

SYSTEM DESCRIPTION

An isometric drawing of the TMI-2 primary system⁵ is shown in Figure 1. The 22.2-cm (8.75-in.) ID pressurizer surge line enters the A-loop hot leg at an elevation of 98 m (321 ft-6 in.). The surge line drops down from the hot leg entrance to an elevation of 94.3 m (309 ft-3 in.), travels approximately 10 m (34 ft) horizontally, and rises up to the pressurizer entrance at an elevation of 95.2 m (312 ft-2 in.) on the inside surface of the pressurizer. This configuration acts as a loop seal for the surge

line, with the entrance of the surge line to the hot leg corresponding to a measured pressurizer liquid level of 163 cm (64 in.). This level is just above the elevation of the pressurizer heaters. The 10-cm (4-in.) pressurizer spray line leaves the primary system at the discharge of the RCP-2A, and enters the pressurizer through the upper head. A control valve is installed near the entrance to the pressurizer for controlling the spray flow rate. The spray line does not have a check valve installed, which would have prevented reverse flow from the pressurizer to the cold leg.

A schematic of the pressurizer-level-measurement system is shown in Figure 2. The level measurement is based upon the difference in the hydrostatic fluid heads of the liquid column in the pressurizer and that of a liquid-filled reference leg, external to the pressurizer. Since the reference legs are external to the pressurizer insulation and are uninsulated, the liquid in the reference legs remains near containment temperature. As a result, there is no need for installation of condensate pots during normal operation, and no condensate pots are installed. There are three independent measurements separated by 120 degrees around the pressurizer. The bottom tap for each is located at an elevation of 96.4 m (316 ft-2 in.), and the top taps are at an elevation of 106.5 m (349 ft-6 in.), for a total span of 1016 cm (400 in.). Between each of these sets of taps is installed a Bailey Instruments differential pressure transmitter, which is setup for a -10 to +10 volt output under an input head of 0 to 1015 cm (0-400 in.) of cold water 293 K (68°F). These transmitters are mounted in instrument racks 424 (RC-1-LT1 and LT2) and 426 (RC-1-LT3), which are located outside of the secondary shield wall in the Reactor Building basement at an elevation of 86.9 m (285 ft). The transmitters are connected to the pressurizer taps using 1.2-cm (1/2-in.) stainless steel tubing as sense lines. The transmitters are zeroed when valved out of the system and vented to atmosphere, i.e., with no load applied to either side. As a result, when the transmitter is valved into the system with an empty pressurizer, the transmitter measures the 1016-cm (400-in.) hydrostatic head of the reference leg. When the pressurizer is full of cold water, the transmitter measures 0.0 cm differential pressure, since the two hydrostatic heads balance each other.

The output from one of the three transmitters is used to calculate the temperature-compensated level in the pressurizer. The transmitter used for this calculation can be selected from the Operators Control Panel, with no record of which one is used; although for normal operation, the RC-1-LT1 transmitter is used. The direct output from any of the transmitters was not recorded on a strip chart during the accident. The temperature compensation is performed to account for the difference in fluid densities between the reference leg and the pressurizer fluid. The level is simultaneously calculated by two methods. The first is performed using an analog circuit, which is part of the NNI, the output of which goes to the ICS for control of the pressurizer liquid level, using the makeup and letdown systems, and also goes to the control panel level indications and strip chart recorder. The second method uses the plant computer to calculate the pressurizer level. In this method, the transmitter output is combined with the specific volumes of the saturated liquid and steam, calculated using the fluid temperatures measured in the pressurizer, to calculate the liquid level. The liquid level, L , is obtained in this method using the following equation:

$$L = \frac{(\rho_r - \rho_g)D - \rho_c DP}{(\rho_f - \rho_g)} \quad (1)$$

where

- ρ_g = the fluid density of the steam in the pressurizer (kg/m³);
- ρ_r = the fluid density for the reference leg, @ 325 K (125°F)
- ρ_c = the fluid density of cold water, @ 293 K (68°F)
- ρ_f = the fluid density of the liquid in the pressurizer (kg/m³)
- D = the distance between the pressurizer taps = 1016 cm (400 in.)
- DP = the measured differential pressure, in cm of 293 K (68°F) water)

Equation (1) accounts for the hydrostatic head of the steam, and is derived in Reference 1. When the primary system temperature is above 325 K (125°F), a reference leg temperature of 325 K (125°F) is assumed for obtaining the reference leg fluid density. The level given by Equation (1) is the collapsed stratified level. If the liquid in the pressurizer was boiling, and, thus, the liquid was filled with voids, the two-phase interface level would be higher than the collapsed stratified level, due to level swell. The results from Equation (1) are available to the operators on the utility printer upon request, and are displayed as alarms on the alarm printer when the range of 508 to 660 cm (200 to 260 in.) is exceeded.

Heater Operation

In order to increase pressure during normal plant operation, the pressurizer is equipped with heaters that are controlled, in the automatic mode by the ICS, based upon pressure. The heaters may also be controlled manually by the operators. The heaters are divided into 13 groups of 126 kW each. These groups are divided into five banks, which is the basic control unit. Each bank can be controlled either manually or in the automatic mode by the ICS. The control mode can be selected by the operators, and the setting is not recorded. During the first day of the TMI-2 accident, the operators apparently switched Heater Banks 4 and 5 into automatic control prior to reactor scram, and left Banks 1, 2, and 3 in manual control mode. Banks 1, 2, and 3 apparently were left energized during the entire first day of the accident. Since these groups were in manual control, operation of the heaters (either on or off) was not recorded on the alarm printer, with the exception of ground fault trips that will be discussed later. Operation of Heater Groups 1 to 5, in Banks

4 and 5, were recorded on the alarm printer as TRIP when each group was de-energized by the ICS, and as NORM when the ICS energized each group. Groups 6 and 7 in Bank 4 were unavailable for operation during the first day of the accident.⁶ Each group also appeared on the alarm printer as a TRIP when the group circuit breaker was tripped due to a ground fault.

Postulated Measurement Problems

Since the March 28, 1979, accident, there have been several arguments concerning problems that might have resulted in invalid measurement of the pressurizer level using the aforementioned measurement system. Twice during the first day of the accident, at 43 and 433 min after the feedwater pump trip, the operators requested output of all three transmitter readings on the utility printer. Both times, the three transmitters agreed within several centimeters. Any arguments discounting the validity of the level measurement must explain this fact. Of the four arguments that have been examined, all were found to be insufficient to explain the observed pressurizer-liquid-level response during the first day of the accident. Each of these four arguments will be presented and discussed next.

The first of these arguments was raised soon after the accident, and involves the possible effervescence of dissolved hydrogen in the reference legs. The argument is that prior to the accident, hydrogen was dissolved in the liquid throughout the primary system to eliminate dissolved oxygen. Following reactor scram, the system pressure decreased from 16.2 to 6.9 MPa (2350 to 1000 psig) within the first 30 min. The dissolved hydrogen would tend to effervesce, or bubble out of the liquid, much like opening a bottle of champagne. In the reference legs of the liquid-level-measurement system, this effervescence could possibly have occurred at a rate fast enough to force a significant portion of the liquid out of the reference leg, thus invalidating the liquid-level measurement. Sandia National Laboratories performed an analysis of this possibility⁷ with the result that [assuming an initially hydrogen-saturated reference leg at 15.2 MPa (2200 psi), and an instantaneous depressurization] a maximum error in the level measurement, due to liquid ejection, was calculated to be 145 cm (57 in.). However, the depressurization was not instantaneous, but took 30 min to reach 6.9 MPa (1000 psig). It was concluded that, "It is apparent that head-loss due to hydrogen effusion is too small to be responsible for the large level changes reported for the accident."

The second argument that has been put forth involves the possible boiloff of liquid from the reference legs during the system depressurization.³ Since the reference legs are outside of the pressurizer insulation, it is unlikely that the fluid temperature in the reference legs would be much above the Reactor Building temperature over any significant length of the reference leg. For boiling to occur, the fluid temperature must be at the saturation temperature for the system pressure, which is 558 K (545°F) at 6.9 MPa (1000 psig). The highest recorded Reactor Building temperature was 353 K (175°F), which occurred at 300 min at an elevation of 101 m (333 ft). It is possible that the fluid in the top few centimeters of the reference legs might have been at a sufficiently high temperature, due to heat conduction from the hot pressurizer, to boil when the system depressurized. However, this would

certainly result in a temporary error of less than 25 cm (10 in.), which would disappear as condensation refilled the reference leg. If condensation did not occur, then to explain the close readings between transmitters would require that the boiloff in each of the reference legs be the same. It appears that this argument cannot be supported by thermodynamic considerations.

The third argument that has been put forth involves damage to the reference legs by a water hammer occurring at 174 min when the RCP-2B was restarted.⁴ This restart of the pump forced liquid into the hot core that quickly boiled into steam, in addition to hydrogen generation, and caused a rapid repressurization of the system and surge into the pressurizer. It has been postulated that the rapid pressure and level increases acted as a water hammer on the reference lines, resulting in damage to the reference lines which subsequently began leaking. The argument continues that the leaks were small, and that the reference lines would refill with condensate during periods of repressurization, resulting in false indications of falling level in the pressurizer. No argument has been made that the water hammer damaged the differential pressure transmitters. There are a number of problems with this argument. First, a water hammer cannot occur in a vessel or line where gas exists. The gas acts as a buffer, absorbing the momentum from the liquid, thus limiting the damage. Second, water hammer results in a pressure spike, whereas the pressure rise in the RCS was at a rate of 2.4 MPa/min (350 psi/min). It is hard to believe that this pressure "pulse" could result in equal damage to all three reference lines. These lines were hydrostatically tested at a pressure of 62 MPa (9000 psig) prior to plant startup. The final problem with this argument is the fact that 259 min after the 2B pump transient (433 min accident time), output from all three of the differential pressure transmitters was recorded on the utility printer and agreed within 13 cm (5 in.) of each other. The case for water hammer damage to the reference lines is very weak.

The fourth argument that has been put forth for disbelieving the level measurement involves the environment to which the transmitters were exposed during the first day of the accident.³ The transmitters were installed in Instrument Racks 424 and 426 in the basement of the Reactor Building. Rack 424 (in which transmitters RC-1-LT1 and LT2 were installed) was in the vicinity of the exhaust from the RCDT rupture disk assembly. The discharge from the PORV was routed to this tank. Consequently, the exhaust had the potential of raising the local temperature above the environmental specifications for the level transmitters. The maximum temperature recorded in the Reactor Building for this vicinity was 353 K (175°F). Specifications for the transmitter are for a maximum operational temperature of 344 K (160°F). However, Bailey Instruments performed autoclave tests on representative units in which the transmitters were maintained in a steam environment above a temperature of 383 K (230°F) for 24 h. During significant portions of this test, the transmitter was submerged in liquid from condensation. Periodically the transmitter was calibrated in-place to check for the environmental effects upon the transmitter calibration. The maximum calibration error experienced during the 24 h-period was less than 5%, primarily a zero shift. It is unlikely that the conditions experienced by the transmitter during the first 24 h of

the accident exceeded the conditions tested for during the autoclave tests. As such, inoperable transmitters or excessive calibration shifts of the transmitters during the first 24 h of the accident are insufficient to explain the observed pressurizer level response.

The major arguments for disbelieving the pressurizer-liquid-level measurements have been presented and discussed. These arguments have all been found to be insufficient to discount the observed pressurizer-level response during the first day of the accident.

THERMAL-HYDRAULIC ANALYSIS

As a result of the evaluation of the pressurizer-level-measurement system, it has been concluded that the measured level was indicating the correct level within a measurement uncertainty, and that the level can be used for analysis of the accident. In this section, the pressurizer-level response to the thermal-hydraulic conditions in the RCS will be discussed. A detailed analysis and discussion of this subject is available in Reference 1; a summary of it will be provided here. Only the major pressurizer-level responses will be presented.

The measured pressurizer liquid level and primary system pressure for the first 150 min of the accident is shown in Figure 3, (time zero is taken as the main feedwater pump trip). During the first 8 s following the feedwater pump trip, the pressurizer level increased to 650 cm (256 in.), from an initial level of 569 cm (224 in.), due to RCS fluid expansion as the average system temperature increased, as a result of reduced heat removal in the steam generators. This initial in-surge was followed by an out-surge from the pressurizer as the RCS fluid contracted following reactor scram (with continued steaming from the steam generators and flow through the PORV). The pressurizer level reached a minimum of 401 cm (158 in.) at 51 s and the level began increasing at approximately 152 cm/min (60 in./min) as the average system temperature increased. At about 1.5 min into the transient, the steam generators secondary pressures began falling, indicating that the steam generators were drying out. Also, at this time, the A-loop hot leg and cold leg temperatures equalized, indicating that energy removal from the steam generator was near zero. At this time, the reactor system was filled with liquid with the exception of the pressurizer steam space. However, at approximately 2 min, the system pressure had dropped sufficiently that the fluid in the vessel upper head reached its saturation pressure [about 11 MPa at 592 K (1600 psig at 605°F)]. This resulted in a reduction of the depressurization rate. As the pressure continued to drop, the upper head void increased and acted as another pressurizer for the system. Indeed, the upper head fluid was probably at a higher temperature than the pressurizer fluid due to heat transfer from the hot vessel walls. The continued decrease in system pressure resulted in reaching saturation pressure in the hot and cold legs at about 5 min. By this time, the continued PORV flow, coupled with the makeup flow and increasing system average temperature, resulted in the pressurizer level increasing to an off-scale high [greater than 1016 cm (400 in.)], where it remained until 10 min.

The pressurizer-level indication was on scale, but high [from 914 to 991 cm (360 to 390 in.)], during the 10 to 73 min time period. Continued

system depressurization and flow out the open PORV, coupled with increased letdown flow and decreased makeup flow as the operators attempted to reduce the pressurizer level, resulted in an increasingly voided RCS. With all four primary coolant pumps running and the steam generators essentially dry, flow throughout the system was predominately homogeneous two-phase flow. This condition existed until the B-loop pumps were shut off at 73 min. At approximately 25 min, output from the out-of-core neutron SRM was increasing. This, coupled with the decreasing loop flow, indicated that the system void fraction was increasing. At 43 min, the operators requested a printout of the values for the three pressurizer differential pressure (level) measurements. These values were listed on the utility printer as RC-1-LT1 = 269 cm (106 in.), LT2 = 279 cm (110 in.), and LT3 = 257 cm (101 in.) [the differential pressure is given in centimeters of water at 293 K (68°F)]. Due to the close agreement between the independent level measurements, it was determined that the pressurizer-level indication was correct. At 73 min, the B-loop pumps were turned off due to low current and high vibration. This allowed phase separation to occur in the B-loop and flow to stagnate, with little or no communication with the A-loop. Indication of the flow stoppage was the falling secondary pressure in the B-loop steam generator. This reduced the energy removal from the primary system.

At 101 min, both A-loop pumps were stopped due to excessive pump vibration. This allowed the previously homogeneous two-phase mixture in the primary systems A-loop to stratify, with a level somewhere in the vicinity of the top of the core (almost certainly below the surge-line elevation in the hot leg). Starting at this time, the liquid pool in the core was boiling, with loss of system mass as steam flowed into the pressurizer surge line and out the PORV. Since the indicated pressurizer level was less than 914 cm (360 in.), continued flow out the PORV was probably saturated steam. While the PORV was open, steam velocities were high enough into the surge line that liquid flow from the pressurizer was limited by the countercurrent flow of steam into the pressurizer surge line. Flooding calculations indicate that the liquid flow out of the pressurizer (into the hot leg) would be zero whenever the RCS pressure was greater than 2.8 to 4.8 MPa (400 to 800 psig) (assuming steam flow into the surge line). The pressurizer liquid level continued to decrease due to steam generation by the heaters in the pressurizer. Between the time that core uncover began (at about 114 to 126 min)⁸ until the PORV block valves were closed at 139 min, the level decreased at a rate of 3.3 cm/min (1.3 in./min). Heater operation at a power of 1386 kW would account for a rate of 2.0 cm/s (0.9 kg/s) [0.8 in./min (2 lbm/s)]. The calculated steam flow out the PORV at 4.8 MPa (700 psig) is 4.5 kg/s (10 lbm/s).

The pressurizer liquid level and the RCS primary pressure are shown in Figure 4 for the 150 to 250 min time frame. This period covers two significant pressurizer fills and one significant out-surge. At 174 min, the RCP-2B was successfully restarted, and ran for 18 min. Within the first minute, the pressurizer heaters were de-energized and the pressurizer spray valve opened. (Note that the spray line originates at the discharge of the RCP-2A and operation of the 2B pump would have resulted in minimal flow through the spray line.) The restart of the pump resulted in significant liquid flow from the 2B cold leg being forced into the core for

the first 20 s of operation, perhaps reflooding the undamaged portions of the core (one estimate of flow is that 28 m^3 (1000 ft^3) entered the reactor vessel).⁵ An indication of additional liquid in the downcomer (and perhaps the core) was the abrupt drop in output from the SRM, as neutrons were absorbed by the liquid. As liquid penetrated the core, a large amount of steam and/or hydrogen was generated, resulting in a rise of RCS pressure of 4.8 MPa (700 psi) in 2 min, with a further 1 MPa (150 psi) increase over the next 16 min. Coincident with this large pressure increase was a jump in the pressurizer level from 762 to 914 cm (300 to 360 in.), with a further slow rise to 991 cm (390 in.). It is postulated that the level rise was due to level swell in the pressurizer as steam from the hot leg entered the pressurizer, condensed, and raised the fluid temperature in the pressurizer. Calculations indicate that condensation, into an initially saturated pressurizer, could have produced the observed level increase with an approximately 10 K (20°F) subcooled pressurizer resulting after 2 min. Since a flow path existed from the pressurizer steam space to the 2A cold leg through the open spray line, condensation may have occurred in the spray line, which would tend to lower the pressurizer pressure. Since there is an indication of reverse flow into the 2A cold leg (the drop in fluid temperature), it is possible that some subcooled liquid may have entered the pressurizer through the spray line, which would result in further steam condensation.

At 192 min, the operators opened the PORV block valve, resulting in a drop in RCS pressure of about 1.4 MPa (200 psi), and a drop of 127 cm (50 in.) in the pressurizer level in 3 min. This was a result of the decreasing system pressure coupled with a nearly saturated pressurizer. As the pressure dropped, the saturated liquid in the pressurizer flashed into steam. A 1.4 MPa (200 psi) drop in pressure would result in formation of 1130 kg (2500 lbm) of steam from the liquid in the pressurizer. This 1130 kg (2500 lbm) of steam would have resulted from flashing 1.9 m^3 (66 ft^3) of saturated liquid, and decreased the pressurizer level by 51 cm (20 in.), as compared to the observed 127 cm (50 in.) drop in level. Another 38 cm (15 in.) drop in level would have resulted from the increased fluid density as the pressure dropped and the fluid saturation temperature decreased. At a pressure of 13.8 MPa (2000 psig), the calculated steam flow rate out the PORV is approximately 15 kg/s (32 lbm/s), for a total steam flow of 2630 kg (5800 lbm) over the 3 min the PORV block valve was open. The steam flow out the PORV would have been a combination of steam generated in the pressurizer and steam flow through the surge line from the hot leg. The decreased steam velocities in the surge line could have permitted some liquid to drain out of the pressurizer, thus accounting for the observed 127 cm (50 in.) decrease in level.

At 195 min, the PORV block valve was closed, resulting in a slow rise in pressure over the next 3 min. This, in turn, resulted in a 102 cm (40 in.) rise in the pressurizer level. As the system pressure increased, the pressurizer became increasingly subcooled relative to the hot leg. The resulting condensation in the steam space reduced the pressurizer pressure and drew steam into the surge line from the hot leg. At 198 min, the pressurizer level exhibited another drain and fill cycle, over a 2 min period. This was due to another open/close cycle of the PORV block valve. Another cycle of the block valve has not been reported within a reasonable

time period of this event. However, as reported in Reference 1, comparison of the RCS and RCDT pressures indicate that another block valve open/close cycle occurred at this time (197.9/198.4 min).

At 200 min, the operators started the makeup pumps in the HPIS mode at an injection rate of approximately 63 L/s (1000 gpm) over the next 15 min, resulting in a continued decrease of the RCS pressure to about 10 MPa (1500 psig). The depressurization was driven by condensation of steam due to the injection of cold makeup liquid. Assuming that the pressurizer was still at saturation, this decrease in RCS pressure would result in liquid boiling in the pressurizer, with the resulting steam formation displacing liquid in the pressurizer, causing a decrease in the liquid level. This depressurization of saturated liquid would generate approximately 20 m³ (700 ft³) of steam, compared to the 13 m³ (450 ft³) of liquid that was displaced. If only the liquid remaining in the pressurizer after the level drop was available for vaporization, then approximately 7.6 m³ (270 ft³) of steam would have been generated. Thus, the observed level decrease is bracketed by these two assumptions and the postulated mechanism of vaporization of saturated liquid is sufficient to explain the observed level decrease. At 204 min, the pressurizer surge line temperature was recorded on the alarm printer as 578 K (581°F), with a system saturation temperature of 592 K (605°F).

At 207 minutes, the pressurizer level decrease stopped; and at 210 min, the pressurizer level began increasing until it increased to an off-scale high by 218 minutes. Coincident with this level increase was a repressurization of the RCS by about 0.6 MPa (80 psi). The pressurizer level increased from 585 to 1016 cm (230 to 400 in.) in 8 min, which corresponds to an injection rate of 22 L/s (350 gpm) of cold water into the system [the in-surge corresponded to 32 L/s (505 gpm) of saturated liquid]. It is postulated that the HPIS injection was sufficient to flood the reactor vessel and hot legs to an elevation above the surge-line entrance in the A-loop hot leg. With increasing RCS pressure and condensation in the pressurizer, liquid was drawn into the pressurizer, causing the large level increase. The HPI injected approximately 57 m³ (15,000 gal) of cold liquid into the system, whereas approximately 38 to 53 m³ (10,000 to 14,000 gal) would be sufficient to fill the cold legs, vessel, and hot leg to the elevation of the surge line in the A-loop hot leg from an initially empty condition. The pressure increased slightly due to compression of the noncondensable gases by the HPI. At 219 min, HPI was reduced to about 6 L/s (100 gpm). At 220 min, the PORV block valve was opened and the pressurizer level returned on-scale, accompanied by a 0.7 MPa (100 psi) pressure drop. The pressure decrease may have allowed the noncondensable gas bubble in the hot leg to expand down to the surge-line elevation, permitting gas flow into the pressurizer and resulting in the level decrease.

There were two significant drain/fill cycles in the pressurizer during the 650 to 900 min period. The pressurizer liquid level and RCS pressure is shown in Figure 5 for this time frame. The first portion of this period is from 650 to 800 min, when there was minimal net makeup into the system [about 3 L/s (50 gpm)], with little or no primary to secondary heat transfer through either steam generator due to isolation of the

secondaries. With the PORV block valve closed and little makeup flow, the core was being cooled by pool boiling, with the level gradually dropping in the downcomer. It is possible that uncovering of the upper region of the core occurred. At 672 min when the PORV block valve was closed (it had been opened at 459 min to depressurize the RCS), the pressurizer responded by beginning a rapid level decrease of 569 cm (224 in.) in 13 min. This dump was due to the fact that the pressurizer was at saturation temperature prior to the valve closure, with the pressurizer heaters supplying 756 kW of energy to the fluid. The flow through the PORV had been maintaining the pressurizer at a lower pressure than the rest of the RCS, thus holding the level up. With the block valve closed, the fluid in the pressurizer continued to boil and the steam displaced the liquid [9.5 m³ (690 ft³) of steam is calculated to have been generated by the heaters, compared to 20.4 m³ (720 ft³) from the level change]. The pressurizer level reached a minimum level of 444 cm (175 in.), which resulted in approximately 20.4 m³ (720 ft³) of liquid leaving the pressurizer.

At 678 min, the makeup flow was increased for 10 min, and the pressurizer level decrease stopped and remained constant. This was concurrent with a slight RCS repressurization. At 689 min, the operators de-energized Heater Groups 1 and 2. At 693 min, the pressurizer began to refill, and reached a level of 1016 cm (400 in.) at 747 min, a refill rate of 10.7 cm/min (4.2 in./min). The pressurizer refill was probably due to the slowly increasing RCS pressure coupled with steam condensation in the slightly subcooled pressurizer. The level in the hot leg would have had to have been above the surge line during this refill. The spray valve was still open during most of this refill (until 726 min), and condensation through this open path may have been the major mechanism for the fill. This argument is supported by the reaction of the cold leg temperature. At 702 min, the A-loop cold leg temperature began to increase, and reached system saturation temperature at 732 min, where it remained until 800 min.

At 803 min, the operators started MUP-1C [increasing net makeup to more than 13 L/s (200 gpm)], and decreased heater power to the pressurizer. The RCS pressure dropped 200 to 350 kPa (30 to 50 psi) (probably due to condensation effects) and the pressurizer level responded by decreasing 280 cm (110 in.) in about 4 min. The addition of 10 m³ (350 ft³) of near-saturated liquid from the pressurizer into the core and continued makeup resulted in a continuous RCS pressure increase from 4.1 to 15.9 MPa (600 to 2300 psig) over the next 70 min. Although the pressurizer temperature remained fairly constant throughout the remainder of this phase, it was increasingly subcooled due to the increasing RCS pressure. The pressurizer level responded to the pressure increase by refilling at a linear rate of 9.7 cm/min (3.8 in./min). This refill was probably condensation induced with liquid available at the surge-line entrance. Once the pressurizer had refilled, the RCS repressurization rate increased. At this time, the pressurizer was probably filled with liquid, unless a small bubble of noncondensable gases existed above the top level tap.

At 930 min, the operators ran the RCP-1A pump for 10 s. This resulted in a brief flow of coolant in the A-loop, which caused a sharp drop in RCS pressure and the temperatures in both the hot and cold legs. Pressure in

the secondary of the A-loop steam generator sharply increased, indicating that primary-to-secondary heat transfer increased due to the start of forced convection. At 950 min, the operators successfully restarted the RCP-1A pump and reestablished forced convection in the system. This action established long-term cooling of the core and essentially recovered control of the plant, although the large quantities of noncondensable gases were not successfully eliminated from the upper head for another 3 to 5 days.

THERMAL-HYDRAULIC EXPERIMENTAL RESULTS

There have been a number of integral systems experiments studying the thermal-hydraulic behavior during a TMI-type accident scenario. The major experimental facilities that have been used for this type of research, in which the experimental results are significant to the current analysis effort, are the Semiscale,⁹ LOFT,¹⁰ and ROSA-IV¹¹ test facilities. In the following section, results from the most significant experiments (those performed in the Semiscale facility) will be presented and discussed with regards to the pressurizer-level response to the systems thermal-hydraulic phenomena.

A total of 10 Semiscale simulations⁹ were performed with the objective of gaining a more fundamental understanding of the thermal-hydraulic phenomena that occurred in the TMI reactor. These simulations used a scaled mock-up of the TMI surge line, including hydraulic resistances, elevations, and point of connection to the loop hot leg in the TMI plant. Several unknown aspects relative to the actual TMI-plant transient required a certain amount of educated speculation in order to complete the tests, such as the value of the actual HPIS flow rate as a function of time and the letdown/makeup flow histories. The primary result of the simulations, with respect to the pressurizer, is that core uncover and core heatup occurred in the Semiscale simulations even though the pressurizer remained filled with liquid. The pressurizer-level response was noted to be generally similar in trend to the measured plant pressurizer-level behavior. Although there were shifts in the timing, the Semiscale level basically showed filling trends as the transient progressed. It was clearly demonstrated that the pressurizer level was an inappropriate reflection of system mass inventory when the system was in a saturated two-phase state.

A comparison of the TMI and Semiscale pressurizer-level variations is illustrated in Figure 6. Two parameters found important in the level variations were the HPIS injection rate and the average system temperature resulting from the auxiliary feedwater flow. During the Semiscale tests, the pumps remained running for the first 100 min, at which time the pumps were shut off. At 100 min, the Semiscale collapsed liquid level was near the top of the core. The pressurizer was nearly full during the entire period of core uncover, even though mass was leaving through the PORV. Thus, an equivalent amount of mass was entering the surge line from the hot leg. The most likely source for the mass entering the surge line was steam produced in the core that eventually condensed in the pressurizer surge line or the pressurizer.

CONCLUSIONS

As a result of the study for which the results have been summarized in this paper, the following conclusions have been reached.

- o The pressurizer-liquid-level measurement was indicating the correct level in the pressurizer, within an uncertainty of approximately 4%. The measured level can be used for comparison to calculated level from systems analysis.
- o The major pressurizer-liquid-level changes have been explained in terms of response to the thermal-hydraulic conditions in the pressurizer and the remainder of the RCS. This study has provided valuable insights into thermal-hydraulic interactions and has helped to determine the boundary conditions for further analysis of the accident.
- o No supporting evidence of damage to the pressurizer liquid level measurement system has been discovered. Neither measured data from the accident nor thermodynamic considerations supports the argument for impaired level measurement.
- o During periods when the pressurizer heaters were undergoing ground fault trips, the available evidence indicates that the pressurizer was full of very-subcooled liquid [as much as 150 K (275°F) subcooled]]. Further investigation of the heater trips is required to resolve the mechanism causing the ground fault. This investigation should include removal and physical examination of the heaters.

REFERENCES

1. J. L. Anderson, Analysis of TMI-2 Pressurizer Level Indications, EGG-TMI-7100, January 1986.
2. J. O. Henrie, Rockwell Hanford, letter to J. C. DeVine, Jr., GPU Nuclear, TMI-2 Accident Analysis, June 13, 1985.
3. T. A. Hendrickson, Burns & Roe, letter to W. H. Hamilton, Chairman of TAAG, TMI-2 Accident Analysis, April 30, 1985.
4. M. L. Picklesimer, The Sequence of Core Damage in TMI-2, PIC Product Company memorandum.
5. M. Rogovin and G. T. Frampton, Jr., Three Mile Island--A Report to the Commissioners and to the Public, Volume II, U.S. NRC Special Inquiry Group, NUREG/CR-1250, Vol. II, January 1980.
6. T. L. Witbeck and J. Putman, Three Mile Island Unit II: Annotated Sequence of Events: March 28, 1979, GPU Nuclear, TDR-044, March 5, 1981.

7. D. A. Powers, "Hydrogen effervescence and the Pressurizer Level Detector," Appendix II.10, pg 763, Vol II, Part 2, Three Mile Island: A Report to the Commissioners and to the Public, (the Rogovin Report), 1979.
8. H. Warren et al., Interpretation of TMI-2 Instrument Data, NSAC-28, May 1982.
9. T. K. Larson et al., Semiscale Simulations of the Three Mile Island Transient - A Summary Report, SEMI-TR-010, July 1979.
10. C. L. Nalezny, Summary of the Nuclear Regulatory Commission's LOFT Program Experiments, NUREG/CR-3214, EGG-2248, July 1983.
11. K. Tasaka et al., "The ROSA-IV Program TMI-2 Scenario Experiments: A Multifaceted Investigation". June 1985.

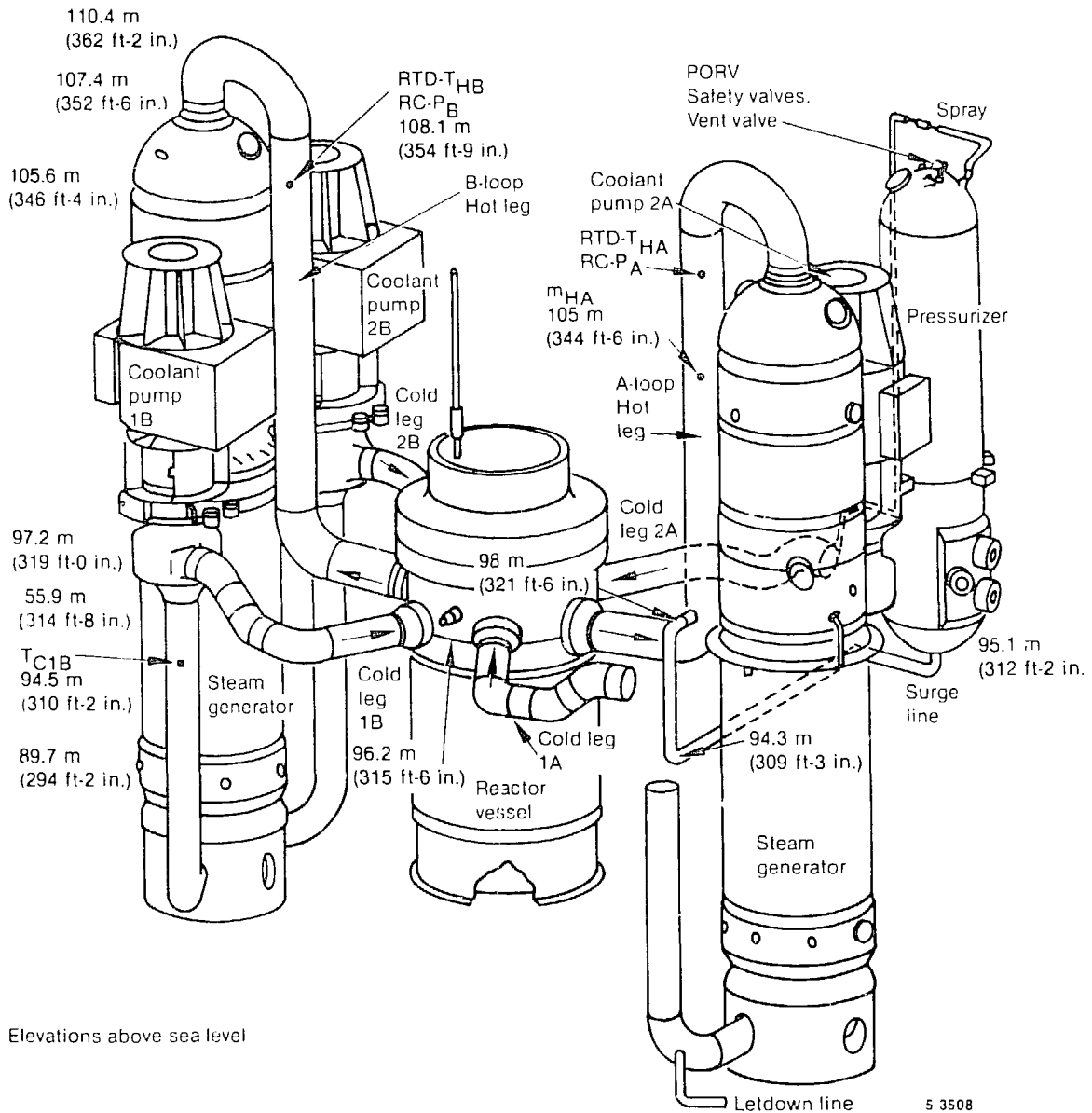
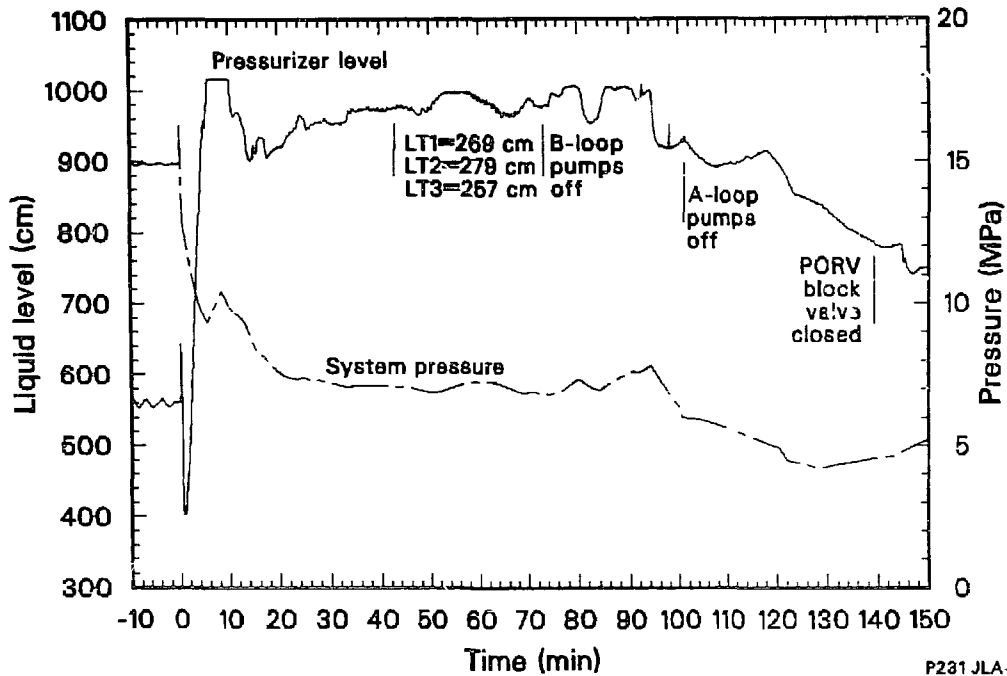
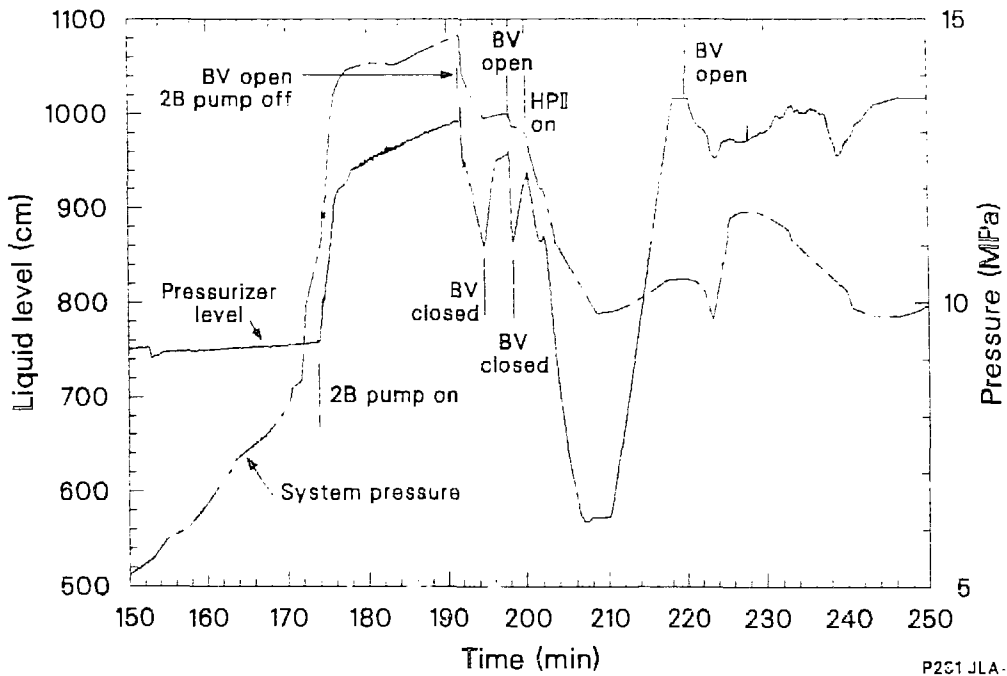


Figure 1. TMI-2 isometric schematic drawing.



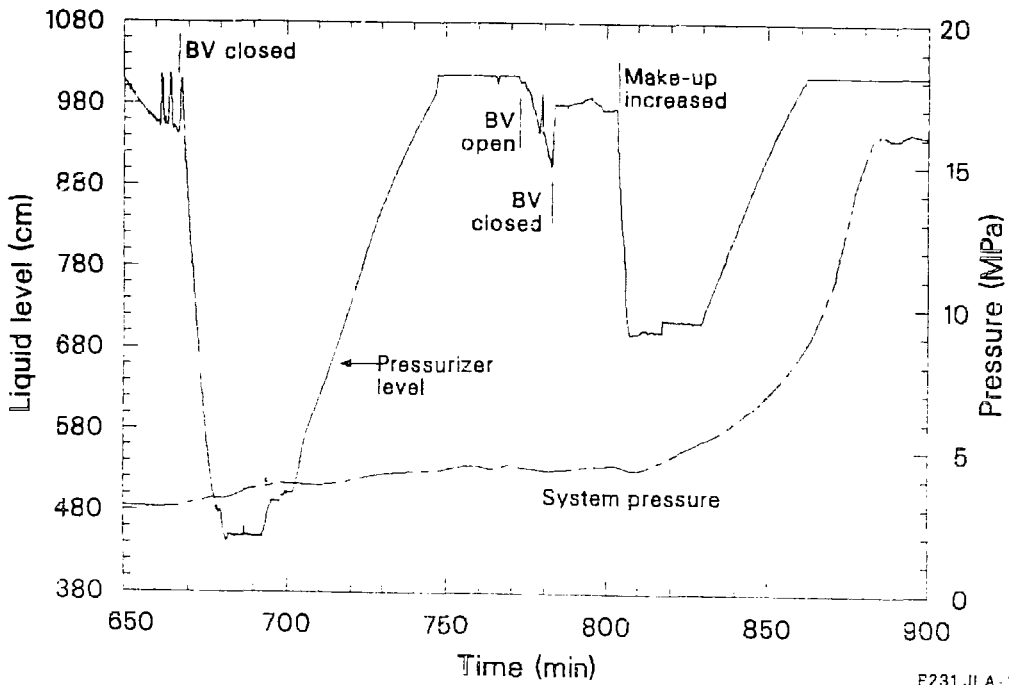
P231 JLA-285-01

Figure 3. Comparison of pressurizer level and primary system pressure (composite).



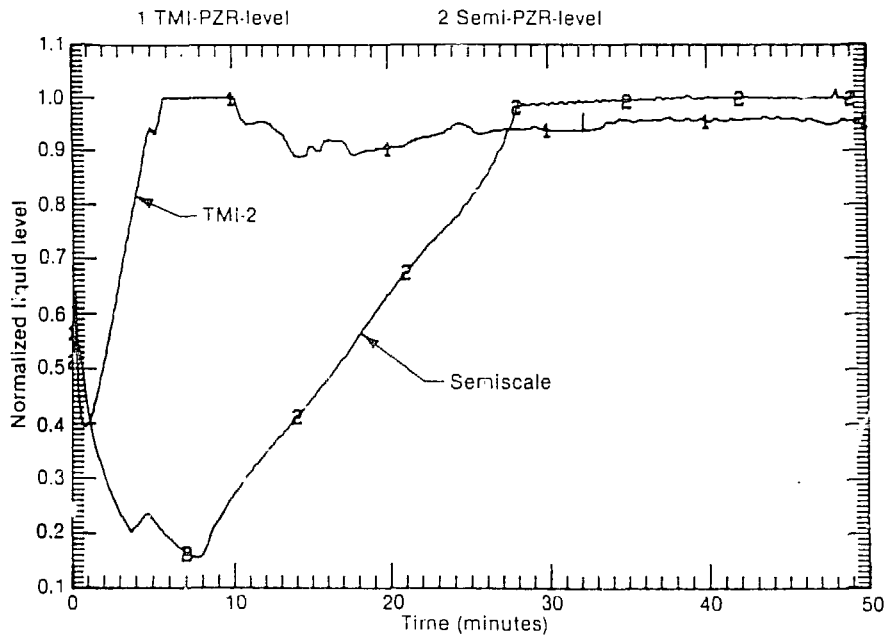
P231 JLA-285-02

Figure 4. Comparison of pressurizer level and primary system pressure (composite).



F231 JLA-285-03

Figure 5. Comparison of pressurizer level and primary system pressure (composite).



6 0650

Figure 6. Comparison of TMI-2 and Semiscale normalized pressurizer liquid levels.

TMI SPND INTERPRETATION

D. J. N. Taylor
Idaho National Engineering Laboratory
EG&G Idaho, Inc.
P.O. Box 1625, Idaho Falls, ID 83415

ABSTRACT

This paper interprets the SPND signals generated during the TMI-2 accident. The interpretation of the signals is based on laboratory and LOFT testing of the SPNDs. The test results are also reported.

INTRODUCTION

The potential for obtaining local core temperatures from the in-core data, if the SPNDs could be calibrated for temperature, has been recognized by TMI-2 accident investigators. Knowledge of local core temperatures could then be used to benchmark the core damage scenarios. For example, the core liquid level has been inferred by using the SPND data. This has been the primary stimulus for the investigation of SPND response. The following is a brief discussion of the TMI-2 accident as it relates to the SPND response.

Just before the start of the TMI-2 accident on 28 March 1979, the reactor was at 97% power. The in-core SPNDs (364 distributed throughout the TMI-2 core) were producing signals between +500 to +850 nanoamps. At the start of the accident (4:00 a.m.), the reactor was tripped. The SPNDs responded as expected with their signals dropping to zero. At 135 min into the accident, the SPNDs produced a negative polarity signal. The magnitude of the negative currents was not recorded. At 150 min, the signals from several of the SPNDs switched polarity to a positive state, and they eventually saturated the data acquisition system at 1500 nanoamps. When the computer resumed recording the data again at 167 min into the accident, most of the SPNDs recorded were generating positive signals. This anomalous signal production occurred during the initial core heatup and initial core damage. The anomalous response of the SPNDs is thought to be due to a combination of the high temperature in the reactor core and also to the physical and chemical environment surrounding the SPNDs and their lead wires in the reactor vessel.

SPND DESCRIPTION AND INSTALLATION

During normal reactor power operation, the SPND measures local thermal neutron flux. Figure 1 illustrates the cross section of the active end of a typical SPND. An individual SPND consists of:

- o A rhodium emitter (0.018-in. dia x 4.75-in. long)
- o Alumina insulation

- A zircaloy-2 center conductor lead wire (0.011-in. dia x 128-ft long)
- An Inconel 600 sheath (.0625-in. O.D. x .0425-in. I.D. x 128-ft long).

Three hundred sixty-four SPNDs were distributed throughout the TMI-2 core in 52 instrument stalks; each contained 7 SPNDs. The vertical spacing between adjacent SPNDs was 20 in.

SPND DATA SOURCES AT TMI

Plant Computer

The state of each of the 364 SPNDs was monitored by the plant computer. Once every minute, the plant computer would interrogate each of the 364 SPNDs in sequential order. The plant computer would then record the state of the SPND on an alarm printer if the SPND had changed states from offscale to onscale or from onscale to offscale during the one-min time interval. The onscale limits ranged between -20 to 2000 nanoamps. Whenever the SPND alarmed offscale, the alarm record consisted of a series of four question marks. The magnitude and sign of the generated signal would be printed when the SPND alarmed onscale. If the SPND did not change states during the one-min time interval, there was no record. The alarm data from 73 to 168 min after turbine trip, were irretrievably lost. The initial core heatup and uncover occurred during this time interval.

Backup Multipoint Recorders

In addition to the plant computer, two multipoint recorders monitored the output signal from 36 selected SPNDs. The range of recording was -20 to 1500 nanoamps. These SPNDs were at the 2 (30-in.), 4 (70-in.), and 6 (110-in.) levels. The parentheses indicate the distance between the center of the emitter of the SPND and the bottom of the reactor core. A data point was printed every 2.5 min (24/h). Once each hour, a channel identification number was printed adjacent to a data point. Just prior to turbine trip and reactor scram, the SPND currents ranged between 500 to 850 nanoamps. At reactor scram, the SPND output dropped to a few nanoamps, indicating a normal shutdown. At 135 min into the accident, the first indication of anomalous signal production by the SPNDs was recorded. The signal was negative and its magnitude was greater than 20 nanoamps. At 150 min, most of the SPND channels on both multipoint recorders began registering positive currents. During the initial study of the SPND response at TMI, the multipoint data was ignored because it was very difficult to associate a channel number with the recorded data point. Recently, 17 channels from one of the multipoint recorders have been decoded and digitized.

The results for the SPND instrument string at the center of the core (H8 position) are plotted in Figure 2. These data suggest a top to bottom core uncover and a top to bottom instrument heatup and damage sequence. Several events are indicated in this figure. At 101 min into the accident,

the "A" loop pumps were tripped. The first negative SPND signals were generated at 135 min. An abnormal radiation release was first indicated at 142 min. At 174 min, the 2B pump was turned on and flow was briefly reestablished in the "B" loop.

SEPARATE EFFECTS (LABORATORY) TESTING

Previous investigators postulated and tested under controlled laboratory conditions several physical mechanisms that could possibly cause the anomaly and SPND signals. Warren¹ from B&W postulated that the elevated temperatures in the reactor core caused the anomalous current generation of the SPNDs. He temperature cycled five SPND assemblies several times in a furnace and on the last cycle, they were heated to their failure point (1310 to 1700 K). Warren's results were qualitatively different from the TMI results. At low temperatures (T less than 810 K), the SPNDs generated small positive signals (they were much smaller than the signals generated at TMI). At higher temperatures, the generated currents changed to a negative polarity and the magnitude increased with increasing temperature. Warren was not able to reproduce the large positive signals generated at TMI.

Warren then postulated that a gamma field in combination with elevated temperatures could produce the positive signals. Baldwin and Warren² next tested a SPND in a gamma radiation field of 2.2×10^5 R/h at temperatures of 589, 811, and 1089 K. The gamma radiation field did not substantially alter the SPND signals at these temperatures. They concluded from these tests that no mechanism had been identified that would produce the large positive signals seen at TMI.

Anderson³ from ORNL next tested a TMI-type SPND in a furnace. The test procedure and test results were similar to the first series of the Warren tests. Anderson concluded that the response of the SPND to increased temperature is dominated by the lead material and not the rhodium emitter.

Cannon⁴ from HEOL tested a Reuter-Stokes⁴ model SPND, which like the B&W instrument, had a rhodium element for detecting neutrons. It also had Alumina as an insulation and Inconel 600 as the outer sheath. It differed from the TMI-type SPND in at least two ways:

- o The center lead wire was Inconel 600 versus zircaloy-2 for the TMI type
- o The length of the emitter was 40 cm versus 12 cm for the TMI type.

Cannon heated the single Reuter-Stokes SPND with a ruptured sheath in a steam environment to temperatures above 1175 K. He observed the following:

- o At high temperatures (T greater than 1175 K), positive output currents were generated by the SPNDs in the range between 2000-3000 nA.

- The output currents generally increased with increasing temperature.
- Steam appeared to be responsible for the positive output signals. When steam was removed the output signal dropped to below 50 nA.
- The effect observed was proportional to the length of the rhodium emitter heated, i.e., reducing the heated length of the emitter by a factor of two reduced the output signal by about a similar factor of two.

The next series of separate effect tests were performed by this author at the INEL. In the first series of tests, a set of SPNDs (different types) with an intact sheath were repeatedly cycled in temperature and heated to failure in a steam envelope. In the second series of tests, the sheath of the SPND was ruptured and the whole assembly was heated in a furnace in an envelope of steam (0.5 atm). The following types of SPNDs were tested:

- Two TMI-type SPNDs with a 4.75-in. rhodium emitter, Alumina insulation, zircaloy-2 lead wire and Inconel 600 sheath
- Two TMI-type SPNDs that were identical to the type described above, except that they did not have the rhodium emitter
- A Reuter-Stokes SPND that had a rhodium emitter, Inconel 600 sheath and lead wire (center conductor), and Alumina insulation
- A Reuter-Stokes SPND without the rhodium emitter,
- A SPND with a rhodium emitter, rhodium lead wire, Alumina insulation, and Inconel 600 oversheath.

In addition to the five types of SPNDs tested, an Inconel 600, zircaloy-2 thermocouple was fabricated and tested in a furnace.

The test results using Type 1 and 2 SPNDs were similar to Warren. The generated currents were positive and small between 650 to 850 K. At temperatures greater than 850 K, the signals became negative and their magnitude became progressively larger with increasing temperature.

The test results from both of the Reuter-Stokes-types of SPNDs were like those reported by Cannon⁴. They generated positive signals of about 10 mA at 1300 K.

The signal generated by the rhodium emitter and rhodium lead wire was negative, and was approximately the same magnitude as the B&W-type SPND.

The Inconel-zircaloy-2 thermocouple produced a negative signal.

The following conclusions can be drawn from the separate effects testing:

- o The large positive currents generated by the B&W-type SPNDs at TMI have not been reproduced in the laboratory.
- o No physical mechanism has been identified for the production of positive signals by the SPNDs.
- o All of the investigators working with B&W-type SPNDs have shown that there is a transition temperature when the current changes polarity (positive to negative) at about 850 K.
- o One physical mechanism for negative current production has been proposed and has had some experimental justification (i.e., the SPND acts like a thermocouple at sufficiently high temperatures.)

LOFT TESTING

Because the separate effects testing failed to reproduce the positive signals recorded at TMI, four SPNDs were installed in the LOFT facility at the INEL for the LP-FP-2 test.

An instrument thimble containing four rhodium-type SPNDs was fabricated by B&W and installed in the center fuel module of the LOFT nuclear core. The top two SPNDs were damaged during installation, which left the bottom two SPNDs functional. The center of rhodium emitters were positioned at 11 in. and 27 in. above the bottom of the core. The individually encapsulated SPNDs and lead wires were 29-ft long. They were identical to those installed at TMI-2 except for their length. At TMI, the SPNDs were 120 to 130-ft long. The difference in hard lead wire length introduced an additional resistance of about 500 ohms in the TMI SPND.

Differences Between LOFT and TMI

At TMI, the active core region consisted of 177 individual fuel assemblies. Each assembly was a 15 x 15 array containing 16 zircaloy guide tubes, 1 zircaloy instrument tube, and 208 fuel rods. The height of the active fuel core was 12 ft. The LOFT core for the LP-FP-2 test contained nine fuel bundles. There were four (15 x 15) full-size, four half-size fuel bundles, and the center bundle was an 11 x 11 array. The height of the LOFT core was 5.5 ft. The LOFT core was about 2% of the volume of the TMI core. All nine fuel bundles at LOFT were uncovered during the LP-FP-2 test; however, the center fuel bundle was the only one that was damaged. To contain the damage, the center fuel bundle was surrounded by a full-length ceramic heat shield that effectively thermally isolated the center fuel bundle from the rest of the core. The LOFT center fuel bundle, like several fuel modules of the TMI-2 core, contained full-length silver-indium-cadmium control rods. The center fuel bundle at LOFT was instrumented with several high-temperature thermocouples to record the heatup. Like parts of the TMI-2 core, the LOFT center fuel bundle overheated, oxidized, melted, and relocated.

Three significant differences between the TMI accident and the LOFT LP-FP-2 test were:

- The volume of the damaged region at TMI was larger.
- The system pressure at LOFT during the heatup and the fuel relocation ranged between 100 to 150 psi; whereas, at TMI the system pressure during the core heatup and core damage phases stayed above 1000 psi.
- The time interval when fuel damage was occurring was much smaller at LOFT than it was at TMI.

LOFT SPND Test Results

The LOFT LP-FP-2 test was a loss of coolant accident with a delayed emergency core cooling. The core was uncovered, and the center fuel bundle overheated, oxidized, melted, and relocated.

There are three major observations in the LOFT test results.

- Both the 11-in. and the 27-in. SPND responded to the core heatup in LOFT. Both initially produced negative signals.
- The 11-in. SPND generated negative signals throughout the test. It did not change polarity.
- The 27-in. SPND changed polarity (negative to positive) at 1430 s into the test. This corresponded to a rapid increase in the temperature of a tungsten-rhenium thermocouple that was attached to the guide tube immediately adjacent to that SPND.

Both the 27-in. and the 11-in. SPND began producing negative polarity signals at 1140 s. At this time, the temperature near the top SPND was near 850 K. At 1430 s, the 27-in. instrument started to produce large positive signals and soon saturated the signal conditioning. The temperature near the transducer was now 1350 K. The highest temperature registered at the closest thermocouple to the bottom SPND did not exceed 1250 K during the test. Figure 3 shows the response of the 27-in. SPND.

SUMMARY OF ANALYSIS

Negative Current Production

A common feature exhibited in most of the separate effects tests and in LOFT was the SPNDs generating negative signals. Some experimental evidence, reported in this paper, indicates that one of the responsible mechanisms was the Seebeck or thermoelectric effect. The three separate elements needed to produce a Seebeck current are:

- The presence of two dissimilar metals
- A circuit (conducting path) made up from the dissimilar metals
- A temperature gradient along the circuit.

The B&W SPND does consist of three different metals; however, a temperature gradient only exists along the Inconel 600 sheath and zircaloy-2 lead wire. The conducting path (junction) joining the two metals could be either or both virtual and real. A virtual junction is caused by a leakage current through the Alumina insulation at a sufficiently high temperature. Pure Alumina is an intrinsic semiconductor. Because it is a semiconductor, its conductivity increases exponentially with temperature. Therefore, at a sufficiently high temperature, Alumina would provide a conductive path that would complete the circuit. The presence of impurities, including residual moisture, in the intact sheathed instrument would tend to increase the conductivity of the Alumina. Virtual junction formation in thermocouples has been studied and modeled by investigators⁵ at ORNL. The estimated threshold temperature where the SPNDs would produce detectable signals on the TMI data acquisition system would be in the range 800 to 925 K.

A real junction connecting the lead wire to the sheath could also have been formed; however, it would require a higher temperature than for virtual junction formation. For example, the SPND could melt and form a metallic bridge, connecting the lead wire to the sheath.

Positive Signal Production

In addition to the thermoelectric effect, a second possible physical mechanism has been proposed as the driving force for the production of anomalous signals in the SPNDs. This mechanism is called electrochemical or galvanic. Three conditions that must be satisfied to produce a galvanic couple are:

- o An oxidation and/or a reduction reaction occurring on the surface of the center zircaloy lead wire (rhodium emitter), and Inconel 600 sheath
- o An electrolyte (current path) connecting the lead wire to the outer sheath
- o A conducting path from the galvanic couple to the data acquisition system.

An analysis indicates that at a high enough temperature ($T > 1400$ K), conditions would have been present at TMI for the production of electrochemical currents from the SPNDs. The separate effects testing neither proved or disproved the viability of electrochemical current production. Additional analysis showed that if the center zircaloy lead wire was undergoing an oxidation reaction, then the SPND would generate negative signals. The electrochemical oxidation of 1 microgram of zircaloy would be sufficient to account for all of the negative signal production from an individual SPND. If the center zircaloy lead wire were undergoing a reduction reaction, then the instrument would generate a positive signal.

CONCLUSIONS AND RECOMMENDATIONS

The results of this investigation lead to the conclusions that:

- o Local temperatures can be deduced only at specific times (i.e., at changes in the signal polarity).
- o Two threshold temperatures have been established; the first is at 850 K when the SPNDs generated detectable negative signals (deduced from both the separate effects and the LOFT tests), and the second is at 1350 K when the SPNDs first produced positive signals (observed only at TMI and in the LOFT test).
- o The results from the analysis of the TMI-SPND data base interpreted through laboratory and LOFT testing has been only partially definitive. There are large uncertainties in the results.

REFERENCES

1. Holland D. Warren, SPND Thermal Currents in a Furnace, Appendix B, Interpretation of TMI-2 Instruments and Data, NSAC-28, 1982.
2. M. N. Baldwin and H. D. Warren, SPND Thermal Currents in a Furnace and Gamma Ray Field, Appendix C, Interpretation of TMI-2 Instruments and Data, NSAC-28, 1982.
3. R. L. Anderson, Thermally Excited Currents in Self-Powered Neutron Detectors, a letter report to EG&G Idaho, dated September 27, 1982.
4. C. P. Cannon et al, Mechanisms for Anomalous Signal Outputs from Self-Powered Neutron Detectors During the TMI-2 Accident, a letter report to the U.S. Dept. of Energy, Middletown, PA, dated October 31, 1984.
5. M. J. Roberts and T. C. Kollie, "Derivation and Testing of a Model to Calculate Electrical Shunting and Leakage Errors in Sheath Thermocouples", Rev. Sci. Instrument, Vol. 48, No. 9, September 1977.

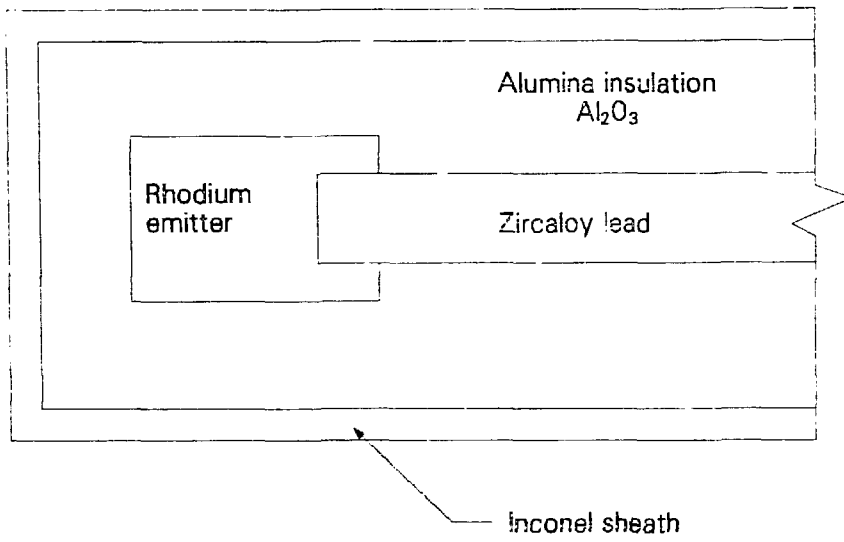
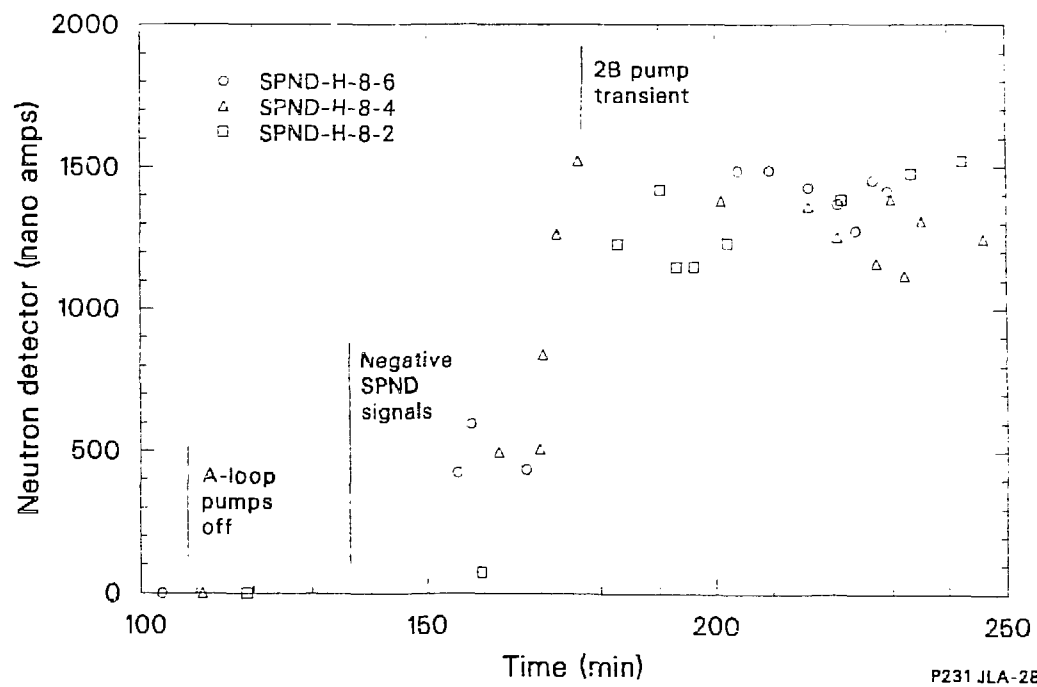


Figure 1. TMI-2 SPND.



P231 JLA-285-05

Figure 2. TMI-2 SPND signals.

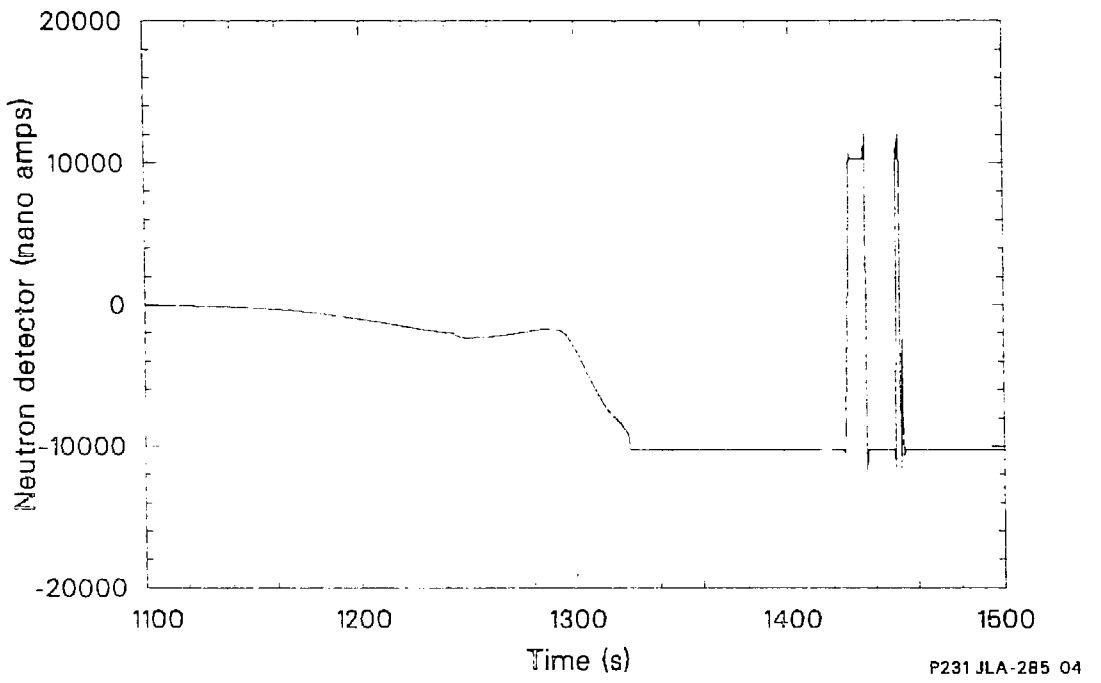


Figure 3. SPND results from LOFT LP-FP-2.

IN-CORE INSTRUMENT SURVIVABILITY

R. D. Meininger
Idaho National Engineering Laboratory
EG&G Idaho, Inc.
P.O. Box 1625, Idaho Falls, ID 83415

NOT RECEIVED IN TIME TO BE
INCLUDED IN THE PROCEEDINGS.

CORE DEBRIS BED AND FISSION-PRODUCT BEHAVIOR

TMI-2 CORE DEBRIS ANALYSIS

B. A. Cook and E. R. Carlson
Idaho National Engineering Laboratory
EG&G Idaho, Inc.
P.O. Box 1625, Idaho Falls, ID 83415

One of the ongoing examination tasks for the damaged TMI-2 reactor is analysis of samples of debris obtained from the debris bed presently at the top of the core. This paper summarizes the results reported in the TMI-2 Core Debris Grab Sample Examination and Analysis Report, which will be available early in 1986. The sampling and analysis procedures are presented, and information is provided on the key results as they relate to the present core condition, peak temperatures during the transient, temperature history, chemical interactions, and core relocation. The results are then summarized.

Figure 1 shows the current condition of the core, as determined from closed-circuit television, core topography, and debris bed probing examinations. It is estimated that the debris bed represents approximately 20% of the original core mass, and is supported by a hard crust below, which is approximately 65% of the core, located between the debris bed and the elliptical flow distributor. Figure 1 also shows the 11 locations where the core debris grab samples were taken. Ten to 20% of the core mass is located in the lower plenum of the reactor vessel.

The samples were obtained from two fuel assembly locations, H8 (center) and E9 (mid-radius). Two different sampling devices were used to extract material from the debris bed. A clamshell-type tool was used to obtain samples from the surface of the debris bed (Figure 2), and a rotating-tube device was used to obtain the subsurface samples (Figure 3). Figure 4 shows Sample 1 (H8, surface) after it was removed from the clamshell sampler. One sample was examined at the B&W Lynchburg Research Center, and 10 samples were examined at the INEL. Of the 10 samples examined at INEL, fragmented chips from 7 particles were examined by Rockwell Hanford Operations using differential thermal analysis, and 22 particles were shipped to ANL (West and East) for metallurgical and chemical analyses.

Physical examinations of the samples included visual and photographic examinations, weighing, bulk tap density measurements, particle-size distribution analysis, and ferromagnetic and pyrophoricity tests. Five types of particles were identified based on visual appearance: (a) obvious fuel pieces; (b) cladding chunks; (c) foamy/porous, prior-molten material; (d) composite particles of fuel and prior-molten material; and (e) metallic-appearing, prior-molten particles.

Bulk tap density measurements indicated that there were two density ranges for the samples. Samples 1, 3, and 6 had densities ranging from 3.5 to 3.8 g/cm³, whereas Samples 9, 10, and 11 had densities ranging

from 5.0 to 5.5 g/cm³. The particle-size distribution analysis indicated that Samples 1 and 3 had the largest fraction of material in the 1680 to 4000- μ m particle-size range, and Samples 9, 10, and 11 showed a bimodal distribution, with peaks at the 1680 to 4000- μ m and 297 to 707- μ m sizes. The bimodal distribution probably resulted in more efficient packing of the debris material and may explain the higher densities of Samples 9, 10, and 11. The particle-size distribution analysis indicated the presence of larger particles (more than 80 wt% greater than 1000 μ m). Stratification of the debris bed into two layers also is indicated by the particle-size distribution: a surface layer, and a lower layer beginning between 36 cm and 56 cm below the debris bed surface. The lower layer contains larger quantities of smaller-sized particles. The measurable ferromagnetic material content of Sample 6, the only sample analyzed for ferromagnetic content, was 0.9% of the total sample weight.

Twenty-nine particles were selected from the 10 core debris grab samples for detailed metallurgical analysis, which included optical and scanning electron microscopy for microstructural information and energy dispersive x-ray spectroscopy and scanning Auger spectroscopy for information on elemental composition. The particles selected for examination were not a random sample, but were selected for specific features of interest, such as obvious molten appearance or mixing of visibly different materials.

Two views of Particle 10A are shown in Figure 5. This sample was taken from the 28-3/4-inch elevation of position E9. It had a shiny glazed surface appearance. The polished cross section of this particle is shown in Figure 6 and higher magnification photographs are shown in Figure 7. This particle is composed entirely of (U,Zr)O₂ with no grain boundary or other phases and practically no inclusions. There are three different zirconium contents within this particle. The high-zirconium-content material is about 7 at.% Zr and is generally found around cracks, edges, and voids. This material tends to be almost pore free and contains a trace of iron (Fe). The middle-zirconium-content material is about 1-1/2 at.% Zr and is found throughout most of the particle. This material contains many small (<10 μ m) voids. The low-zirconium-content material is about 0.5 at.% to no zirconium and is found in a small central region. This was the only material in this particle to exhibit a grain structure; the grain size is approximately 28 μ m.

The particle has a previously molten appearance. The small amount of Zr or other impurities indicates a melting temperature approaching the UO₂ melting temperature of approximately 3100 K. This particle appears to have been a piece of fuel that interacted with ZrO₂ near the UO₂ melting point. The prior-molten ceramic material has a dense, almost glassy appearance, indicating temperatures somewhat above the liquidus temperature and then rapid cooling. No grain structure could be found outside of the central restructured zone, either during the optical examination using etches or during the SEM examination.

Particle 3L is shown in Figures 8 and 9. This particle exhibits several layers, with different porosity in each of the regions. This particle is predominantly (U,Zr)O₂ with slight variations in the Zr/U

ratios between the regions. The only occurrence of other elements is in and around a few large pores. A minimum melting temperature for the (U,Zr)O₂ has been established at 2810 K. The melting temperatures were found to increase only for compositions near UO₂ (melting point = 3120 K) or ZrO₂ (melting point = 2973 K). It also has been demonstrated that a foamy structure with large voids is formed very near the melting point, but the (U,Zr)O₂ displays a much more dense structure upon exposure to temperatures above the liquidus.¹ Particle 3L also shows dendritic freezing in the (U,Zr)O₂--separation of the UO₂-ZrO₂ homogeneous liquid into U-rich and Zr-rich phases--indicating slow cooling from above the liquidus (Figure 9). Therefore, the particle indicates peak temperatures above 2800 K with slow cooling and layering of molten materials.

Particle 10F (Figure 10) is another example of a prior-molten material with layering and large pores. The region containing the small, irregular-shaped pores is composed of (U,Zr)O_{2+x} with a trace of Fe. There is very little grain boundary or second-phase material in this region. The other region contains large round pores and also is composed of (U,Zr)O_{2+x} with a trace of Fe. The Zr-to-U ratio is slightly higher in the second region and there are extensive amounts of grain boundary phases containing Cr, Fe, and Ni. There is also a fine-grained second-phase material found in the second region that contains the same constituents as the base material, but with more Fe, slightly more Zr, and less oxygen. The second-phase material is hypostoichiometric, while the base material is hyperstoichiometric.

Particle 1A is a recognizable fuel piece with the cladding attached (Figures 11 and 12). This particle provided information on how the liquified material (UO₂ dissolved by molten Zr) relocates. This phenomena is important in the calculation of the peak temperatures achieved. If the molten Zr relocates immediately upon melting, then the temperature escalation, as a result of the exothermic oxidation reaction of the Zr and the steam, stops. If the molten Zr is held in place by an outer ZrO₂ layer, as seen in Particle 1A, then the oxidation continues and the temperature continues to rise. Figure 12 shows an outer layer of ZrO₂ and oxygen-stabilized alpha Zr containing a layer of prior-molten metallic (U,Zr,O), and then a fragment of a UO₂ fuel pellet. The peak temperature of this particle was greater than 2170 K (the melting point of the Zr), but below 2245 K (the melting point of the oxygen-stabilized alpha Zr).

Prior-molten structural materials were observed in a few samples. Two examples are shown in Figures 13, 14, and 15. Particle 9D consists of metallic Ag mechanically bonded to several small pieces of U-Zr ceramic material. The metallic Ag material has round inclusions containing Ni, Sn, and traces of Fe. The U-to-Zr ratio in the ceramic material varies from piece to piece. This indicates significant mixing of the core materials, especially after melting and oxidation of the U-Zr material (Zr and Ag will interact in the absence of O). Sample 9G is a particle containing mostly Ag with small amounts of Ni included. Very little Ag material was found in the debris samples.

The examination of the core debris from the upper part of the TMI-2 core has provided indication of the present core condition, the peak

temperatures achieved during the transient, the temperature history, chemical interactions between the core components, and core relocation. Some principal fuel behavior observations/conclusions from the examination of the core debris samples are:

- 80 wt% of the debris is greater than 1000 μm in size
- Two layers exist in the debris bed, with the lower layer containing larger quantities of small particles
- Many particles indicate temperatures greater than 2800 K
- A few particles indicate temperatures up to 3100 K.
- There is evidence of candling and multiple temperature ramps, with molten metallic Zr flowing inside ballooned rods
- There was significant interaction between fuel rods, grid spacers, and the stainless steel structural components.

The Ag-Zr alloy was not found in the debris bed, indicating oxidation of the molten Zr before contact with the Ag.

The core debris was well mixed on a macrographic scale, but heterogeneous on a particle scale.

REFERENCE

1. P. Hofmann, private communication, KFK, Federal Republic of Germany, SFD Program Meeting, Idaho Falls, ID, April 16-19, 1985.

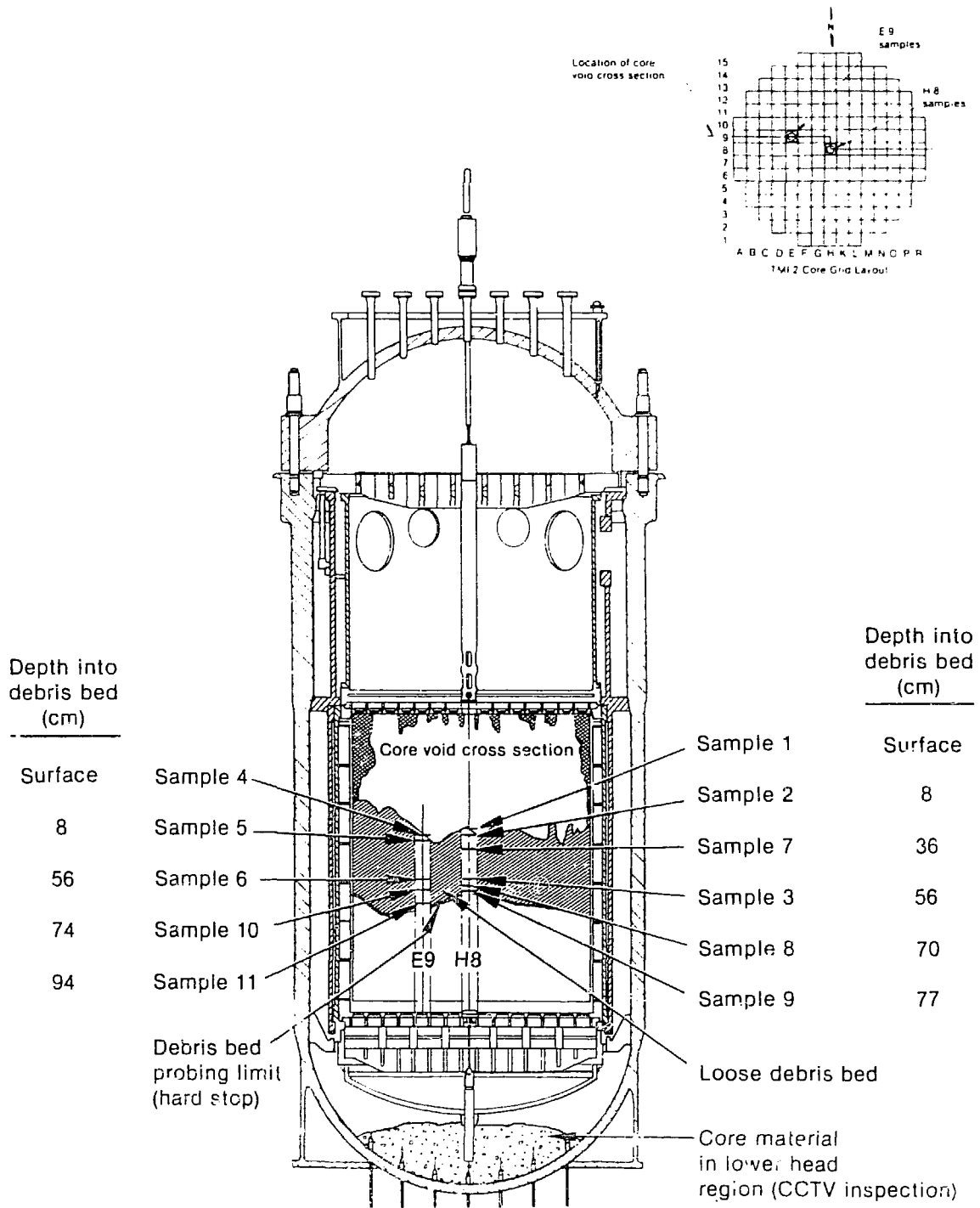


Figure 1. TMI-2 core debris grab samples

5 3264

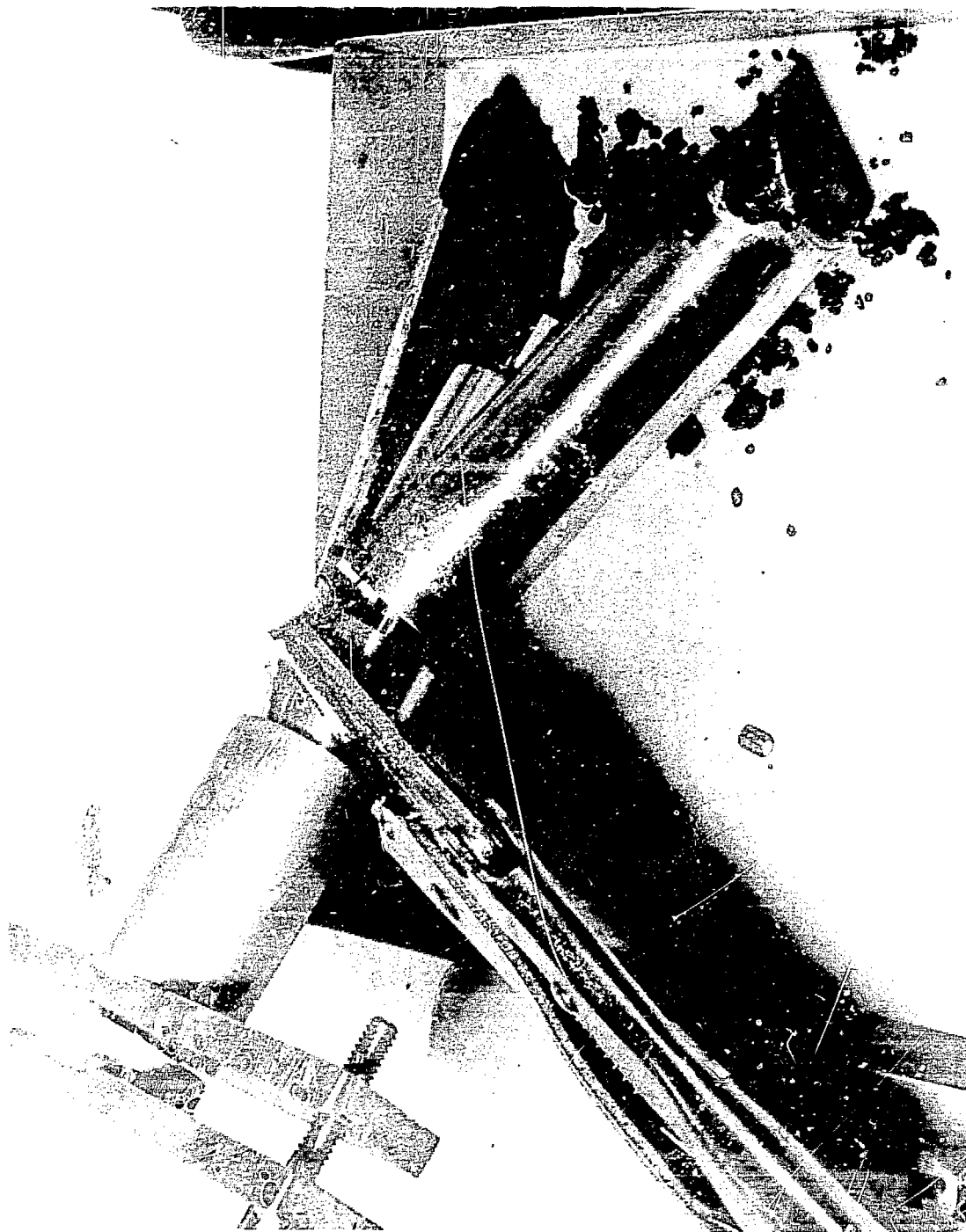


Figure 2. TMI-2 core debris Sample 1 being removed from clamshell (surface-H8)



Figure 3. Stratified material in sampling tool for Sample 3
(H8, 55 cm)

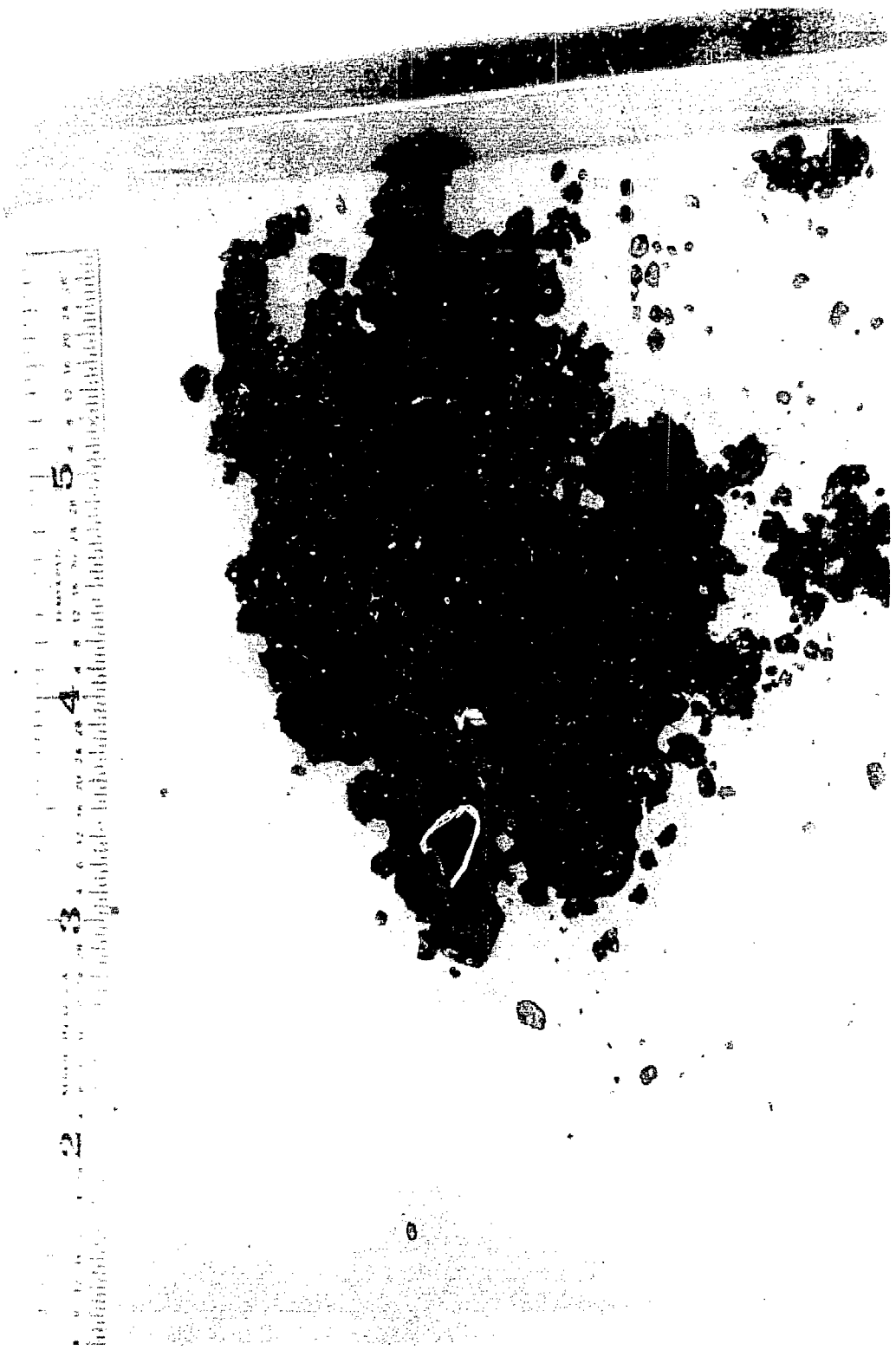


Figure 4. The bulk material for Sample 1 (H8, surface)

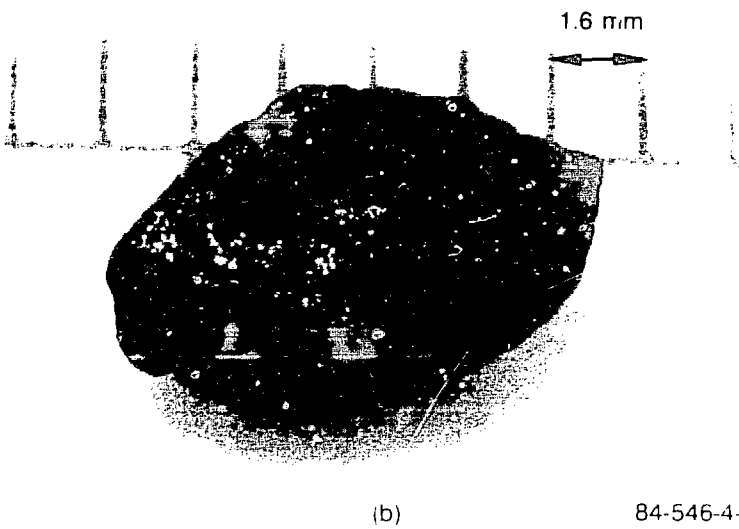
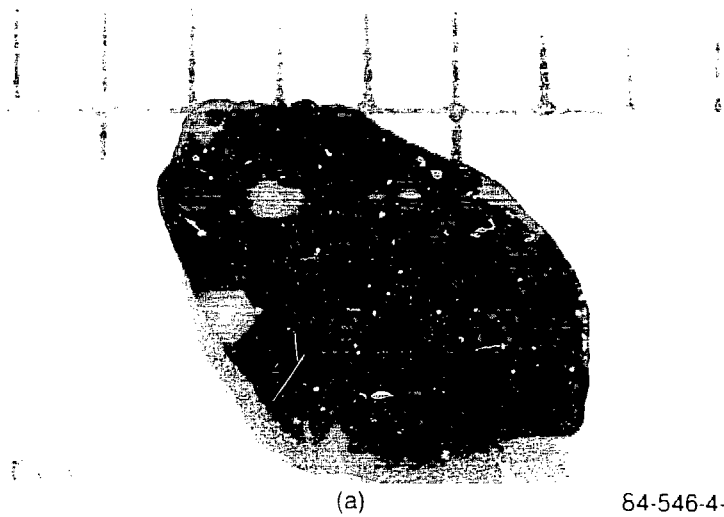


Figure 5. Particle 10A from the 28-3/4-in elevation at location 19

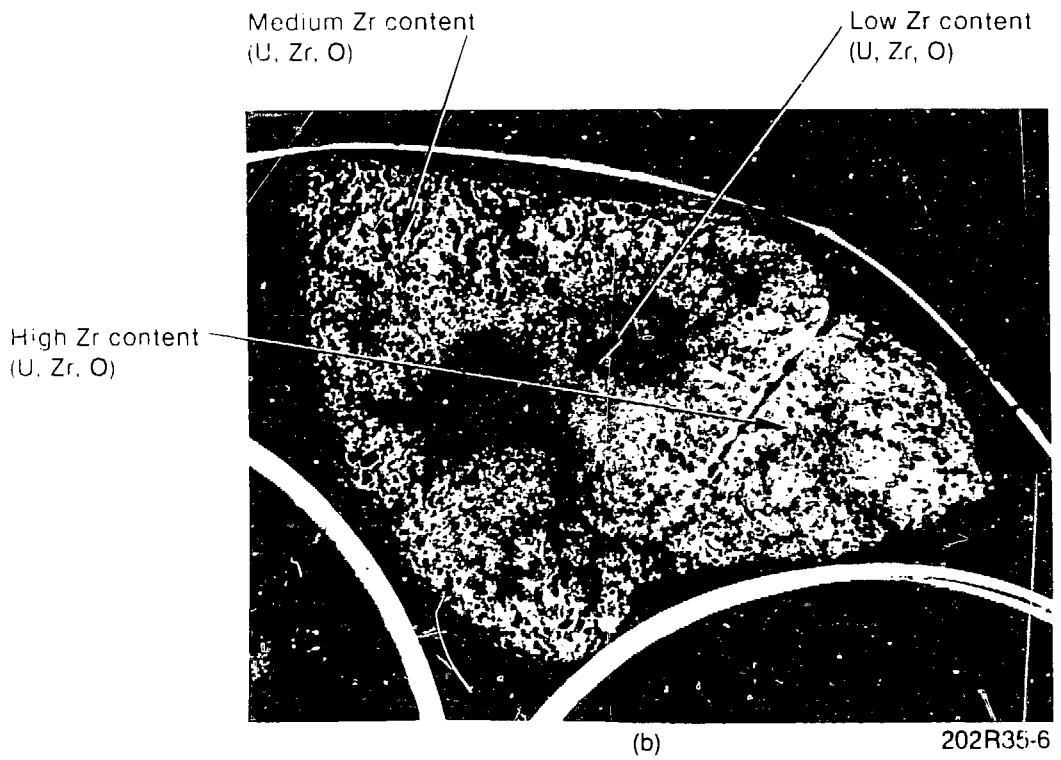
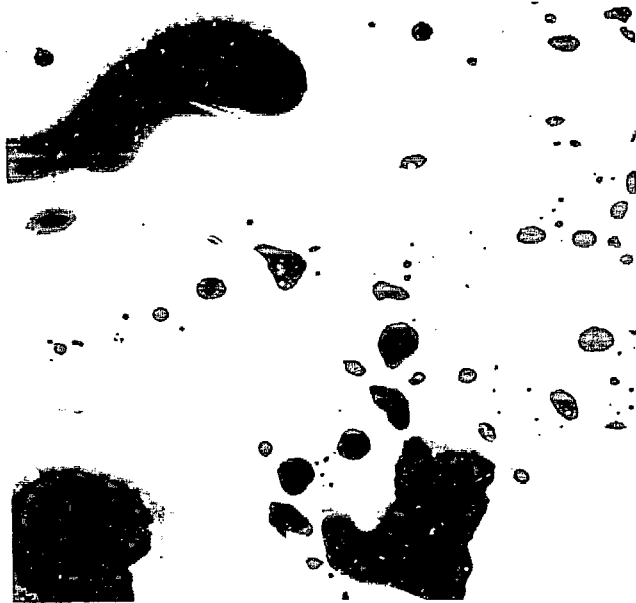
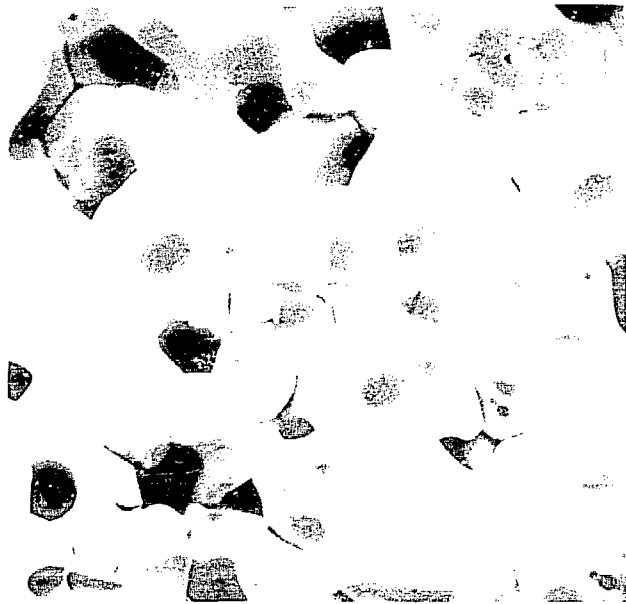


Figure 6. Particle 10A from the 28-3/4-in. elevation at location E9

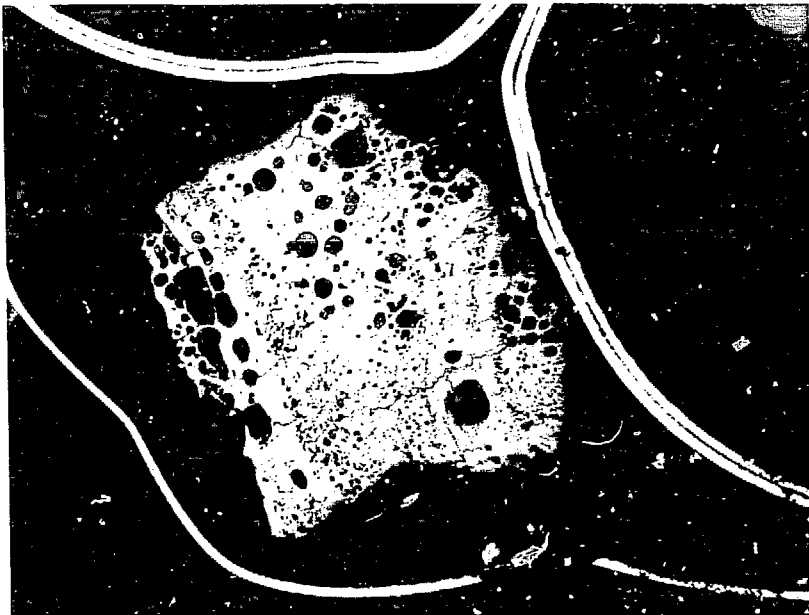


(a) Medium Zr content region



(b) Low Zr content region

Figure 7. Particle 10A from the 28-3/4-in. elevation at location E9



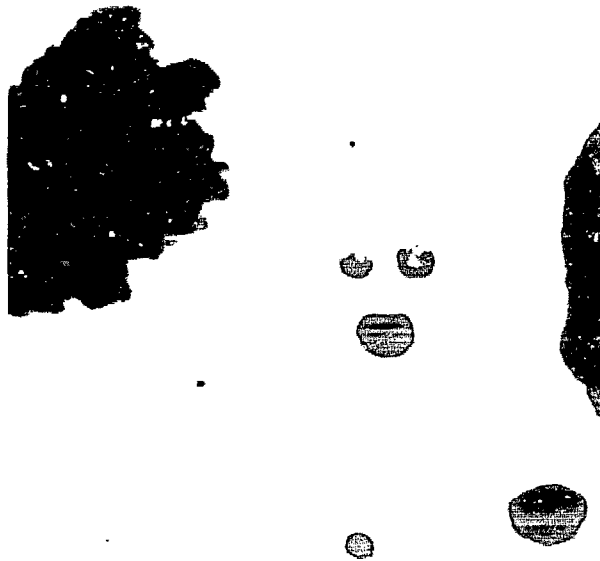
202R28-3

Figure 8. Particle 3L from the 22-in. elevation
at location H8



(a) Microphotograph after a heavy etch showing no grain structure.

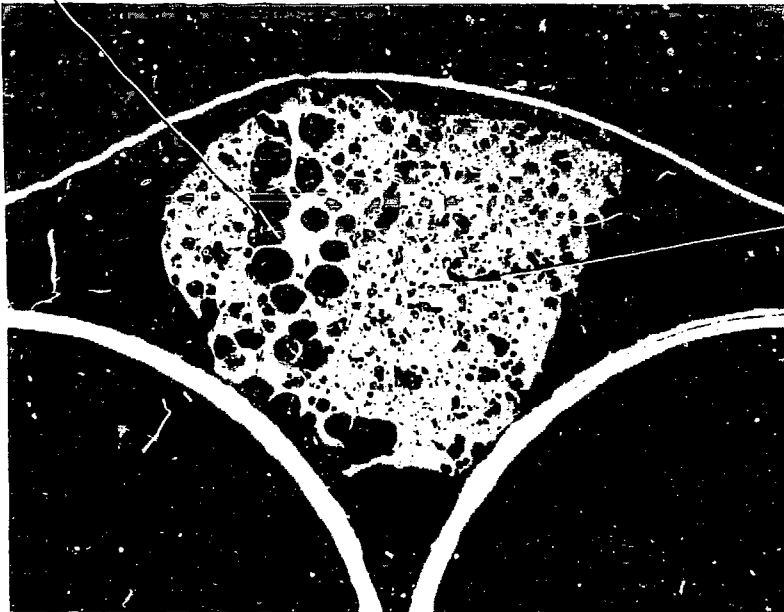
202R28-8



(b) SEM image showing dendritic freezing structure

Figure 9. Particle 3L from the 22-in. elevation at location H8

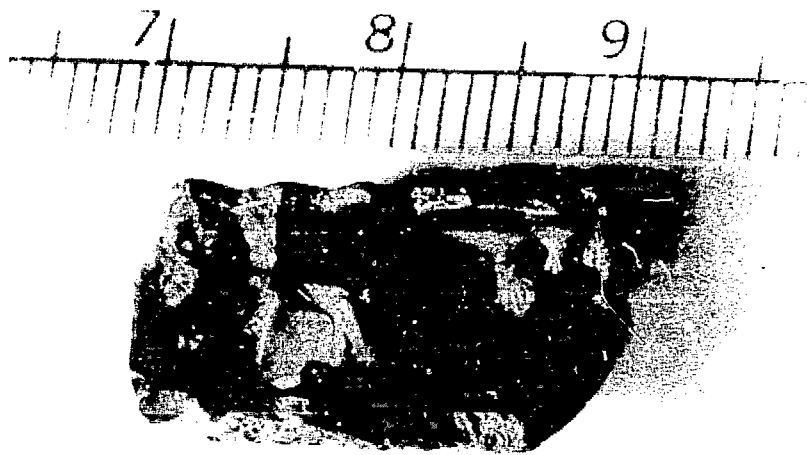
Large pore region
(higher Zr, major
contamination with
Cr, Fe, and Ni)



Small pore region
(lower Zr, less
contamination
with Cr, Fe, and Ni)

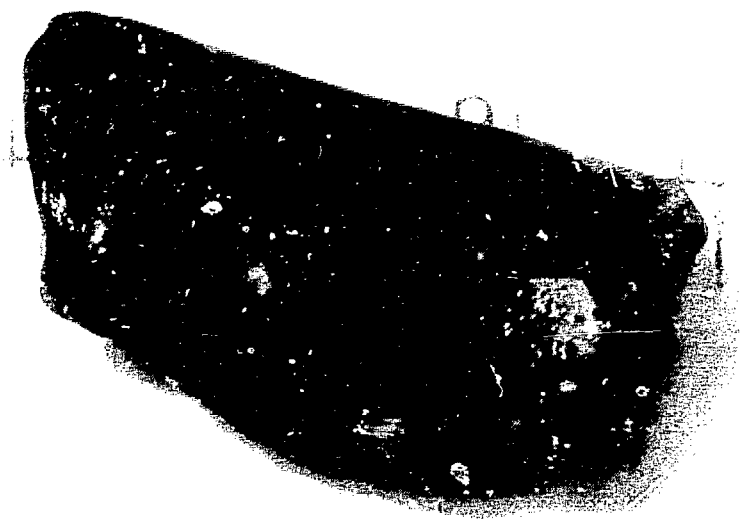
202R32-1

Figure 10. Particle 10F from the 28-3/4-in. elevation
at location E9



(a)

84-216-2-22



(b)

84-216-2-30

Figure 11. Particle 1A from the surface at location H8



Figure 12. Photomicrograph of Particle 1A from the surface at location H8

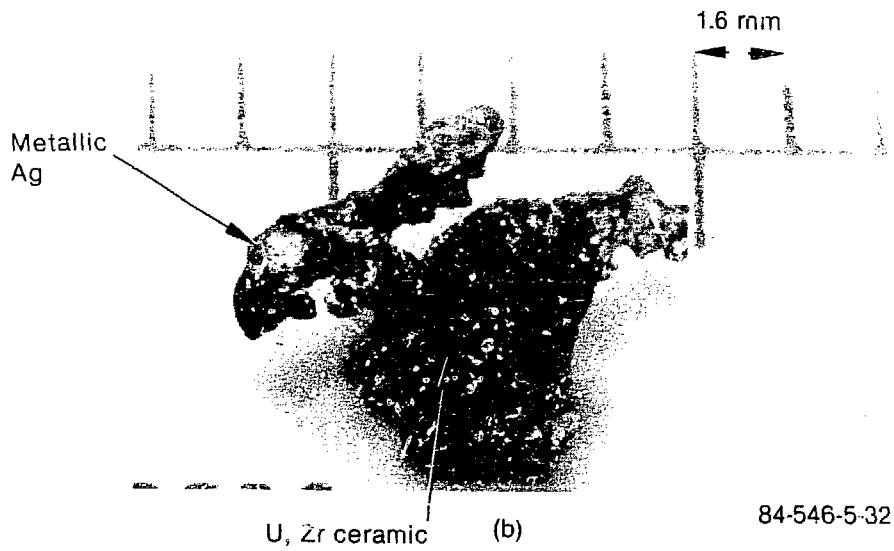
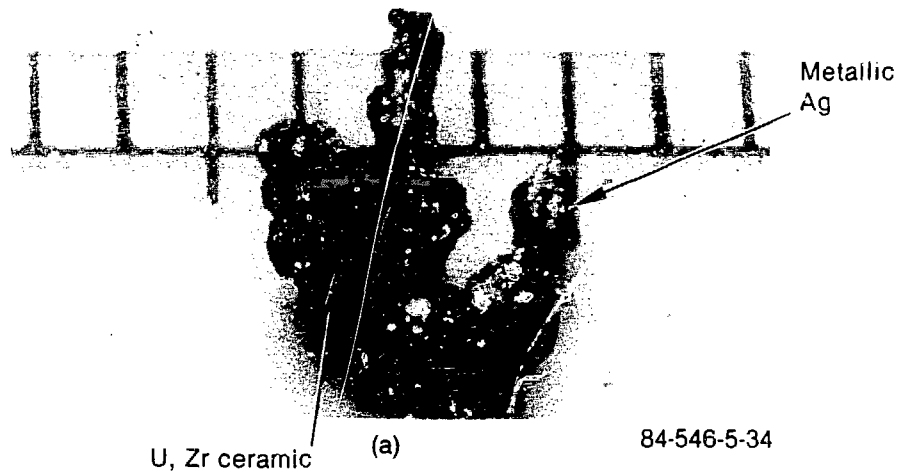


Figure 13. Particle 9D from the 30-1/2-in. elevation at location HB

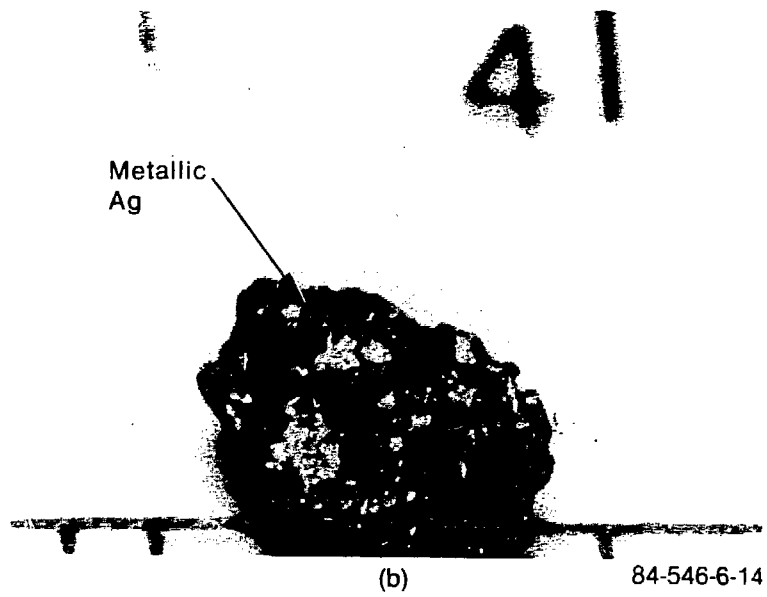
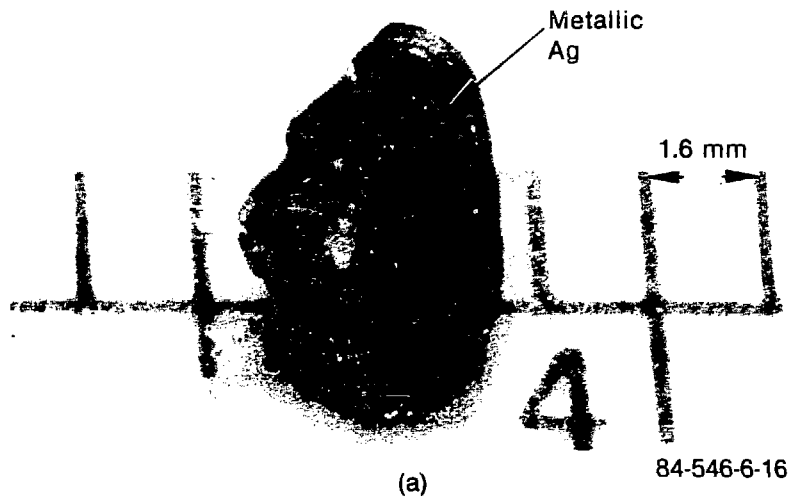


Figure 14. Particle 96 from the 30-1/2-in. elevation at location H8

FISSION PRODUCT TRANSPORT AT THREE MILE ISLAND^{a,b}

Dennis E. Owen^c
Nuclear Engineering Consultant
Hummelstown, PA 17036

Tom E. Cox
Bechtel National, Inc.
Middletown, PA 17057

James M. Broughton
Idaho National Engineering Laboratory
EG&G Idaho, Inc.
P.O. Box 1625, Idaho Falls, ID 83415

ABSTRACT

TMI-2 radionuclide analyses are reviewed and summarized in this paper to determine how fission products moved to various parts of the reactor system at the time of the accident. In spite of high fuel temperatures and major core damage, the core retained a very large fraction of most radionuclides. Reactor coolant, either remaining in the primary system or released to various sumps and tanks, retained significant quantities of cesium and iodine. Noble gases were effectively retained within the Reactor Building, with the exception of small releases to the environment. Long-term deposition and retention on vessel, piping, and building surfaces were insignificant for all isotopes examined. The measured partitioning of radionuclides within those systems is tabulated, and recommendations for additional analyses are presented.

INTRODUCTION

The 1979 accident at TMI-2 damaged a large fraction of the reactor core. More than 100 t of fuel rods were subjected to varying degrees of oxidation, fragmentation, and melting. Of the approximately 10^{10} Ci of radionuclides present in the core at the time of the accident, over 10^8 Ci were released from the UO₂ fuel, but only about 10^6 Ci--virtually all noble gases--were released to the environment. Recognition that the environmental source term was so small, in spite of major core damage, has prompted numerous investigations of LWR radionuclide retention mechanisms and examinations of the extent to which earlier accident release estimates may have overestimated the danger to the public.

- a. This paper is reprinted in these Proceedings with the permission of the American Ceramic Society.
- b. The TMI-2 mass balance data base discussed in this paper is funded by DOE. Compilation of data is being performed by NUS Corporation and EG&G Idaho, Inc. Preparation of this paper was supported by EPRI.
- c. Member, Affiliated Nuclear Consultants.

TMI-2 radionuclide analyses play an important role in this ongoing reevaluation of LWR accident source terms. They provide a benchmark to physical reality. Small-scale separate effects and integral behavior experiments have provided, and will continue to provide, detailed knowledge of the subtleties of fission-product behavior during an accident. Yet such experiments--and the computer codes resulting from them--ultimately must describe the behavior of a power reactor, with its 100 t of fuel, more than 300,000 L of coolant, and more than 100 km of piping. Unfortunately, the characteristic that makes the TMI-2 accident so important to source-term studies--it involves a full-size power plant--precludes TMI-2 from ever being the source of a precise fission-product mass balance. The dynamics of the TMI-2 plant, including fission-product decay, relocation of contamination, cleanup and offsite shipment of radioactive wastes, etc., make a precise postaccident mass balance impossible. Nevertheless, characterization of TMI-2 fission-product behavior is important, since it leads to a good general understanding of fission-product release, transport, and deposition in a large power reactor. That general understanding can be further refined by experimentation and analysis.

The goal of this paper is to reduce the more than 7000 analyses performed on TMI-2 solid, liquid, and gaseous samples to a simple, concise description of the immediate postaccident fission-product partitioning. The partitioning will be reduced to the amounts of fission products that are:

- Retained in the fuel and core debris within the vessel
- Released from the fuel, but retained on in-vessel surfaces and primary system piping surfaces
- Released to the coolant and remaining within the primary system
- Released from the primary system to various tanks and sumps
- Released to the reactor and Auxiliary Building surfaces
- Released to the Reactor Building air
- Released to the environment.

In some instances, the partitioning description will be compromised by analytical uncertainties, incomplete or missing analyses, system unknowns (such as true Reactor Building or primary system piping surface areas), and the inability to backtrack the likely location of fission products that have chemically and physically changed because of reaction and decay. Nevertheless, the resultant source term should provide an initial estimate of TMI-2 fission-product behavior, a basis for comparison with source-term experiments, and a guide for recommending future TMI-2 fission-product analyses.

TMI-2 FISSION-PRODUCT INVENTORY

At the time of the TMI-2 accident in March 1979, the Unit 2 reactor had been operating for about six months and had accumulated 95 effective full-power days of operation, attaining a core average burnup of 3175 MWd/t. The radionuclide inventory for selected radioisotopes at the time of the accident--as calculated by the ORIGEN-2 computer code¹--is summarized in Table 1,² which lists the principal isotopes being measured at TMI-2 by the DOE Mass Balance Program. The list also includes most of the specific isotopes or chemical species identified by NRC as contributing to the health hazards of reactor accidents.³ Table 1 also helps put these inventories in perspective by expressing their quantities in more familiar units of mass and volume.^a

It is important to realize that these hazardous isotopes constitute only a small portion of the total fission-product inventory; over 75% of the TMI-2 inventory consists of stable (nonradioactive) species.⁴ In the following discussion of TMI-2 fission-product transport, about 27 kg of radionuclides (out of a total of ~275 kg) are being tracked within the very large reactor system.

CORE DAMAGE AND FISSION-PRODUCT MOVEMENT WITHIN THE TMI-2 REACTOR SYSTEM

Based on video camera examination of the damaged reactor core and analysis of core-debris specimens, the following core-damage events--summarized schematically in Figure 1--occurred at TMI-2:

- Of approximately 37,000 fuel rods in the core, all but about 7000 shattered
- The top approximately 2.5 m of the rods shattered, and the rod debris collapsed to form a void at the top of the core and a debris bed approximately 1 m deep
- The fuel rods that did not shatter constitute a ring of generally intact fuel at the core periphery
- Stainless steel control rod cladding failed, and the Ag-In-Cd control alloy in these rods melted
- Portions of the stainless steel and Inconel structural material near the top of the fuel assemblies melted and oxidized

a. Conspicuously absent from Table 1 are the tellurium isotopes, principally Te-132 and the stable isotopes Te-128 and Te-130. Because only very limited analyses exist, we have elected to exclude tellurium data. However, the existing tellurium data are briefly referred to in the Summary and Conclusions sections of this paper.

- Liquefied fuel material was produced when zircaloy melted and UO_2 dissolved in the melt
- UO_2 melting occurred (as revealed by metallography of a small number of core-debris specimens), but its extent in the core is unknown
- A large quantity of debris, composition as yet unknown, exists on the bottom of the reactor vessel.

The release path of fission products from the damaged core has been studied extensively.⁵⁻⁷ Figure 2 is a time line that summarizes some of these events. Briefly, the release pathways were as follows. Fuel rod failure began about 2 h-20 min into the accident. At this time, the reactor coolant pumps were off. The water level in the reactor vessel was down because reactor coolant had been lost through the stuck open PORV. A block valve in the PORV line was closed at about this time, stopping the primary system leakage. Approximately the lower one-half of the vessel only contained water; the top half of the vessel contained steam. Uranium-oxide fuel temperatures were high, so that both volatile and gaseous fission products were released into the steam. More fission products were released when (approximately 3 h into the accident) a large fraction of the oxidized and embrittled fuel rods were shattered by thermal shock due to temporary resumption of pump flow. Thus, fission products were released to the RCS water in the vessel and to the steam and hydrogen atmosphere above the water. [The hydrogen was being produced by the reduction of steam by the hot zircaloy cladding.]

At this time, no direct liquid pathway out of the reactor vessel existed because the water level was below the reactor vessel coolant exit lines (the "hot legs") and the system was closed. Fission-product gases, however, flowed out of the hot legs to the once-through steam generators and also entered the pressurizer inlet pipe, where they mixed with the pressurizer fluid. The PORV remained stuck open, but the block valve on the line remained closed, preventing loss of coolant. However, some of these radioactive gases were released from the primary system during subsequent periods in which the PORV block valve was cycled open. Thus, some of these gases were carried out of the pressurizer to the RCDT. Since the RCDT had previously filled with RCS water and then overflowed into the Reactor Building basement, these fission gases would also have escaped from the RCDT and been released into the Reactor Building air atmosphere.

Later in the accident (~16 h), after the reactor coolant pumps had been restarted and coolant flow reestablished throughout the primary system, fission products would have been carried through other parts of the primary system piping, including the letdown/makeup system. This system, which maintains the water purity and boron concentration for the RCS, consists of a letdown line that draws primary coolant through coolers and then into the Auxiliary Building. Auxiliary Building components then lower the water pressure and clean the water by passing it through various filters and demineralizers. The water then collects in makeup tanks and is pumped back into the reactor. Radioactive gases, released from the letdown water during cooling and depressurization, collected in various vent

headers and ultimately discharged via the building stack to the environment. Similarly, radioactive gases accumulating above the water in the makeup tanks passed through the makeup tank headers and leaked into the Auxiliary Building ventilation system. The letdown/makeup system piping also leaked, so that water spilled onto the Auxiliary Building floor and released gases, which were carried by the ventilation system to the environment. Radioactive gases also entered the Auxiliary Building ventilation system via two other principal paths. The RCDT is equipped with a vent header, which carried gases to holdup tanks in the Auxiliary Building. Various vent headers leaked radioactive gases into the building ventilation system. Radioactive water accumulating in the Reactor Building sump also was pumped into the Auxiliary Building sump. Sump capacity was exceeded, causing the water to back up through drains and onto the floor in both the Auxiliary and Fuel Handling Buildings. While not all of the above pathways operated at all stages of the accident (some were recognized and valved off), together they account for most of the onsite transport and offsite releases of radioactivity from TMI-2.

Very small liquid releases to the environment occurred through the IWTS. The IWTS collects normally nonradioactive water from various sumps, filters it, and discharges it into the Susquehanna River. Because various Auxiliary Building tanks had overflowed, contaminated water collected in certain sumps served by the IWTS. The IWTS also processes the Turbine Building sump water. Steam generator tube leaks contaminated the TMI-2 secondary system, and radioactive, secondary-side steam leaked from the turbine and condensed in the Turbine Building sump.

Generally stable conditions were achieved approximately 16 h into the accident, when one reactor coolant pump was restarted and remained on. Cold shutdown with natural circulation was achieved about one month later, on April 27, 1979. For the purposes of this paper, the accident will be considered over about April 1, since at that time most of the environmental releases had stopped. It is important to try to define the partitioning of fission products at this particular time, because the postaccident environment was quite dynamic. Not only are the processes of radioactive decay occurring, but there has been considerable subsequent movement of gas (deliberate containment venting) and water (system leakage and pumping to storage locations). Also, over the following months and years, various radionuclides became concentrated or moved to other locations as water cleanup systems, Reactor Building decontamination, and offsite shipment of wastes were conducted. The radiological conditions at TMI-2 immediately after the accident were as follows:

- o The reactor core was damaged to the extent described earlier in this section
- o Forced convection was established and the primary system was essentially full of highly radioactive water (some minor gas pockets remained)
- o About 1.1×10^6 L of highly radioactive RCS water had leaked to the Reactor Building
- o About 1.2×10^5 L of RCS water had leaked to the Auxiliary Building

- The Reactor Building atmosphere consisted primarily of air, water vapor, and hydrogen, but also contained substantial gaseous fission products.

FISSION-PRODUCT PARTITIONING AT TMI-2

Analysis of TMI-2 samples began the day of the accident and continues at present. DOE and its contractors are assembling a computerized data base of the TMI-2 radionuclide analysis results. Analysis results through 1983 have been entered into the data base, but the preliminary TMI-2 mass balance report⁸ only discusses data through 1979. Work to expand the data base and qualify the analytical results continues. The DOE data base will ultimately be the definitive compilation of TMI-2 fission-product behavior.

Fission Products in the Fuel and Core Debris

A very large quantity of the TMI-2 radionuclide inventory remains within the fuel, in spite of the high temperatures and extensive fuel damage. Examination of the damaged core with video cameras and sonar-like equipment has shown a large void at the top of the core, with a ring of oxidized but generally intact fuel at the core periphery. The 1-m deep, loose, granular debris bed beneath the void has been sampled and analyzed. The condition of the core beneath this loose debris is unknown, although recent (March 1985) video-camera observations of a very large quantity of slag-like debris at the bottom of the vessel makes it very likely that the high temperatures that produced the damage at the top of the core also were present in the lower core region. Observation of a large quantity of debris on the bottom of the vessel also seems to indicate that little fuel debris was swept out of the vessel, as was initially assumed when the large core void was found. Accordingly, as a first step, the existing core can be simplistically modeled as a ring of intact fuel rods (equivalent to approximately 33 intact fuel assemblies out of a total 177, based on sonar data⁹), with the balance of the core (approximately 144 fuel assemblies) being debris.

Because the exact nature of the core damage beneath the loose debris is unknown, the entire core--with the exception of the peripheral standing fuel--was assumed to have the fission-product content of the loose, granular debris. Radionuclide analyses of the debris have been made,^{10,11} and a best-estimate curie content has been prepared.¹² The estimated radionuclide retention in the core, based on the debris bed sample analyses and the simple core-damage model described above is summarized in Table 2. Estimated radionuclide retention ranges from approximately 13% for the noble gases to approximately 100% for cerium. Even in the fuel debris, which experienced high accident temperatures and long-time water immersion, retention was high for all species measured.

Fission Products on Vessel and Piping Surfaces

Since the establishment of the very low environmental releases at TMI-2, there has been considerable speculation on the role of inherent

mechanisms of fission-product retention during a core-damage accident. Among the mechanisms generally assumed to reduce radionuclide release are deposition of volatile fission products on the high surface area structures within the reactor vessel and on the internal surfaces of the reactor system piping. Radionuclide retention on TMI-2 upper vessel internal surfaces can be estimated using measurements that have been made of the surface deposition on two control rod drive leadscrews. The leadscrews are approximately 7-m long, threaded, stainless steel rods to which the TMI-2 control rod assemblies are attached (see Figure 1). The leadscrews pass through the large surface area stainless steel plenum assembly (Figure 1), so that the surface deposition on the leadscrews may be taken as representative of the plenum assembly itself (which has not yet been sampled or analyzed). The leadscrews were not removed until July 1982; thus, they were subjected to over three years of immersion in hot water. Nevertheless, detailed analysis of the leadscrews¹³ showed that they retained both loose surface deposits (which were removable by brushing) and tightly bound deposits, which probably formed when the leadscrews were in an atmosphere of hot steam, hydrogen, and fission products during the accident. The available leadscrew data and the extrapolation to deposition on vessel internal surfaces is summarized in Table 3.

Only one small specimen from the inside surface of the TMI-2 primary system piping has been examined thoroughly. The thermowell, which housed the RTD located in the "A" hot leg near the steam generator, was removed for analysis in early 1984. The thermowell is a small-diameter, closed-end, stainless steel tube that protrudes through the pipe wall and into the primary coolant. The thermowell, which has an exposed surface area of approximately 15 cm², was immersed in hot coolant for five years prior to analysis. Table 4 is a summary of the radionuclides measured on the thermowell¹⁴ and the extrapolation to radionuclide deposition on TMI-2 primary system piping is presented.

Combining the data of Tables 3 and 4, it is noted that the current deposition on vessel and piping surfaces accounts for less than 1% of the radionuclides measured.

Fission Products in the Primary Coolant

The radionuclide content of the 250,000 L RCS has been monitored from the day of the accident. General trends for cesium and strontium are shown in Figure 3. The large decreases in cesium content, commencing about 1200 d after the accident, were due to processing of RCS coolant through specially designed zeolite and resin water cleanup systems. The smaller fluctuations resulted from changes in water chemistry (e.g., variations in boron and dissolved oxygen levels) and from the dilution action of the letdown/makeup system. Because of the wide variation in RCS radionuclide content over time, only analyses made soon after the accident were used to calculate RCS inventory.¹⁶ The radionuclide concentration of the RCS at the time of the accident is compared with the initial TMI-2 radionuclide inventory in Table 5. Note that the primary coolant retained significant--and approximately equal--percentages of both iodine and cesium. The uncertainty in the strontium value is particularly high because, as shown in Figure 3, strontium levels in the coolant were changing rapidly at the time of the accident.

Fission Products in Miscellaneous Tanks and Sumps

Major collection points for contaminated RCS coolant during the TMI-2 accident were the Reactor Building basement sump, the Auxiliary Building sump, and the various associated collection tanks. A simplified schematic of these sinks and their respective volumes is shown in Figure 4. High radiation levels and component access limitations made sampling of these liquid sinks difficult. Thus, no early (April 1979) analyses of these components are available. Accordingly, the radionuclides released to these locations were calculated using the measured RCS coolant activity levels (from Table 5) and the calculated coolant leakages summarized in Figure 4. The results (Table 6) indicate that about five RCS volumes leaked from the TMI-2 primary system to the Reactor and Auxiliary Building tanks and sumps, and that significant quantities of cesium and iodine accumulated there.

Fission Products on Reactor and Auxiliary Building Surfaces

There is considerable uncertainty about the actual quantity of radionuclides deposited on Reactor Building and Auxiliary Building surfaces, because of the inability to measure true surface areas of complicated structures and the limited number of thorough surface analyses available. Reactor Building surface areas (metal and concrete combined) have been estimated at $2.42 \times 10^8 \text{ cm}^2$.¹⁷ Surface contamination, of course, varies substantially, depending upon location in the Reactor Building, the type of surface being examined, and surface orientation. Reactor Building surface contamination data obtained almost three years after the accident is summarized in Table 7.¹⁸ Note the broad range of surface contamination measured. Even using the maximum reported surface contamination, the results indicate that Reactor Building surfaces retained a very small fraction of the radionuclide inventories. Although Auxiliary Building surface areas and surface contamination levels have not been tabulated, they are generally much less than those in the Reactor Building. Incorporating the Auxiliary Building data probably would not alter the above conclusion.

Fission Products in the Reactor Building Atmosphere

Analysis of airborne radioactivity within the TMI-2 containment is a critical source-term parameter, since many past accident-effect studies have assumed that a rapid and large containment breach could occur during a severe LWR accident. Recent research^{4,19} has shown that containment failure--if it does occur--will probably occur many hours after accident initiation via small, pressure-sensitive leak paths. (The TMI-2 containment structure did not fail or leak directly to the environment.) Regardless of the hypothesized containment failure mechanism, TMI-2 containment airborne radioactivity data are important because they do represent a potential environmental source term. A few measurements of containment gases were made near the time of the accident, with most of the measurements obtained during the first 100 d after the accident. The available data²⁰ are summarized in Table 8. Note that, essentially, only noble gases are present in the containment atmosphere.

Fission Products Released to the Environment

Radioactivity releases to the environment via the gas and liquid release pathways described earlier in this paper were thoroughly analyzed after the TMI-2 accident (References 4 and 6). Those releases are summarized in Table 9. Efforts were made to measure many different isotopes; therefore, the absence of an isotope from Table 9 means it was not detected, or it was detected at background levels resulting from atmospheric weapons testing. Although the noble gas release estimated by GPU Nuclear²¹ is a factor of 10^5 higher than the other release measurements (see Table 9), there is good general agreement that noble gas releases were about 1% of inventory, radioiodine releases were extremely small (less than 1/10,000 of 1%), and releases of other radionuclides were immeasurable.

SUMMARY AND CONCLUSIONS

The results to date on fission-product partitioning within the TMI-2 reactor system are presented in Table 10. Although the uncertainty in these measurements is no doubt high, for the reasons discussed in the "Introduction" section of this paper, the following conclusions are clear:

- ⊙ For all of the elements examined, except the noble gases, a very large fraction of the radionuclides were retained in the fuel debris. This was true in spite of fragmentation of most of the fuel rods and the apparent presence of a large quantity of once-molten core material.
- ⊙ Permanent deposition of radionuclides on nearby steel components (reactor internals and primary system piping) is small and does not appear to significantly impede radionuclide release from the primary system. This conclusion is based on analyses of components that were flushed with coolant for many months prior to examination. High radiation levels prevented early access to those components to confirm their behavior in the first hours and days after the accident. Without that early data, it is impossible to determine whether those components retain significant radionuclides prior to coolant flushing. Data from reactor experiments that can measure radionuclide deposition on structural material surfaces in real time should be reviewed to verify this conclusion.
- ⊙ The reactor coolant retains a significant quantity of the cesium and iodine released from the fuel. Even if the coolant escapes the pressurized primary system piping and enters tanks or open sumps, cesium and iodine retention remain high.
- ⊙ Though the Reactor Building contains a very large surface area that is cold (relative to the core and coolant temperatures) and consists of a variety of materials (carbon steel, stainless steel, concrete, plastics), only small amounts of radionuclides have been found on its surfaces. The high-humidity conditions inside the Reactor Building after the accident and the resulting

evaporation and condensation probably removed some surface deposits. However, during later Reactor Building decontamination efforts, it was found that water was a poor surface decontamination agent (except under high pressure). Thus, it appears likely that even at the time of the accident, the Reactor Building surfaces retained relatively small quantities of radionuclides.

- The Reactor Building atmosphere retained about 50% of the noble gases. They were effectively retained for over one year, until they were deliberately vented to the environment.
- Except for noble gases, radionuclide releases to the environment during the TMI-2 accident were extremely small and without measurable health effects (References 4 and 6). That they remained small in spite of the loss of a large quantity of the primary coolant and the consequent substantial fuel damage is a vindication of the defense-in-depth principles under which LWRs are built and operated.

Because TMI-2 tellurium data are very limited, they were not included in this paper. We are well aware, however, of the importance of tellurium contributions to LWR accident source terms and the debates over tellurium behavior. Therefore, we wish to call attention to tellurium analyses reported for the leadscrews (Reference 13) and the RCS coolant.²² Using the reported values, we calculate that tellurium deposition on reactor vessel internal surfaces could be approximately 2% of tellurium inventory, tellurium retention in the RCS coolant is less than 0.1%, and tellurium retention in Reactor and Auxiliary Building tanks and sumps is less than 1%.

With the exception of the sampling and analysis of the reactor core, few analyses beyond those performed already can help further define the immediate, postaccident fission-product transport. At this time (May 1985), the Reactor Building has been vented, the Reactor and Auxiliary Buildings have been extensively decontaminated, contaminated coolant in the primary system and that collected in tanks and sumps have been processed, and a variety of wastes has been consolidated and transported offsite for disposal.

One additional area that should be analyzed is the radionuclide penetration into the concrete surfaces in the Reactor Building basement. Water depth in the basement after the accident was greater than 2 m. Even though the basement water was removed and processed (in late 1981)--leaving only a few inches of residual water and sludge--radiation levels in the basement remain quite high. It is believed that the high radiation levels result, in part, from radionuclide penetration into the basement walls. Although personnel have not yet entered the basement because of the high radiation, a robot vehicle has surveyed the basement and photographed the "bathtub ring" on the basement walls. We have made estimates of the surface areas involved and of the possible extent of cesium penetration into the concrete, and have calculated that the basement surfaces could

hold as much as 3% of the TMI-2 cesium inventory. Because retention of this much cesium--and perhaps other fission products--would alter the conclusion that the Reactor Building surfaces (at least those surfaces immersed in water) retain an insignificant fraction of the core inventory, it is important that these surfaces be sampled and analyzed. Since personnel access to the basement might require decontamination of the basement walls, provisions will be made to obtain early, representative core samples of the basement surfaces, using the TMI-2 robot vehicle. The basement sampling will include core samples of both floors and walls and the various surfaces present, including unpainted high-density concrete, epoxy-painted, high-density concrete, and low-density concrete block.

The most important region requiring additional sampling and analysis is the damaged fuel, because it clearly retains most of the TMI-2 radionuclide inventory. Only one portion of the core debris--the loose, granular debris bed--has been sampled and analyzed. Most of the fuel structure remains to be examined, including the partially intact peripheral fuel assemblies, the as-yet unseen fuel structures beneath the granular debris bed, and the slag-like debris observed at the bottom of the vessel. We believe that the wide spectrum of fuel structures remaining to be analyzed ultimately will be found to contain most of the fission products as yet unaccounted for in Table 10. DOE (along with the other participants in the TMI-2 research program--GPU Nuclear, EPRI, and NRC) is planning extensive additional analyses of the reactor core and also is alert for other analyses that might contribute to the understanding of TMI-2 fission-product transport. It is recognized that the TMI-2 fission-product partitioning summarized herein is, of necessity, tentative. It is important that these additional analyses be performed so the TMI-2 radionuclide mass balance be as complete as possible and, thereby, serve as a definitive measure of LWR reactor safety.

REFERENCES

1. A. G. Groff, ORIGEN-2--A Revised and Updated Version of the Oak Ridge Isotope Generation and Depletion Code, ORNL-5621, July 1980.
2. Inventory calculated by EG&G Idaho, Inc. using ORIGEN-2 computer code, private communication, D. W. Akers, EG&G Idaho, Inc., April 1985.
3. U.S. Nuclear Regulatory Commission, Technical Bases For Estimating Fission-Product Behavior During LWR Accidents, NUREG-0772, June 1981.
4. American Nuclear Society, "Report of the Special Committee on Source Terms," September 1984.
5. Staff of the Special Inquiry Group, M. Rogovin, Director, Three Mile Island--A Report to the Commissioners and to the Public, NUREG/CR-1250, Vol. 2, Part 2, 1980.
6. Nuclear Safety Analysis Center, Analysis of the Three Mile Island Unit 2 Accident, NSAC-80-1, March 1980.

7. The President's Commission on the Accident at Three Mile Island, J. G. Kemeny, Chairman, "The Accident at Three Mile Island, Technical Assessment Task Force, Vol. 4," October 1979.
8. R. J. Davis et al., Radionuclide Mass balance for the TMI-2 Accident: Data Through 1979 and Preliminary Assessment of Uncertainties, GEND-INF-047, November 1984.
9. L. S. Beller and H. L. Brown, Design and Operation of the Core Topography Data Acquisition System for TMI-2, GEND-INF-012, May 1984.
10. D. W. Akers and B. A. Cook, Preliminary Report: TMI-2 Core Debris Grab Samples--Analysis of First Group of Samples, EGG-TMI-6630, Draft June 1984.
11. G. O. Hayner, TMI-2 HBA Core Debris Sample Examination--Final Report, Babcock & Wilcox, RDD:85:5097-01:01, July 1984.
12. R. Rainisch, "Radiological (Source Term) Characterization of TMI-2 Core Debris Grab Samples--Summary of Data Report by B&W and EG&G," GPU Nuclear Data Management and Analysis Memorandum, November 1984.
13. K. Vinjamuri et al., Examination of H8 and B8 Leadscrews from Three Mile Island Unit 2, EGG-TMI-6685, April 1985.
14. Private communication from T. E. Cox, EG&G Idaho, Inc., to C. B. Leek, Letter No. TEC-54-84, dated September 25, 1984.
15. Letter report, E. J. Bateman (Babcock & Wilcox) to i. H. Lilien (GPU Nuclear), "List of Materials Weited by the Reactor Coolant System at TMI-2," December 20, 1984.
16. GPU Nuclear, Reactor Coolant System Sample Results, TMI-2 Technical Planning Department, TPG/TMI-122, Rev. 0, July 1984.
17. C. A. Pelletier et al., Preliminary Radionuclide Source Term and Inventory Assessment for TMI-2, GEND-028, March 1983.
18. R. J. Davis, Information On Reactor Building Surface Contamination, NUS-TM-352, June 1983.
19. A. R. Buhl, et al., "IDCOR--Supporting the Technical Foundation and the Decision Process for Source Term Reduction," ANS Executive Conference on Ramifications of the Source Term, Charleston, South Caroline, March 10-13, 1985, to be published.
20. J. K. Hartwell et al., Characterization of the Three Mile Island Unit 2 Reactor Building Atmosphere Prior to the Reactor Building Purge, GEND-005, May 1981.
21. K. Woodard, Offsite Radiation Release, GPU Nuclear Report GPU-TDR-059, February 1980.
22. C. A. Pelletier et al., Iodine-131 Behavior During the TMI-2 Accident, NSAC-30, September 1981.

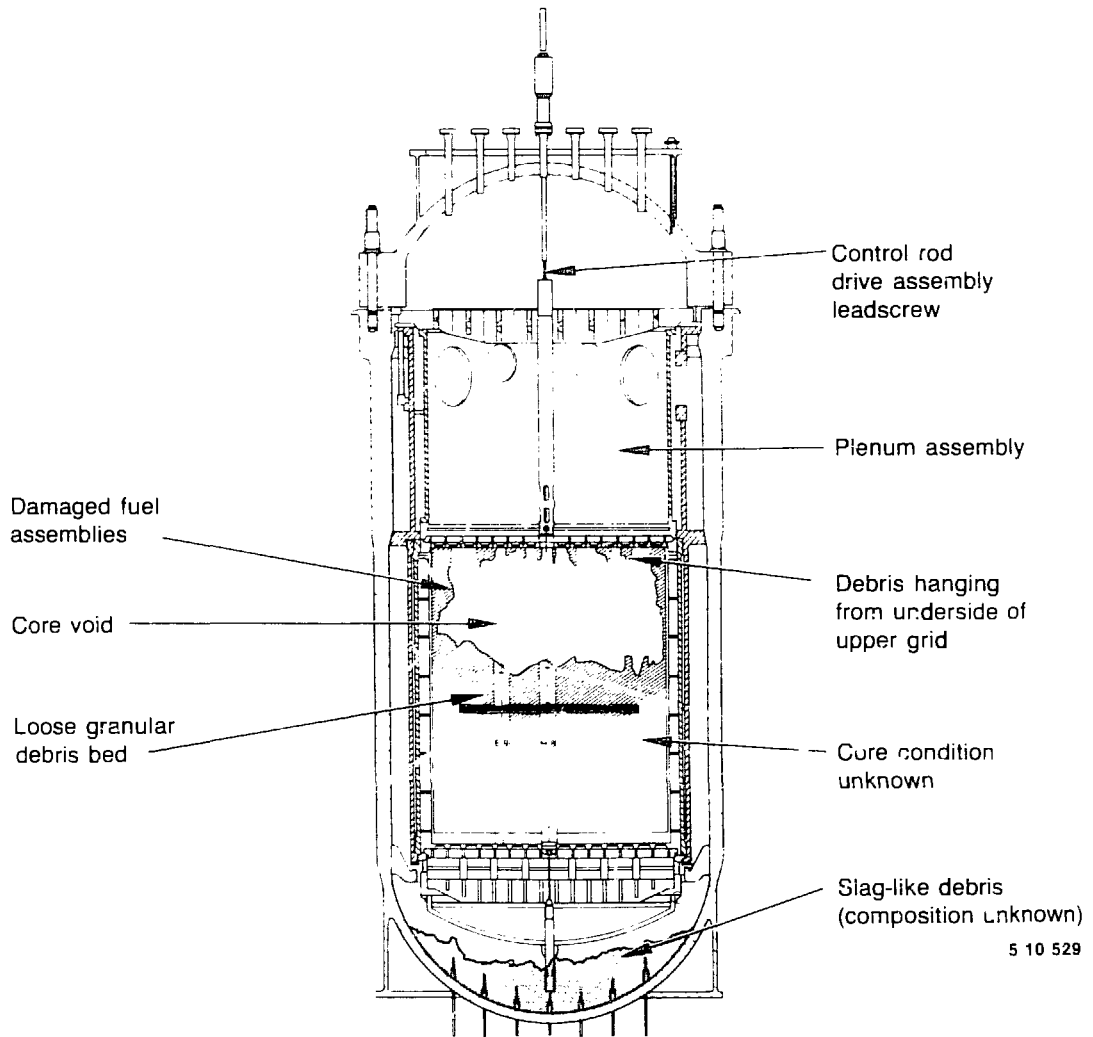
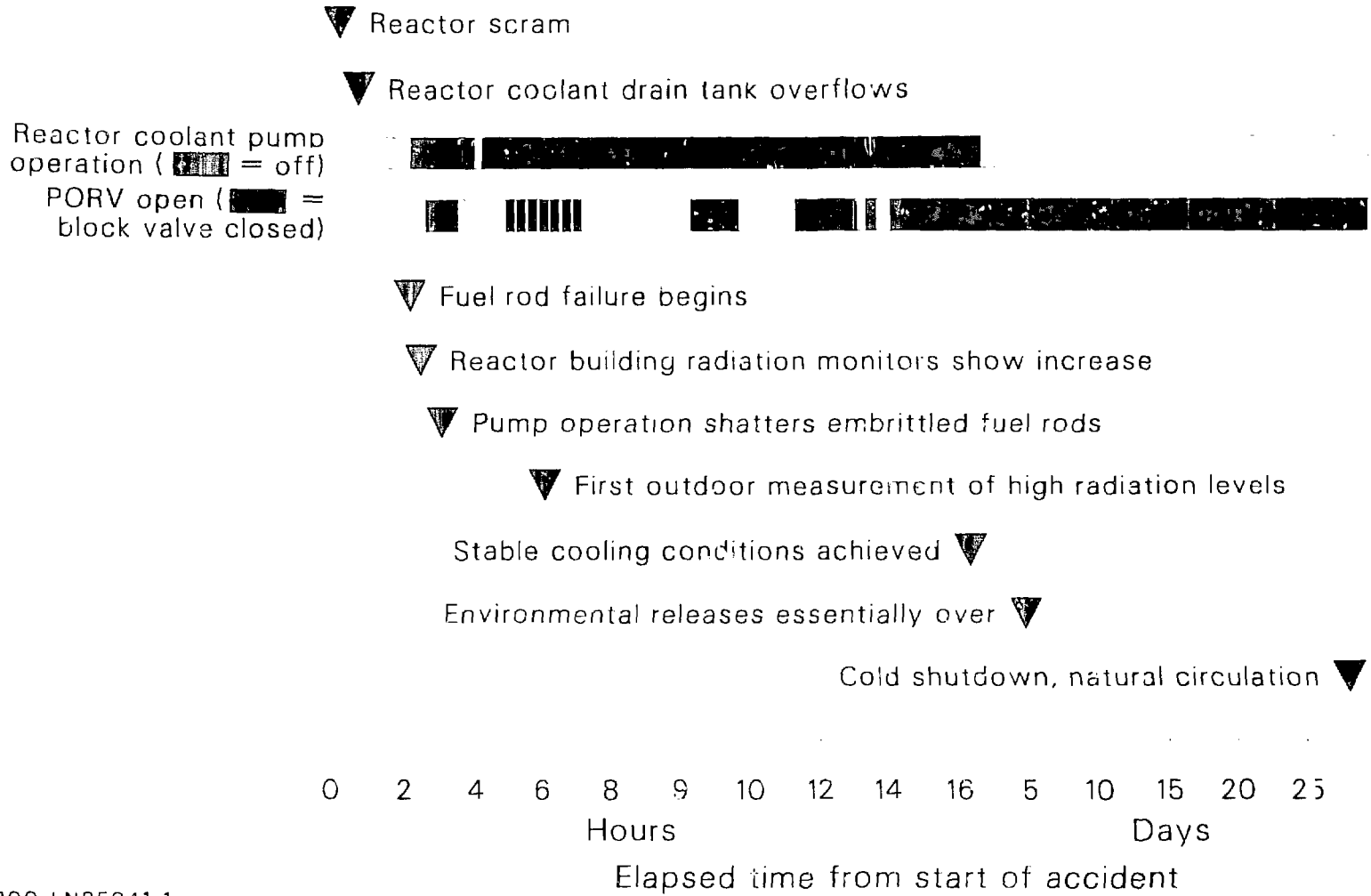


Figure 1. TMI-2 core and reactor vessel conditions.



P200-LN85041-1

Figure 2. Release path of fission products.

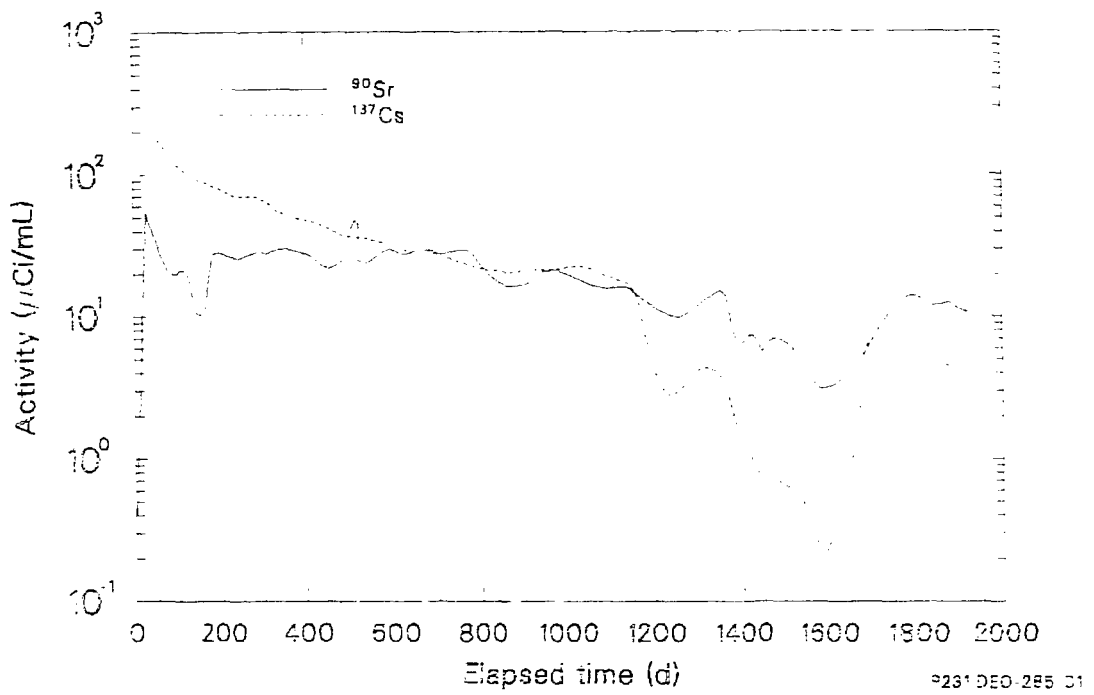
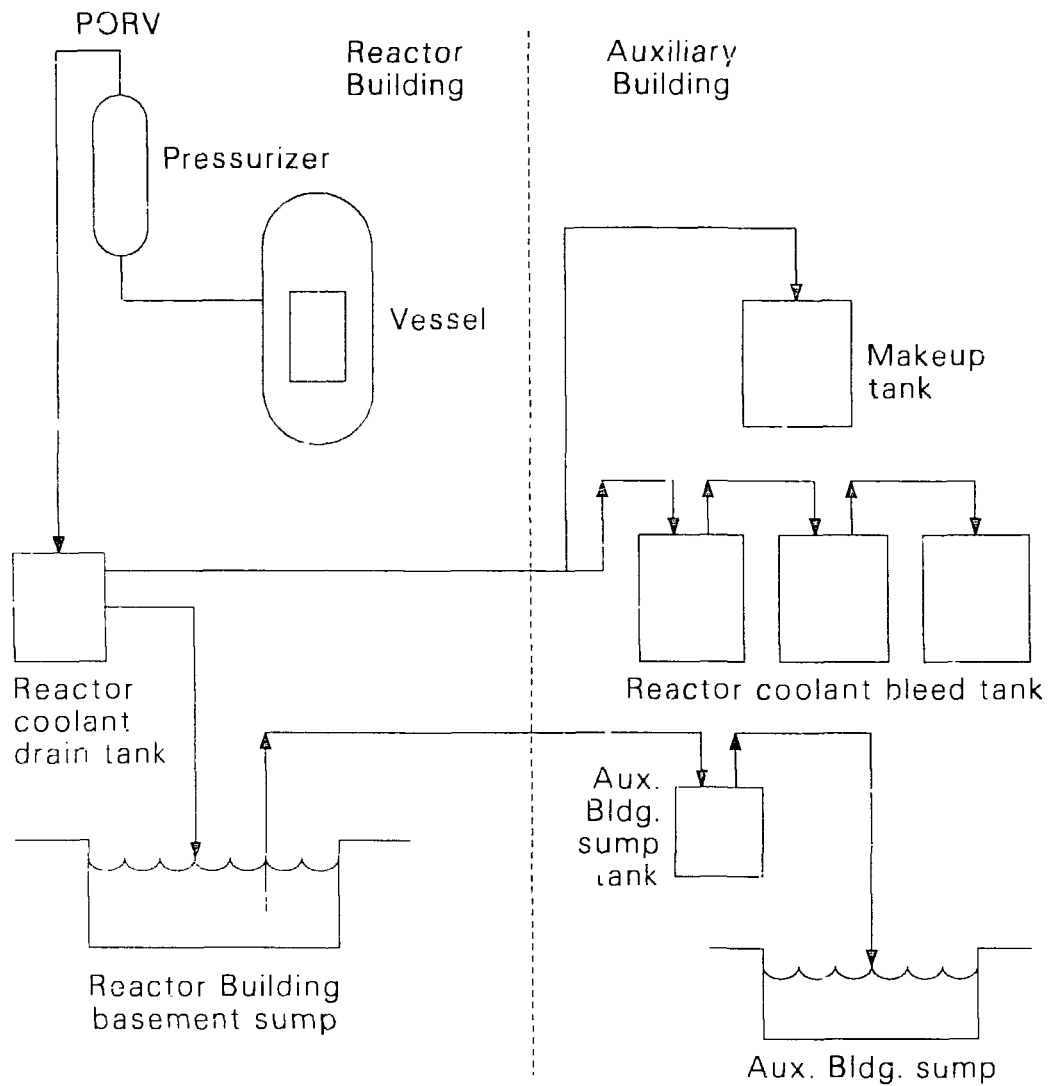


Figure 3. Radionuclide levels in the TMI-2 reactor coolant.



Volume Summary Early April 1979

Component	Vol. of RCS Water Leakage (L)
Reactor coolant drain tank	1.1 x 10 ⁶ (ref. 8)
Reactor Building basement sump	
Reactor coolant bleed tanks	1.2 x 10 ⁵ (calculated by authors)
Aux. Bldg. sump & sump tank	

P201-LN85042 1

Figure 4. Collection points for contaminated RCS coolant.

TABLE 1. INVENTORY OF SELECTED TMI-2 RADIONUCLIDES AT SHUTDOWN

Isotope	Half-Life	Inventory			
		Curies ^a	$\mu\text{Ci/g UO}_2^{\text{b}}$	Volume (L at STP)	Mass (g)
Kr-85	1.8 y	9.7×10^4	1.0×10^3	63	240
Sr-90	29 y	7.5×10^5	9.1×10^3	--	5300
Ru-106	368 d	3.6×10^6	3.9×10^4	--	1100
Sb-135	2.7 y	1.2×10^5	1.3×10^3	--	85
I-129	1.6×10^7 y	2.2×10^{-1}	2.4×10^{-3}	--	1400
I-131	8.1 d	6.7×10^7	7.2×10^{-5}	--	540
Xe-133	5.3 d	1.5×10^8	1.6×10^6	136	810
Cs-134	2.1 y	2.0×10^5	2.2×10^3	--	155
Cs-137	30 y	8.5×10^5	9.1×10^3	--	9800
Ce-144	284 d	2.4×10^7	2.6×10^5	--	<u>7500</u>
				TOTAL =	~27000

a. As calculated by ORIGEN-2 (Reference 2).

b. Core average, based on 9.3×10^7 g UO_2 .

TABLE 2. ESTIMATED RADIONUCLIDE RETENTION IN THE TMI-2 FUEL AND CORE DEBRIS

Isotope	Rubble		Intact Rods	Total Estimated Activity in Fuel ^c (Ci)	Percent Retention ^e in Core
	Average Measured Specific Activity ^a ($\mu\text{Ci/g UO}_2$)	Estimated Activity ^b (Ci)	Estimated Activity ^c (Ci)		
Kr-85	nm	0 (assumed)	1.3×10^4	1.3×10^4	13
Sr-90	4.1×10^3 ^f	3.1×10^5	1.1×10^5	4.2×10^5	115
Ru-106	2.3×10^4	1.7×10^6	5.2×10^5	2.2×10^6	61
Sb-125	6.1×10^2	4.6×10^4	1.7×10^4	6.3×10^4	41
I-129	5.5×10^{-4} ^f	4.1×10^{-2}	3.2×10^{-2}	7.3×10^{-2}	33
Cs-134	3.3×10^2	2.5×10^4	2.9×10^4	5.4×10^4	27
Cs-137	1.4×10^3	1.0×10^5	1.2×10^5	2.2×10^5	28
Ce-144	2.9×10^5	2.2×10^7	3.5×10^6	2.6×10^7	108

nm = not measured.

a. From Reference 12, decay corrected to shutdown.

b. Based on 9.3×10^7 g UO_2 in the core, of which 81% (144 out of 177 fuel assemblies) is rubble.

c. Based on 19% of the core being intact (33 out of 177 fuel assemblies) and containing 100% of its initial inventory. Based on burnup calculations, the peripheral fuel assemblies each contain about 75% of the fission-product inventory of the core average fuel assembly.

d. Sum of Columns 3 and 4.

e. Calculated percentage of initial inventory (from Table 1) remaining in the core.

f. Private communication from EG&G Idaho, Inc. Data should be considered preliminary.

TABLE 3. ESTIMATED RADIONUCLIDE DEPOSITION ON TMI-2 REACTOR VESSEL INTERNAL SURFACES

Isotope	Average Measured Surface Deposition on Leadscrews ^a ($\mu\text{Ci}/\text{cm}^2$)	Estimated Deposition on Vessel Surface ^b (Ci)	Percent Deposition on Vessel Surfaces ^c
Sr-90	18	126	~0.02
Ru-106	194	1360	~0.04
Sb-125	30	210	0.18
I-129	5.2×10^{-5}	3.6×10^{-4}	0.16
Cs-134	51	357	0.18
Cs-137	181	1270	0.15
Ce-144	645	4520	~0.02

a. From Reference 13, decay corrected to shutdown.

b. Assuming surface area of vessel internals = $7.0 \times 10^6 \text{ cm}^2$ (sum of lead screws and plenum).

c. Calculated percentage of initial inventory (from Table 1).

TABLE 4. ESTIMATED RADIONUCLIDE DEPOSITION ON TMI-2 PRIMARY SYSTEM PIPING

Isotope	Measured Deposition ^a ($\mu\text{Ci}/\text{cm}^2$)	Estimated Deposition on Internal Piping Surfaces ^b (Ci)	Percent Deposition on Piping Surfaces ^c
Sr-90	10.6	2650	0.4
Sb-125	0.5	125	0.1
I-129	7.9×10^{-8}	2.0×10^{-4}	<0.01
Cs-134	5.7	1425	0.7
Cs-137	22.2	5550	0.7
Ce-144	33.7	8425	~0.04

a. From Reference 14, decay corrected to shutdown.

b. Assuming uniform deposition on a piping surface area of $2.5 \times 10^8 \text{ cm}^2$ (Reference 15).

c. Calculated percentage of initial inventory (from Table 1).

TABLE 5. ESTIMATED RADIONUCLIDE CONTENT OF THE TH1-2 REACTOR COOLANT SYSTEM

Isotope	Average Measured Activity ^a ($\mu\text{Ci/mL}$)	Estimated Activity in RCS ^b (Ci)	Percent Retention in RCS ^c
Sr-90	14	3440	0.5
Ru-106	0.36	89	<0.01
I-129	7.4×10^{-5}	1.8×10^{-2}	8.0
I-131	1.8×10^4	4.4×10^6	7.0
Xe-133	1.4×10^3	3.4×10^5	0.2
Cs-134	78.5	1.9×10^4	10.0
Cs-137	311.0	7.7×10^4	9.0

a. From Reference 16, decay corrected to shutdown.

b. Based on RCS volume = 2.46×10^5 L at operating temperature.

c. Calculated percentage of initial inventory (from Table 1).

TABLE 6. ESTIMATED RADIONUCLIDE CONTENT OF TMI-2 SUMPS AND TANKS

Isotope	Average Measured Activity for RCS Liquid ^a ($\mu\text{Ci/mL}$)	Estimated Activity			Percent Retention for All Sumps and Tanks ^e
		Reactor Building ^b (Ci)	Auxiliary Building ^c (Ci)	Total ^d (Ci)	
Sr-90	14.0	1.5×10^4	1.7×10^3	1.7×10^4	2.0
Ru-106	0.36	396	43	439	~0.01
I-129	7.4×10^{-5}	8.1×10^{-2}	8.9×10^{-3}	9.0×10^{-2}	41.0
Xe-133	1.4×10^3	1.5×10^6	1.7×10^5	1.7×10^6	1.0
Cs-137	311.0	3.4×10^5	3.7×10^4	3.8×10^5	45.0

a. From Table 5.

b. Based on 1.1×10^6 L of RCS liquid released to the Reactor Building (see Figure 4).

c. Based on 1.2×10^5 L of RCS liquid released to the Auxiliary Building (see Figure 4).

d. Total of Columns 3 and 4.

e. Calculated percentage of initial inventory (from Table 1).

TABLE 7. ESTIMATED RADIONUCLIDE DEPOSITION ON TMI-2 REACTOR BUILDING SURFACES

Isotope	Measured Surface Activity ($\mu\text{Ci}/\text{cm}^2$)	Estimated Deposition on Reactor Building Surfaces ^b (Ci)	Percent Deposition on Reactor Building Surfaces ^c
Sr-90	$1.4 \times 10^{-3} - 1.7 \times 10^{-1}$	41	<0.01
I-129	$3.7 \times 10^{-7} - 6.8 \times 10^{-7}$	1.6×10^{-4}	~0.07
Cs-137	$4.0 \times 10^{-2} - 3.6$	670	0.1

a. From Reference 18, decay corrected to shutdown.

b. Assuming maximum value from Column 2 and a Reactor Building surface area of $2.42 \times 10^8 \text{ cm}^2$ (Reference 17).

c. Calculated percentage of initial inventory (from Table 1).

TABLE 8. ESTIMATED RADIONUCLIDE CONTENT OF THE TMI-2 REACTOR BUILDING ATMOSPHERE

Isotope	Measured Concentration ^a ($\mu\text{Ci}/\text{cm}^3$)	Estimated Activity in Reactor Building Atmosphere ^b (Ci)	Percent Retention in Reactor Building Atmosphere ^c
Kr-85	0.93	5.2×10^4	54.0
Sr-90	1.6×10^{-10}	8.9×10^{-6}	<<0.01
I-129	5.7×10^{-11}	3.2×10^{-6}	<0.01
Cs-134	2.1×10^{-10}	1.2×10^{-5}	<<0.01
Cs-137	7.2×10^{-10}	4.0×10^{-5}	<<0.01

a. From Reference 20, decay corrected to shutdown. Values are for measured Reactor Building conditions of 9.55×10^4 Pa (716 torr) and 299 K.

b. Based on Reactor Building free volume of 5.58×10^{10} cm³ (Reference 17).

c. Calculated percentage of initial inventory (from Table 1).

TABLE 9. TMI-2 RADIONUCLIDE RELEASE TO THE ENVIRONMENT

Isotope	Estimated Quantity Released ^a (Ci)	Percent Release ^d
Kr-88 ^c	3.8×10^5	0.6
Xe-133	1.6×10^6	1.1
Xe-133 ^d	8.4×10^6	5.6
Xe-133m ^c	2.3×10^5	1.1
Xe-135 ^c	3.0×10^5	0.9
Xe-135m ^c	2.5×10^4	1.0
I-131 (via gas path)	15	<<0.01
I-131 (via liquid path)	0.11	<<0.01

a. From Reference 5, decay corrected to shutdown.

b. Calculated percentage of initial inventory (from Table 1).

c. Inventories for these isotopes are not listed in Table 1. They are

- Kr-88 = 6.9×10^7 Ci
- Xe-133m = 2.1×10^7 Ci
- Xe-135 = 3.3×10^7 Ci
- Xe-135m = 2.6×10^7 Ci.

d. From Reference 21.

TABLE 10. TMI-2 FISSION PRODUCT PARTITIONING

Plant Location	Estimated Percentage of Inventory at Time of Accident							
	Cs	I	Xe	Kr	Sr	Sb	Ru	Ce
Fuel and core debris within the vessel	27	33	13 ^a	13 ^a	115	41	61	~100
Vessel internals and primary system piping	~1	<1	nm	nm	<1	<1	<<1	<<1
Primary system coolant	~10	~8	<1	nm	~1	nm	<<1	nm
Reactor and Auxiliary Building sumps and tanks	~45	~41	nm	nm	~2	nm	<1	nm
Reactor and Auxiliary Building surfaces	<1	<1	nm	nm	<<1	nm	nm	nm
Reactor Building atmosphere	<<1	<<1	nm	54	<<1	nm	nm	nm
Environment	nd	<<1	1	~1	nd	nd	nd	nd
Total accounted for (%)	83	82	68 ^b	68	118	41	61	100

nm = not measured.

nd = not detected above background.

a. Calculation only; assumes the apparently intact fuel rods contain their initial inventory.

b. Assumes Xe retained in Reactor Building atmosphere to the same extent as Kr, but had decayed at time of measurement.

FISSION PRODUCT AND CORE MATERIAL BEHAVIOR

S. Langer, M. L. Russell, D. W. Akers
Idaho National Engineering Laboratory
EG&G Idaho, Inc.
P.O. Box 1625, Idaho Falls, ID 83415

INTRODUCTION

The paper by Owen¹ discussed the location of the fission products and the fraction of the initial core fission product content that has thus far been inventoried. Knowledge of the location and inventory of fission products are essential to plant cleanup and are measurable quantities. This paper continues the discussion of fission products and will emphasize the mechanisms of fission-product transport and the pathways through which the fission products were moved from their initial locations in the core to their final locations in the plant systems. Thus, we seek to determine:

- HOW they got there
- WHEN they got there.

The first question relates to transport mechanisms, while the second relates to the question of whether transport took place during the accident or subsequent to it. These are NOT measurable quantities after termination of the sequence of events, but require either modeling, systems analysis, or inference.

Detailed results of the fission-product inventory analyses will also be discussed to demonstrate how data from the damaged core can be used to enhance our knowledge of the accident phenomenology and aid in resolution of SFD accident source-term issues. Understanding of the transport mechanisms and behavior of the fission products and other core materials in the TMI-2 plant systems can contribute to resolving technical issues that are of importance to source-term research. Tolman² has discussed how fission-product data from TMI-2 can be used to aid in resolving the following source-term issues:

- Release of control materials
- Modeling of the in-vessel behavior of fission products including
 - Release of less volatile fission products
 - Chemical reactions which affect transport
- Behavior of tellurium
- Fission-product and aerosol deposition in the RCS

- Revaporization of fission-product plateout in the upper plenum region.

BACKGROUND AND CHRONOLOGY IMPORTANT TO FISSION-PRODUCT RELEASE

The study of the TMI-2 accident fission-product behavior requires determining both the chronology of significant events affecting the escape of fission products and the escape pathways. Both information categories are crucial to determining how and when the fission products moved to their final locations. The escape-path studies also help to focus the fission-product inventory search to the most productive areas, buildings, equipment, and components.

Events Important to Releases During the Accident

Many events occurred during and after the TMI-2 accident that affected the character and distribution of core materials and fission products that escaped from the reactor vessel and the RCS to other locations in the plant. The most significant events (neglecting minor release pathways) include the following:

Time

(2 h) 138 min	Fission products and small fractions of uranium were released in the reactor vessel when fuel rod rupture commenced. Reactor coolant circulation had ceased and the available escape paths (shown in Figure 1) from the RCS were through: (a) the stuck-open PORV to the RCDT, where liquid could escape to the Reactor Building basement floor through the rupture disk, and vapor could escape through vent lines to the Radwaste Disposal Vent Gas System in the Auxiliary Building; and (b) the letdown line downstream of RCP-1A that led to the Makeup/Purification or Radwaste Disposal Systems in the Auxiliary Building.
142 min	The pressurizer/PORV escape path was closed.
150 min	Zircaloy-steam reaction became significant, releasing hydrogen and other chemical-reaction products into the RCS. Core material temperatures eventually reached or exceeded 3100 K, which could (a) generate aerosols from low volatility materials and from chemical reactions, and (b) accelerate the escape of fission products from the uranium dioxide. Sufficient damage to the in-core instrument guide tubes probably occurred to allow coolant to enter the calibration tubes that extend to a "Seal Table" at the Reactor Building 347-ft elevation.
174-192 min (3 h)	The RCP-2B was energized, although it pumped coolant only for seconds. ³ This event is believed to have reflooded the overheated core region, fragmented most of the standing

fuel in the upper core region, and caused circulation of core-material particles and fission products throughout the RCS.

- 192-197 min
220-318 min
340-550 min
565-589 min
600-668 min
756-767 min
772 780 min
- The PORV to RCDT escape path was reopened repeatedly during these time periods.
- 200-267 min
- The HPI pumps were operated alternatively and intermittently during this period, effectively terminating the periods when the total supply of coolant to the core was essentially zero.
- 227 min
- A significant relocation of core material from the core region to the flooded reactor vessel lower plenum region probably occurred. This event probably would increase the escape of core material and fission products to the Letdown System.
- (4 h)
236 min
- The radioactive gas escape path to the Radwaste Disposal Gas Vent System through the RCDT vent was closed during Reactor Building isolation.
- 266 min
- Overpressure in the Makeup Tank lifted the 552 kPa (80 psi) set point liquid relief valve and discharged contaminated RCS liquid to the RCBHTs, which also overflowed and became overpressurized.
- The RCBHT overpressure probably lifted the 138 kPa (20-psi) set point relief valves a short time and allowed unfiltered vapor escape to the atmosphere, via the Radwaste Disposal Gas Relief Header and the Vent Stack. It also is believed that liquid from the RCBHT vents entered the Radwaste Disposal Gas Vent Header, where it is separated and drained to the Auxiliary Building sump.
- 267-544 min
(5 h)
- A Sustained HPI period commenced.
- 370-670 min
- TMI-2 Control Room air became contaminated (both particulate and noble gas channel alarms) requiring use of personnel face masks and particulate filters.
- 590-596 min
(10 h)
- A hydrogen burn occurred in the Reactor Building causing a 193 kPa (28 psig) peak pressure and actuation of the RB Spray, which injected chemically treated (boron and sodium hydroxide) water into the RB during a 6-min-duration actuation period.

949 min (20 h)	Forced circulation cooling of the reactor was resumed through the A-loop with RCP-1A.
1230 min	Overpressure in the Letdown System lifted the 904 kPa (130-psi) set point relief valve MU-R-3 around midnight allowing reactor coolant escape to the RCBHT. The RCBHT relief valves are believed to also have lifted, allowing unfiltered vapor escape to the atmosphere, and probable entry of liquid to the Auxiliary Building Sump through the Radwaste Disposal Gas Vent Header. This condition lasted longer than 40 min.
1331 min	TMI-2 Control Room air became contaminated requiring use of personnel face masks and particulate filters for 64 min.
1475 min	An escape path was created by opening the makeup tank vent valve to the Radwaste Disposal Gas Vent Header. This pathway was reopened periodically for the next several days.
(30 h) 2050 min	A helicopter measured 3 R/h beta-gamma and 410 mR/h gamma at 15 ft above the TMI-2 Vent Stack.
30 d-10 h	Natural circulation cooling of the reactor commenced April 27, 1979.
30 d	Auxiliary Building decontamination commenced April 27, 1979.
5 month	EPICOR-II cleanup of medium contamination water commenced October 1979.
16 month	Reactor Building gas cleanup and venting commenced and included reopening of the Vent Stack.
28 month	SDS/EPICOR-II cleanup of the highly contaminated water from the Reactor Building basement commenced and included cleanup of an equivalent of four RCS volumes of reactor coolant water.
36 month	Reactor Building decontamination commenced in March 1982.

An estimated 2.4×10^6 L (643,000 gal) of contaminated water collected in the Reactor Building basement between accident initiation and interaction of SDS cleanup of the water. The steadily increasing depth of water in the basement at key accident-sequence events was as follows:

<u>Time After Accident Initiation</u>	<u>Event</u>	<u>Basement^a Water Depth (m)</u>
227 min	Major core material relocation to reactor vessel lower plenum region	2.5 x 10 ⁻¹ (10 in.)
15 h-40 min	Commence sustained forced-circulation cooling of core	8.1 x 10 ⁻¹ (2 ft-8 in.)
30 d-10 h	Commence natural circulation cooling of core	1.3 (4 ft-3 in.)
910 d (9-23-81)	Commence SDS cleanup of RB basement	2.6 (8 ft-6 in.)

a. Assumes linear relationship of liters of water to water depth; 2.4 x 10⁶ L (643,000 gal) equals 2.6-m (8 ft-6 in.)-water depth.

The basement water is believed⁴ to have been composed of the following sources on 9-23-81:

<u>Water Source</u>	<u>Percent</u>
Reactor Coolant System water: first 72 h of accident	41
next 907 d	28
Reactor Building Spray System water	3
Susquehanna River water	<u>28</u>
	<u>100</u>

The spray system water contained boron and sodium-hydroxide chemicals and the river water (from leaks in the river water cooling system) silt was composed of the following major elements in order of concentration: Fe, Si, Mn, Pb, Ca, K, S, Al, Ba, Na, and Ti.

The TMI-2 buildings and equipment are still being decontaminated. The decontamination process commenced April 27, 1979, 30 d after accident initiation. All fluid systems have been flushed, fluid and gas filters removed, fluid treatment resin beds removed or decontaminated, and TMI-2 accident liquid effluent decontaminated. The decontamination has not yet reduced radiation to personnel-entry levels in the following areas:

- The Reactor Building basement, which includes the letdown coolers, the RCDT, sediment containing fission products and core materials, and concrete that has absorbed liquid contaminated with fission products and core materials.
- The Reactor Building D-ring compartments, which contain the components of the Reactor Coolant Loops.

- The Fuel Handling Building Makeup and Purification Valve Room, which contains the letdown system block orifice and piping.

The above conditions mean that (a) samples that are representative or traceable to plant conditions that existed during the accident are no longer numerous, and (b) sample acquisition from personnel exclusion areas is limited to what can be obtained with remote-operated tools and robots.

The event sequence shows a chronological separation of the core-damage events and the offsite radiation releases. The core damage probably ended about 3 h-20 min after accident initiation when the HPI refill of the RCS commenced, whereas offsite radiation releases apparently began with the measurement of TMI-2 Control Room air contamination at 6 h-10 min after accident initiation. (It is believed that the Control Room air was contaminated by the outside air.) The offsite radiation releases continued for several days until the makeup tank venting was no longer necessary.

The measurement of the offsite radiation source characteristics showed that noble gases were the dominant contributor to the offsite source term and cesium and iodine contributions were negligible.⁵ This observation indicates that effectively all of the nongaseous fission-product (cesium, iodine, strontium, etc.) inventories were retained by the TMI-2 buildings and equipment during the TMI-2 accident sequence (Reference 5).

Pathways for Release

The pathways for release of the core fission products and materials during and after the TMI-2 accident are described in this section. The escape paths that contributed to the major releases to plant systems are emphasized.

A map (Figure 2) has been developed to show schematically the TMI-2 equipment, buildings, and areas that are believed to be either migration paths or destinations of core fission products or materials during and after the TMI-2 accident sequence. The purpose of the map is to provide an aid to explaining and studying the fission-product behavior during and after the accident sequence.

TMI-2 accident studies have concluded that the major fission-product escape paths from the RCS during the accident sequence were as follows (in descending order of importance): (See Figure 1 also for a schematic diagram of the major escape paths.)

- Through the PORV/RCDT rupture disk route to the Reactor Building basement floor and free volume.
- Through the Letdown System to the Makeup/Purification System, Radwaste Disposal Liquid System, Radwaste Disposal Gas Vent and Relief Systems, AFHB free volume and air exhaust system, and the Vent Stack to the atmosphere.

The minor escape pathways include the: PORV/RCDT vents, RCS sample line, B-loop steam generator tube leaks, and Secondary Steam System.

The reactor vessel bottom and core instrument cable chase regions have not been explored sufficiently to determine whether or not an escape path developed from the RCS to the Reactor Building free volume through the core instrument train tubes beneath the reactor vessel. Fission products did not escape to the Auxiliary Building by Reactor Building sump pump action, because the escape path was closed prior to fuel rod rupture.

After the commencement of core cooling by natural circulation (April 27, 1979) all fission-product escape paths were controlled including: (a) the venting of Reactor Building radioactive gases through filters and the Vent Stack to the atmosphere, and (b) the transport to offsite repositories of filters and ion-exchange resin from cleanup and decontamination of the TMI-2 accident liquid. The water cleanup systems included the following:

- The already-installed EPICOR-I system at TMI-1 for water with less than 1 $\mu\text{Ci/mL}$ contamination.
- The EPICOR-II system, which was specially installed for cleanup of water with 1 to 100 $\mu\text{Ci/mL}$ contamination.
- The SDS, which also was specially installed in the TMI-2 AFHB spent-fuel storage pool for cleanup of water with greater than 100 $\mu\text{Ci/mL}$ contamination.

APPLICATION OF FISSION-PRODUCT ANALYSES TO ACCIDENT PHENOMENOLOGY

This section discusses the retention of several core-material constituents in the debris bed. These data are then utilized, in conjunction with fission-product retention data reported in the paper by Owen¹, to speculate on mechanisms by which these materials were removed from the core region, thus enhancing our knowledge of the accident phenomenology.

The concentrations of uranium and zirconium in eight samples from two locations in the upper core debris bed are shown in Figure 3. The upper dashed line represents the initial average concentration of uranium in the core, while the lower line represents the average concentration of zirconium. Within experimental error, these data show essentially quantitative retention of uranium in the debris bed. On the other hand, not a single sample has a Zr concentration equal to the initial core average and it is clear that a significant depletion of Zr in the core has occurred. (The remaining fraction of the samples is mostly oxygen.) This is more evident in the E9 sample than in the H8 samples and is further evidenced by the higher average U concentration in the E9 samples. There is no obvious dependence of U or Zr concentration with depth into the bed.

Since neither Zr nor ZrO_2 has a significant volatility and are quite insoluble in water, the transport of Zr from the core-debris region probably occurred by melting of the Zr-4 cladding and relocation of Zr to lower regions of the core or the reactor vessel. Clearly, this process must have occurred during a period of core uncovering.

The retention of control rod materials in the debris bed is shown in Table 1. The retentions of Cd and In are below the limits of analytical detection, which are 0.03 and 0.36 fractions of the (initial) core inventory, respectively. Only about 0.09 fraction of the predominant control rod material, Ag, remains in the debris bed. Cd is the most volatile element in the control rod alloy, having a partial pressure of 41.9 MPa at 1700 K,^{6,7} the approximate failure temperature of the control rod. At this temperature, the partial pressures of Ag and In are ~10⁻⁵ MPa (References 6 and 7) and, thus, are unlikely to be lost by volatilization of the metal. While aerosol formation of the metal or oxide are considered possible modes of transport for the control rod material⁸, <3% of the Ag inventory has been found in the upper pressure vessel plenum and the RCS where aerosol particles would have been expected to deposit had they been transported from the core as aerosols. It seems likely, therefore, that the control materials relocated from the core-debris region in the same manner as the Zr, by melting and gravity-induced flow to lower portions of the core or to the RPV lower plenum.

The retention of ceramic burnable poison materials in the debris bed is shown in Table 2.^a The TMI-2 core contained burnable poisons in the form of $B_4C-Al_2O_3$ and $Gd_2O_3-UO_2$ pellets clad in zircaloy-4. Table 2 shows that the Al has been largely depleted from the core while the Gd has been fully retained. Al_2O_3 is a stable oxide (ΔG° (298 K) = -527.4 KJ/mol O) but is thermodynamically reduced to aluminum metal by Zr at 2000 K. Thus, upon reduction, Al can be lost from the core either by vaporization ($p_{Al} = 0.27$ MPa at 3000 K)⁹ or by dissolution in the liquid Zr and flow to the lower regions of the core. A similar mechanism would seem to be applicable to gadolinia, which is less stable than alumina and, thus, also thermodynamically unstable with respect to Zr. However, gadolinia is in solid solution with UO_2 at low concentrations and is, therefore, stabilized by the UO_2 . The analytical data show that the UO_2 was fully retained in the core; it would, therefore, be expected that the Gd_2O_3 would also be retained. These data on the burnable poison materials provide further evidence of relocation of certain species from the debris bed by gravity-induced flow to lower regions of the core.

Table 2 also indicates major depletion of structural materials from the core-debris region. These may also have been lost by relocation to lower portions of the vessel by melting prior to formation of molten ceramic phases in the core materials.

a. Because of the high concentration of boron in the reactor coolant, required to keep the system subcritical, boron concentrations in any sample of core or RCS material has no significance.

Fission-product release data can also be applied to elucidating transport mechanisms and degradation phenomenology. In his paper, Owen showed that 27% of the cesium and 33% of the iodine were retained in the debris bed, while 45 and 41% of these species were relocated to the sumps, tanks, and basements of the Reactor and Auxiliary Buildings. Cubicciotti¹⁰ has calculated thermodynamically that, at the temperatures estimated by metallographic analysis of leadscrews in the plenum, virtually quantitative plateout of the thermodynamically expected volatile species containing these fission products would occur on plenum surfaces as condensed vapor on aerosol particles. We can, therefore, look at Cs and I transport as three-phase processes in which they were (a) initially volatilized from the hot core during core uncovering, (b) plated out in the RPV upper plenum, and (c) subsequently transported to the ex-RCS tankage and the RB basement by reactor coolant upon recovery of the core during the B-pump transient or after 200 min into the accident when HPIS cooling was resumed or following the resumption of forced circulation following the accident.

It is not yet known what fraction of the fission products found in the ex-RCS system were transported during the accident and what fraction may have been leached directly from the core itself subsequent to the resumption of sustained core cooling. Figure 4 shows the concentrations of four fission-product species in the reactor coolant during approximately the first year following the accident. Since the data in Figure 4 are decay-corrected, a horizontal line would indicate a constant concentration. It is evident that the concentrations of Cs, I, and tritium (T) are decreasing with time, while Sr has increased. That is, even if Cs, I, and T were being leached from the core during this time period, the removal rate by dilution, demineralizer processing, and precipitation (in the basement) exceeds the input rate by leaching. For Sr, however, the input by leaching exceeds the removal rate; in fact, roughly 90% of the Sr in the coolant has been introduced by leaching since termination of the accident. (Strontium in the coolant does not exceed about 1% of the core inventory.) The evidence thus indicates that accident release and postaccident release may be different for the various fission product species.

FISSION-PRODUCT RELEASE AND TRANSPORT MECHANISMS

The release of fission products from the TMI-2 core and their subsequent transport to other parts of the reactor system must be considered as a three-stage process involving:

- Initial release of volatile species or aerosols from the core
- Probable plateout on surfaces in the RPV on aerosol particles
- The leaching of soluble species from the plateout films or the transport of the aerosol particles by coolant water as hydrosol to other portions of the plant.

From an accident evaluation viewpoint, the first-stage process is of primary importance; from a plant recovery viewpoint, the latter process is likely of primary importance.

Previous studies of fission-product release from the reactor core have considered only release from a partially uncovered core (References 7, 8, and 10). This is, of course, quite logical since fuel rod rupture and subsequent release require loss of cooling and core uncovering to permit core heatup to the point of rod failure. The release mechanism is assumed to be volatilization of fission products in their equilibrium chemical form into a stream of H_2 and H_2O in time-varying ratios. The H_2/H_2O ratio may affect the dominant volatile species for each chemical element. However, the TMI-2 accident was not quite so simple, nor quite so severe. The core was both HOT AND UNCOVERED and HOT AND COVERED during the time period from 138 to 200 min into the accident. Two periods of core uncovering, 138 to 174 min and 190 to 200 min (based on the present best estimate scenario and SCDAP calculations), were separated by a period during which the core was recovered during the B pump transient. Thus, the possibilities are release by volatilization into an H_2/H_2O stream and the release directly into coolant by leaching of species from fuel surfaces and accessible grain boundaries. One may postulate that release during the short (~15 min) period following the B pump transient is small, but that is far from established fact. In actuality, we do not know in which state the dominant release occurred.

In addition to the uncertainty concerning the release during the various periods during the accident, the release subsequent to the resumption of sustained core cooling is also unknown. The release directly to the coolant by leaching during the long (~5 y) postaccident period may exceed the release during the accident itself for certain species. Presently, it is simply not known for all species, since neither the accident release or the postaccident leach release can be measured. While the total release can be measured, the quantity needed to compare with severe accident code calculations is the direct release during the accident.

The only means of obtaining the direct release during the accident is by subtracting from the measured total release the release during the postaccident period. This latter quantity may possibly be obtained in two ways:

- By estimating it from the records of the reactor coolant volume passing through the system and the concentrations of fission products in that system as a function of time following the accident
- By calculating it from models of the leaching of irradiated, damaged fuel based on separate effects leaching experiments.

To date, neither of these techniques has been successfully applied to TMI-2, although attempts are underway.

The mechanisms of fission-product transport discussed above, volatilization, aerosol formation, leaching, are probably sufficient to account for the transport of fission products to other portions of the RCS and to other plant systems. However, in the case of TMI-2, there was an additional mechanism for transport of fission products and other core

materials out of the core. The finding of 10 to 20 t of core material in the lower plenum region of the RPV strongly suggests that fission products may have been transported by other core materials as they relocated by melting and gravity-induced-flow to the lower head of the RPV. Until a sufficient number of samples of the lower head debris is obtained to fully characterize and assay the 10 to 20 t of material, including its fission-product content, a complete analysis of the accident release and the leach release is not possible.

The different fission-product species may be expected to have exhibited different behavior during the various accident phases and during the postaccident leaching based on the relative volatilities of the dominant vapor species and the solubilities of the condensed-phase compounds in water (or in the molten core material that relocated to the lower plenum). Any model developed on the basis of the behavior of one fission product must be validated by demonstrating that it can also account for the behavior of other species that had different volatility and solubility properties.

Resolution of the remaining issues concerning fission-product behavior await the acquisition of samples from unexplored portions of the core, the lower plenum, and the Reactor Building basement. The specific technical issues remaining to be addressed include:

- Core damage progression/core slump and collapse/reactor vessel failure modes
- Release of control rod materials
- Release of low-volatility fission products
- Chemical interactions affecting fission-product transport
- Tellurium behavior.

SUMMARY

This paper has (a) discussed the mechanisms, pathways, and chronology of fission-product and core-material transport during and after the TMI-2 accident, (b) shown how analysis of fission-product transport can enhance our knowledge of the accident scenario, and (c) outlined the plan to complete the TMI-2 fission-product behavior study.

The sequence of significant events that affected the character and distribution of fission products that escaped from the reactor vessel clearly show a chronological separation of the core damage event sequence and the development of the offsite radiation releases.

The escape paths for the fission products from the RCS can be divided into major and minor pathways. The major pathways are through the Letdown System and Radwaste Disposal Gas Vent and Relief Headers to the Auxiliary Building free volume and offsite atmosphere, and the PORV/RCDT rupture disk

to the Reactor Building basement floor and free volume. The minor pathways are the PORV/RCDT vents, the RCS sample line, and through B-loop steam generator tube leaks to the Main Steam System. The core instrument tube regions have not been examined sufficiently to determine if they are significant escape paths. (A reactor vessel bottom leak path is not anticipated because the vessel appears to be leak tight.)

Detailed analysis of core-debris samples for major core constituents and several fission-product species has shown essentially complete retention of uranium and gadolinium in the upper debris bed, but significant depletion of zirconium; the control materials Ag, Cd, and In; and the structural materials and aluminum. It is believed that the volatile fission products Cs and I vaporized from the core, while the core metals relocated to the unexplored lower core regions or the lower plenum.

The relocation of several of the fission products in TMI-2 is considered as a three-stage process, involving initial transport from the core to other locations in the RPV where plateout or collection on aerosols occurred, with subsequent transport in an aqueous medium to other locations in the plant. Complicating the analysis of this accident release is the long-term leaching of the core and transport of soluble fission products to other portions of the RCS. Additionally, the fission products found in the lower plenum of the RPV must be considered a part of the accident release, although they did not contribute to the source term. It is possible that the various fission-product species behaved differently in each of these relocations based on their chemical form or solubility in the coolant, or in phases flowing to the lower plenum of the RPV.

The TMI-2 Accident Evaluation Program includes a Sample Acquisition and Examination Plan and a Fission-Product Inventory Evaluation Plan, which together will complete the study of the TMI-2 accident fission-product behavior and focus the research findings towards resolving a number of severe core damage accident technical issues.

REFERENCES

1. D. E. Owen, T. E. Cox, J. M. Broughton, "Fission Product Transport at Three Mile Island", Proceedings of the First International Information Meeting on the TMI-2 Accident, Germantown, MD, October 21, 1985.
2. E. L. Tolman, "TMI Accident Evaluation Program Overview", Proceedings of the First International Information Meeting on the TMI-2 Accident, Germantown, MD, October 21, 1985.
3. Nuclear Safety Analysis Center, Analysis of Three Mile Island Unit 2 Accident, NSAC-80-1, 1980.
4. C. V. McIsaac and D. G. Keefer, TMI-2 Reactor Building Source Term Measurements: Surface and Basement Water Sediment, GEND-042, October 1984.
5. M. Rogovin, Three Mile Island, A Report to the Commissioners and to the Public, NUREG/CR-1250, January 1980

6. D. Kubaschewski, E. L. Evans, C. B. Alcock, Metallurgical Thermochemistry, 4th Ed., Pergamon Press, Oxford, 1967.
7. D. Cubicciotti and B. R. Sehgal, "Vaporization of Core Materials in Postulated Severe Light Water Reactor Accidents", Nucl. Tech., 67, 191 (1984).
8. R. P. Wichner and R. D. Spence, Quantity and Nature of LWR Aerosols Produced in the Pressure Vessel During Core Heatup Accidents: A Chemical Equilibrium Estimate, NUREG/CR-3181 (ORNL/TM-8683), 1984.
9. D. R. Stull and H. Prophet, JANAF Thermochemical Tables, 2nd Ed., NSRDS-NBS-37, 1971.
10. D. Cubicciotti and B. R. Sehgal, "Vapor Transport of Fission Products in Postulated Severe Light Water Reactor Accidents", Nucl. Tech., 65, 266 (1984).

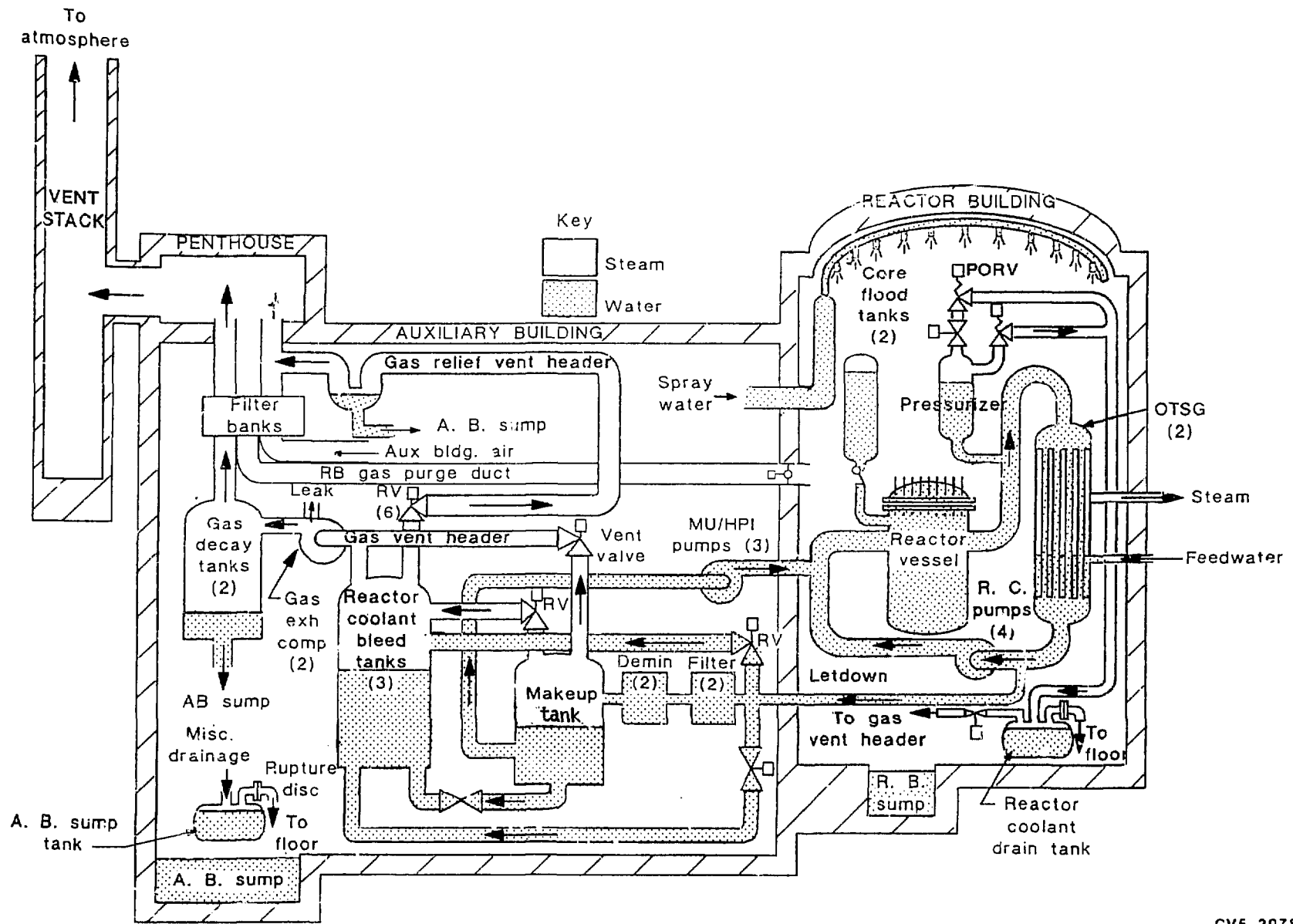


Figure 1. TMI-2 accident fission product escape paths schematic.

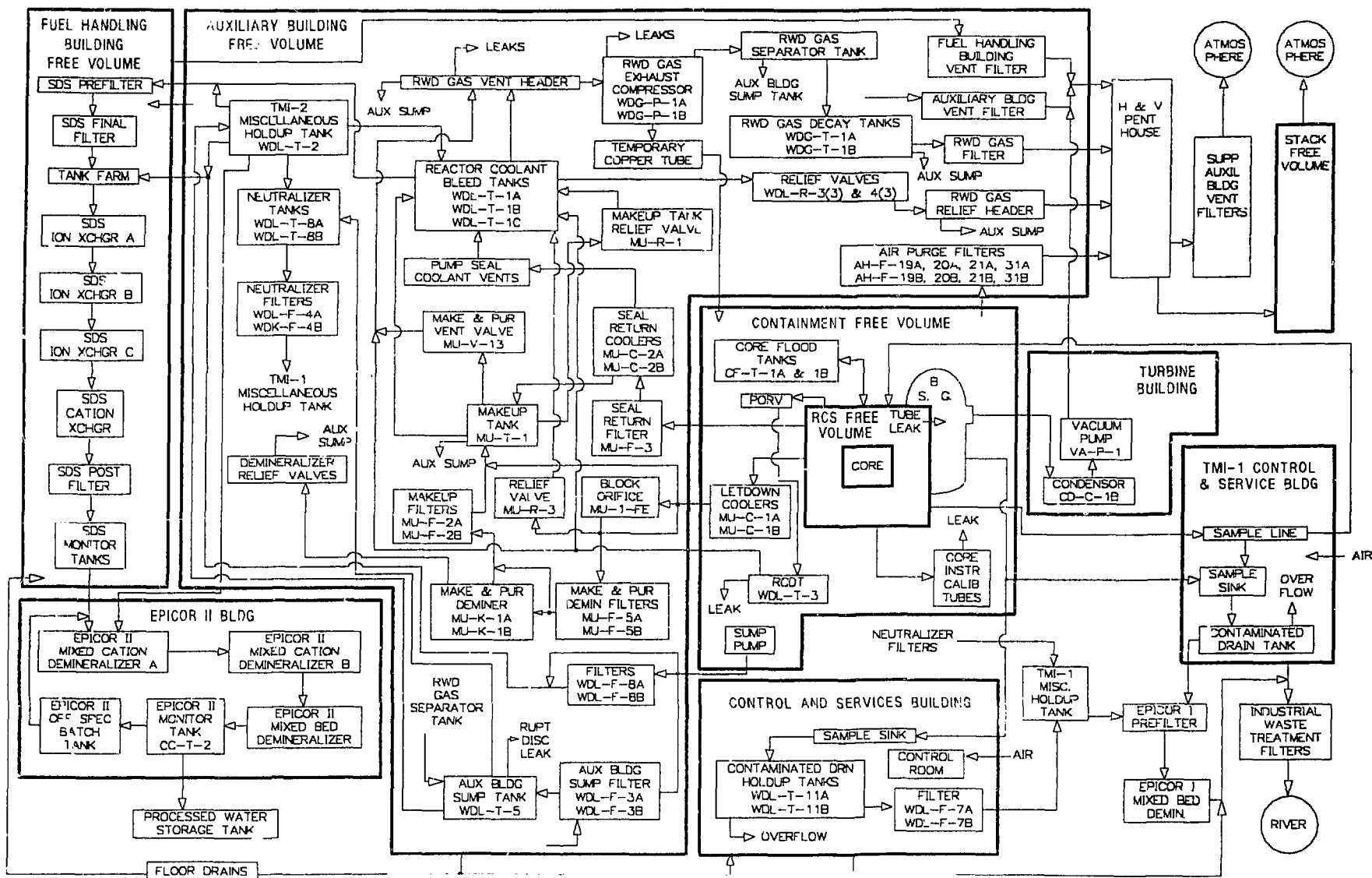


Figure 2. Radioactive material location map.

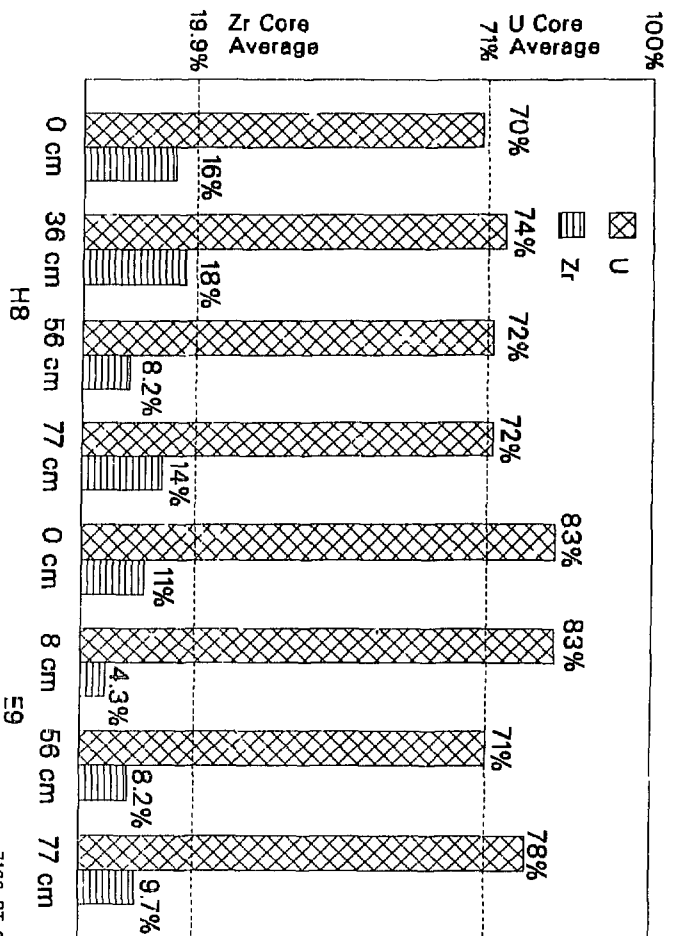


Figure 3. Bulk sample Zr/U concentrations in the reactor core.

2165-ST-0127 '83

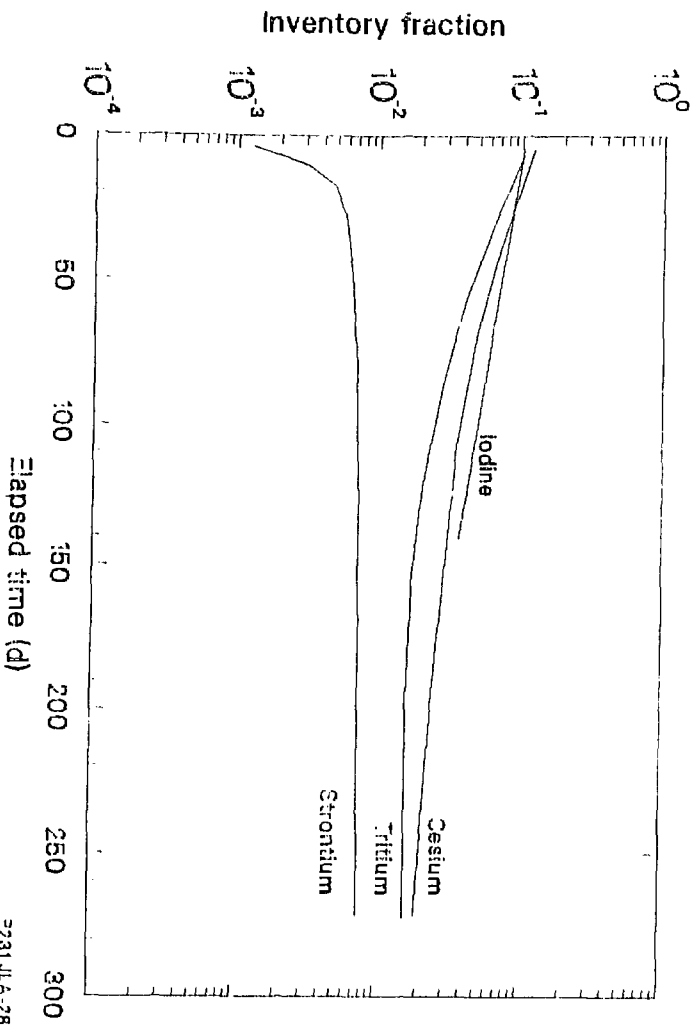


Figure 4. Trends in reactor coolant inventories.

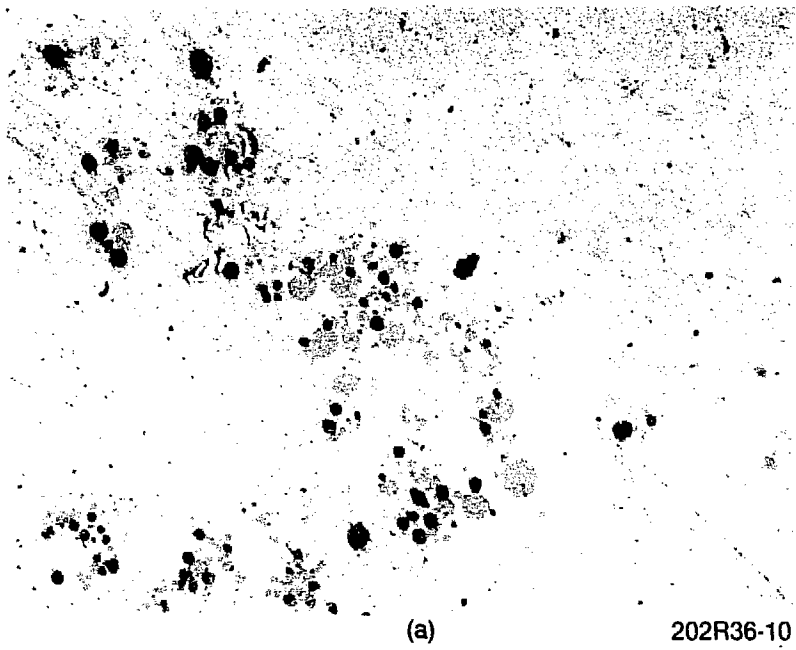
TABLE 1. CONTROL ROD MATERIAL RETENTION IN THE DEBRIS BED

<u>Element</u>	<u>Mol Fraction (wt%)</u>	<u>Core Average Concentration Debris Bed (wt%)</u>	<u>Measured Concentration (wt%)</u>	<u>Fraction of Core Inventory</u>
Cd	5	0.12	<3.3E-3	<0.03
In	15	0.33	<0.12	<0.36
Ag ^a	80	1.75	0.15	0.09

a. <3% of Ag inventory has been found in the plenum and RCS.

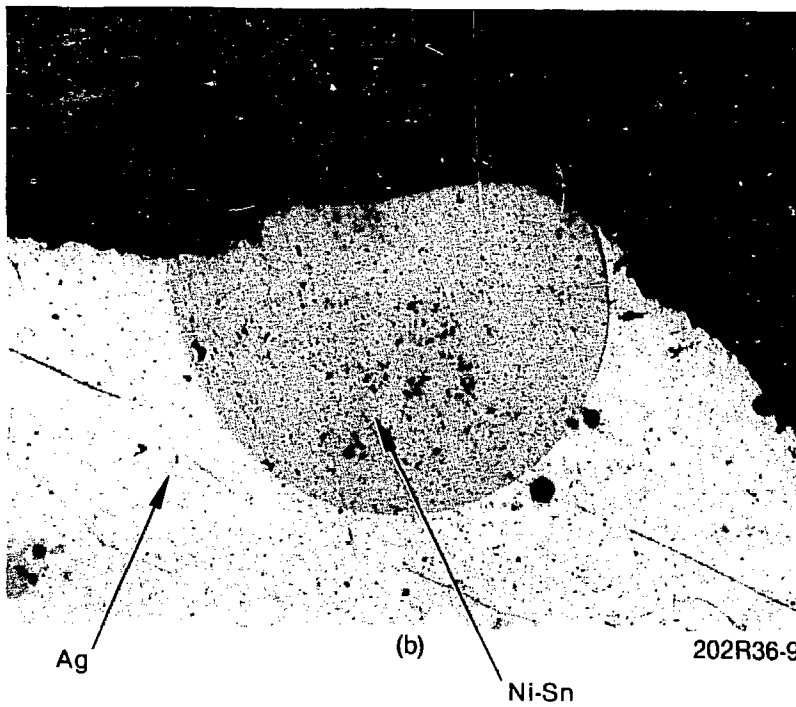
TABLE 2. POISON AND STRUCTURAL MATERIAL RETENTION IN DEBRIS BED

<u>Material</u>	<u>Core Average Expected Concentrations (wt%)</u>	<u>Measured Concentrations (wt%)</u>	<u>Fraction of Core Inventory</u>
<u>Poison Rod</u>			
Al (B ₄ C-Al ₂ O ₃)	0.18	<7E-2	<0.39
Gd (Gd ₂ O ₃ -UO ₂)	0.01	~5.9E-2	>1.0
<u>Structural</u>			
Fe	3.0	6.8E-1	0.23
Mn	0.09	4.5E-2	0.50
Ni	0.91	0.46	0.51
Cs	1.00	0.21	0.22



(a)

202R36-10



Ag

(b)

Ni-Sn

202R36-9

Figure 15. Particle 96 from the 30-1/2-in. elevation at location HB

CORE AND POTENTIAL STRUCTURAL DAMAGE

CORE RELOCATION PHENOMENOLOGY

Robert E. Henry, Hans K. Fauske, Michael Epstein
Michael N. Hutcherson, Marc A. Kenton
Fauske & Associates, Inc.
16W070 West 83rd Street
Burr Ridge, Illinois 60521

ABSTRACT

Analyses have been performed to determine the water inventory in the TMI-2 reactor core during the time interval between the B-loop pump start at 174 min and 227 min when core material possibly was transported into the reactor vessel lower plenum. These analyses are accompanied by estimates of the net steam generation at specific times during this interval, as well as the thermal behavior within a badly damaged core that has progressed to a liquified or molten central region. These analyses demonstrate that the core was covered with water at approximately 200 min into the accident and the net steam generation rate at best only approached the decay power. As a result, the average core temperature was increasing. This probably continued until the event at 227 min resulted in core geometry changes and an ultimately coolable configuration.

The evaluation of thermal propagation for a severely damaged core indicates that thermal attack alone does not appear to be sufficient to explain the progression of material into the lower plenum. However, considerations of chemical attack (eutectic formation) or significant primary system pressure changes could lead to a local failure of the core-support structure, as evidently occurred.

INTRODUCTION

During approximately the first 2.5 h of the TMI-2 accident, about half of the primary system coolant was lost to the containment through a stuck open PORV on the pressurizer. At approximately 100 min into the accident, the last set of reactor coolant pumps were tripped, allowing the remaining primary coolant to separate into liquid and vapor phases. As a result, limited water inventory was available to maintain core cooling, and within minutes, the top of the core was uncovered and began to overheat. The core degradation continued until approximately 174 min into the transient when the RCP-2B was started and a significant quantity of water was added to the core. This resulted in a pressurization of the primary system from about 9 to 14 MPa over the next 2 min.

In the 45 min following the RCP-2B pump start, the pressurizer MOV (also referred to as RC-V2) and the HPI were activated at different times. These actions and the response of the reactor system provide insight into the core coolability at key times through assessments of the apparent core steaming rates at these times. In addition, the injection caused water to drain from the pressurizer and cover the reactor core. Consequently, this is a critical time interval in the progression of the TMI-2 accident.

Steam condensation and cooling of noncondensable gases resulting from the HPI caused a rapid decrease of the primary system pressure between 200 and 207 min. This depressurization caused a substantial amount of water to drain from the pressurizer and ultimately onto the overheated core. The combination of this and the injection water caused the core to be completely covered, and the reactor vessel filled to the top of the hot legs within this 7-min interval. During this time, the cold legs evidently developed a sizable gas volume, as indicated by the primary system pressure and the measured cold leg temperatures. At about 207 min, the pressurizer level reached a minimum, stayed constant for about 3 min, and then increased at approximately 0.5 m/min. This response provides insight into the water inventory within the primary system and will be discussed in the next section.

During the period that the MOV was open (192 to 197 min), the primary system pressure decreased approximately 1.4 MPa. This was accompanied by a drop of about 0.4 m in the pressurizer-water level. High pressure injection using MUP-1A and -1C, in the ESF mode was initiated at 200 min and continued for 17 min. This cold leg injection condensed steam and cooled noncondensable gases, thereby causing the primary system pressure to decrease and drain water from the pressurizer. Specifically, during this period, the pressure decreased from 13.3 to 10.2 MPa and the pressurizer-water level dropped 3.5 m. The rate of change in the primary system condition caused by these state changes provides insight into the net core steaming rate at various times during the interval between 174 and 227 min.

Assuming the core to be badly damaged during this interval before the core changed configuration at 227 min, analyses were carried out to assess the thermal propagation of a core with a molten center. These analyses have concentrated on the general progression of thermally dominated events to determine if downward propagation could be achieved through thermal mechanisms alone. Key elements of these analyses include the driving forces for internal circulation and the possible crusts to be formed at the upper and lower pool boundaries. In addition to the thermal propagation, additional mechanisms due to eutectic formation between the fuel and unreacted Zircaloy, as well as the primary system pressure changes during this interval, are also considered.

WATER INVENTORY

The onset of HPI in the ESF mode at 200 min provides a strong condensation and cooling source within the cold legs. Condensation of steam and cooling of noncondensable gases in the four cold legs caused the primary system pressure to decrease rapidly. As a result, the pressurizer drained water into the A-loop hot leg and subsequently into the core. Both the HPI water and the water drained from the pressurizer increased the water inventory in the core region, as demonstrated by a rapid decrease in the signal from the source range monitors at this time¹. The subsequent accumulation of water within the primary system is determined by the extent of injection, the water drained from the pressurizer, and the specific regions in which the water accumulation occurs.

Water Accumulation in the Reactor Vessel

Injection of cold water into the cold legs condensed steam and cooled the hydrogen accumulated in these regions, thus causing the local pressure to decrease. A pressure differential of about 2 kPa between the cold legs and the reactor vessel upper plenum was sufficient to open the flapper valves at the top of the downcomer (see Figure 1). This would allow more steam and hydrogen to enter the cold legs to maintain an essentially equal pressure throughout the primary system. As a result, the cold legs accumulated hydrogen to essentially offset the condensation of steam. Consequently, the gas/vapor mixtures in this region became rich in hydrogen, which is in agreement with the recorded behavior of the primary system pressure and cold leg temperatures (well below saturated steam). At the beginning of the HPI, the recorded cold leg temperatures averaged about 490 K with the corresponding vapor pressure at 2.3 MPa, as compared to the primary system pressure of about 13 MPa. At the end of the injection, the cold leg temperatures averaged approximately 420 K corresponding to a vapor pressure of 1.1 MPa, with the primary system pressure at about 10.7 MPa. With a gas pocket formed in the cold legs and downcomer, the water drained from the pressurizer into the reactor vessel would be held within the core. This is due to the movement of the water from the core into the downcomer and cold legs that compressed the gas trapped in this region. At the elevated primary system pressures recorded during this time interval, the cold leg and downcomer gas volumes need only be compressed slightly (about 1%) to maintain the static head of water sufficient to fill the reactor vessel to the hot leg nozzles. As a result, water drained from the pressurizer into the core region would be maintained within the core, and the trapped, noncondensable gases would prevent the downcomer from filling.

In essence, the same arguments are true for the HPI water that is injected into the cold legs. As the water drains into the downcomer and attempts to fill it, this accumulation compresses the gas space in the cold legs, downcomer, and upper plenum. Consequently, any attempt to fill the downcomer and compress the cold leg and downcomer gas volumes would result in pushing the water from the downcomer into the core region. Thus, the HPI water ultimately is transferred into the core region, and the downcomer would remain essentially filled with gas.

Water Inventory in the Reactor Vessel

To analyze the filling of the reactor vessel, it is convenient to begin late in the ESF-injection period and work backward toward the time of initiation. As illustrated in Figure 2, the pressurizer level reaches a minimum at about 207 min and remains constant for approximately 3 min before increasing again to a completely full condition. When the pressurizer level begins to rise, the water level in the A-loop hot leg must be at the height of the surge line (see Figure 3). Working backward from this point in time at the filling rate of the primary system determined by the pump curve (Figure 4), the 180 s of constant pressurizer level corresponds to the time required to fill a portion of the vapor/gas space in the RPV upper plenum, the downcomer region, and the hot legs from an elevation equal to the top of the not-horizontal section (Figure 5) to

the surge-line entrance. The particular volume of injected water deposited within these regions is such that the fractional change in gas/vapor space in these regions is approximately equal. In other words, the start of the constant pressurizer level condition, designated as point "A" in Figures 2 and 4, corresponds to a completely filled horizontal hot leg. The flapper valves were decoupled from the large gas volume in the vertical section of the hot legs and the gaseous volumes in the steam generators. At this time, the area for additional steam condensation and cooling of noncondensable gases decreased from a value typical of the entire cross-sectional area of the reactor vessel (about 25 m²) to the cross-sectional flow area of the hot legs (about 1.5 m²). This volumetric decrease caused the primary system depressurization to terminate (Figure 6) and also stopped the draining of the pressurizer.

The formation of large gas pockets in the cold legs is also in agreement with the recorded reactor coolant pump behavior. At 248 min, RCP-1A was started (Reference 1) and both the starting and running currents were measured. The latter was very low; therefore, the pump was tripped after about 1 min of operation. This low-current reading suggests that the pump could not be primed, indicating a gas volume had accumulated in the A-loop cold legs.

Determining points A and B in Figures 2 and 4 and concluding that the downcomer and cold legs would be substantially filled with gas allows the calculation of the reactor vessel water inventory to be extrapolated from point A back to the point of HPI initiation, point C in Figure 4. This is illustrated in Figure 7 considering the volume of the upper plenum region and the core that must be filled by the injection water. As illustrated in Figure 4, the water level at the time of HPI initiation is less than about 1 m above the bottom of the core, which is consistent with the effective steaming rate calculations for this time that will be discussed later. These calculations demonstrated that the net core steaming at this point in time was nil since the core was almost completely uncovered. Hence, these calculations are consistent.

Primary System Pressurization

At 207 min when the pressurizer stopped draining, the primary system pressure began to rise as a result of the reduced heat transfer area and the continued HPI flow. A demonstration of the consistency in the calculations can be shown by equating the primary system pressurization rate due to the HPI after 210 min, assuming negligible heat transfer and condensation, and comparing this with the measured rate of pressure increase. A strip chart record of the primary system pressure indicates that the pressure rose about 0.7 MPa in 430 s, i.e., an average pressurization rate of about 1600 Pa/s. At the prevailing primary system pressure (about 10.7 MPa), the pump head curves for the HPI pumps indicate an injection rate of approximately 45 L/s. Considering the upper region of the primary system to behave as an isothermal gas volume being pressurized by this liquid displacement, the primary system pressurization rate can be estimated by

$$\frac{dP}{dt} = - \frac{P}{V} \frac{dV}{dt} \quad (1)$$

where P is the pressure and V is the gas volume in the primary system. For an average primary system pressure during this interval of 10.7 MPa and an approximate gaseous volume of 120 m³, Equation (1) yields a pressurization rate of about 4000 Pa/s. While this is somewhat larger than the actual measured behavior, the difference may well be due to continued condensation and heat transfer. This calculation illustrates that the primary system pressurization rate is consistent with water injection at a rate typical of the ESF-HPI system during this interval.

NET STEAM GENERATION FROM THE CORE

Core Steaming When the MOV Was Open

To assess the coolability of the core, the core steaming rate can be estimated when the MOV was open during the interval 192 to 197 min. The MUP-1A also was running during this period, but at a highly throttled condition. Also, the RCP-2B was operating for the first 25 s that the valve was open. The core-water level was probably at or below the core midplane at this time.²⁻⁵

During this period, the reactor primary system can be approximated as a large volume partially gas/vapor filled and partially water filled (see Figure 8) with the pressurizer initially venting gas/vapor when the MOV opened. It is during this period that simplified calculations can be employed to estimate the steam generation within the core. When the valve was open, the gas/vapor volume depressurization rate (dP/dt) can be related to the mass flow rate out of the pressurizer relief line (m_{g,x}) and the vapor mass generation rate within the primary system (m_{g,gen}) as

$$\dot{m}_{g,gen} = \dot{m}_{g,x} + \frac{V_g}{RT_g} \frac{dP}{dt} \quad (2)$$

where V_g is the vapor volume within the primary system, R is the gas constant, and T_g is the vapor temperature. In this representation, the vapor has been assumed to be steam behaving as an ideal gas. MAAP calculations show the voided volume of the primary system to be about 150 m³, and the pressurizer temperature approaches 600 K at this time. These approximate values are sufficient to analyze important trends in the primary system behavior.

The vapor mass flow rate through the relief line (m_{g,x}) can be calculated as

$$\dot{m}_{g,x} = G_c A_{RV} \quad (3)$$

where A_{RV} is the flow area through the relief valve, and G_C is the exiting critical mass flux that depends on whether all steam or a two-phase, steam-water mixture is discharging from the pressurizer. For all steam discharge, the critical mass flux G_C is given by

$$G_C^2 = \frac{\gamma P_0^2}{RT_g} \frac{2}{\gamma + 1} \frac{\gamma + 1}{\gamma - 1} \quad (4)$$

where P_0 is the stagnation pressure within the pressurizer, T_g is the steam temperature (taken as the saturation temperature corresponding to the P_0), and γ is the isentropic expansion coefficient.

Opening of the MOV and the subsequent depressurization could have caused sufficient level swell within the pressurizer to cover the discharge port with a steam-water mixture. For such conditions, the mass flux through the relief line would increase and can be expressed as

$$G_C^2 = 2 \rho_L (1 - \alpha_x) P_0 (1 - \eta) \quad (5)$$

where ρ_L is the saturated liquid density, α_x is the exiting void fraction, and η is the critical pressure ratio (about 0.8 for steam-water critical flow at these pressures). The exiting void fraction can be related to the pressurizer average void fraction ($\bar{\alpha}$) as

$$\alpha_x = \frac{2 \bar{\alpha}}{1 + C_0 \bar{\alpha}} \quad (6)$$

where C_0 is a constant (about 1.2). In addition, the pressurizer average void fraction can be related to the superficial vapor velocity (u_g) by

$$\bar{\alpha} = \frac{u_g}{2 + C_0 u_g} \quad (7)$$

and also to the collapsed (h_0) and swelled liquid levels (h_s) as

$$\bar{\alpha} = \frac{h_s - h_0}{h_s} \quad (8)$$

The superficial vapor velocity exiting the pressurizer can be expressed as

$$u_g = \frac{\dot{m}_{g,x}}{\rho_V A_V} \quad (9)$$

where ρ_v is the saturated vapor density, and A_v is the cross-sectional area of the pressurizer (about 3.6 m^2). Assuming no slip between the liquid and vapor phases (homogeneous), the exiting vapor flow can be related to the total exiting flow ($\dot{m}_{g,x}$) can be related to the total exiting flow ($\dot{m}_x = G_c A_{RV}$) as

$$\dot{m}_{g,x} = x_x \dot{m}_x \quad (10)$$

where

$$x_x = \frac{v_l \alpha_x}{v_l \alpha_x + v_v (1 - \alpha_x)} \quad (11)$$

where the v_v and v_l are the saturated steam and water specific volumes, respectively. Equation (8) provides the criterion for determining whether this two-phase discharge occurred during the blowdown of the pressurizer when the MOV was open, i.e., if the swell level equaled or exceeded the level of the discharge port, a two-phase discharge would have occurred. Equation (10) for two-phase discharge from the relief line is then equivalent to Equation (3) for all vapor discharge.

Carrying out this analysis during the period the MOV was open, the estimated net steaming rate is about 14 MW, indicating the average core temperature was increasing since the decay power at this time was about 26 MW. Assuming the difference of 12 MW to be the principal heating source (oxidation heating is neglected), this translates into a core average temperature rise of approximately 90 K during this period (7 min).

Core Steaming With HPI-ESF

The actuation of MUP-1A and MUP-1C in the ESF mode resulted in a rapid depressurization of the primary system causing drainage from the pressurizer into the A-loop hot leg and subsequently into the core. Steam condensation and cooling of noncondensable gases in the reactor cold legs, as well as that drawn from the hot legs through the flapper valves in the reactor plenum assembly, caused this depressurization. The effective steaming rate within the core region during this period can be estimated by comparing the condensation rate of steam due to cold injection water to the rate of pressure decrease within the primary system, Figure 9. The heating rate of the injection water from the condensing steam and cooling gases required to bring the ECCS water to saturation (\dot{Q}_L) is

$$\dot{Q}_L = \dot{m}_{inj} c_l (T_{sat} - T_e) \quad (12)$$

where \dot{m}_{inj} is the ECCS injection rate, c_l is the specific heat capacity of the enter injection water, T_{sat} is the saturation temperature corresponding to the prevailing primary system pressure, and T_e is the

temperature of the injection water (about 300 K). In this calculation, it is assumed that sufficient steam is always available to heat the water to saturation. As such, the condensation is maximized in this analysis.

Assuming the steam in the primary system can be represented as an ideal gas, and it behaves essentially isothermally during this process, the steam condensation rate (\dot{m}_g) can be related to the measured depressurization rate (dP/dt) as

$$\dot{m}_g = \frac{V_g}{RT_g} \frac{dP}{dt} \quad (13)$$

where V_g is the volume of the steam space, and T_g is the steam initial temperature. The cooling rate required to remove steam from the vapor space at this rate, \dot{Q}_g , is then

$$\dot{Q}_g = \dot{m}_g h_{fg} \quad (14)$$

where h_{fg} is the latent heat of vaporization.

During the depressurization, a substantial fraction of the water inventory in the pressurizer could also flash. This can be estimated by assuming the water is initially saturated and remains in equilibrium during the decompression. The quality associated with this flashing process can be estimated as

$$x = \frac{h_{f,i} - h_{f,f}}{h_{fg}} \quad (15)$$

where $h_{f,i}$ is the water initial enthalpy (assumed saturated) and $h_{f,f}$ is the final, saturated liquid enthalpy. The product of this quality and the total fluid mass in the pressurizer is approximately the steam mass formed by the depressurization. The product of the average steam generation rate over this interval and the latent heat of vaporization is then the heat removal rate that must also be supplied by the ECCS injection (\dot{Q}_{pZR}) to condense this steam.

As discussed earlier, additional water pools accumulated in the RCP suction lines and steam generators appear to have been subcooled during this period. Hence, they would not be flashing into the steam space and would, consequently, not require additional heat removal by the ECCS injection. Thus, the net cooling rate from within the primary system (\dot{Q}_{net}), based upon an upper limit of the condensation heat flux Q_L , is then

$$\dot{Q}_{net} = \dot{Q}_L - \dot{Q}_g - \dot{Q}_{pZR} \quad (16)$$

The decay heat was approximately 26 MW or about 1% of full thermal power (2720 MW).

In analyzing the primary system pressure and pressurizer-level histories, Figures 6 and 2, respectively, the period from when the HPI system was activated in the ESF mode (200 min) to when the primary system pressure and pressurizer level reached a minimum (about 207 min) shows the overall apparent core cooling rate to be approximately equal to the decay power (Figure 10). It should be remembered that this is based upon an assumption which maximizes the condensation on the injection water and, therefore, maximizes the calculated core cooling rate. Realistically, the condensation is a fraction of the maximum value; hence, the net core cooling rate would be a fraction of the decay power. However, the major finding is that when the overheated core is covered with water, the core cooling rate is, at most, only about equal to decay power, i.e., no rapid quenching of the damaged core.

There is one particularly interesting 1-min period beginning at about 202 min when the primary system pressure decreased at a somewhat slower rate (Figure 11). This is perhaps indicative of the quenching of the loose debris on top of the core material that originally comprised the upper region of the core. During this period, the net cooling rate from the debris could have been as much as about 21 MW--slightly less than the product of the critical heat flux at this pressure and the cross-sectional area inside the core barrel (an approximate debris bed quenching model). This change in the primary system pressure is accompanied by a change in the pressurizer drainage (Figure 12). With an average quenching rate of 21 MW over an interval of about 70 s, the energy extracted is about 1.5×10^9 J. Considering the debris bed on the top of the core to be approximately 20% of the core material, and assuming the temporary change in pressurizer and primary system pressure behavior to result from quenching of this debris, the bed temperature prior to the quenching would have been about 130 K greater than water saturation at the primary system pressure. Using an adiabatic heatup rate of about 1/2 K/s indicates that the heatup commensurate with this cooling rate would have started about 260 s earlier. This was slightly after when the RCP-2B was tripped.

CORE BEHAVIOR

Stability of a Thermally Driven TMI Molten Pool

During the probing of the TMI-2 reactor core, a hard, impenetrable layer of material was discovered at an elevation of about 1.5 m above the bottom of the core. This finding as well as other considerations led to the hypothesis that a region of molten core material (or pool) existed just below the unbreakable layer prior to 225 min. In fact, it is speculated that the unbreakable layer was once the upper frozen boundary of the pool. The floor (or lower crust boundary) of the pool is believed to have been located ~0.9 m above the bottom of the core, as the evidence suggests continuous water delivery to this level. The pool lifetime is estimated to be about 1 h. It has been postulated that the pool phase ended suddenly as a result of a general weakening or remelting of the lower crust that opened

the way for the flow of molten material into the lower plenum. Some evidence for rapid fuel movement comes from the pressure and temperature signals recorded during the course of the accident as well as the anomalous behavior of Levels 1 and 2 SPNDs. Also, a large quantity of what appears to be previously molten core material has been observed in the lower plenum (15 to 20 t). The draining of the pool phase occurred at a time when the core is believed to have been completely submerged in water, Figures 3 and 4.

To investigate the thermal structure of the postulated molten core pool and the possibility of remelting its lower crust boundary, the molten pool is assumed to be in a steady-state heat balance. That is, the heat loss from the bounding crust surfaces is equal to the heat produced by radioactive decay within the interior. If the crusts are thermally stable, the steady-state condition will be attained.

The model for the molten pool is illustrated in Figure 13. The pool is treated as a horizontal layer of large extent and the heat transfer correlations obtained with water pools (e.g., see References 6 and 7) are assumed applicable to the molten core materials. The pool is sandwiched between two frozen layers of pool material. In water experiments with internal heat generation, it has been observed that the flow is very turbulent in the upper, unstable portion of the pool and relatively calm and quiescent in the lower, stable, stratified portion. Very slow random motion does exist, however, down to the bottom surface in the stable portion of the layer. The temperature profile sketched in Figure 13 reflects these observations.

As already mentioned, the pool has been postulated to be sandwiched between the impenetrable layer and the water level located 1.5 m and 0.9 m, respectively, above the bottom of the core. This suggests a pool depth $D = 0.6$ m. The rate of volumetric heat production within the pool is estimated to be $\dot{Q} = 2.8 \text{ MW m}^{-3}$. Based on currently available data for molten UO_2 , a thermal conductivity $k = 3 \text{ W m}^{-1} \text{ K}^{-1}$, a thermal diffusivity $\alpha = 7 \times 10^{-7} \text{ m}^2 \text{ s}^{-1}$, a kinematic viscosity $\nu = 6 \times 10^{-7} \text{ m}^2 \text{ s}^{-1}$, and a coefficient of volumetric expansion $\beta = 10^{-4} \text{ K}^{-1}$ are reasonable approximations.

The appropriate Rayleigh number for a heat generating fluid layer is

$$R_a = \frac{g \beta \dot{Q} D^5}{\alpha \nu k} \quad (17)$$

The fraction n of internally generated heat transferred downward and impinging on the lower crust is given by the following correlation²:

$$n = R_a^{-0.0785} \quad (\text{for } R_a > 10^3) \quad (18)$$

Using the physical properties given above, the Rayleigh number for the core pool is about 1.7×10^{14} . Then from Equation (18), η is approximately 0.076 indicating only about 7.6% of the heat generated is transported to the lower crust.

Almost all the heat is lost from the pool by radiation, and the surroundings (water) are at so low a temperature that the back-radiation from them is not appreciable^a. Equating the sum of the heat generated in the lower portion of the pool and that in the lower crust with the radiation heat loss gives

$$\eta \dot{Q}D + \dot{Q}\delta_L = \epsilon \sigma T_L^4 \quad (19)$$

where ϵ is the emissivity of the crust surface (~ 0.7), σ is the Stefan-Boltzman constant, T_L is the temperature at the underside of the lower crust, and δ_L is the thickness of the lower crust. The temperature drop across the lower crust can be estimated by solving the one-dimensional conduction equation. The result is

$$T_{mp} - T_L = \frac{\dot{Q}\delta_L^2}{2k} + \frac{\eta \dot{Q}D\delta_L}{k} \quad (20)$$

where T_{mp} is the melting point of the pool material and assumed equal to 3100 K. Equations (19) and (20) represent an algebraic system for the two unknown quantities T_L and δ_L . Solving for these quantities produces

$$\delta_L = 0.029 \text{ m and } T_L = 1517 \text{ K.} \quad (21)$$

It is obvious that in order to determine the quantities δ_u and T_u for the upper crust, the following system must be solved

$$(1 - \eta)\dot{Q}D + \dot{Q}\delta_u = \epsilon \sigma T_u^4 \quad (22)$$

$$T_{mp} - T_u = \frac{\dot{Q}\delta_u^2}{2k} + \frac{(1 - \eta)\dot{Q}D\delta_u}{k} \quad (23)$$

a. It is assumed that the conditions external to the pool are such that the water undergoes film boiling at the outside surfaces of the crusts. Also, it is assumed that thermal radiation is neither absorbed nor emitted in the steam film or at the surfaces of the supporting fuel pins (see next section).

These equations provide the results

$$\delta_u = 0.0011 \text{ m and } T_u = 2509 \text{ K} \quad (24)$$

for the upper crust. It may be of some interest to determine the temperature within the core of molten pool (T_{pool}). This can be accomplished by concentration on the upper unstable portion of the pool for which the relation between the heat flux and the temperature difference is well known and given by (see Reference 7)

$$Q(1 - \eta)D = 0.16 \frac{g\beta D(T_{\text{pool}}^3 - T_{\text{mp}}^3)^{1/3}}{\alpha\nu} \cdot \frac{k(T_{\text{pool}} - T_{\text{mp}})}{D}$$

Solving for T_{pool} yields

$$T_{\text{pool}} = T_{\text{mp}} + 3.95 \frac{\alpha\nu}{g\beta}^{1/4} \cdot \frac{Q(1 - \eta)D}{k}^{3/4}$$

from which the following estimate is obtained

$$T_{\text{pool}} = 3100 + 347 = 3447 \text{ K}$$

The result for the upper crust thickness is at odds with the notion that the impenetrable layer at the 1.5-m core elevation once served as the upper boundary of a molten core pool. The upper pool crust is much too thin to identify the crust as the upper boundary. Moreover, it does not seem reasonable that a molten UO_2 pool, once established, will suddenly drain by the remelting of its lower boundary. Thermal radiation alone appears capable of maintaining the pool in a stable configuration. Considering the fact that the 2.9-cm thick lower crust is supported from below by the fuel pin matrix, the crust will probably not give way under the weight of the pool. (The pool exerts a hydrostatic pressure of 59 kPa at its lower surface.)

In the foregoing evaluation, the pool material was assumed to be pure UO_2 ($T_{\text{mp}} = 3100 \text{ K}$). However, interaction of the Zr cladding, UO_2 , and steam can result in a metallic-like, core-pool material with a melting temperature as low as $\sim 2100 \text{ K}$ and thermal conductivity $k \approx 20 \text{ W m}^{-1}\text{K}^{-1}$. Repeating the calculations with these physical properties yields $\delta L = 0.05 \text{ m}$ and $\delta u = 0$ for the thicknesses of the lower and upper crust, respectively.^a The lower crust is thicker than that predicted previously, and, therefore, is probably thick enough to prevent the downward movement of core material. A crust plate is not predicted to form at the upper surface of the pool.

a. The internal-heating rate in both the pool and the crusts was maintained at $Q = 2.8 \text{ MWm}^{-3}$.

On first sight, at least three complications appear to stand in the way of agreement between the steady-state pool model presented here and the observations at TMI-2. These are:

- The film boiling layer on the underside of the TMI-2 pool may have been sufficiently thick to cause the intact fuel pins to shield a portion of the thermal radiation leaving the lower crust surface and impinging on the steam-water interface below.
- The interior motion in the molten core material pool may be driven by "forces" other than thermal.
- The core melt-down phase of the TMI-2 accident sequence may not have involved the formation of a large molten core pool.

These complications will be considered in order in the sections that follow.

Thickness of the Vapor Film on the Lower Boundary of the Postulated TMI-2 Molten Pool

To estimate the thickness of the film boiling layer on the underside of the TMI-2 molten pool, it is assumed that the film flows from the center towards the radial end of the pool (the edge of the lower crust) and up around the pool side wall as an intact vertical film (see Figure 14). Heat is transferred from the lower crust to the liquid-vapor interface by radiation through the vapor film. No effort is made here to include the effect of thermal radiation on the vertical flow of vapor along the side of the pool, although this could readily be included in the analysis. Thus, the vertical vapor film remains uniform in thickness as it moves upward due to buoyancy.

The vapor film on the underside of the pool flows along a surface that is normal to the gravity field. The vapor motion in this case depends upon the variation of both the hydrostatic pressure and vapor temperature with changes in the film thickness along the surface. The variation in the vapor temperature causes the velocity component normal to the surface to decrease with increasing distance from the center of the crust. By virtue of mass continuity, this induces a radial outward movement of vapor. This natural convection phenomena is subtle and difficult to deal with analytically. For this reason, the vapor film will be assumed to be isothermal and its motion governed by hydrostatic pressure alone. The hydrostatic "mechanism" for vapor movement is likely to be much weaker than the natural convection mechanism. Moreover, in the presence of natural convection (temperature gradients), the hydrostatic pressure will tend to retard the outward movement of vapor and thicken the vapor film. Nevertheless, the isothermal vapor-film assumption will serve to illustrate that natural forces are present that are capable of thinning the vapor film and ensuring that the vapor-liquid interface remains close to the radiating surface of the lower crust.

The x-direction momentum equation can be shown to reduce to a simple balance between the hydrostatic pressure gradient and the viscous force (see Figure 14 for nomenclature) as

$$\mu \frac{\partial^2 u}{\partial z^2} = g(\rho_L - \rho_V) \frac{d\delta}{dx} . \quad (25)$$

Solving for u and using the boundary conditions $u = 0$ at $z = 0$ and $u = 0$ at $z = \delta$ yields

$$u = - \frac{g(\rho_L - \rho_V)}{2\mu} \frac{d\delta}{dx} (z\delta - z^2) . \quad (26)$$

The average radial vapor velocity is

$$\bar{u} = \frac{1}{\delta} \int_0^{\delta} u dz = - \frac{g}{12\mu} (\rho_L - \rho_V) \frac{d\delta}{dx} \delta^2 . \quad (27)$$

A mass balance across a radial increment dx of vapor film yields

$$\frac{1}{x} \frac{d}{dx} (x\bar{u}\delta) = v_e \quad (28)$$

where v_e is the steam production velocity at the vapor-liquid interface; it is related to the radiation heat flux q by

$$q = \rho_V h_{VL} v_e . \quad (29)$$

Substitution of Equations (27) and (29) into Equation (28) yields

$$\frac{1}{x} \frac{d}{dx} x\delta^3 \frac{d\delta}{dx} = - \frac{12 \mu g}{g\rho_V(\rho_L - \rho_V)h_{VL}} = - A . \quad (30)$$

This is the differential equation for the thickness of the upper film on the underside of the pool.

If δ_{\max} is denoted as the maximum film thickness (at the center of the crust plate, i.e., at $x = 0$) and δ_{\min} as the film thickness at the edge of the crust plate (at $x = R$), the boundary conditions then become

$$\delta = \delta_{\max} \text{ at } x = 0 ; \delta = \delta_{\min} \text{ at } x = R . \quad (31)$$

Solving Equation (30) subject to these boundary conditions produces

$$\delta^4 = \delta_{\min}^4 + A(R^2 - x^2) . \quad (32)$$

Specification of the film thickness at the crust edge depends upon the upflow condition at the edge. Here, it will be assumed that δ_{\min} is equal in thickness to that of the vertical film flow along the side of the pool, which is readily shown to be given by

$$\delta_{\min} = \left(\frac{1}{2} RA\right)^{1/3} . \quad (33)$$

Thus, from Equation (33), the maximum film thickness at the center of the crust plate is

$$\delta_{\max}^4 = \frac{1}{2} RA^{4/3} + AR^2 . \quad (34)$$

A simple mass balance over the total crust surface yields the following expression for the average vapor film velocity at the crust edge:

$$\bar{u}_{x=R} = \frac{Rq}{2 \delta_{\min} \rho_v h_{v\ell}} . \quad (35)$$

The downward radiation heat flux from a 0.6-m deep molten pool is about $q = 0.13 \times 10^6 \text{ W m}^{-2}$ (7.6% of the total heat generated). Taking the system pressure to be 10 MPa yields $A \approx 1.2 \times 10^{-10} \text{ m}^2$. For a molten pool radius of $R = 1.6 \text{ m}$, the following quantities are inferred: $\delta_{\min} = 0.46 \text{ mm}$, $\delta_{\max} = 4.2 \text{ mm}$, and $u_{x=R} = 3.1 \text{ m s}^{-1}$. The film is rather thin, even at the center of the crust where it is a maximum. The predicted velocity at the edge of the crust is rather large, and it may be questionable whether the vapor could turn the corner and cling to the side of the pool. The vapor may detach itself from the crust at this location and rise through the water in the form of a bubble plume. This should not, however, substantially change the estimate of the film thickness nor the conclusion that the vapor film on the underside of the pool is much too thin for the intact pins to interfere with the thermal radiation field.

Melting- or Boiling-Driven Pool Convection

The natural convection flow in the core material pool may not be caused entirely by the effect of temperature gradients, but perhaps also by the introduction of a lighter material species. The latter is often the largest effect.

Consider the situation where the core material pool is located above a lighter material that is miscible with the pool. For example, during the core disruption, UO_2 may collapse onto Zr cladding. During the subsequent heatup of the UO_2 fuel, the underlying cladding in contact with the fuel will melt and chemically attack the intervening fuel crust. This may result in the disintegration of the UO_2 crust and thereby permit the injection of the lighter molten Zr into the pool from below (see

Figure 15). In this situation, the hydrodynamics governing the downward heat transfer process are primarily driven by the density difference between the fuel and cladding (see Reference B for a discussion of natural convection melting). Unlike the thermally driven-convection process with its stable lower layer, density-driven motion of this type will cause most of the internally generated heat to be transferred downward and thereby result in the formation of a thick crust at the upper pool interface. It would, therefore, be possible for the fuel pool to penetrate the underlying clad by this mechanism and enter into the lower plenum. Consequently, natural convection melting (or dissolution) may be an explanation of the relocation of core material into the TMI-2 lower plenum.

During the disrupted core heatup phase, volatile materials such as cadmium may be injected into the growing molten region. This is another example where convection in the pool may be governed by a buoyancy mechanism arising from the presence of a lighter species. Again, increased downward heat transfer is anticipated when compared with that for pure thermal convection. However, it may be difficult to quantify the influence of a vaporizing or boiling species on the heat fluxes to the pool boundaries.

Melt-Down in the Absence of a Pool Phase

The possibility that the core melt-down phase of the TMI-2 accident sequence did not involve the formation of a significant molten core pool should also be considered. Two alternative processes involving the continuous downward migration of molten fuel are suggested below.

A crust plate would be expected to form at the core water level. The core melt-down rate is much too slow for the molten material to penetrate any significant distance below the surface of the water without refreezing. Extremely thin films of molten material drain from the downward moving core-melt front. Such films cannot flow very far without refreezing, especially in water. Thus, the molten fuel that first arrives at the water surface blocks its own channel by refreezing there. The melt flow that follows is thereby forced to move horizontally into adjacent channels. Thus, a crust forms and becomes progressively wider (spreads), and the number of channels open to the water pool below is gradually reduced until only a few openings remain. These open channels must accept the full flow of molten core material from above. The flow enters these channels with a velocity much larger than that of the draining material above because the available flow area that penetrates the crust is now much less than the flow area through the melting core above. Once the molten material drains through this crust, it can then work its way down to the bottom of the vessel without much interference from the freezing process.

Another process proposed to bypass the pool-formation phase is the possible shattering of the solid fuel shell as internal melting takes place. It is envisioned that as the solid fuel melts, the volume increase associated with the phase change causes sufficient pressure to fragment or crack the surrounding solid and force some of the melt through the crack(s) before the crack reseals itself. This could be followed by additional

melting and pressure buildup at a rate proportional to the melting rate until the stresses once again give rise to cracks through which molten fuel is ejected. This continuous melting-cracking process may prevent the formation of a large region of molten fuel. Instead, large-scale downward movements of the fuel may occur as a result of repeated fuel-melt ejections.

The primary system pressure changes considerably during the interval from 174 to 227 min, as indicated in Figure 6. Specifically, it increases from 9 to 14 MPa at 174 min, decreased from 13 to 10 MPa at 200 min, increases to 11 MPa at 207 min, and decreases to 10 MPa before 227 min. These changes could substantially stress such a crust. Such considerations are particularly important after 200 min when the core was covered by water. Of particular note is the pressure increase at 207 min that could have forced water into overheated debris, thereby causing a local pressurization that could disrupt the crust and allow debris to flow into the lower plenum.

The difficulty with the foregoing hypotheses is that it does not explain the existence of the impenetrable layer located ~1.5 m above the bottom of the core. Further consideration is needed to assemble the various parts of the complicated picture of the melt-down phase of the TMI-2 accident.

SUMMARY

Assessment of the primary system behavior as a result of ECCS injection into the cold legs indicates the pressurizer also drained into the core during the period of such injection. The ensuing steam condensation apparently resulted in the formation of gaseous (hydrogen) pockets in the cold legs and downcomer. As a result of this water accumulation, the core was essentially covered shortly after the HPI initiation at 200 min. This is consistent with the observation from the pressurizer and the primary system pressure that appears to show a quenching of a limited amount of overheated core debris as the pressurizer drains. Following this quenching, the net steaming rate from the core was somewhat less than decay power indicating the quenching process was very slow and that the central region of the damaged core could have continued to increase in temperature.

The primary system pressure and pressurizer water level records appear to be completely consistent with covering the core and filling the reactor vessel to the top of the horizontal section of the hot legs at 207 min. The pressurizer itself begins to fill once the vertical section of the hot legs has been filled to a level equal to the surge-line entrance, which occurs at approximately 210 min. This requires that gas volumes (principally hydrogen) are trapped in the cold legs. Such conditions are consistent with the measured cold leg temperatures and the failure of the RCP-1A to "prime" itself at 248 min when it was started.

The steaming rate from the damaged TMI-2 core was evaluated during two periods of the excursion that were readily amenable to such an analysis: (a) when the MOV was open with no makeup to the primary system, and

(b) when the ESF injection was initiated and the primary system was closed. The purpose of this evaluation was to determine if the core was being adequately cooled during this period considering it was probably surrounded by water, particularly when the MUP-1A and -1C were operating in the ESF mode. This analysis indicates the damaged core was heating when the MOV was open, and this heating process may well have started after water injected into the core by the RCP-2B had evaporated. The core also was apparently heating when the MUP-1A and -1C were running, even though the core was probably covered with water during this period. The heatup of the loose debris bed in the upper core region, which apparently quenched following ESF injection, appears to have begun about when the RCP-2B tripped.

Assessments of the thermal stability for a badly damaged core that has evolved into a pool configuration show that such a state would be stable in the absence of other perturbations, such as primary system pressure changes. However, chemical attack, such as eutectic formation between uranium-dioxide fuel and unreacted Zircaloy could explain the downward attack of the core material and its eventual migration into the lower plenum. In addition, considerations of pressure changes within the primary system, especially when the core has been completely covered by water, show that these could also provide for localized failures of the supporting crust and transport of once molten material into the lower plenum.

REFERENCES

1. "Analysis of Three Mile Island - Unit 2 Accident," NSAC-1 Revised March 1980, Nuclear Safety Analysis Center, Electric Power Research Institute, Palo Alto, CA.
2. B. Tolman, "Thermal Hydraulic Features of the TMI Accident," Presentation to TMI-2 Tech. Adv. and Analysis Group, EG&G, March 26, 1985.
3. Modular Accident Analysis Program (MAAP), Best Estimate Prediction at 10443 s, Marc A. Kenton, Fauske & Associates, Inc., Burr Ridge, IL, August 22, 1985.
4. J. O. Henries, "Hypothesis Concerning TMI-2 Core Conditions," Presentation to Tech. Adv. and Analysis Group, Rockwell International, March 1985.
5. G. R. Thomas, "TMI-2 Core Conditions Hypothesis Plus IDCOR MAAP Analysis of TMI-2", Presentation to Tech. Adv. and Analysis Group, EPRI/NPD, March 26, 1985.
6. P. Boon-Long, T. W. Lester, R. W. Faw, "Convective Heat Transfer in an Internally Heated Fluid Layer with Unequal Boundary Temperatures," Int. J. Heat Mass Transfer, Vol. 22, pp. 437-445, 1979.

7. K. B. Katsaros, W. T. Liu, J. A. Businger, J. E. Tillman, "Heat Transport and Thermal Structure in the Interfacial Boundary Layer Measured in an Open Tank of Water in Turbulent Free Convection," J. Fluid Mech., Vol. 83, pp. 311-335, 1977.
8. M. Epstein and M. A. Grolmes, "Natural Convection Characteristics of Pool Penetration into a Melting Miscible Substrate," J. Heat Transfer, in press, 1985.

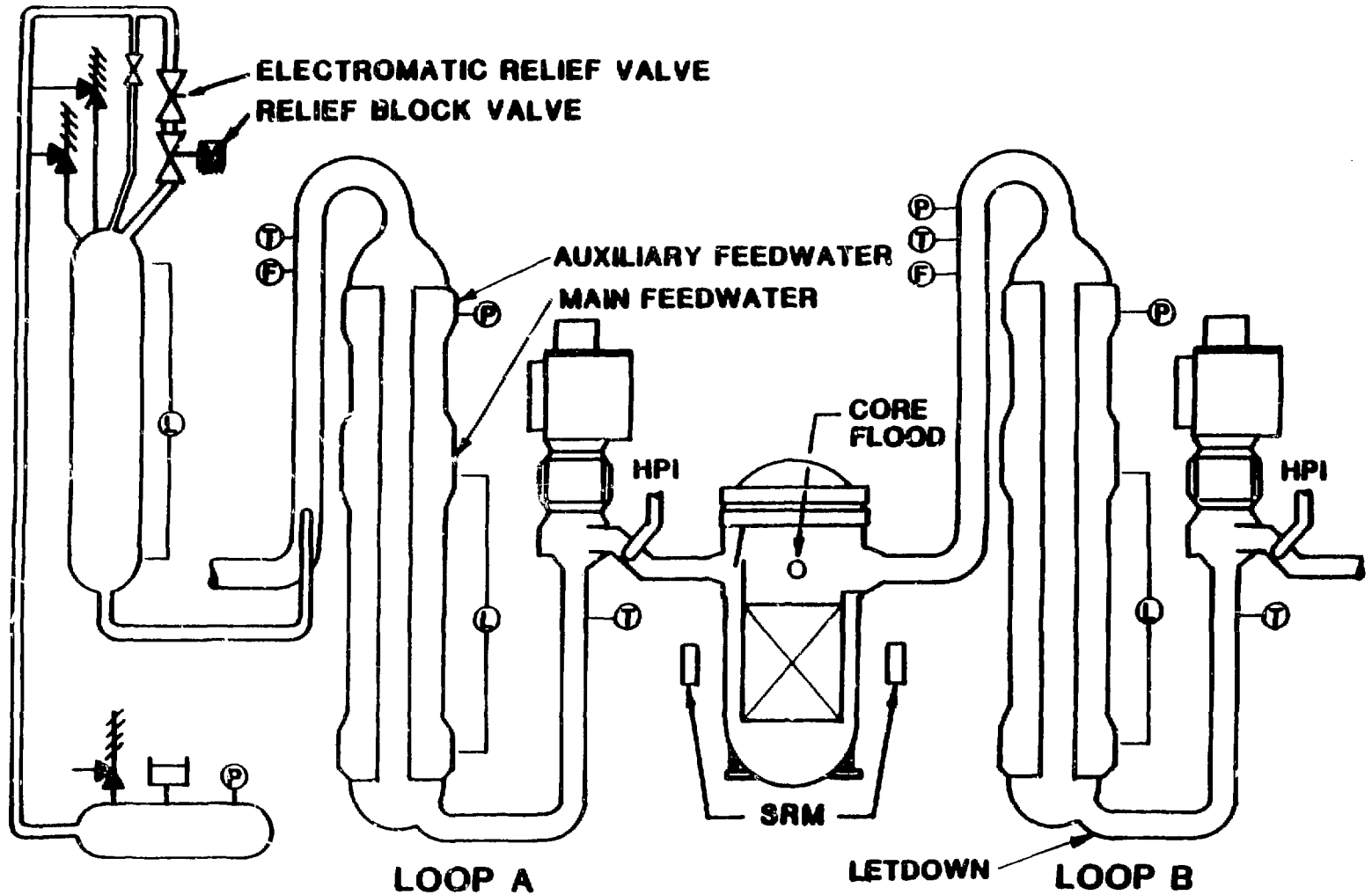


Figure 1. Schematic of the TMI-2 reactor coolant system.

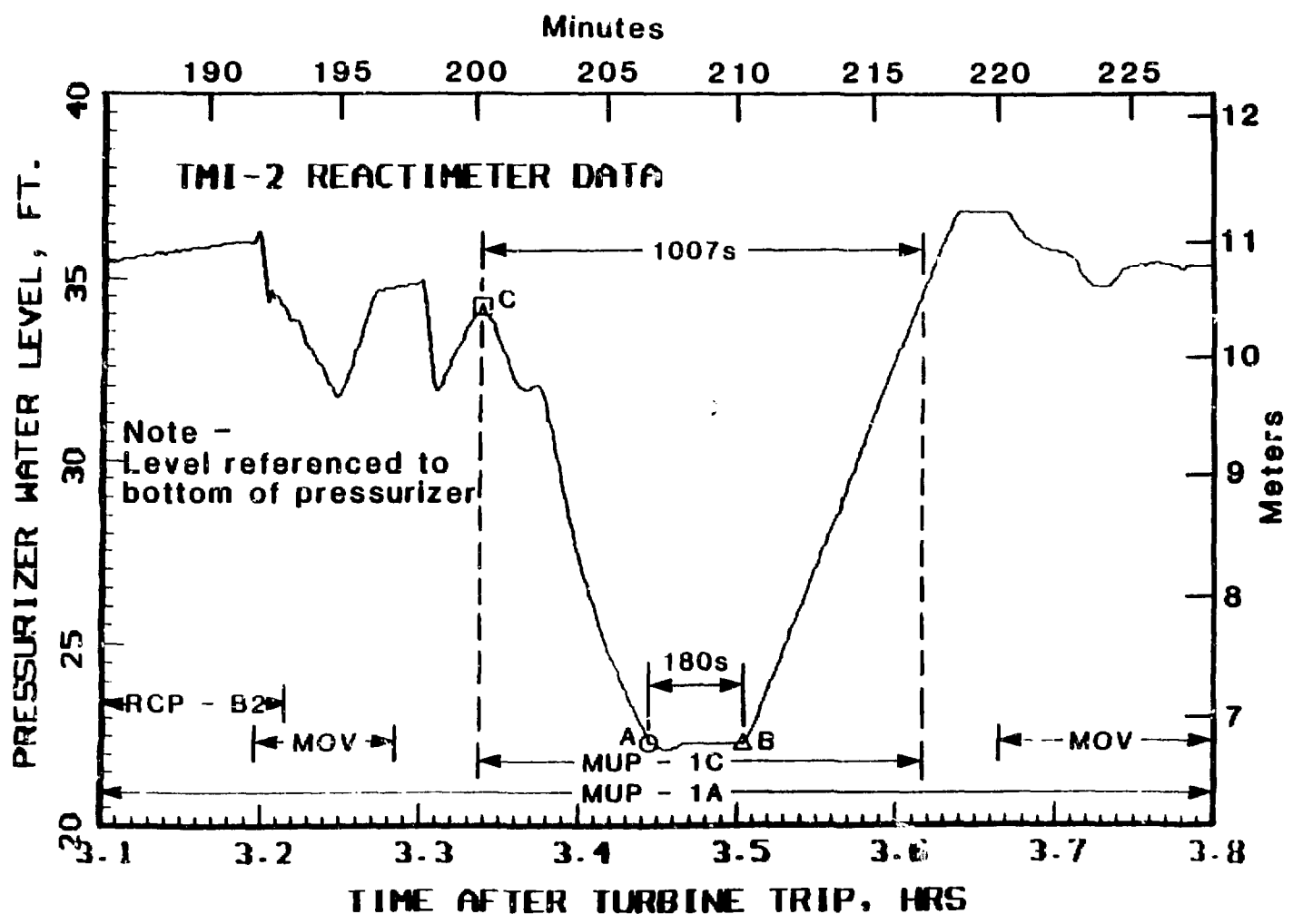


Figure 2. Pressurizer water level when MUP-1C running (200-217 min).

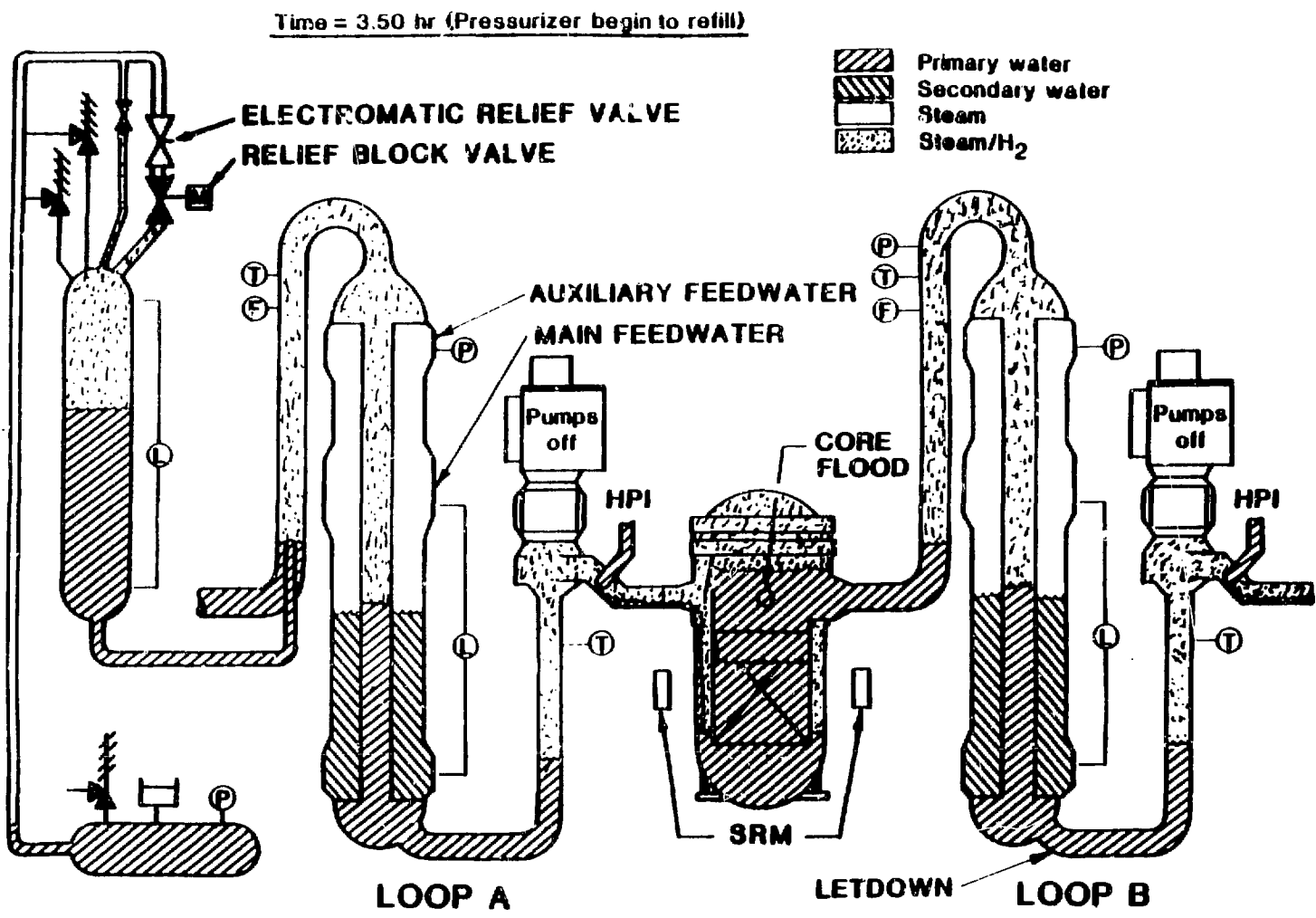


Figure 3. Schematic of the fluid levels in the RCS when the pressurizer began to refill at 3.50 hours.

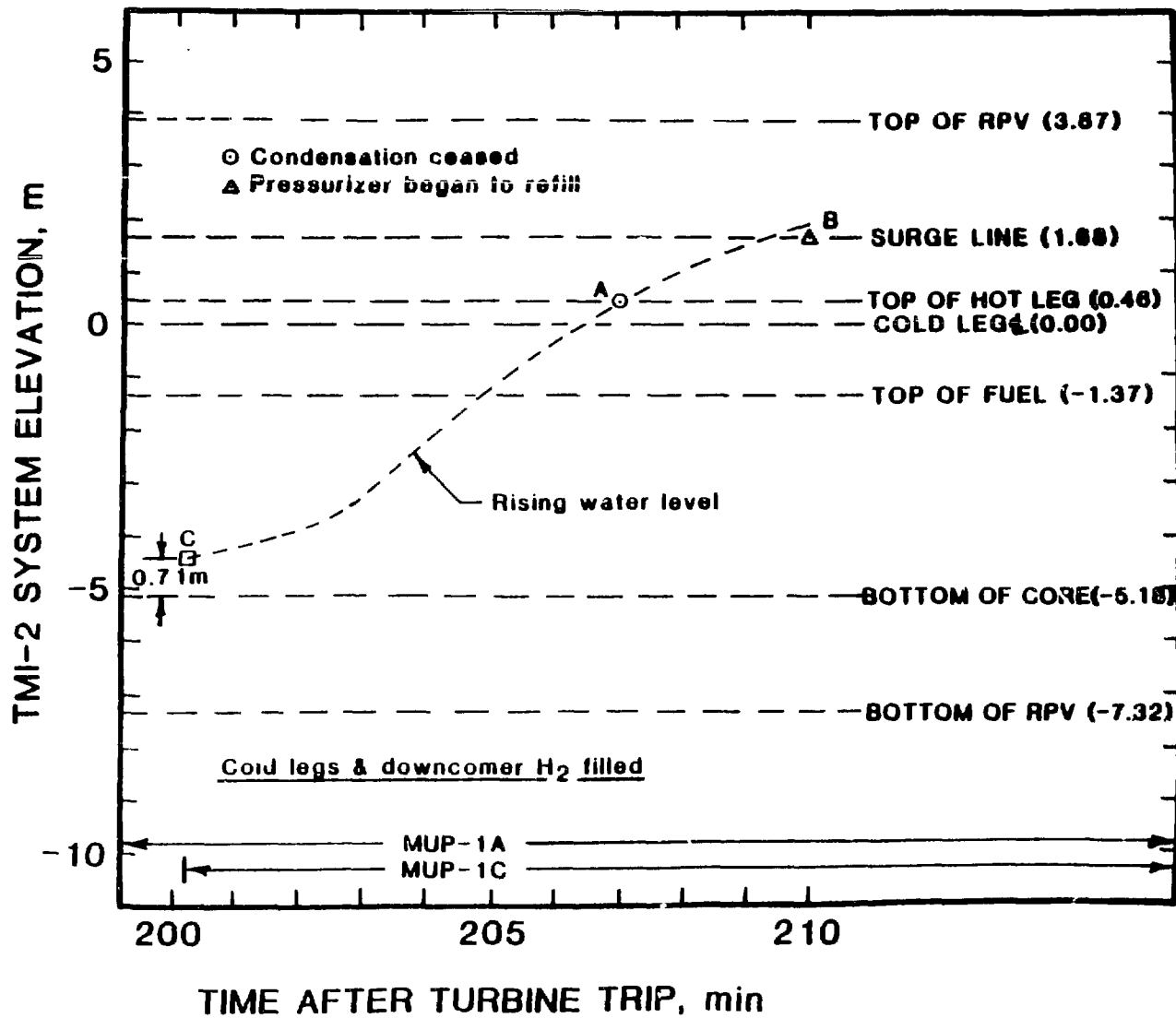


Figure 4. Rising water level in the RPV and upper piping when the MUP-1A and 1C were running.

Time = 3.45 hr (Hot legs water filled)

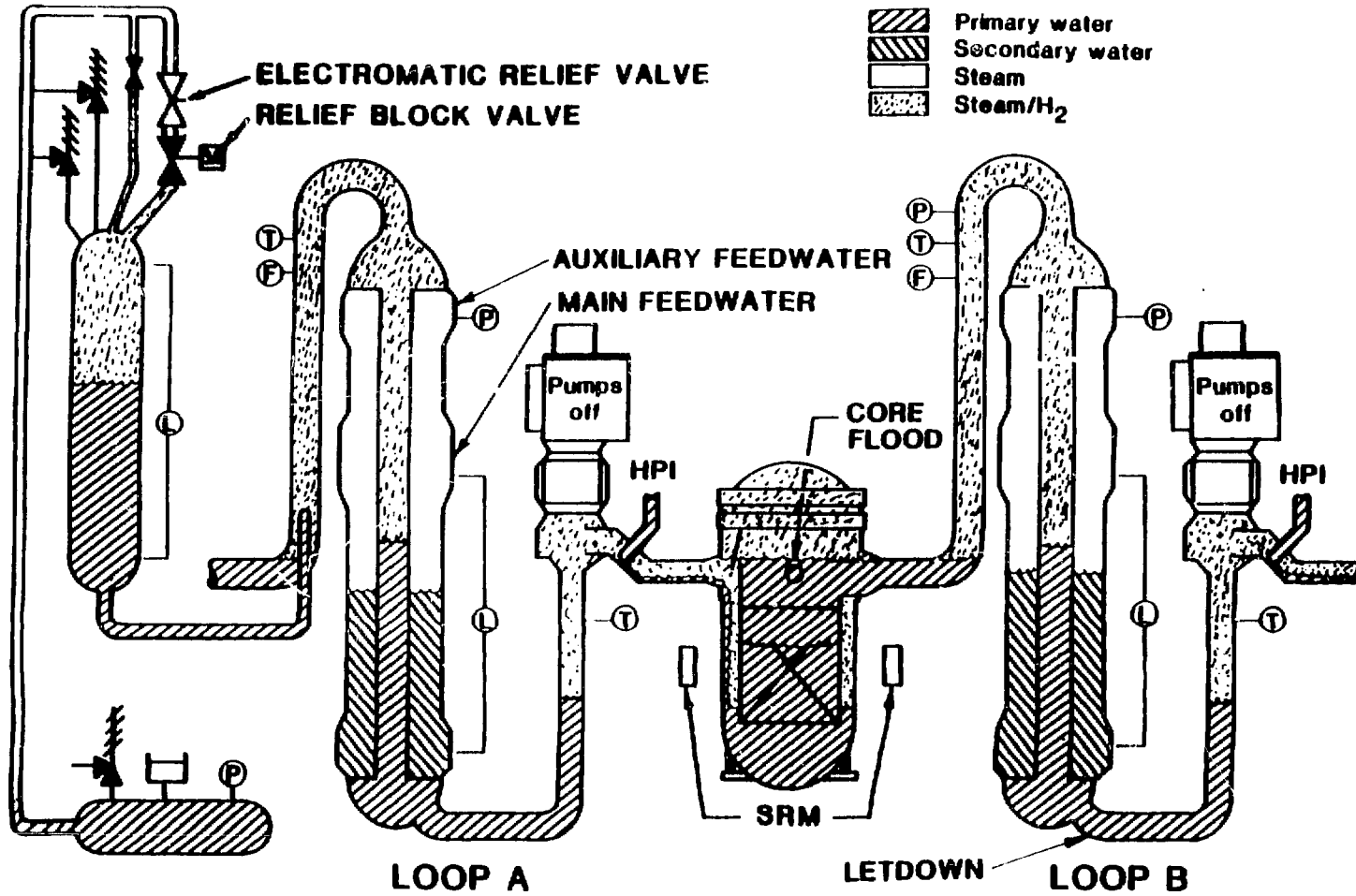


Figure 5. Schematic of the fluid levels in the RCS when the horizontal runs of the hot legs apparently filled at 3.45 hours.

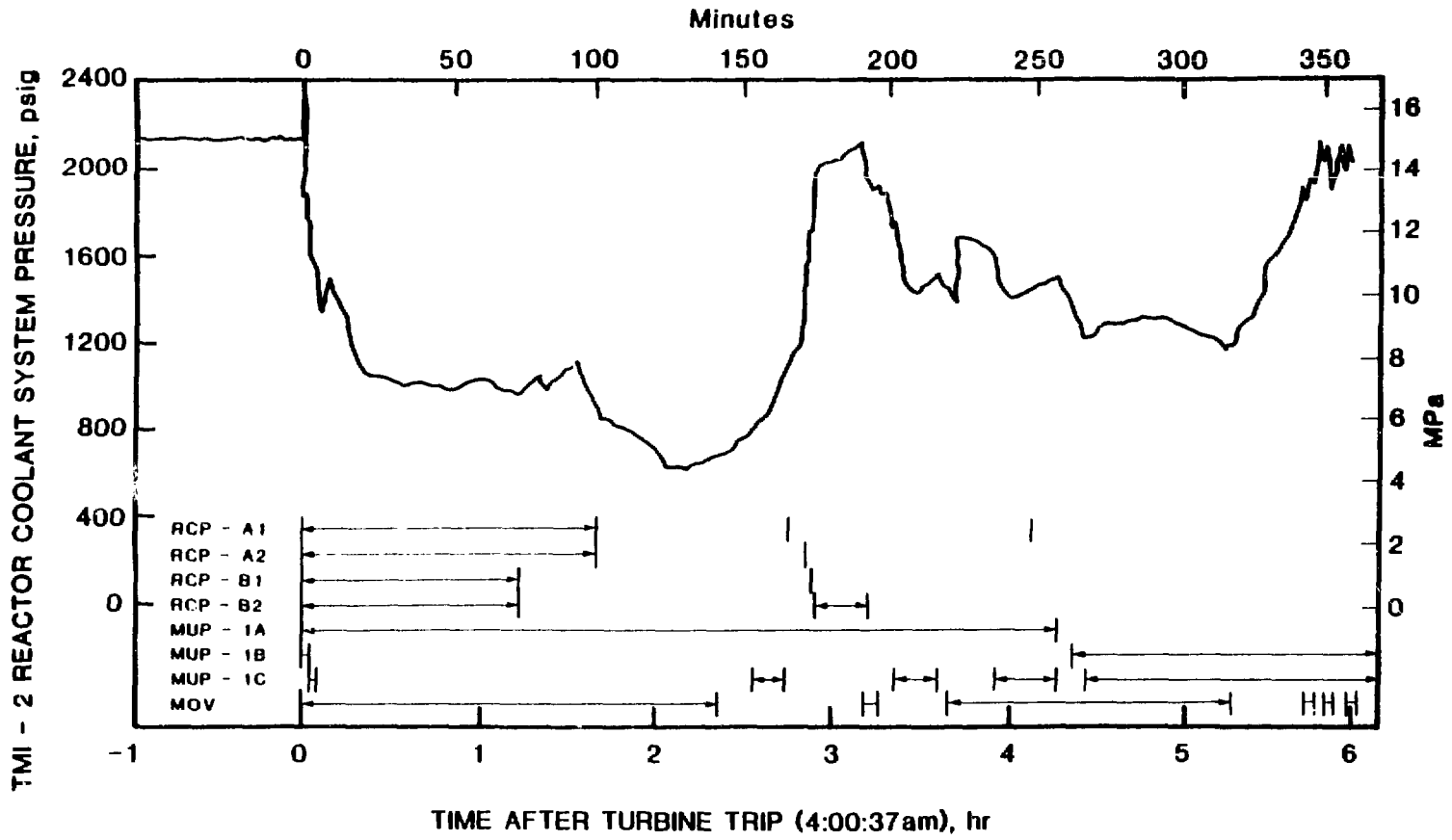


Figure 6. Primary system pressure and various operator interactions during the first 6 hours of the TMI-2 incident.

Time = 3.34 hr (MUP-1C started)

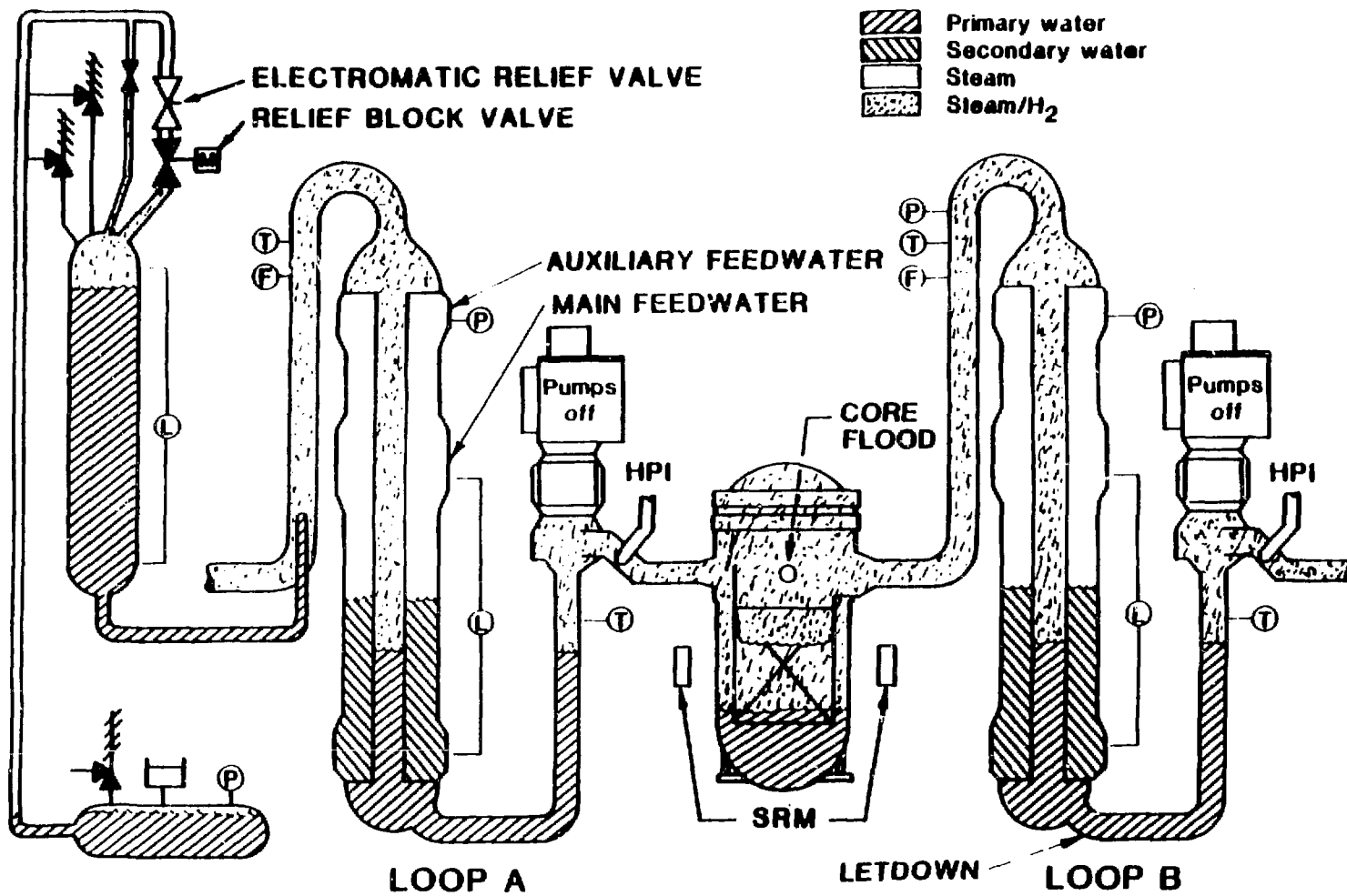


Figure 7. Schematic of the fluid levels in the RCS when the MUP-1C started at 3.34 hours.

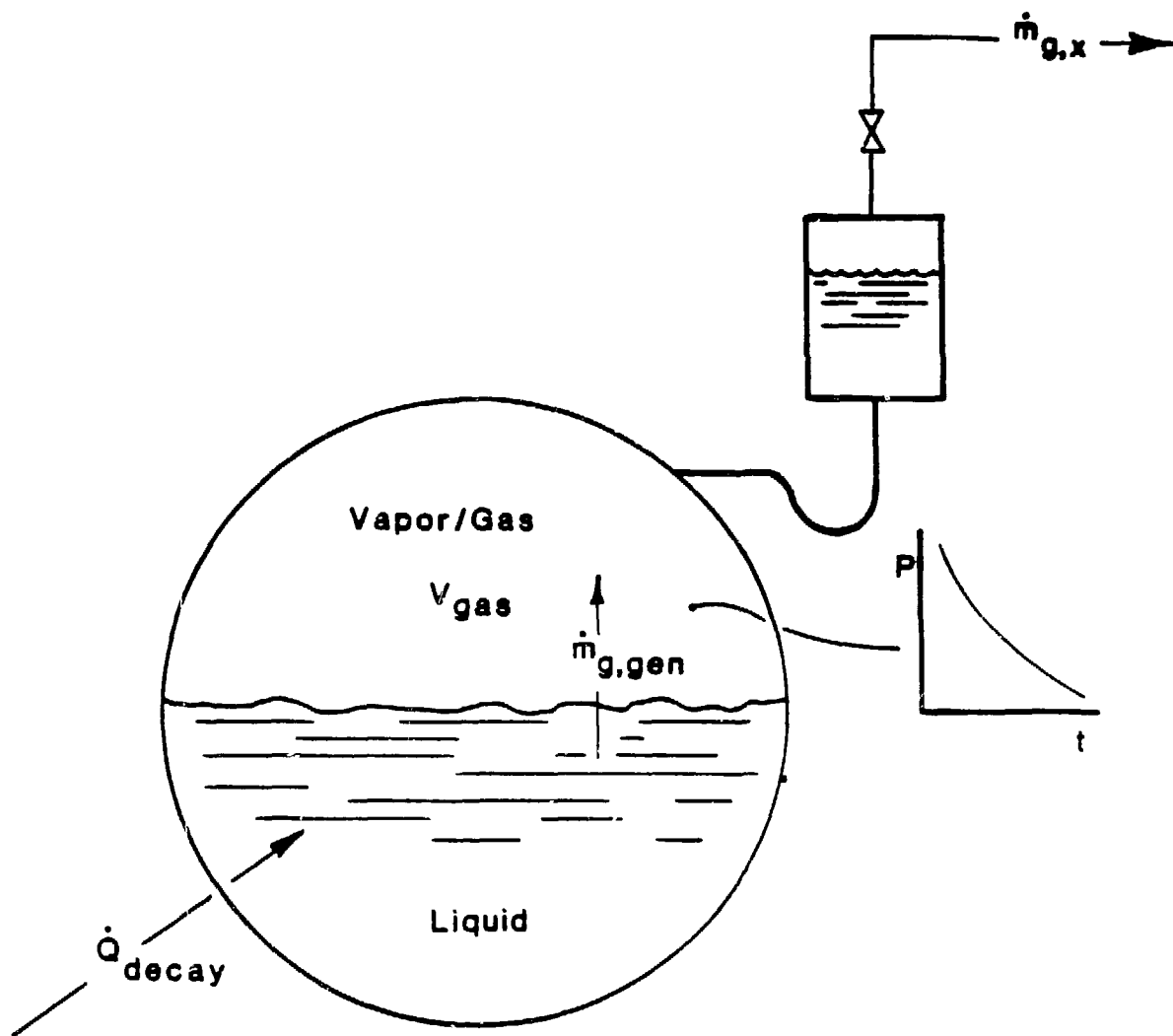


Figure 8. Schematic representation for the primary system when the MOV was open at 192 minutes.

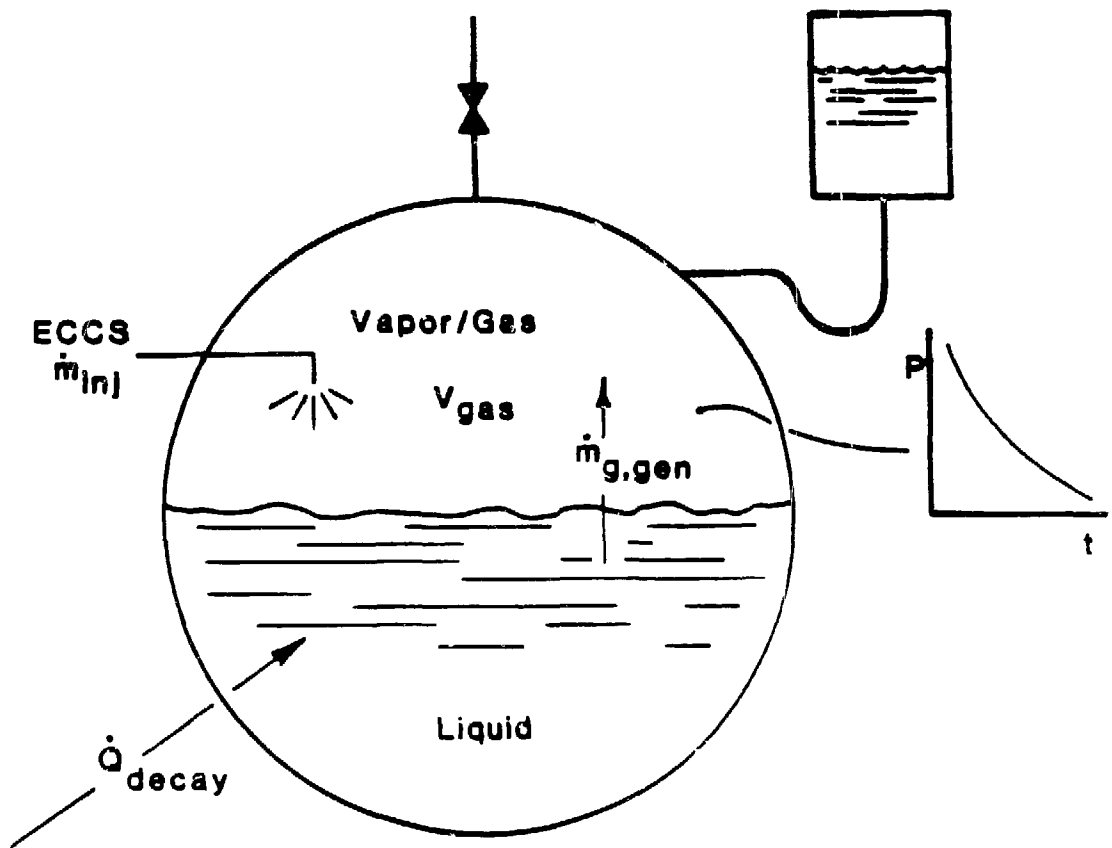


Figure 9. Schematic representation of the primary system when HPI was initiated at 200 minutes.

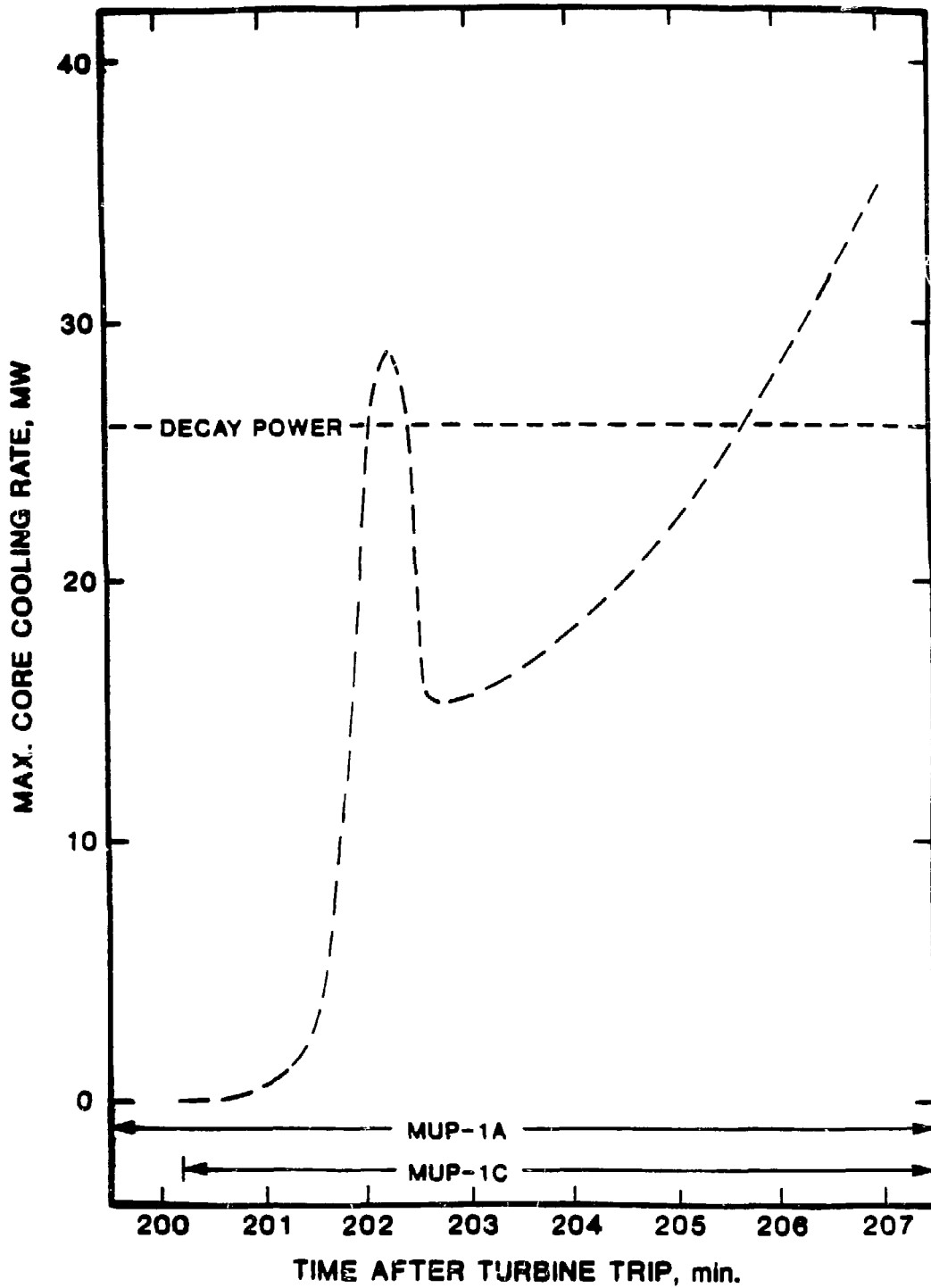


Figure 10. Maximum core cooling rate during ESF-HPI when primary system pressure and pressurizer water level were falling (200-207 min.).

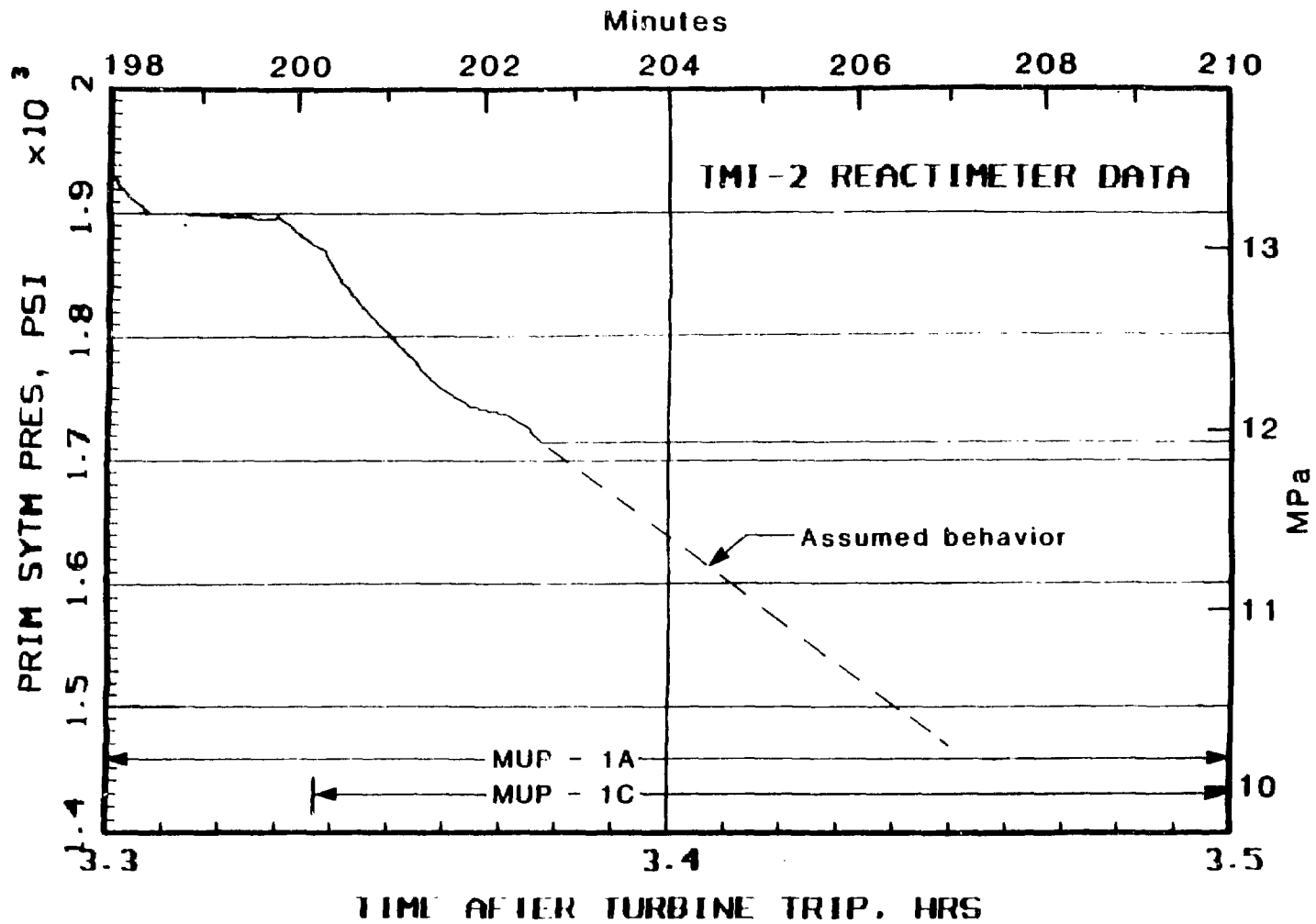


Figure 11. TMI-2 primary system pressure when HPI was initiated in the ESF mode at 200 minutes.

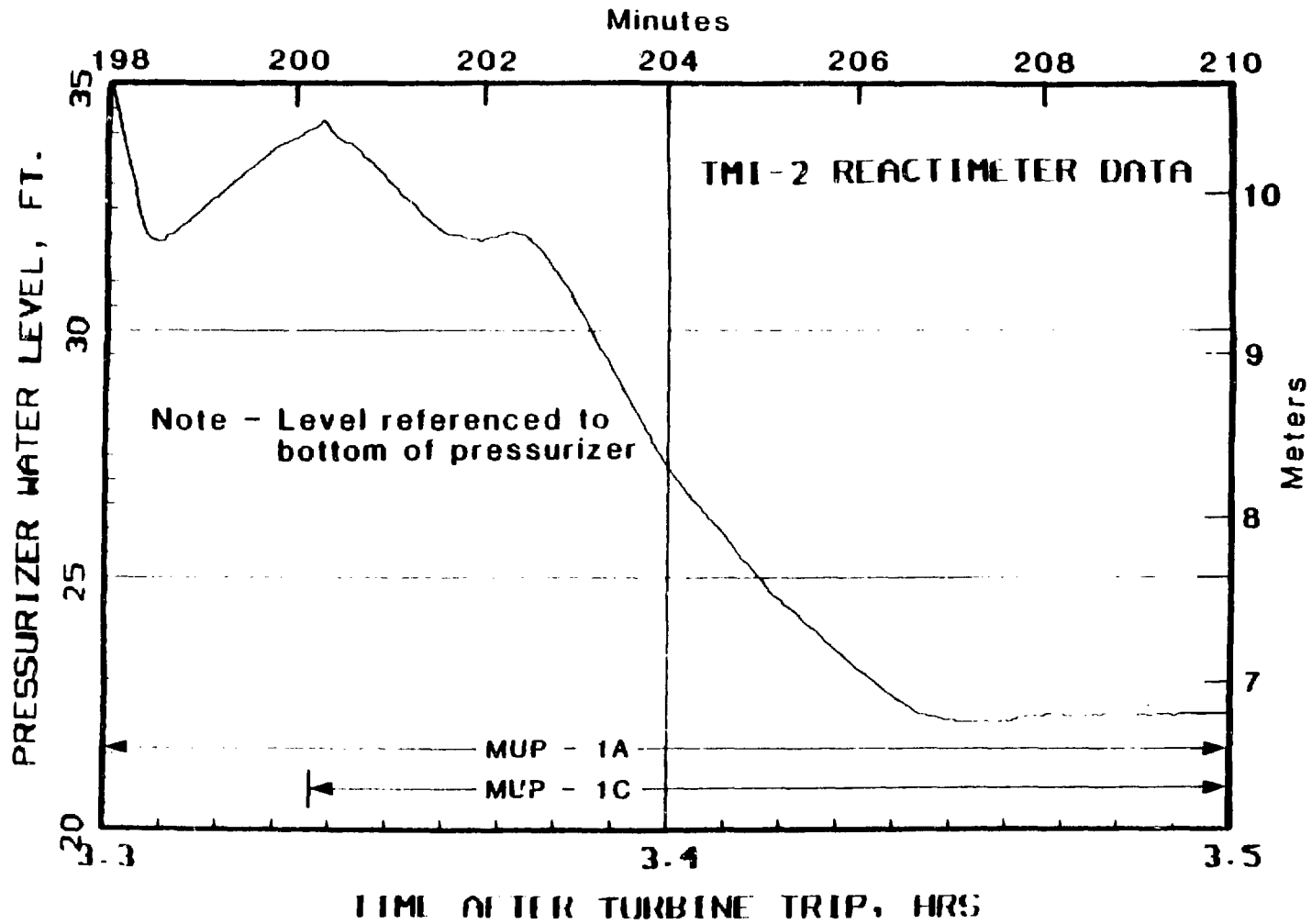


Figure 12. Pressurizer water level following ECCS activation at 200 minutes.

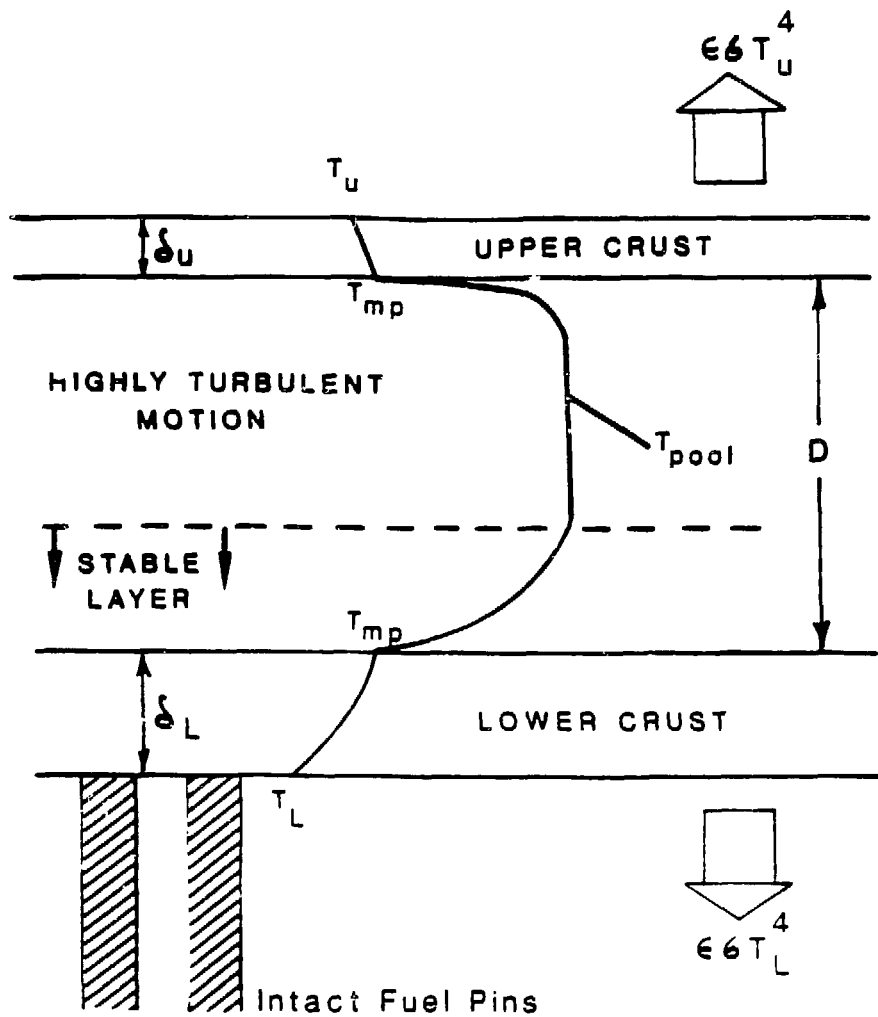


Figure 13. Schematic of heat generating pool indicating temperature profile and nomenclature.

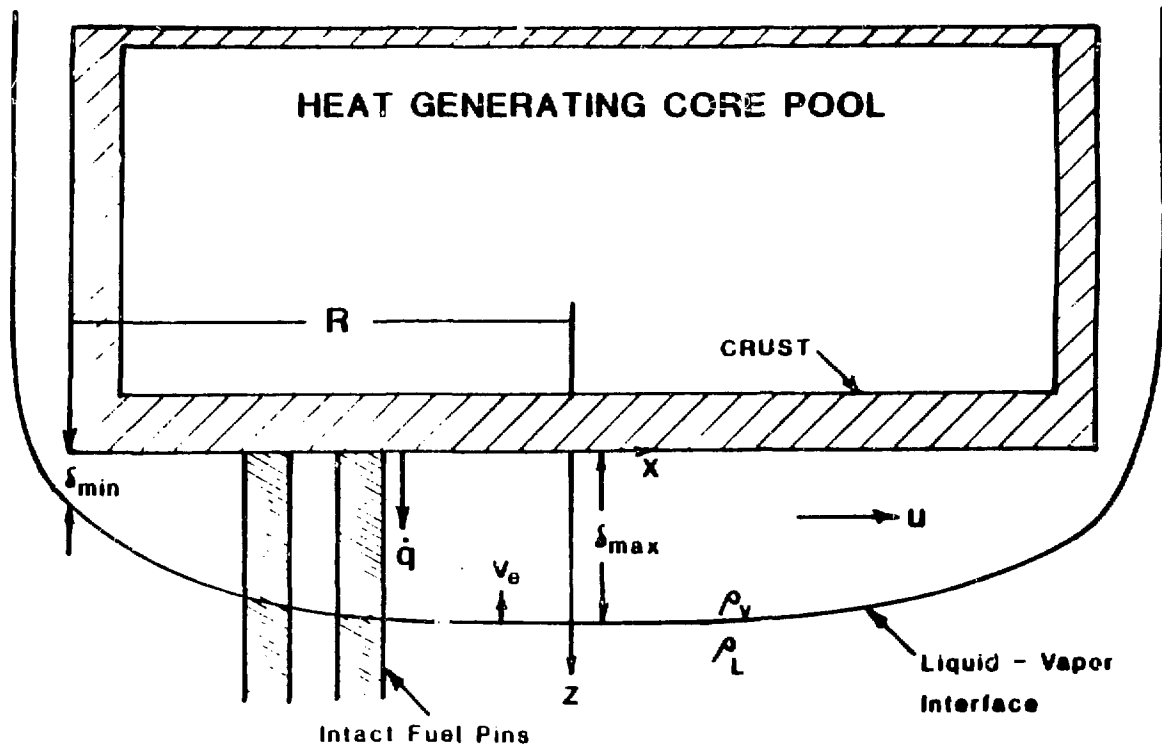


Figure 14. Vapor film profile for isothermal film flow along the bottom of the molten core pool.

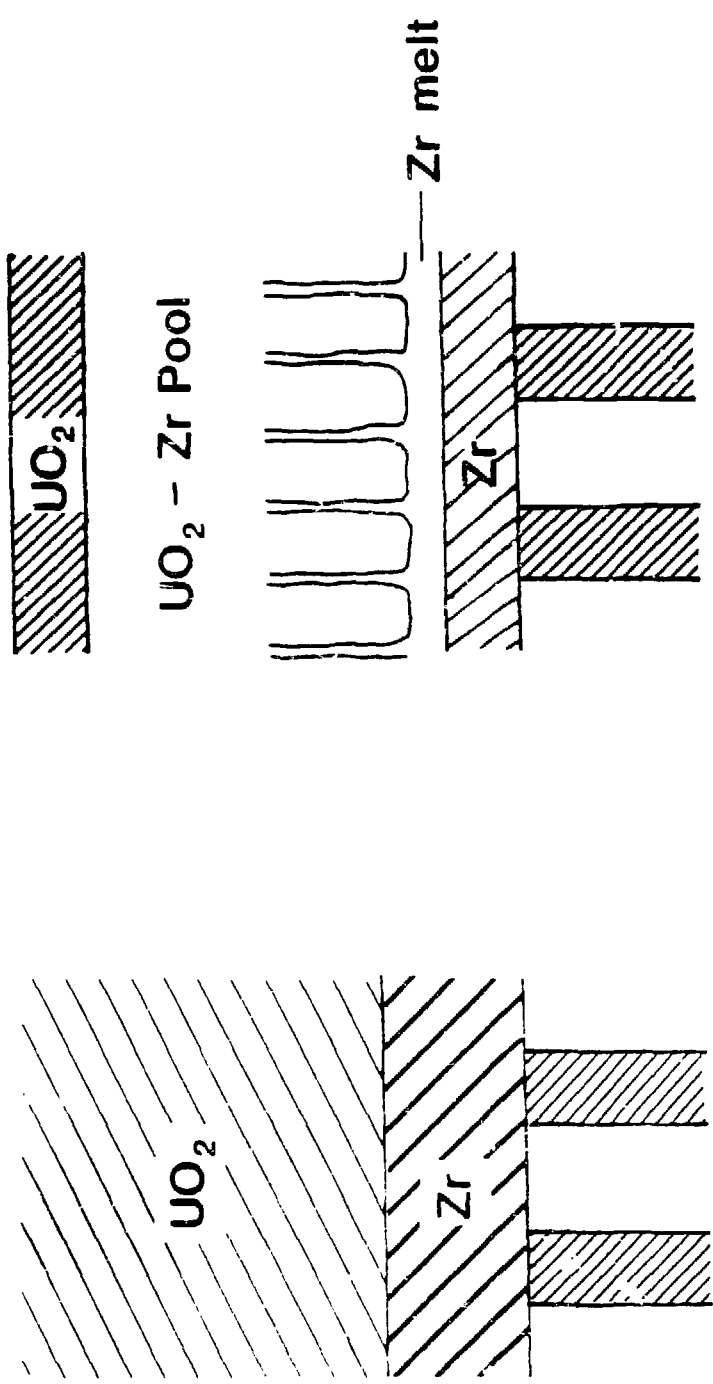


Figure 15. Melting-penetration mechanism leading to fuel draining.

DEBRIS THERMAL INTERACTION WITH LOWER PLENUM STRUCTURES

August W. Cronenberg
Engineering Science and Analysis, ESA
836 Claire View, Idaho Falls, ID 83402

Stephen R. Behling, William F. Domenico, James M. Broughton
Idaho National Engineering Laboratory
EG&G Idaho, Inc.
P.O. Box 1625, Idaho Falls, ID 83415

ABSTRACT

The damaged core of the TMI-2 reactor contains a wealth of information that will aid in understanding severe accidents. That information is being obtained by pursuing a research effort of core examination in concert with analysis aimed at understanding observed phenomena. This paper presents a preliminary analysis of the potential damage state of the lower plenum resulting from thermal interaction between hot core debris and lower head structures. Analysis indicates that the instrument penetration nozzles in TMI-2 could have experienced melting at localized hot-spot regions, with attendant debris drainage and plugging of the instrument guide tubes. Only minor thermal attack on the vessel liner is predicted.

INTRODUCTION

Recent video inspections of the TMI-2 lower plenum indicate that a significant amount of core debris relocated to that area of the reactor. Originally, this core relocation was not thought to have occurred. Consequently, the TMI-2 findings have heightened interest in the issues of debris coolability, melt progression, and debris thermal attack on lower plenum structures. The latter issue is the subject of this paper.

To interpret the consequences of debris thermal interaction with lower plenum structures, first a brief description is presented of what is currently known about characteristics of the TMI-2 debris. Analyses of debris interaction with the bottom-entry instrument penetration tubes and the reactor lower head are then presented for a range of debris thermal conditions. Conclusions are drawn regarding the potential damage state of the lower plenum structures.

DEBRIS CHARACTERISTICS

To assess the possible range of damage consequences due to potential debris thermal interaction with lower plenum structures, first it is necessary to characterize the debris with respect to composition and thermal and geometric properties. Characterization efforts to date are summarized briefly herein.

In September 1983, two axial strings of solid-state neutron track detectors were installed in the annular gap between the TMI-2 reactor vessel and the biological shield.¹ The resulting axial flux profile differed significantly from what would be expected for a normal core, showing significant neutron streaming from fuel in the lower plenum. Predictions indicate that approximately 10 to 20 t of fuel debris may have relocated to that region of the reactor. Such findings prompted initiation of subsequent video inspections of the lower plenum.

During February 1985, and again in July 1985, video inspections were performed of the lower plenum.² Figure 1 is a schematic showing the configuration of the lower plenum and includes camera orientations for views of the debris shown in Figure 2. Estimates of the debris depth range from 25 to 70 cm above the top surface of the interior of the lower head. The debris appears to be segregated radially, with loose sand/gravel-type material near the center and larger agglomerations up to several centimeters in diameter towards the edges. Specific characteristics of some of the lower plenum debris can be seen in Figure 2. Figure 2a shows what appears to be frozen debris suspended from a hole in the flow distributor plate. The debris appears to extend to about half the diameter of the hole (15.24 cm dia) and probably is agglomerated, once-molten material. Figure 2b shows what appears to be solid sharp-edge debris fragments in the vicinity of the gusset that is welded to the stainless-steel guide tube. Figure 2c presents a view of the debris bed near the junction of the Inconel penetration nozzle and the stainless-steel guide tube. The Inconel penetration nozzle appears to be intact above the surface of the rather densely packed debris bed. However, this may not be the case below the surface of the debris, where coolant penetration into the debris bed may have been quite limited. Thus, the question arises as to the physical state of the Inconel penetration nozzles (which have a melting point of ~1615 K).

After the first video inspection, a series of wire (0.15 cm dia) probings³ of the instrument penetration tubes were attempted in March 1985. Sixteen of 17 locations probed were found to be blocked at positions below the reactor vessel. The one location (L-11) that was clear when probed, subsequently was gamma profiled. Results of that study⁴ indicate increased activity with increased height above the reactor vessel, suggesting the existence of a non-fuel layer at the very bottom of the lower head (which may represent resolidified Ag-In-Cd alloy, with an overlayer of fuel debris). It should be noted, however, that analysis of the gamma profile data is subject to an inexact parameter variation of weight percent of fuel and non-fuel materials, as well as assumptions regarding the radioactivity in the debris. Thus, significant uncertainties exist as to inferred debris stratification characteristics.

In July 1985, studies were performed to investigate characteristics of the debris when agitated with a hydraulic spray.⁵ Borated water was delivered from a nozzle jet at pressures of approximately 17.2 and 34.5 MPa. Visibility in the water deteriorated as soon as the jet was activated. The finer debris material became suspended but settled quickly; and water clarity was reestablished 30 min after the disturbance. Since the debris was found to be loose, a follow-up study was made, and samples

were obtained⁶ using a long manipulating tool with a finger gripper at the end. The retrieved samples contained particles ranging from 0.6 to 6 cm dia. Planned analyses will determine the material composition and fission-product content of those samples to support debris recovery efforts.

Based on such findings to date, characteristics of the lower plenum debris can be summarized as follows:

- Approximately 10 to 20 t of core debris may have relocated to the lower plenum
- The apparent depth of the debris is approximately 25 to 70 cm
- The debris ranges in size from sand/gravel to particles 15 cm dia
- The debris can be characterized as being composed of solid fragments and once-molten agglomerations
- Data indicate the apparent existence of a stratified bed, with an underlayer of primarily non-fuel material and an overlayer of fuel/structural debris in a loose rubble configuration
- The majority of instrument penetration tubes appear blocked or subject to structural damage.

ANALYSIS

One consequence of debris migration to the lower plenum is the potential for debris thermal attack on the lower plenum structures, where thermal degradation of the bottom-entry penetration tubes and lower head are of primary concern. These two damage modes are assessed in this paper. From the outset, it should be cautioned that such analyses are used primarily to define a maximum damage state that could have occurred at localized regions within the lower plenum, that is at regions depleted of coolant as the debris settled into a close-packed or agglomerated bed. Such analyses were initiated to help identify lower plenum inspection efforts and material-interaction studies that would further the understanding of questions pertaining to vessel integrity.

Thermal Analysis of Penetration Tubes

Both B&W (TMI-2) and Westinghouse PWRs contain instrument tubes that penetrate through the lower head and serve as entry ports for neutron flux monitors and other in-core instrumentation. Because of the large number of penetrations (52 for TMI-2) and the three-dimensional type of thermal attack these tubes can experience, such penetrations may be subject to early failure and the attendant potential to duct core material into the containment.

In this analysis, the thermal response of the Inconel penetration nozzle just above the lower head is investigated with respect to attack by hot core debris. The analysis is based on the configuration shown in Figure 3. For conditions of good debris/nozzle contact, the thermal relaxation time^a for the nozzle wall thickness (X = 1.746 cm) can be estimated as

$$t_t = \frac{X^2}{4\alpha} \quad (1)$$

where α = thermal diffusivity. Using Inconel properties (see Table 1), the thermal relaxation time is estimated to be ~22 s. If the heat of fusion for nickel (the main component of Inconel) is taken into account, the thermal relaxation time for melting ($t_{t,m}$) can be approximated as:

$$t_{t,m} = \frac{X^2}{4\alpha a^2} \approx 45 \text{ s} \quad (2)$$

where a = the dimensionless solidification constant (~0.7 for Inconel), which is estimated from the following expression⁷:

$$[C_p \bar{T}_{mp}/L(\pi)^{0.5}]_n = a \exp(a^2) [(k\sqrt{\alpha}_f)/(k\sqrt{\alpha}_n) + \text{erf}(a)] \quad (3)$$

where C_p = specific heat, \bar{T}_{mp} = melting point, L = latent heat, k = conductivity, and α = thermal diffusivity, and the subscripts n and f refer to the nozzle wall material (Inconel) and fuel properties, respectively. For localized hot-spot regions, nozzle melt-through can occur rather quickly if the debris temperature exceeds the Inconel melting point of ~1615 K.

To assess the debris temperature and particle-size conditions that could lead to nozzle melt-through, the steady heat-conduction equation for spherical geometry with constant properties is applied; as follows:

$$T(r) = T_s + \frac{q'''}{6k} (R^2 - r^2) \quad (4)$$

where T_s = surface temperature, q''' = volumetric heat generation rate, k = thermal conductivity, R = radius, and r = radial position. Using the TMI-2 burnup condition and a 5-h decay-period, the volumetric heat

a. Thermal relaxation time, t_t , can be defined as the time period for a temperature-forcing function at the surface of a heat-conducting body to be transmitted to some interior position, X .

generation rate can be approximated as 10^6 W/m^3 . For an effective conductivity of 5 W/m-K and particle diameters (D_p) less than or equal to the 15.24-cm dia holes of the lower flow distributor, the center temperature (T_0) of the debris for a surface contact temperature (T_s) equal to the Inconel melting point (1615 K) is estimated to be:

D_p	T_0
(cm)	(K)
2.54	~1629
10.16	~1700
15.24	~1810

Because the eutectic melting point of $\text{UO}_2/\alpha\text{-Zr(O)}$ is about 2170 K, the debris need not be molten to cause surface melting of the Inconel penetration nozzles. In other words, fuel debris particles smaller than the hole size of the flow distributor can be in a solid condition and still cause surface melting of the Inconel nozzle. Again, it should be noted that such analysis applies only to the case of a closely packed debris configuration in contact with an Inconel penetration nozzle, where coolant penetration into the debris bed would be significantly degraded.

The above analysis assumes that heat-generating fuel debris is in good thermal contact with the nozzle wall. However, the debris in the lower regions of the plenum may be composed primarily of non-fuel, structural material. In that case, structural debris must possess sufficient sensible heat to raise the temperature of the nozzle wall to the Inconel melt temperature. For non-fuel debris, a heat balance is written for a segment of the penetration nozzle (heat sink) and the associated debris (heat source) in immediate contact with it, using the following expressions:

$$\text{Sensible heat of debris particle} = \left(\frac{\pi n^3}{6}\right) (\rho C_p) (T_{p,0} - 1615) \quad (5)$$

$$\text{Sensible heat of nozzle wall thickness} = \left(\frac{\pi D}{4}\right) [OD^2 - ID^2] (\rho C_p) [1615 - T_{n,0}] \quad (6)$$

$$\text{Latent heat of nozzle wall thickness} = \left(\frac{\pi D}{4}\right) [OD^2 - ID^2] (\rho L) \quad (7)$$

where D_p = debris diameter and the height of the nozzle associated with each debris particle, $T_{p,0}$ = initial debris temperature, 1615 K is the melting point of Inconel, $T_{n,0}$ = initial nozzle temperature [which is taken as the saturation temperature of water at 10.3 MPa (i.e., 586 K)], and the other parameters are as previously defined. Equating the sensible heat given up by the debris to the sensible and latent heat gain needed for nozzle melting, the debris temperature can be expressed as

$$T_{p,o} = 1615 \text{ K} + \frac{3 [OD^2 - ID^2] \rho_{\text{wall}}}{2 D_p^2 (\rho C_p)_{\text{debris}}} [C_{p, \text{wall}} (1029 \text{ K}) + L] \quad (8)$$

Thus, the temperature conditions leading to nozzle melting are estimated to be

Particle diameter (D_p)	$T_{p,o}$ (K)
10.16 cm	2122
15.24 cm	1840

Since the melt temperature of stainless steel is 1640 K, structural debris on the order of 10 to 15 cm dia need only be 200 to 400 K above its melting point to cause adiabatic nozzle wall heating to a melt condition. It should be noted that in the above analysis, melting of the entire nozzle wall thickness is assumed, where failure may occur with only partial melting.

Such analysis indicates that thermal degradation of the Inconel penetration nozzles could have occurred during the TMI-2 accident. Thus, the possibility exists that molten debris entered the penetration nozzles and flowed downward to colder regions of the reactor vessel, where refreezing occurred. An order-of-magnitude estimate of penetration distance (X_p) for plug solidification can be assessed from the "bulk freezing" model first advanced by Ostensen and Jackson.⁸ This model assumes that turbulence within the flowing molten material prevents the formation of a stable frozen crust layer at the channel wall. Thus, the leading edge of the melt is considered a "slush" and freezing is complete when the latent and sensible heat are removed from the slush by turbulent heat loss to the wall. Figure 4 illustrates the essential features of the problem, where a heat balance between a cold wall with constant temperature T_w and a molten plug at temperature T_o above the melting point leads to the following algebraic expression for the penetration distance (X_p):

$$X_p = \frac{D_h}{2f} \frac{L_f/C_p + (T_o - T_{mp})}{T_o - T_w} \quad (9)$$

where D_h = hydraulic tube diameter, f = wall friction factor, and the other parameters are as previously defined. Assuming molten-debris drainage through the annular space between the inside surface of the penetration nozzle and the outside surface of the instrument string, the penetration distance is estimated to be about 8 cm for molten Inconel and approximately 2 to 4 cm for molten UO_2 , for $T_w = 500 \text{ K}$ and $T_o = 50 \text{ K}$ above the melting point of the molten material. Since the lower head is approximately 14 cm thick, plugging occurs within the vessel head, preventing breach of the pressure-vessel boundary.

generation rate can be approximated as 10^6 W/m^3 . For an effective conductivity of 5 W/m-K and particle diameters (D_p) less than or equal to the 15.24-cm dia holes of the lower flow distributor, the center temperature (T_0) of the debris for a surface contact temperature (T_s) equal to the Inconel melting point (1615 K) is estimated to be:

D_p (cm)	T_0 (K)
2.54	~1629
10.16	~1700
15.24	~1810

Because the eutectic melting point of $\text{UO}_2/\alpha\text{-Zr(O)}$ is about 2170 K, the debris need not be molten to cause surface melting of the Inconel penetration nozzles. In other words, fuel debris particles smaller than the hole size of the flow distributor can be in a solid condition and still cause surface melting of the Inconel nozzle. Again, it should be noted that such analysis applies only to the case of a closely packed debris configuration in contact with an Inconel penetration nozzle, where coolant penetration into the debris bed would be significantly degraded.

The above analysis assumes that heat-generating fuel debris is in good thermal contact with the nozzle wall. However, the debris in the lower regions of the plenum may be composed primarily of non-fuel, structural material. In that case, structural debris must possess sufficient sensible heat to raise the temperature of the nozzle wall to the Inconel melt temperature. For non-fuel debris, a heat balance is written for a segment of the penetration nozzle (heat sink) and the associated debris (heat source) in immediate contact with it, using the following expressions:

$$\text{Sensible heat of debris particle} = \left(\frac{\pi D_p^3}{6}\right) (\rho C_p) (T_{p,0} - 1615) \quad (5)$$

$$\text{Sensible heat of nozzle wall thickness} = \left(\frac{\pi D_p}{4}\right) [OD^2 - ID^2] (\rho C_p) [1615 - T_{n,0}] \quad (6)$$

$$\text{Latent heat of nozzle wall thickness} = \left(\frac{\pi D_p}{4}\right) [OD^2 - ID^2] (\rho L) \quad (7)$$

where D_p = debris diameter and the height of the nozzle associated with each debris particle, $T_{p,0}$ = initial debris temperature, 1615 K is the melting point of Inconel, $T_{n,0}$ = initial nozzle temperature [which is taken as the saturation temperature of water at 10.3 MPa (i.e., 586 K)], and the other parameters are as previously defined. Equating the sensible heat given up by the debris to the sensible and latent heat gain needed for nozzle melting, the debris temperature can be expressed as

$$T_{p,o} = 1615 \text{ K} + \frac{3 [OD^2 - ID^2] \rho_{\text{wall}}}{2 D_p^2 (\rho C_p)_{\text{debris}}} [C_{p, \text{wall}} (1029 \text{ K}) + L] \quad (8)$$

Thus, the temperature conditions leading to nozzle melting are estimated to be

Particle diameter (D_p)	$T_{p,o}$ (K)
10.16 cm	2122
15.24 cm	1840

Since the melt temperature of stainless steel is 1640 K, structural debris on the order of 10 to 15 cm dia need only be 200 to 400 K above its melting point to cause adiabatic nozzle wall heating to a melt condition. It should be noted that in the above analysis, melting of the entire nozzle wall thickness is assumed, where failure may occur with only partial melting.

Such analysis indicates that thermal degradation of the Inconel penetration nozzles could have occurred during the TMI-2 accident. Thus, the possibility exists that molten debris entered the penetration nozzles and flowed downward to colder regions of the reactor vessel, where refreezing occurred. An order-of-magnitude estimate of penetration distance (X_p) for plug solidification can be assessed from the "bulk freezing" model first advanced by Ostensen and Jackson.⁸ This model assumes that turbulence within the flowing molten material prevents the formation of a stable frozen crust layer at the channel wall. Thus, the leading edge of the melt is considered a "slush" and freezing is complete when the latent and sensible heat are removed from the slush by turbulent heat loss to the wall. Figure 4 illustrates the essential features of the problem, where a heat balance between a cold wall with constant temperature T_w and a molten plug at temperature T_o above the melting point leads to the following algebraic expression for the penetration distance (X_p):

$$X_p = \frac{D_h}{2f} \frac{L_f/C_p + (T_o - T_{mp})}{T_o - T_w} \quad (9)$$

where D_h = hydraulic tube diameter, f = wall friction factor, and the other parameters are as previously defined. Assuming molten-debris drainage through the annular space between the inside surface of the penetration nozzle and the outside surface of the instrument string, the penetration distance is estimated to be about 3 cm for molten Inconel and approximately 2 to 4 cm for molten UO_2 , for $T_w = 500 \text{ K}$ and $T_o = 50 \text{ K}$ above the melting point of the molten material. Since the lower head is approximately 14 cm thick, plugging occurs within the vessel head, preventing breach of the pressure-vessel boundary.

From synthesis of the above analysis, the following observations can be drawn relative to the potential damage state of the instrument penetration nozzles. Of particular note is the fact that fuel debris need not be in a molten state in order to cause melt failure of the nozzle. This is due to the fact that the nozzle is made of relatively low melting-point/high-strength Inconel, which, although capable of withstanding high system pressures, offers little resistance to thermal attack by hot debris. This is particularly true at locations within the lower plenum of a close-packed debris configuration, where coolant penetration for cooling the debris and nozzles could have been severely limited. However, calculations of melt-penetration distance indicate a refreezing distance of less than the thickness of the lower head (~14 cm), so that integrity of the pressure-vessel boundary is predicted.

Thermal Analysis of the Lower Head

Although debris thermal attack on the penetration nozzles is the more likely failure mode for reactors that incorporate bottom-entry instrumentation, massive collapse of core debris onto the lower plenum could also lead to thermal degradation of the lower head. An assessment of the thermal response of the lower head as a consequence of contact with hot-core debris is presented, based on an estimate of the instantaneous contact temperature for the configuration shown in Figure 5. To assess if surface melting of the stainless-steel liner will occur, the following expression is applied for the instantaneous contact interface temperature (T_I) for two semi-infinite slabs⁹

$$T_I = \frac{T_H (k/\alpha)^{0.5}_H + T_C (k/\alpha)^{0.5}_C}{(k/\alpha)^{0.5}_H + (k/\alpha)^{0.5}_C} \quad (10)$$

where k is the conductivity, α is the thermal diffusivity, and H and C refer to the hot debris and cold vessel wall, respectively. Applying the above equation to both ceramic-UO₂- and metallic-U-Zr-O-type debris in contact with the stainless-steel liner, the following interface temperatures are predicted:

<u>UO₂ Debris</u>	<u>U-Zr-O Debris</u>
$T_h = 3150 \text{ K}$	$T_h = 2170 \text{ K}$
$T_c = 580 \text{ K}$	$T_c = 580 \text{ K}$
$T_I = 1200 \text{ K}$	$T_I = 1400 \text{ K}$

As indicated, the interface temperature takes on a value closer to the higher conductivity material, so that for ceramic-UO₂-type fuel debris, T_I is less than that for metallic-like U-Zr-O debris. However, in either case, the interface temperature is less than that required for melting stainless steel or establishing a significant molecular diffusion couple for Zr-Fe eutectic melting (i.e., $T > 1400 \text{ K}$). Therefore, significant melt attack on the stainless-steel liner is not predicted.

CONCLUSIONS

Based on the foregoing analyses, the following conclusions are drawn relative to the potential damaged state of the lower plenum:

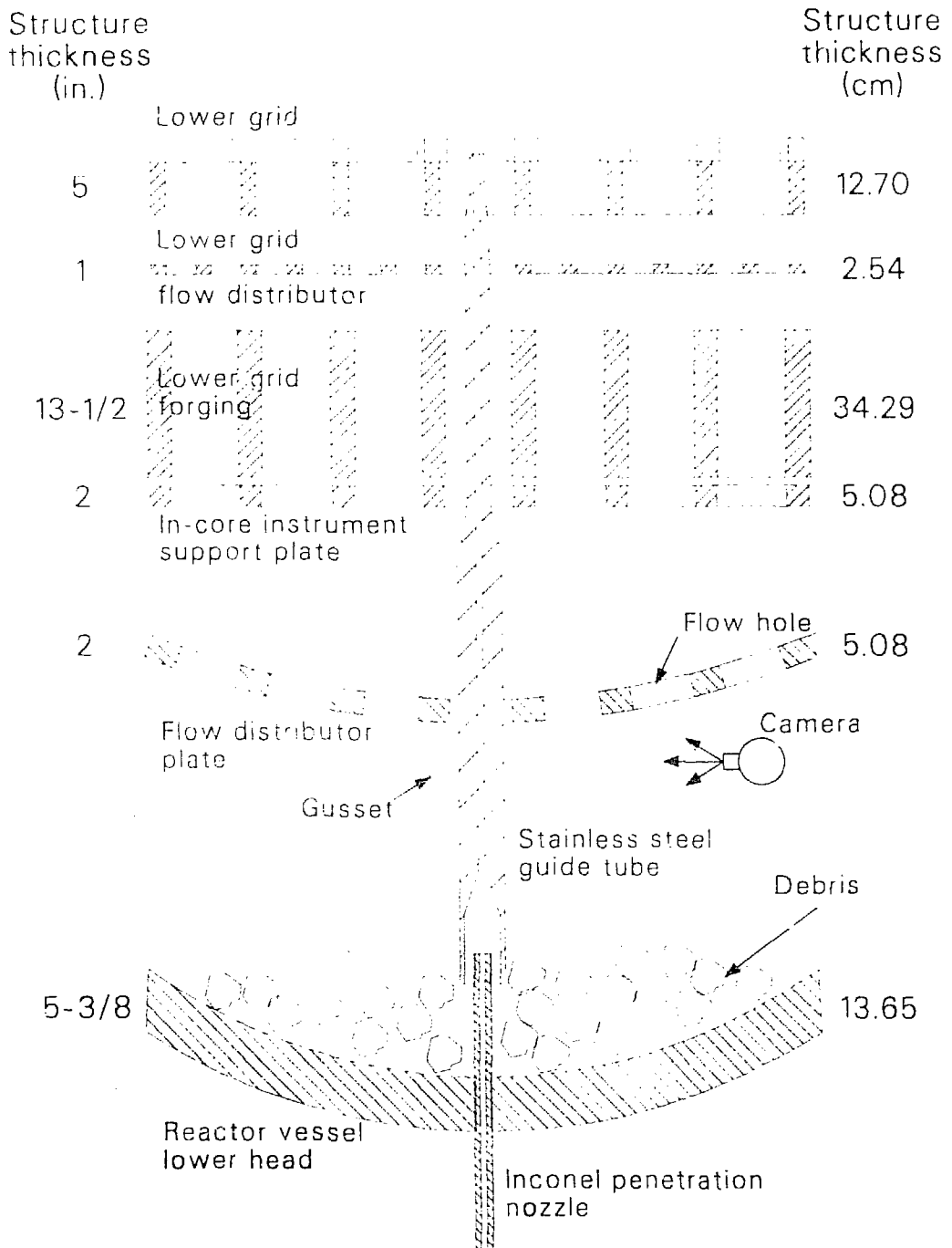
- Analysis of debris thermal interaction with the Inconel instrument nozzles indicates that thermal degradation of such nozzles may have occurred at regions where the debris bed was in a close-packed coolant-impenetrable configuration.
- For failed penetration nozzles, molten debris may have entered those nozzles, leading to debris drainage and plugging of the instrument guide tubes. Modeling of the penetration distance indicates that either molten UO_2 or Inconel will refreeze within the thickness of the pressure vessel lower head (~14 cm), maintaining the integrity of the pressure boundary.
- Significant eutectic Zr-Fe melting of the stainless-steel liner at the inside surface of the lower head is not predicted, for contact with either molten ceramic or metallic debris.
- A range of lower plenum damage and material interaction conditions is possible, which is largely dependent on debris composition and rubble bed cooling conditions.

In conclusion, it is suggested that acquisition of TMI-2 data should include assay of the debris decay-heat source and composition, damage state of the Inconel penetration nozzles relative to potential melting, as well as that of the stainless-steel liner.

REFERENCES

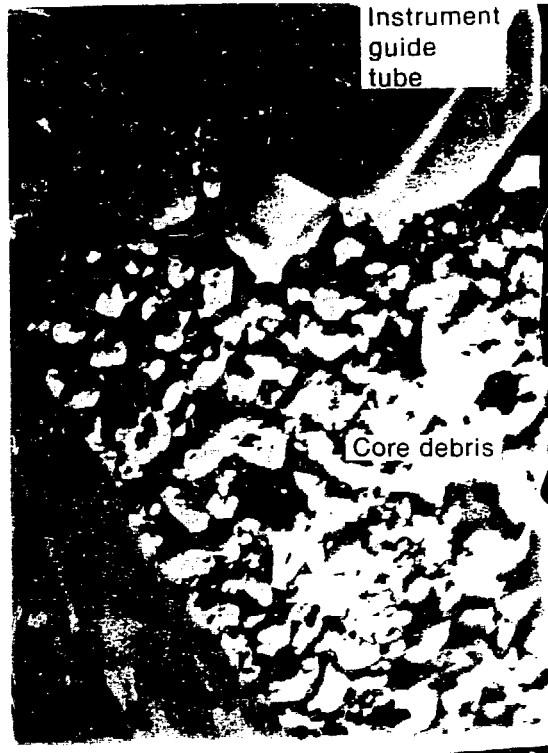
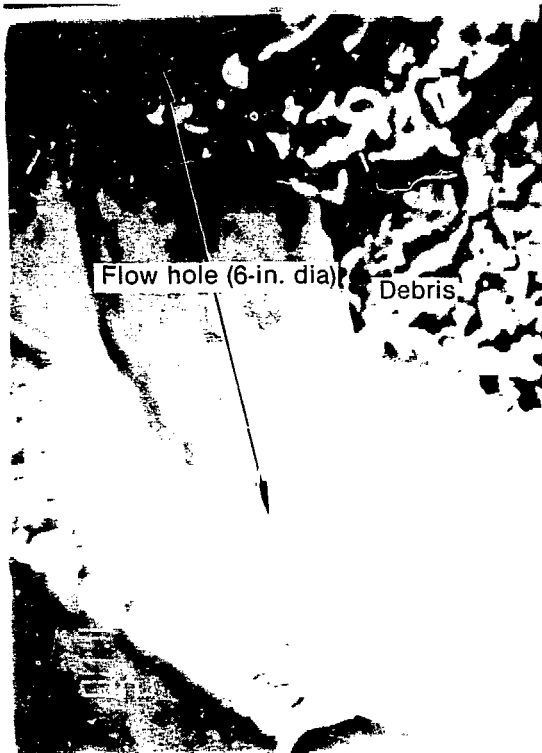
1. Technical Planning Department, Determination of Fuel Distribution in TMI-2 Based on Axial Neutron Flux Profile, TPO/TMI-165, Rev. 0, GPU Nuclear Corporation, April 1985.
2. V. R. Fricke, "Reactor Lower Head Video Inspection," TMI-2 Technical Planning Bulletin, February 26, 1985.
3. D. G. Keefer, "In-Core Instruments Tube Probing," EGG-Interoffice Correspondence, April 1, 1985.
4. R. Rainisch, Analysis of Gamma Scanning of In-core Detector No. 18 (L-11) in Lower Reactor Vessel Head, GPU-Nuclear Report TPO/TMI-175, June 1985.
5. V. R. Fricke, "Hydraulic Disturbance of the Debris in the Bottom Head of the TMI-2 Vessel," TMI-2 Technical Planning Bulletin, TPB-85-20, July 26, 1985.
6. G. Worku, "Core Debris Sample Retrieval from the Lower Head Region," TMI-2 Technical Planning Bulletin, TPB-85-21, July 29, 1985.

7. M. S. El-Genk and A. W. Cronenberg, "An Assessment of Fuel Freezing and Drainage Phenomena in a Reactor Shield Plug Following a Core Disruptive Accident," Nucl. Engr. Design, 47, pp. 195-255, (1978).
8. R. W. Ostensen and J. F. Jackson, Intended Fuel Motion Study, ANL-RDP-18, 1973.
9. H. S. Carslaw and J. C. Jaeger, Conduction of Heat in Solids, 2nd Edition, Oxford University Press, Oxford England, 1959, pg. 88.



LN86011-4

Figure 1. Schematic of the TMI-2 lower plenum, including camera orientations for views of the debris shown in Figure 2.



(a) Once-molten debris suspended from a flow hole in the flow distributor plate.

(b) Debris in the vicinity of the gasket welded to the stainless steel guide tube.



(c) View of the debris bed near the junction of the Inconel penetration nozzle and stainless steel guide tube.

Figure 2. Still frames taken from video inspections of the lower plenum.

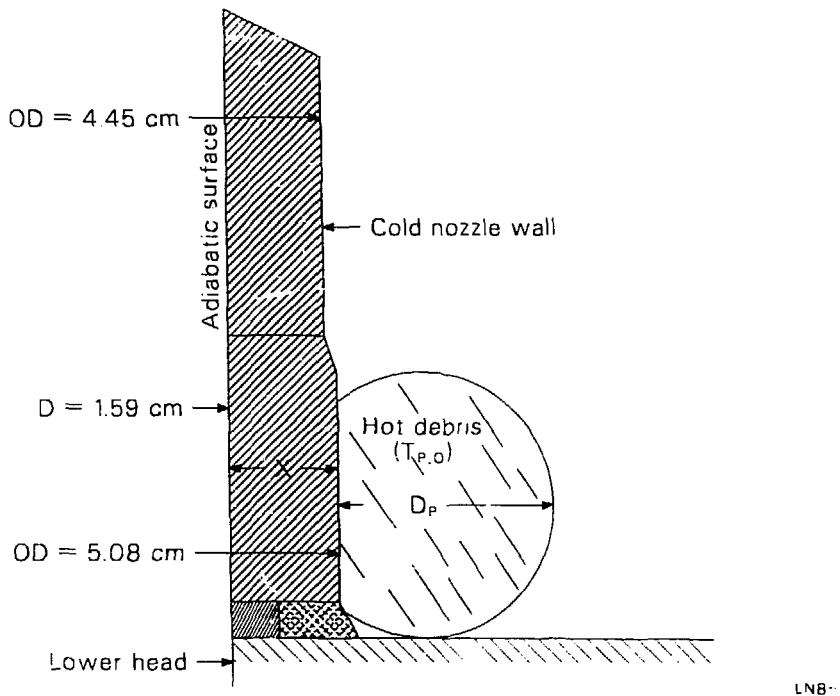


Figure 3. Configuration of the wall of the Inconel penetration nozzle in contact with hot debris.

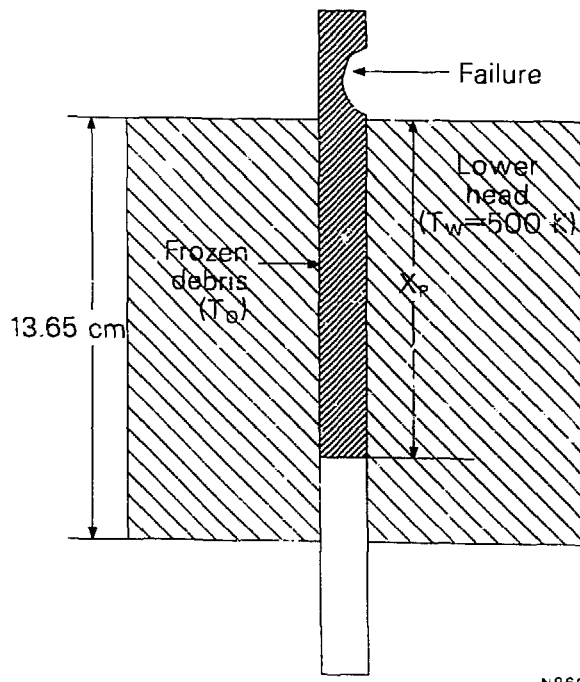
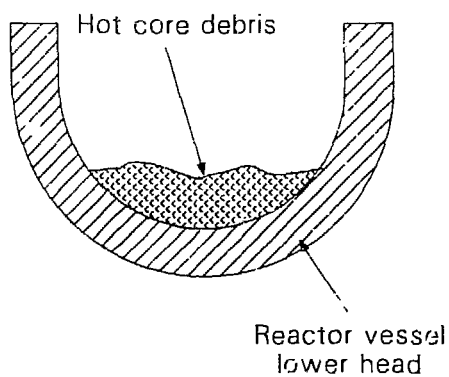
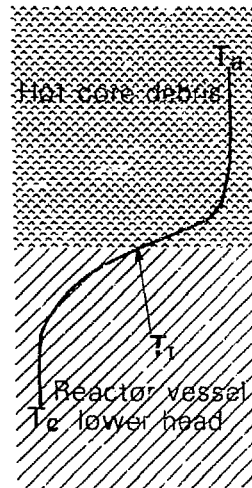


Figure 4. Schematic of the molten debris penetration distance (x_p) within the lower head thickness.



(a) Lower head failure caused by direct thermal attack of hot core debris.



(b) Illustration (rotated) of instantaneous contact-interface temperature for slab geometry.

LNB6C : 2

Figure 5. Illustration of thermal attack by hot core debris on the lower head.

TABLE 1. THERMOPHYSICAL PROPERTIES OF CORE MATERIALS

<u>Property (Units)</u>	<u>Symbol</u>	<u>UO 2</u>	<u>Values Inconel</u>	<u>Stainless-Steel</u>
Melt Temperature (K)	T_{mp}	3150	1616	1640
Specific heat (cal/g-K)	C_p	0.12	0.106	0.12
Conductivity (W/m-K)	k	3.7	12	16
Density (kg/m ³)	ρ	105	80	80
Latent Heat (cal/g)	L	65	71	65
Diffusivity (cm ² /s)	α	0.0083	0.035	0.04

CHEMICAL INTERACTION BETWEEN CORE AND STRUCTURAL MATERIALS

E. R. Carlson and B. A. Cook
Idaho National Engineering Laboratory
EG&G Idaho, Inc.
P.O. Box 1625, Idaho Falls, ID 83415

Recent camera inspection of the TMI-2 lower plenum has shown a significant (~20 metric ton) amount of debris present. In order for material to reach the lower plenum, it must either flow as a liquid or fall as a solid through the lower core-support structure. This observation raises the possibility that significant interaction (thermal and/or chemical) may have occurred between upper core materials and lower core support and reactor vessel materials. The purpose of this paper is to investigate the possible chemical interactions between core materials (control material, UO_2 , zircaloy, Inconel) and the lower core-support structures. This analysis will be used in conjunction with thermal analyses to determine what, if any, challenge may have occurred to the integrity of the internal structure and the primary system pressure boundary.

The composition of the active core region including the assembly end fittings is shown in Table 1, grouped by material type. Fuel-rod materials (UO_2 and zircaloy) make up about 92% of the active core, while the remaining 8% is primarily structural material (stainless steel and Inconel) and control material (Ag, In, Cd). Table 2 is a ranking of the various elements (excluding oxygen) found in the active core region from all of the material types. A complete list of possible interactions would include all possible combinations of the elements listed in Table 2, plus oxygen. However, the first six elements (U, Zr, Fe, Ag, Cr, Ni) comprise over 98% of the active core region; so for the purpose of this paper, the remaining elements (including fission products) are ignored. The omission of the minor elements is justified primarily because of their relative scarcity, but it can also be justified because their inclusion generally would not add to the variety of interactions; in effect, they are lumped with the elements that are considered.

Table 3 is a matrix of the potential binary reactions between the six most abundant elements plus oxygen. The feasibility of the reactions is summarized in this table. Uranium is considered as UO_2 and the only additional source of oxygen is assumed to be H_2O . In addition to the reactions of individual metallic elements, the interaction between the various metal oxides must also be considered. Binary phase diagrams are available for most of the interactions in Table 3 and ternary information is available (usually with oxygen as the third element) in a few instances. Beyond that the data is very limited.

Since the objective of this analysis is to estimate damage to the reactor vessel and lower core-support structures, the number of material interactions can be narrowed to those between stainless steel (Fe, Cr, Ni)

and active core materials. Therefore, the relocation of three groups of materials can be considered that cover all important interactions:

- $(U,Zr)O_{2+x}$ containing small amounts of Al, Cr, Fe, Ni oxides
- Control rod materials (Ag) with variable amounts of Zr
- Zr(O) (metallic) with variable amounts of oxygen and uranium.

The first case considered involves ceramic material consisting of $(U,Zr)O_2$ with small amounts of other oxides falling from the active core region as a solid or liquid and contacting stainless-steel structural material. The standard free energy diagram for oxide formation of the active core region constituents is shown in Figure 1. This diagram can be used to determine:

- Feasibility of oxide interactions and to determine equilibrium partial pressures of oxygen for particular oxidation reactions
- Equilibrium partial pressure ratios P_{H_2}/P_{H_2O} for hydrogen reduction reactions.

Since the Gibbs' free energy change must be negative for a reaction to proceed, the oxides with greater stability (lower on the chart in Figure 1) will reduce oxides of lesser stability. Since UO_2 and ZrO_2 are stable relative to the stainless-steel constituents, these elements will not reduce UO_2 or ZrO_2 . Phase diagrams show there are no eutectic-type interactions between these elements and the oxides of Zr and U, although there are small solubility limits of Cr and Fe in solid UO_2 (Reference 1). However, there are interactions between the oxides of stainless-steel constituents and oxides of U and Zr. For example, see Figure 2, which illustrates the ZrO_2 and iron oxide phase diagram, showing that liquids can be present at as low as 1600 K.

In considering control rods interaction, the control material (Ag, In, Cd) melts at 1234 K, the stainless-steel cladding will fail at about 1700 K due to melting, and the molten materials can interact with the zircaloy guide sleeve. The molten control materials then flow down and contact the lower core-support structures and, possibly, the reactor vessel. During the relocation process, the control materials may contact zircaloy and dissolve a significant amount of Zr. The Zr-Ag phase diagram, shown in Figure 3, indicates that at 1500 K, Ag can dissolve about twice its weight in Zr. The control materials themselves (especially Ag) are not expected to interact with stainless steel as seen in the phase diagrams between Ag and Fe, Cr, and Ni and between In and Fe in Figures 4-7. The Ag-Cr and In-Ni phase diagrams in Figure 8 do indicate interactions, but there is evidence that significant interaction of molten Ag-In-Cd alloy with stainless steel does not occur.² The reasons may be that silver reduces the melting point of chromium only to about the melting point of stainless steel and not below, and indium and nickel are relatively minor components. Zirconium does interact with stainless steel, but the interaction of Ag-Zr alloy with stainless steel is not known.

The third potential interaction involves the melting of metallic zircaloy between 2030 K and 2245 K (depending on the amount of dissolved oxygen), which flows downward possibly interacting with UO₂ fuel and Inconel grid spacers before contacting the lower support structure. The binary phase diagrams between pure Zr and the stainless-steel components are shown in Figures 9-11. Based on these diagrams, a eutectic between zircaloy and stainless steel would be expected to form at about 1200 K or above. Dissolved oxygen is expected to have a relatively minor effect until ZrO₂ begins to precipitate out above about 30 at.% oxygen (see Reference 1). The addition of metallic uranium might be expected to lower the eutectic point with Zr and Fe based on the binary U-Fe diagram shown in Figure 12, except that two moles of oxygen are usually added for each mole of uranium.

Experiments have been performed at KFK in the Federal Republic of Germany to study the melting point of U-Zr-stainless steel alloys (see Reference 1). In these experiments, UO₂ inside of zircaloy cladding and bounded by stainless steel was heated up to UO₂ melting temperatures under various conditions and then examined. The phase composition was determined, and the specimens were remelted to determine melting points of various phases. These results indicate that metallic corium^a compositions that are rich in stainless steel do not melt until near the melting point of stainless steel. This is also indicated by the Zr-Fe phase diagram in Figure 9. Therefore, the Zr-Fe phase diagram may be reasonable to use for Zr-stainless-steel interaction even with dissolved oxygen and uranium, bearing in mind that UO₂ or ZrO₂ that precipitates out does not react with stainless steel.

This review of potential material interactions between the TMI-2 core and structural materials indicate the only reaction of concern is probably between zircaloy and stainless steel. At the eutectic point (~1220 K), the stainless steel-zircaloy reaction is believed to proceed very slowly; however, at temperatures 200 K or more above the eutectic point, the reaction approaches equilibrium in a matter of minutes.³ Using the Fe-Zr phase diagram (Figure 9) at 1450 K, the equilibrium liquid concentration is 0.65 at.% or 0.75 wt% Zr. This means that zircaloy would dissolve up to about one-third of its weight in stainless steel. There are other eutectic points on the Fe-rich side of the phase diagram at 1570 K, so at temperatures above ~1600 K, zircaloy could be expected to dissolve about seven times its weight in stainless steel. However, the reduction in the melting point of stainless steel is only about 100 K. The heat of reaction between Zr and stainless steel is not known, but is not expected to be a significant factor in the metal-metal interaction. While control rod materials by themselves are not expected to react with stainless steel, Ag can dissolve Zr which, in turn could react with stainless steel. However, the Ag-Zr-stainless-steel system must be studied to quantify this potential reaction. Critical interaction temperatures are summarized in Figure 13.

a. Corium = mixtures of fission products and core materials simulating irradiated fuel

REFERENCES

1. P. Hofmann et al., Konstitution und Reaktionsverhalten von LWR-komponenten beim Coreschmelzen, KFK-2242, February 1976.
2. D. A. Petti, Ag-In-Cd Control Rod Behavior in Severe Reactor Accidents, MIT Thesis, December 1985.
3. P. Hofmann, private communication, KFK, Federal Republic of Germany, Idaho Falls, Idaho, August 1985.
4. J. J. Moore, Chemical Metallurgy, London, Butterworths and Co., LTD, 1981.
5. P. Hofmann, Simulation of the Chemical State of Irradiated Oxide Fuel; Influence of the Internal Corrosion on the Mechanical Properties of Zry-4 Tubing, KFK-2785, March 1979.
6. C. E. Wicks and F. E. Block, Thermodynamic Properties of 65 Elements - Their Oxides, Halides, Carbides, and Nitrides, Bureau of Mines Bulletin 605, 1963.
7. E. M. Levin et al., National Bureau of Standards, Phase Diagram for Ceramists, American Ceramic Society, 1969.
8. D. L. Hagerman, A Model for Solubility of Zirconium Cladding in Ag-In-Cd Neutron Absorber, FIN No. A6050, September 1985.
9. M. Hansen and K. Anderko, Constitution of Binary Alloys, New York, McGraw Hill Book Co., 1969.
10. W. G. Moffatt, Binary Phase Diagrams Handbook, Schenectady, New York, General Electric Company, 1976.
11. F. A. Shunk, Constitution of Binary Alloys, Second Supplement, New York, McGraw Hill Book Co., 1969.
12. American Society for Metals, Bulletin of Alloy Phase Diagrams, Vol. 5, No. 2, April 1984.
13. D. Coleman et al., TMI-2 Accident Core Heatup Analysis, A Supplement, NSAC-25, June 1981.

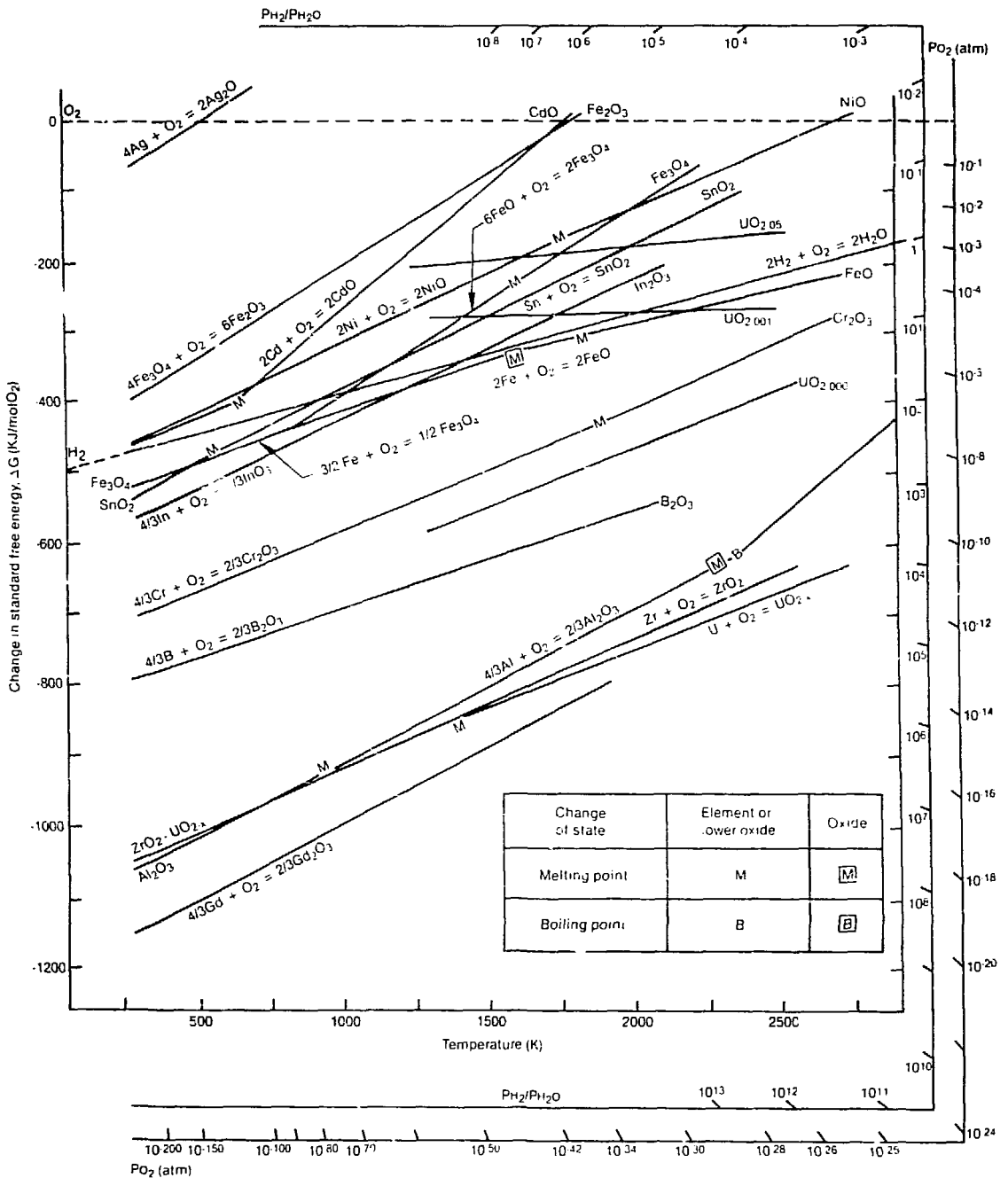
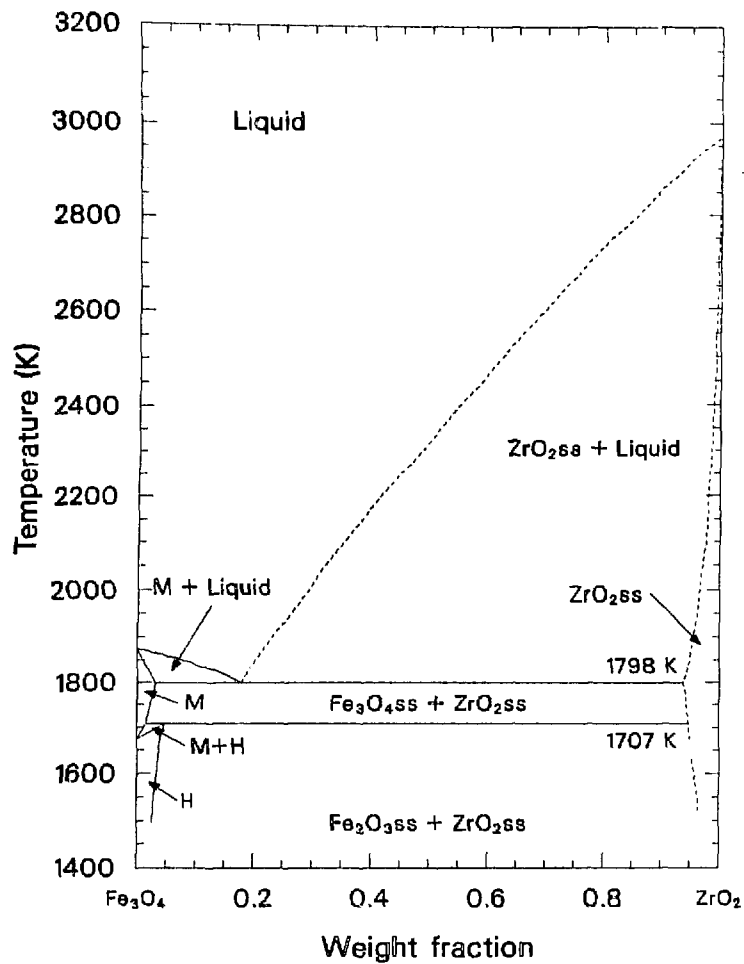
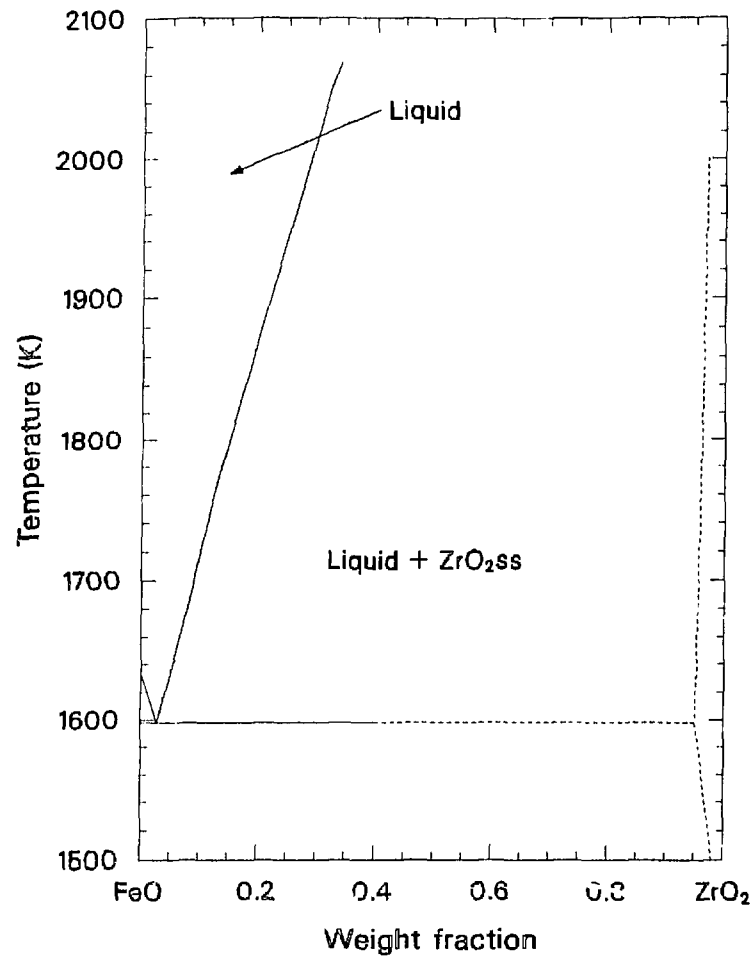


Figure 1. Standard free energy diagram for active core region materials (References 4-6).

System $\text{Fe}_3\text{O}_4\text{-ZrO}_2$ 

(a)

System FeO-Zr_2 

(b)

Figure 2. Iron oxide- ZrO_2 phase diagram (Reference 7).

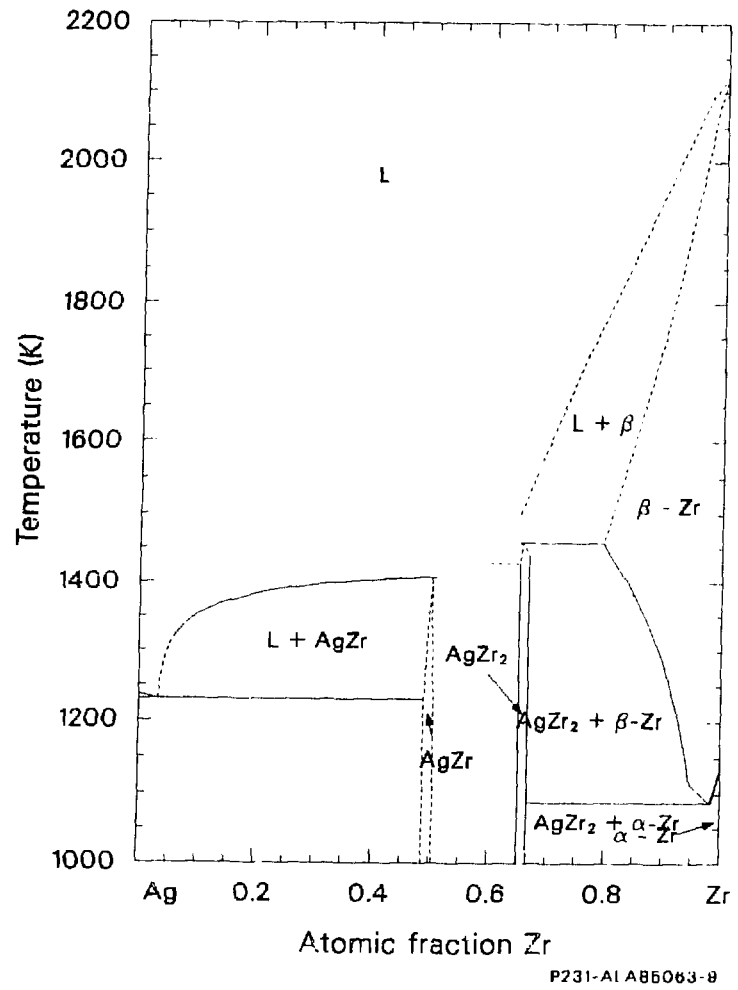


Figure 3 Ag-Zr phase diagram (Reference b).

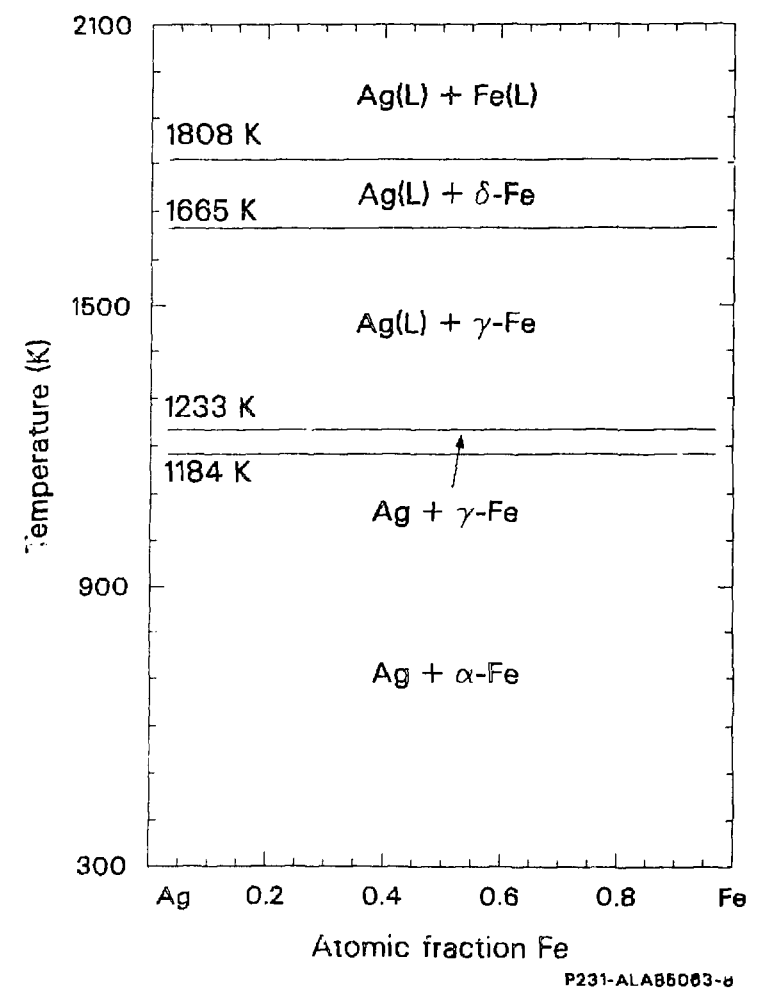
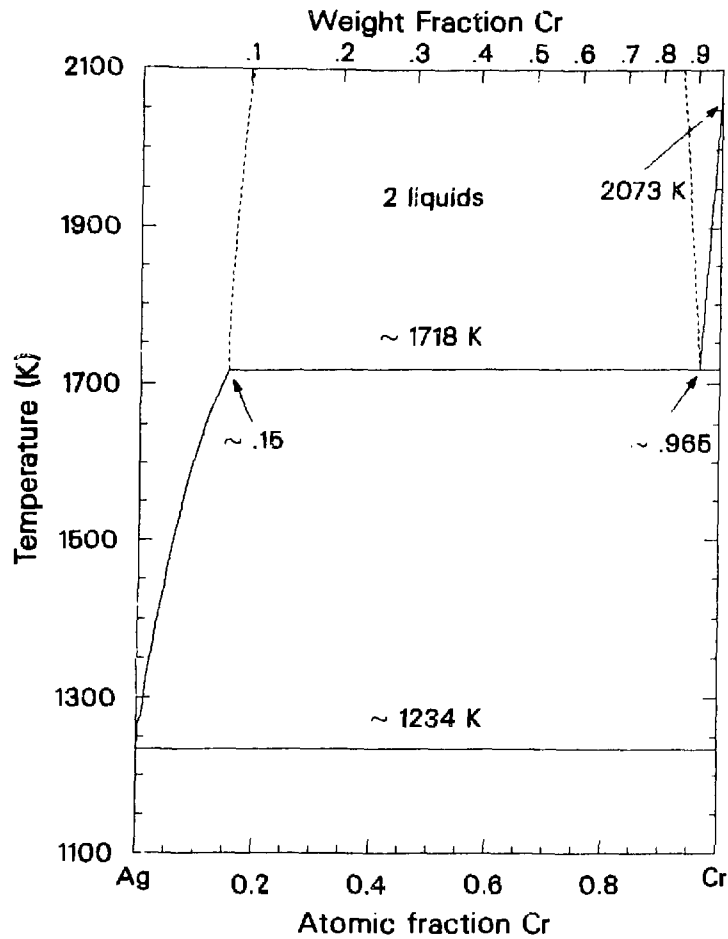
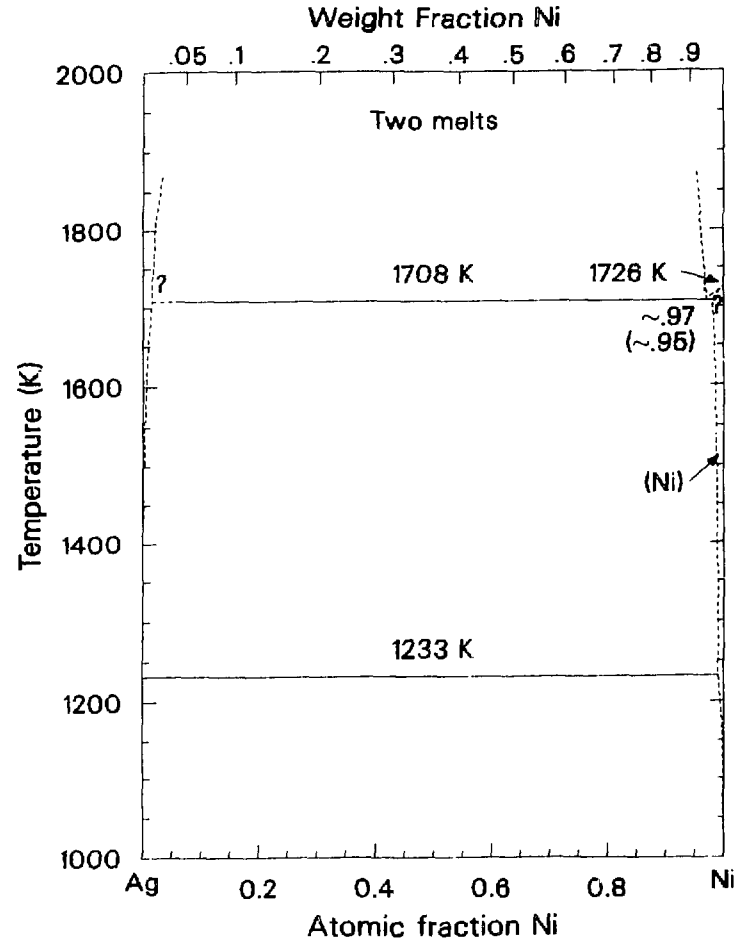


Figure 4 Fe-Ag phase diagram (Reference 3).



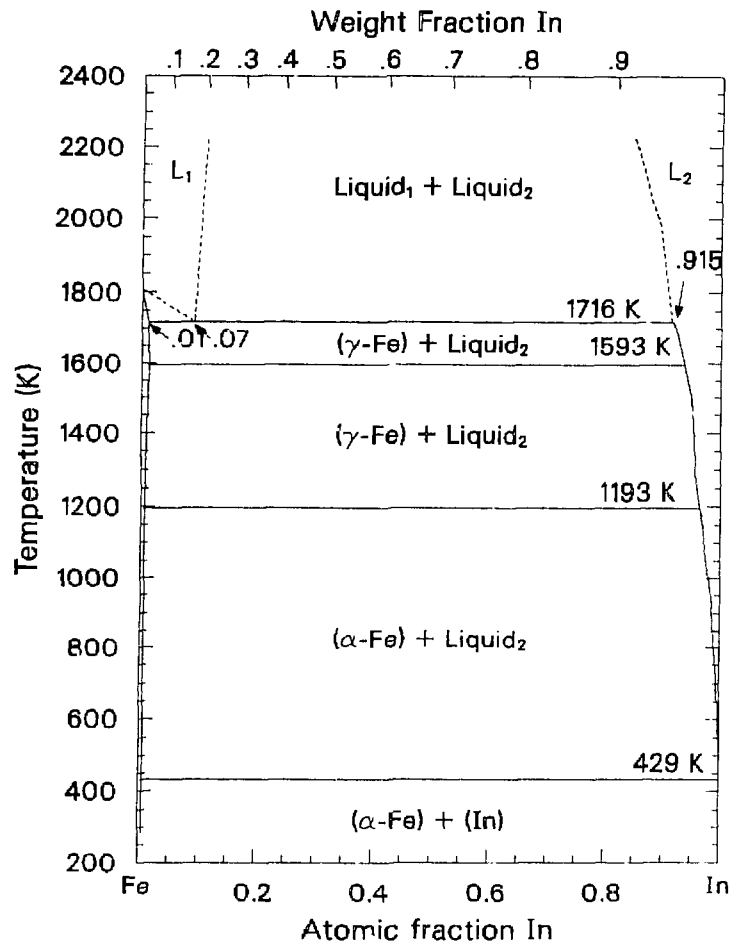
P231-ALA85063 10

Figure 5. Ag-Cr phase diagram (Reference 9).



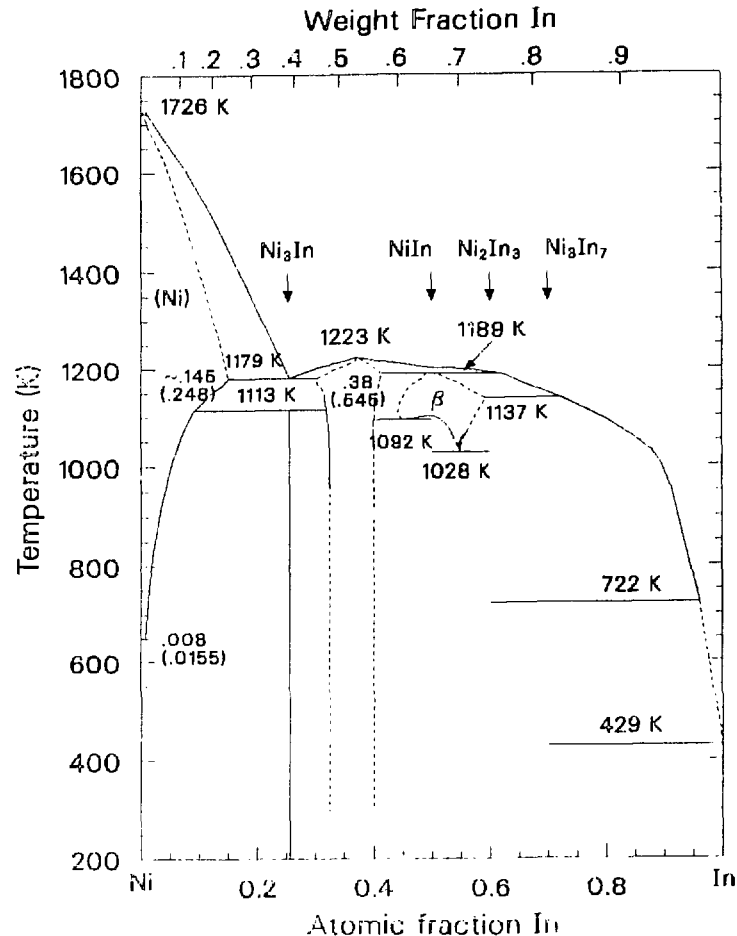
P231-ALA85063 11

Figure 6. Ag-Ni phase diagram (Reference 9).



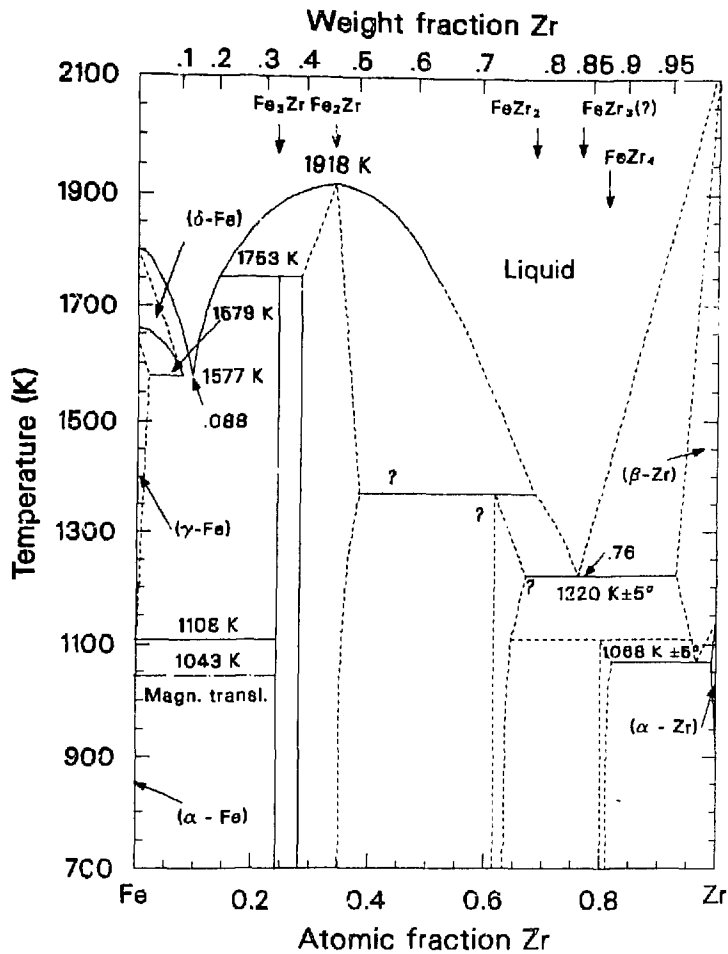
P231-ALAB5083-12

Figure 7. Fe-In phase diagram (Reference 10).



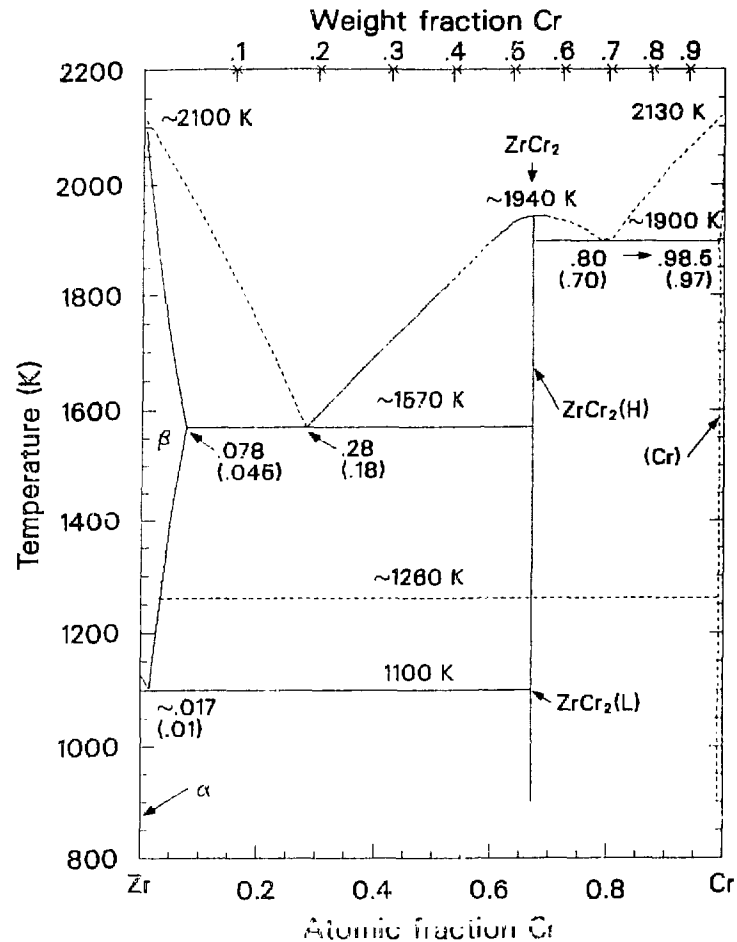
P231-ALAB5003-10

Figure 8. Ni-In phase diagram (Reference 9).



P231-ALA8608.3 14

Figure 9. Fe-Zr phase diagram (Reference 11).



P231-ALA860 13

Figure 10. Cr-Zr phase diagram (Reference 9).

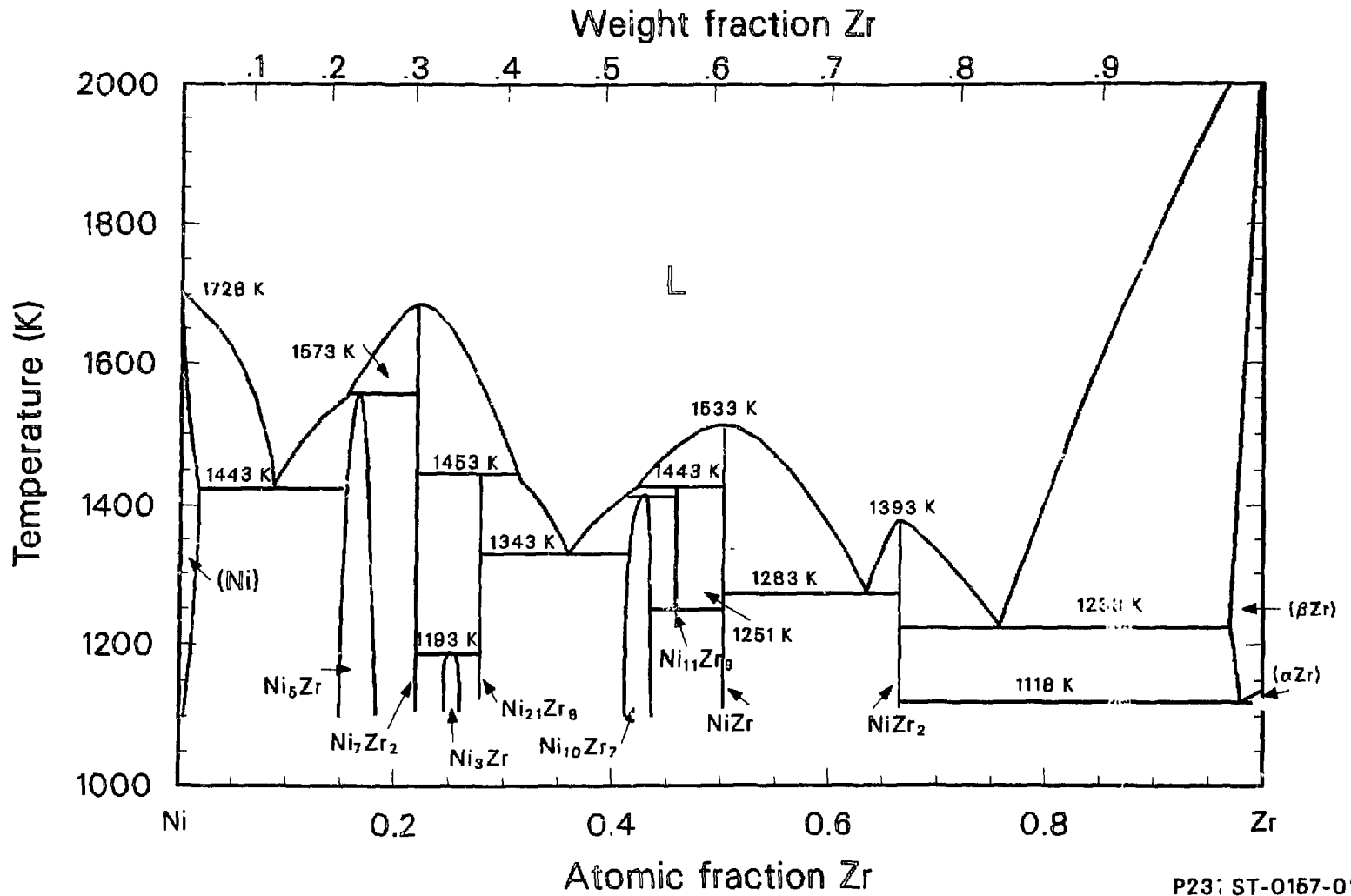


Figure 11 Zr phase diagram
(Reference 12).

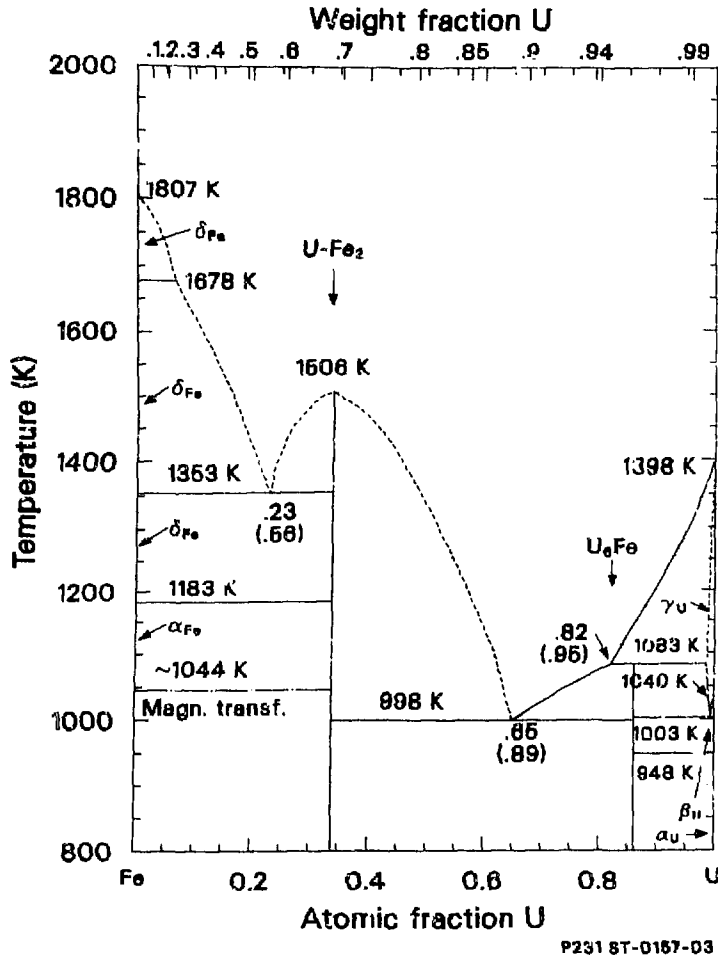


Figure 12. U phase diagram (Reference 9).

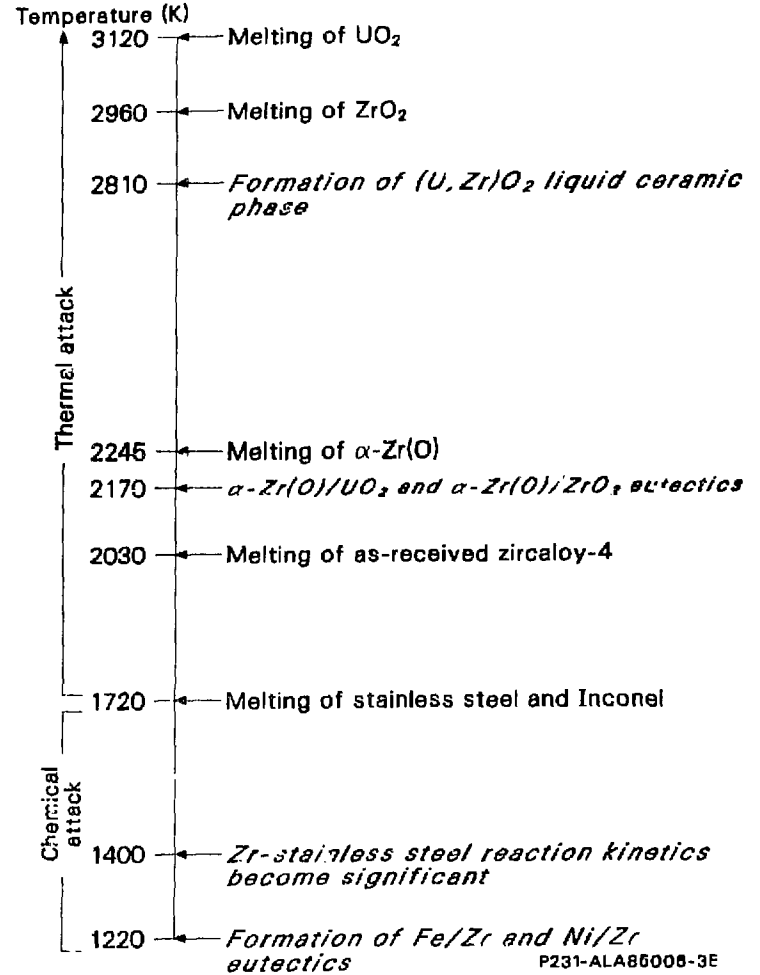


Figure 13. Chemical interactions and formations of liquid phases.

TABLE I. CORE MATERIAL COMPOSITION (Reference 13)

	Material			Element	Weight Percent	Material					
	Weight		Melt Temperature (K)			Weight		Melt Temperature (K)	Element	Weight Percent	
	(kg)	(%)				(kg)	(%)				
UO ₂	93050	74.0	3120	Zr	2.265	Inconel-718	1211	1.0	1720	Ni	51.900
				235U	85.882					Cr	19.000
				238U	11.853					Fe	18.000
				O						Nb	5.553
Zircaloy-4	23029	18.3	2030	Zr	97.907					Mo	3.000
				Sn	1.60					Ti	0.800
				Fe	0.225					Al	0.600
				Cr	0.125					Co	0.470
				O	0.095					Si	0.200
				C	0.0120					Mn	0.200
				N	0.0080					N	0.130
				HF	0.0078					Cu	0.000
				S	0.0035					C	0.040
				As	0.0024					S	0.007
				Ti	0.0020						
				V	0.0020						
				Mn	0.0020	ZrO ₂	331	0.3	2960	Zr	74.0
				Ni	0.0020				O	26.0	
				Cu	0.0020						
				W	0.0020						
				H	0.0013						
				Co	0.0010	Ag-In-Cd	2749	2.2	1050	Ag	80.0
				B	0.000033					In	15.0
				Cd	0.000025					Cd	5.0
				U	0.000020						
Type 304 and Unidentified Stainless Steel	4636	3.7	1720	Fe	68.635	B ₄ C-Al ₂ O ₃	626	0.5		Al	34.33
				Cr	19.000					O	30.53
				Ni	9.000	Al ₂ O ₃			2320	B	27.50
				Mn	2.000	B ₄ C			2620	C	27.50
				Si	1.000						
				N	0.130	Gd ₂ O ₃ -UO ₂	131.5	0.1	Gd	10.27	
				C	0.080					U	77.72
				Co	0.080	Gd ₂ O ₃			2670	O	12.01
				P	0.045						
				S	0.030						

Total Inventory = 125.8 Metric tons

TABLE 2. TMI-2 CORE COMPOSITION BY ELEMENTAL WEIGHT PERCENT

<u>Element</u>	<u>Weight Percent</u>
U	71.77
Zr	19.89
Fe	3.01
Ag	1.75
Cr	1.00
Ni	0.91
In	0.33
Sn	0.32
Al	0.18
B	0.14
Cd	0.12
Mn	0.09
Nb	0.05
Si	0.04
C	0.04
Mo	0.03
Gd	0.01
Ti	0.01
N	0.01
Co	0.01
S	0.01
Ca	0.01
P	0.01
Hf	0.01
V	0.01
W	0.01

TABLE 3. BINARY REACTION MATRIX

	UO ₂	ZrO ₂ Zr	H ₂ O	Fe	Cr	Ni	Ag
UO ₂	X						
ZrO ₂ Zr	Yes Yes	X					
H ₂ O	Yes	No Yes	X				
Fe	No	No Yes	Yes	X			
Cr	No	No Yes	Yes	X	X		
Ni	No	No Yes	Yes	X	X	X	
Ag	No	No Yes	No	No	No	No	X
FeO Cr ₂ O ₃	Yes	Yes Yes	X	X	X	X	No

P231-ALA86083-4A

SUMMARY

FUTURE MEETINGS AND INFORMATION TRANSFER

Sidney Langer
Idaho National Engineering Laboratory
EG&G Idaho, Inc.
P.O. Box 1625, Idaho Falls, ID 83415

This paper describes how information from the TMI-2 Accident Evaluation Program will be disseminated to industry and the general public via meetings and publications.

This First International Information Meeting on the TMI-2 Accident is the first of presently planned annual meetings on the TMI-2 Accident Evaluation Program. Papers presented at these meetings will be published annually in Proceedings. As was true this year, future meetings will be held in conjunction with Water Reactor Safety Research Meetings sponsored by NRC.

The Materials Science and Technology Division of the ANS has tentatively scheduled a topical meeting for early October 1987, entitled "The TMI-2 Accident: Fuel and Materials Technology." Further information on this meeting will be available by October 1986.

Plans for future meetings and publications will be governed by progress in defueling the TMI-2 reactor. The present schedule for defueling the reactor; removing, transporting, and examining samples; and reporting results is depicted in Figure 1. As the figure shows, defueling will be completed in the fall of 1987, with analysis of data from samples probably completed in late 1988 or early 1989.

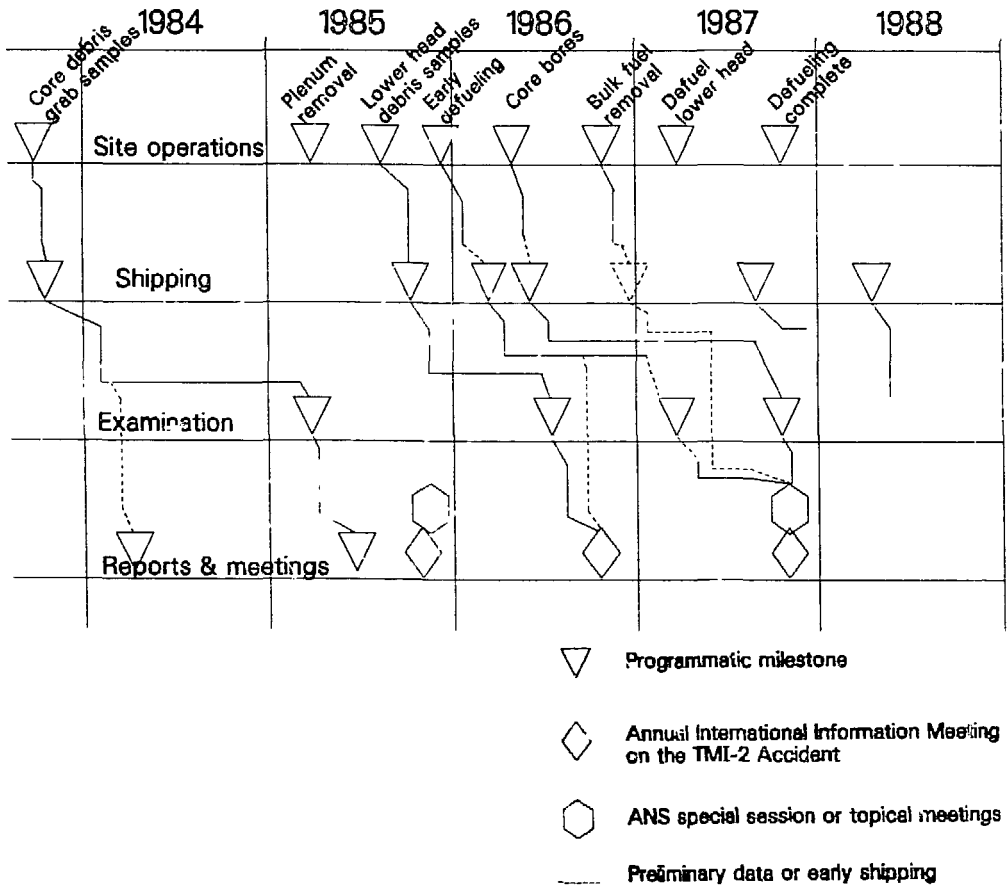


Figure 1. TMI schedule.